Microwave absorbing materials based on epoxy foam loaded with long carbon fibers

Aicha El Assal

▶ **To cite this version:**

Aicha El Assal. Microwave absorbing materials based on epoxy foam loaded with long carbon fibers. Networking and Internet Architecture [cs.NI]. Université de Rennes; Université Libanaise, 2021. English. NNT : 2021REN1S013 . tel-03337128

HAL Id: tel-03337128

https://theses.hal.science/tel-03337128

Submitted on 7 Sep 2021

HAL is a multi-disciplinary open access archive for the deposit and dissemination of scientific research documents, whether they are published or not. The documents may come from teaching and research institutions in France or abroad, or from public or private research centers.

L'archive ouverte pluridisciplinaire **HAL**, est destinée au dépôt et à la diffusion de documents scientifiques de niveau recherche, publiés ou non, émanant des établissements d'enseignement et de recherche français ou étrangers, des laboratoires publics ou privés.

UNIVERSITÉ DE RENNES 1

الجامعة اللبنانية
UNIVERSITE LIBANAISE

THESE DE DOCTORAT DE

L'UNIVERSITE DE RENNES 1 EN COTUTELLE AVEC
L'UNIVERSITE LIBANAISE

ECOLE DOCTORALE N° 601
Mathématiques et Sciences et Technologies de l'Information et de la Communication
Spécialité : *Télécommunications*

Par

Aicha EL ASSAL

Matériaux absorbants en hyperfréquences à base de mousse époxy chargée en fibres longues de carbone

Thèse présentée et soutenue à Saint-Brieuc, le 09 Mars 2021
Unité de recherche : IETR, Institut d'Électronique et des Technologies du numéRique
Thèse N° :

Rapporteurs avant soutenance :

Xavier BEGAUD	Professeur des Universités, Telecom Paris, Palaiseau
Julien SARRAZIN	Maître de conférences HDR, Sorbonne Université, Paris

Composition du Jury :

Président :			
Examinateurs :	Eric	LHEURETTE	Professeur des universités, IEMN, Villeneuve d'Ascq
	Philippe	POULIGUEN	Docteur /HDR, Agence de l'Innovation de Défense, Paris
	Xavier	BEGAUD	Professeur des Universités, Telecom Paris, Palaiseau
	Julien	SARRAZIN	Maître de conférences HDR, Sorbonne Université, Paris
	Ali	HARMOUCH	Maître de conférences, Université Libanaise, Tripoli
	Akil	JRAD	Professeur des universités, Université Libanaise, Tripoli
Dir. de thèse :	Ala	SHARAIHA	Professeur des universités, Université de Rennes 1, Rennes
Co-dir. de thèse :	Ratiba	BENZERGA	Maître de conférences, Université de Rennes 1, Rennes
Invité	Gilles	FOURNIER	Ingénieur R&D, ArianeGroup, Les Mureaux

Acknowledgement

Because everything starts with a dream that could not be realized without the support of some people…

I would like, first of all, to thank all the jury members who gave me the honor to participate, by their presence or by Visio, to the defense of my thesis during this very hard period of a sanitary crisis. So, many thanks to the rapporteurs and examiners of my thesis work: Prof. Xavier Begaud, Dr. Julien Sarrazin, Prof. Eric Lheurette and Dr. Philippe Pouliguen; many thanks for taking time to read my manuscript and to give me your insightful comments which enabled me to improve it. I want also to thank the guest Gilles Fournier for giving me a part of his time to read and to participate to my defense.

I wish to thank Professor Ronan Sauleau for hosting me in the IETR Lab and also Loïc Jegou and Jacques Berthoux, successive directors of the IUT of Saint-Brieuc for hosting me for three years at the IUT of Saint-Brieuc.

I address also my thanks to the IETR staff, IUT staff and the "SGM department" (Loïc, Stéphane, Claire, Xavier, Laurent, Jean-Pierre, Tual, Maël, Philippe, Yvonne, Florence, Ernest) and "ID composite" (Josselin, Côme and Charles) and PhD colleagues: Hanadi, Mohamad, Aladdin, Bacem, Chloé, Fatou, Florent, Younes, Bachir, Mathieu, Mathieu (Mich-mich), Quentin and Maëlle, for providing me a friendly environment that made me feel home. I want also to thank my Lebanese friends in Rennes: Sahar, Mariam, Maria, Asma, Imane, Ghina… for their high support during my third year of my thesis in Rennes.

Furthermore, many thanks to Chloé Méjean for her great help at the beginning of my thesis for the characterization, by coaxial probe method and in the anechoic chamber, and for the extraction of the dielectric properties of our materials. I want also thank Hanadi Breiss, my partner in work, in office, in residence and in Saint-Brieuc. Thank you Hanadi for being by my side during my sorrows and my happiness. Thank you for your support in my defense and for everything.

I want also to thank Jérôme Sol, for his help allowing me to successfully characterize the composite materials and my numerous prototypes in the anechoic chamber of the IETR, and all the members of the IETR mechanical department for the prototypes' cutting and the metamaterial realization.

A special thanks goes to Ludo, our computer specialist in IUT of Saint-Brieuc, for his continuous support to solve the problems of my computer and for supporting me during my defense. Ludo, your friendship and sincere tears mean a lot to me, thank you for everything.

I want also to express my gratitude to Dr. Akil Jrad and Dr. Ali Harmouch, my supervisors in Lebanon, for their supervision, comments, their encouragement, and their permanent support to me during my thesis.

I would like also to thank Prof. Ala Sharaiha for giving me the opportunity to start my thesis under his supervision. Thank you Dr. Ala for your availability, your encouragement, your investment and your many advices that enriched the work of this thesis.

I address also my most sincere thanks and gratitude to Dr. Ratiba Benzerga who has supervised me during this thesis. Thank you Dr. Ratiba for everything, for your high supervision, your encouragement,

your very useful comments and advice that helped me a lot to broaden my knowledge and to progress in everything. Thank you also for continuously pushing me to go further in my research and for allowing me to attend national and international conferences and to encourage me to write journal articles. Actually, I have learned so much from you and I will be forever grateful to you; my success is because of you. I will not also forget your humanity, your friendly personality and your permanent support and help in a foreign country in which I do not know so much people. I will never forget what we have shared during four years and I will never forget you.

Last but not least, I would like to thank my family members. I will start by my backbone, my mother and my father who offered me unlimited support since my first breath till reaching my dream. No words can express my thankful and grateful for both of you. Without you, this dream would have been possible. I owe a lot for both of you.

I wish also to thank my aunt Emneh who was also by my side since the first step in high school till reaching my dream now. Thank you very much for your unlimited support and prayers.

I would like also to thank my sisters Aya and Fatat, my brothers Aboudi and Omar, my parents in law (Widad and Zakaria) and my sisters in law Jihane and Jinane and my brother in law Mohamad. They have also supported me during these three years and I owe to them very much. I don't want also to forget my little nephews Ibrahim and Ilias who have brought me so much happiness by their birth in the same period of my thesis.

Finally, I would like to thank my fiancé Jamil for his continuous support during these three years. Jamil, you were beside me all time and in every step I do; without your encouragement, I could not be able to reach my dream that became also yours from the first day. I am very lucky to have you in my life. Thank you for everything.

Saint-Brieuc, 2021

Résumé de thèse en Français

Résumé de thèse en Français

Au cours des dernières décennies, et en raison de l'augmentation rapide des télécommunications, les matériaux absorbant les micro-ondes ont suscité un regain d'intérêt, et sont redevenus un sujet de recherche substantiel dans la plupart des technologies et des environnements où la de réduction du niveau des ondes électromagnétiques (EM) est nécessaire. Les absorbants EM sont aujourd'hui utilisés dans des applications diverses allant du militaire (furtivité) au civil (télécommunications, interférences EM, systèmes médicaux et dans les environnements de caractérisation électromagnétique). Des critères de plus en plus exigeants pour ces absorbants, émanent des applications émergentes, motivent aujourd'hui la communauté scientifiques à développer de nouveaux absorbants légers, avec une très bonne performance d'absorption, fonctionnant sur une large bande de fréquences tout en maintenant leur compacité. Le but de cette thèse s'inscrit dans cet objectif, à savoir, **proposer de nouveaux designs d'absorbants plans fonctionnant en large bande, présentant une bonne performance d'absorption, tout en maintenant une certaine compacité.** Le cahier des charges de ces absorbants sera détaillé au fur et mesure de ce résumé.

Le manuscrit de thèse est constitué de quatre chapitres. Le chapitre I est un chapitre de l'état de l'art. Le chapitre II traite des absorbants plans à multicouches et le chapitre III propose une optimisation de ces absorbants multicouches. Le chapitre IV quant à lui traite des absorbants à métamatériaux multi-résonants et des absorbants hybrides.

Ce résumé présente, d'une façon succincte, les principaux résultats des différents travaux menés lors de ma thèse et des résultats présentés dans les différents chapitres. Ce résumé est constitué de quatre parties qui détaillent les quatre chapitres de la thèse, rédigée en anglais, suivis par une conclusion et des perspectives.

Le chapitre I de la thèse est un chapitre de l'état de l'art ; il résume tout d'abord la théorie et les principes qui régissent le phénomène d'interaction ondes/matière. Dans cette partie, la notion de réflexion, de transmission et d'absorption des ondes EM sont d'abord introduites, suivies de la définition des propriétés diélectriques et magnétiques des matériaux (permittivités, perméabilités et pertes) qui contrôlent ces phénomènes.

Dans ce même chapitre, quelques matériaux absorbants de la littérature sont présentés. En effet, une grande variété d'absorbants a été utilisée ou étudiée au fil des ans. Ces matériaux peuvent être répertoriés de deux façons distinctes : leurs bandes d'absorption ou leurs compositions. Dans ce chapitre, des exemples de ces absorbants ont été présentés.

Dans le premier classement (en fonction de la bande d'absorption), les absorbants résonants sont tout d'abord présentés. Ici, les écrans de Salisbury, les couches de Dällenbach ou encore, les couches Jaumann sont montrés et leur principe de fonctionnement (principe de quart d'onde) est brièvement abordé. Les

absorbants à métamatériaux, autant qu'absorbants résonants, sont également cités. Des exemples illustrant les différents absorbants résonants (et donc à faible bande) sont présentés dans ce chapitre. Par la suite, les absorbants large-bande sont présentés et le principe d'adaptation d'impédance est introduit. Dans cette partie du chapitre, quelques exemples d'absorbants (déjà commercialisés ou à l'étude), tels que les absorbants pyramidaux ou multicouches, sont présentés. Dans cette partie, plusieurs exemples d'absorbants multicouches sont aussi donnés comme il s'agit du même type d'absorbant traité dans cette thèse. Par ailleurs, quelques solutions, proposées en littérature, pour élargir la bande passante des absorbants à métamatériaux sont également montrés, comme par exemple, des solutions basées sur la modification des dimensions, ou l'association de plusieurs dimensions de résonateurs. Une autre possibilité, très souvent utilisée en littérature, est celle de la superposition (en 2D ou 3D) de plusieurs motifs de métamatériau ; cette solution est expliquée au travers de plusieurs exemples. Les gammes de fréquence de fonctionnement de ces absorbants sont systématiquement données ainsi que leurs performances d'absorption. Une dernière solution, présentée dans le manuscrit, est celle de l'incorporation d'éléments passifs sur les éléments résonants du métamatériau.

Dans le second classement (en fonction de la composition), les absorbants sont groupés sous les catégories d'absorbants à bases de pertes diélectriques ou de pertes magnétiques. Pour les absorbants à pertes magnétiques, les matériaux absorbants les plus répondues sont présentés tels que les absorbants à base de ferrites, de Fer carbonyle ou encore à base de charges métalliques (particules de Fer…). Ici, les avantages et les inconvénients de ces matériaux sont expliqués et des exemples de littératures, donnant leurs épaisseurs, leurs taux de charges ainsi que leurs réflectivités, sont présentés. Concernant les absorbants à pertes diélectriques, différentes sous catégories ont été identifiées et présentées. Il s'agit des absorbants à base de polymères conducteurs, des absorbants à base de matrices diélectriques chargées en particules diélectriques (comme le SiC), ou encore, des absorbants à base de matrices diélectriques chargées en particules conductrices. Pour ces derniers, les charges métalliques (cuivre ou tungstène) et les charges carbonées (noir de carbone, nanotubes de carbone, graphite, graphene et fibres de carbone) ont été abordées. Plusieurs exemples illustrant ces différents matériaux absorbants ont été présentés dans ce chapitre. En fin de cette partie, quelques exemples de matériaux absorbants associant des pertes diélectriques et des pertes magnétiques, très étudiés récemment dans la littérature, ont été cités.

Dans la dernière partie du chapitre I, une introduction aux matériaux utilisés dans cette thèse a été faite. Ces matériaux, à base de mousse époxy chargée en fibres de carbone (FC), ont été développés récemment dans l'équipe FunMAT de l'IETR, située à St Brieuc. Les avantages apportés par ces matériaux, comparés à ceux du commerce, sont présentés ainsi que quelques résultats antérieurs de prototypes réalisés.

Le chapitre II présente l'étude menée sur la conception et la réalisation d'absorbants plans à multicouches, utilisant le matériau absorbant à base de la mousse époxy chargée en fibres de carbone.

Au début de ce chapitre, la notion de réflexion d'un absorbant plan est tout d'abord abordée. Dans le cas d'absorbant monocouche, la réflexion (qui intervient à l'interface air/matériau et les réflexions qui interviennent aux interfaces matériau/plaque métallique mais aussi matériau/air (Figure 1(a)) sont rappelées. Les différentes formules, ainsi que les différentes approximations, permettant le calcul du coefficient de réflexion de l'absorbant sont données pour le cas d'une incidence normale des ondes EM. Le model est par la suite élargie à un absorbant multicouches avec N couches (Figure 1(b)).

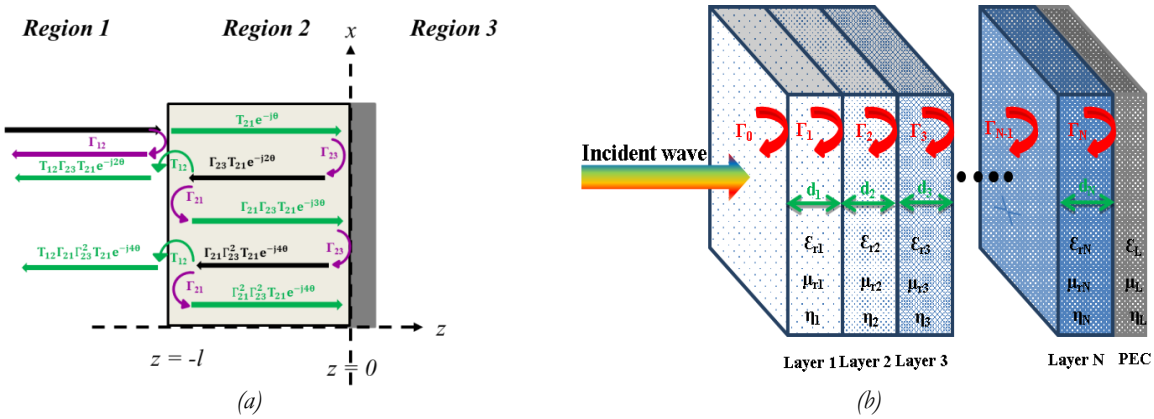

Figure 1 : Coefficient de réflexion d'un absorbant (a) monocouche et (b) multicouche.

Dans le cadre de cette thèse, un programme MATLAB a été développé pour calculer la réflexion totale d'un absorbant multicouche. Le détail de ce calcul (code) est expliqué dans la thèse. Par ailleurs, et afin de valider ce code, une simulation d'un absorbant a été réalisé avec le logiciel commercial CST et a été comparée à la réflexion calculée par ce code (Figure 2) ; ici, la géométrie ainsi que les propriétés mesurées sur un absorbant du commerce AH 125 (de SIEPEL) ont été utilisées pour les deux méthodes. La Figure 2 montre des coefficients de réflexion très similaires, hormis ceux calculés dans la gamme de fréquence comprise entre 2.3 GHz et 4.9 GHz. Cette différence est due à la différence de points utilisés par les deux méthodes. En effet, le calcul par MATLAB utilise les 51 points issus de la mesure par sonde coaxiale des propriétés diélectriques, alors que CST génère 1005 points lors de la simulation. Ceci a été vérifié par simulation réalisée avec des propriétés diélectriques mesurées sur une gamme de fréquence plus étroite (entre 2 et 6 GHz seulement). Pour la suite du travail, ce problème ne se posera plus, car les propriétés diélectriques de nos matériaux seront extraites des caractérisations en chambre anéchoïque ; cette dernière méthode permet d'acquérir 3452 points simultanément par mesure.

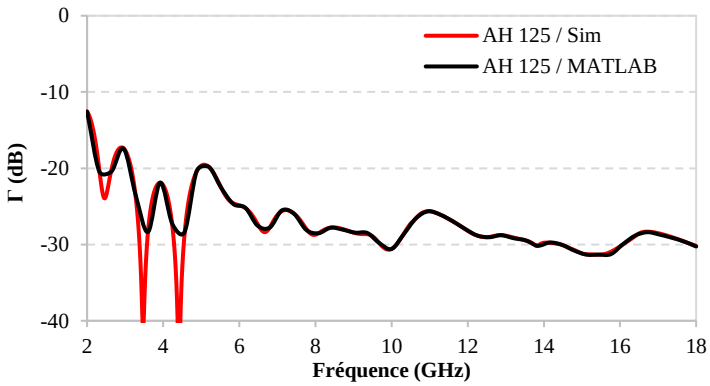

Figure 2 : Comparaison entre les coefficients de réflexion simulé (CST) et calculé (MATLAB) pour l'AH 125.

Il faut noter ici que le programme MATLAB élaboré lors de cette thèse permet de calculer le coefficient de n'importe quel multicouche en moins de 3 secondes, alors que le logiciel commercial de simulation CST prend plusieurs heures à faire cette même simulation ; ceci nous a donc permis un gain considérable en temps de calcul. Par ailleurs, ce même code nous permet, contrairement à CST, de calculer la réflexion à chaque interface du multicouche, ceci nous permettra, comme on le verra par la suite, d'identifier les sources de réflexion dans nos absorbants.

Dans la deuxième partie de ce chapitre II, la méthode d'élaboration des matériaux utilisés, ainsi que la technique utilisée pour leur caractérisation en chambre anéchoïque, ont été tout d'abord présentées. Pour ce chapitre, des mousses époxy chargées avec différents taux (entre 0.25 wt.% et 1 wt.%) de fibres de carbone de différentes longueurs (entre 3 mm et 12 mm) ont été utilisés. Les Figures 3, 4 et 5 regroupent les propriétés (permittivités (a) et pertes diélectriques (b)), dans la gamme de fréquence comprise entre 0.75 et 18 GHz, des différents matériaux que j'ai élaborés pour ce chapitre.

Ces figures montrent d'une part une augmentation des propriétés diélectriques en fonction du taux de charge, quelle que soit la longueur des fibres utilisée, et d'autre part, que pour un même taux de fibre, les pertes diélectriques augmentent avec la longueur des fibres.

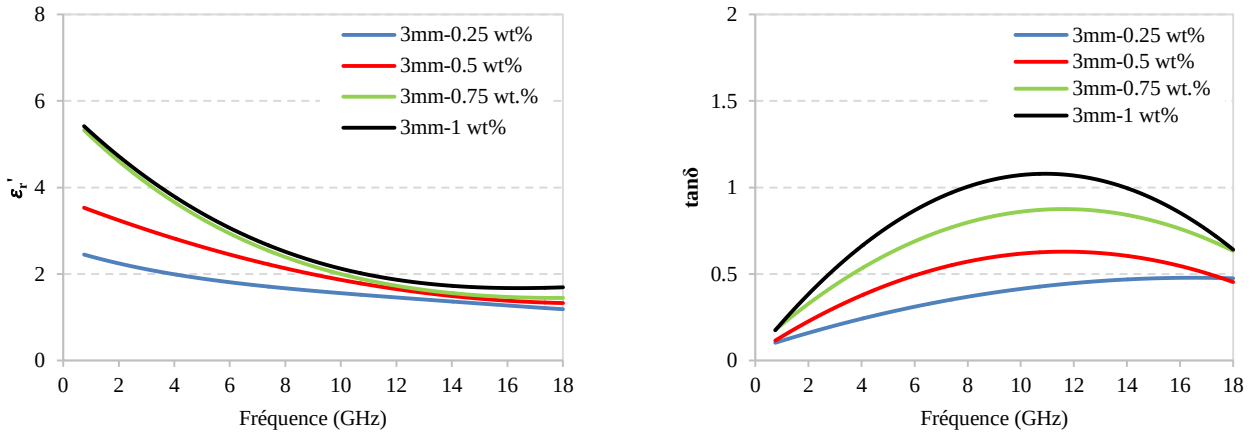

Figure 3 : Propriétés diélectriques ε'_r (a) et tanδ (b) des composites élaborés avec des fibres de 3 mm de long.

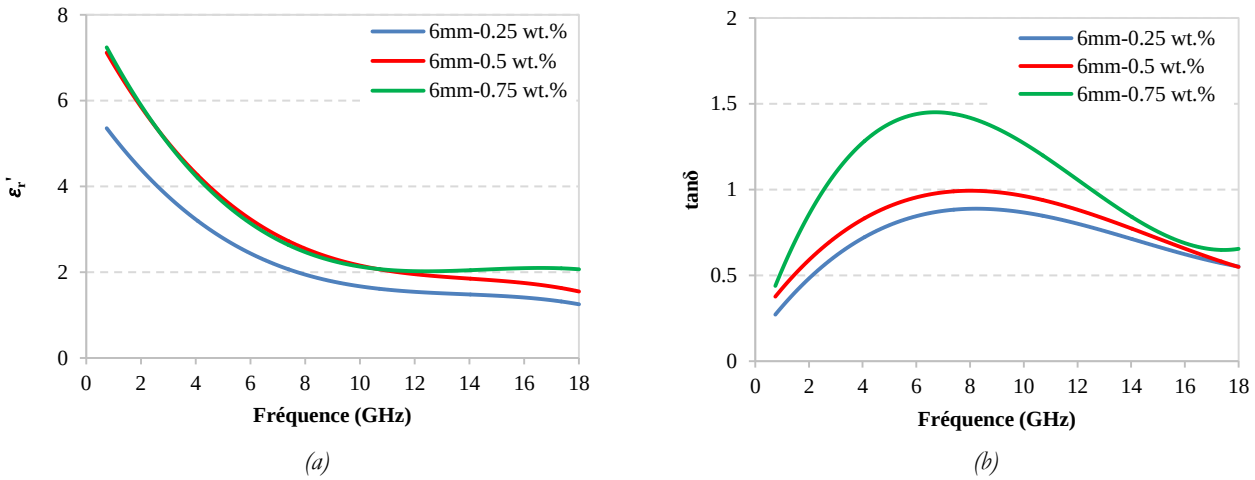

Figure 4 : Propriétés diélectriques ε'_r (a) et tanδ (b) des composites élaborés avec des fibres de 6 mm de long.

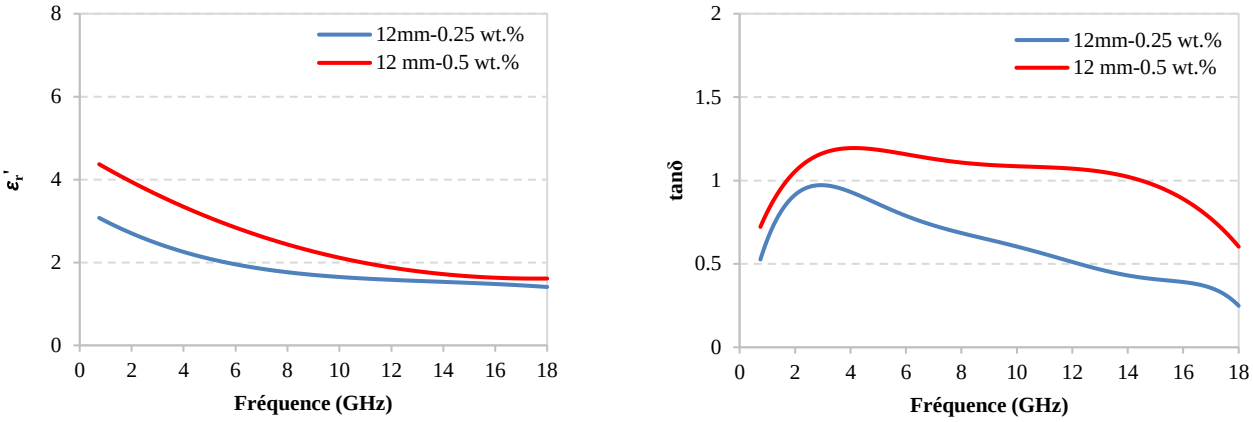

Figure 5 : Propriétés diélectriques ε_r' (a) et tanδ (b) des composites élaborés avec des fibres de 12 mm de long.

L'influence de la longueur des fibres sur les pertes diélectriques est plus facilement visible sur la Figure 6 qui regroupe les matériaux élaborés avec 0.25 wt.% de fibres de 3, 6 et 12 mm de longueur. Cette figure met en avant par ailleurs un autre aspect très intéressant ; il s'agit de l'influence de la longueur des fibres sur la gamme d'absorption (ou sur la fréquence du maxima des pertes diélectriques). Il apparait que plus les fibres sont longues, plus le maximum des pertes shift vers les basses fréquences ; ceci voudrait dire que les fibres courtes seraient plus intéressantes pour l'absorption en hautes fréquences alors que les fibres longues seraient plus efficaces pour l'absorption en basses fréquences.

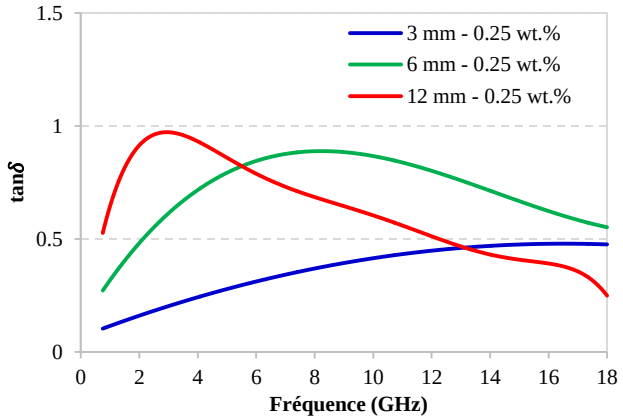

Figure 6 : Pertes diélectriques des mousses époxy charges avec 0.25 wt.% de 3, 6 et 12mm-CFs.

Par ailleurs, et dans ce même chapitre, les méthodes pouvant être utilisées pour choisir la composition des différentes couches d'un absorbant à multicouches, afin de réduire sa réflectivité, et donc augmenter son absorption, sont expliquées. Elles peuvent se baser directement sur les propriétés diélectriques des matériaux (permittivité et pertes diélectriques) ou sur le calcul de l'impédance intrinsèque de chaque matériau. Dans les deux cas, un gradient des propriétés, ou des impédances, doit être utilisé pour garantir une transition progressive des ondes, donc une réflexion minimale des ondes EM aux différentes interfaces (air/matériau, matériau/matériau et matériau/plaque métallique). Ceci permettra aux ondes d'être transmises dans les différentes couches et être progressivement atténuées dans ces dernières.

Dans le but de choisir les différentes couches, parmi celle présentées en Figures 7, l'impédance caractéristique des différents matériaux a été calculée en utilisant les propriétés diélectriques des couches (Figures 3, 4 et 5) ainsi que la formule suivante :

$$\eta_c = \eta_0\sqrt{\widetilde{\mu_r}/\widetilde{\varepsilon_r}} = \sqrt{\mu_0/\varepsilon_0}\sqrt{\widetilde{\mu_r}/\widetilde{\varepsilon_r}} = 377\sqrt{1/\widetilde{\varepsilon_r}}$$

Ou η_c est l'impédance caractéristique du matériau, η_0 est l'impédance de l'air (377 Ω), $\widetilde{\mu_r}$ et $\widetilde{\varepsilon_r}$ sont respectivement, la perméabilité et la permittivité complexes du matériau. Il faut noter ici que nos matériaux sont purement diélectriques, leur perméabilité magnétique est donc égale à 1.

La Figure 7 regroupe les différentes impédances caractéristiques des matériaux présentés en Figures 3, 4 et 5; ces impédances sont comparées à celle de l'air (trait en pointillé bleu) et à celle de la mousse époxy non chargée (trait gris). Cette figure montre que grâce aux différentes longueurs et aux différents taux de charge, un panel d'impédances intrinsèques est obtenu. Celui-ci permettrait de réaliser donc un multicouche avec un gradient d'impédance, ce qui devrait permettre de réduire la réflexion aux interfaces et donc d'avoir une bonne performance d'absorption. Mais il faut noter, notamment en basses fréquence, le gap entre la première couche (ici la mousse non chargée) avec une impédance de 344 Ω et la deuxième couche (mousse chargée avec 0.25 wt.% de FC de 3mm) d'une impédance de 240 Ω @ 0.75 GHz. Ce gap relativement important pourrait produire, en basses fréquences, une forte réflexion au niveau de l'interface entre les deux premières couches.

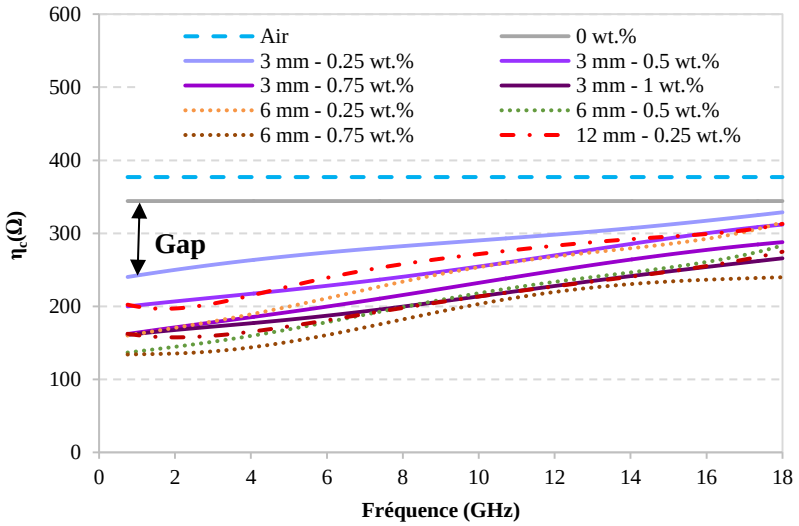

Figure 7: Les impédances caractéristiques calculées pour les différents composites élaborés.

Se basant sur le principe de transition d'impédance, quatre couches, parmi celles présentés en Figure 7, ont été choisies pour réaliser le premier prototype d'absorbant. La première couche choisie est celle de la mousse époxy non chargée qui présente l'impédance la plus proche de celle de l'air. Cela permettrait de réduire la réflexion au niveau de l'interface air/absorbant. Pour la dernière couche de l'absorbant, la mousse époxy chargée avec 0.75 wt.% de FC de 6 mm de long a été choisie. Ce matériau présente l'impédance la plus faible, donc, la plus proche de celle de la plaque métallique de 0 Ω, positionnée au dos

de l'absorbant lors des simulations et des mesures pour estimer la performance d'absorption. Pour les deux autres couches centrales (2ième et 3ième couches de l'absorbant), des matériaux avec des impédances intrinsèques intermédiaires ont été choisie pour assurer la bonne transition/gradient d'impédance. Il s'agit des mousses époxy chargées avec 0.25 wt.% de FC de 3 mm et de 0.25 wt.% de FC de 12 mm. Le design et les impédances caractéristiques des différentes couches choisies sont présentés dans la Figure 8. Pour ce premier prototype, une épaisseur totale de 250 mm a été choisie pour le multicouche ; cette épaisseur est l'une des épaisseurs standards utilisées pour les absorbants plans du commerces fonctionnant dans la gamme de fréquence 1 – 18 GHz. Par ailleurs, une épaisseur plus grande (70 mm) a été choisie ici volontairement pour la première couche afin de garantir une bonne transition entre l'air ambiant et les différentes couches absorbantes.

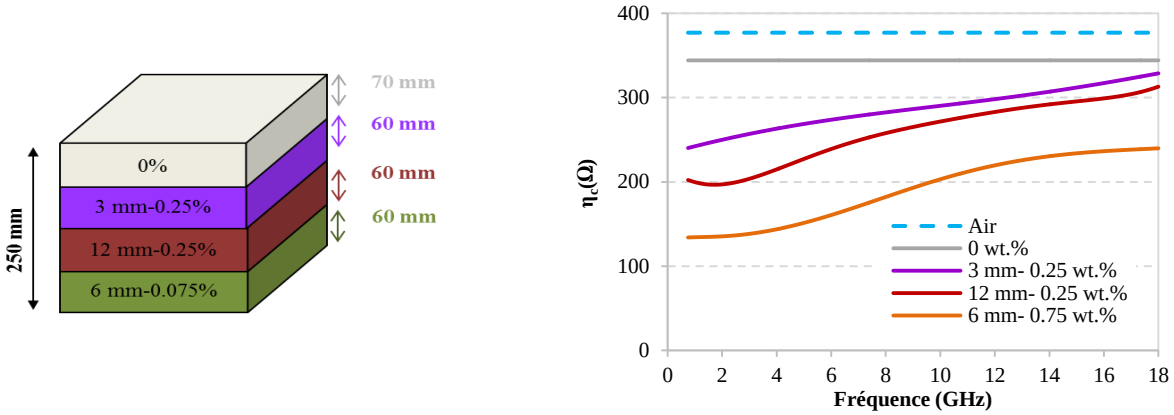

(a) *(b)*

Figure 8 : Design du prototype MLA250 (a) et impédances caractéristiques des composites choisis pour la réalisation de ce prototype (b). (L'impédance de l'air est représentée en trait discontinu bleu).

Le prototype schématisé en Figure 8.a, nommé ici MLA250, a été réalisé et caractérisé en chambre anéchoïque. La photo de ce prototype ainsi que son coefficient de réflexion mesuré sont montrés en Figure 9(a) et 9(b), respectivement. Le résultat de mesure est comparé à celui de la simulation sur cette même figure.

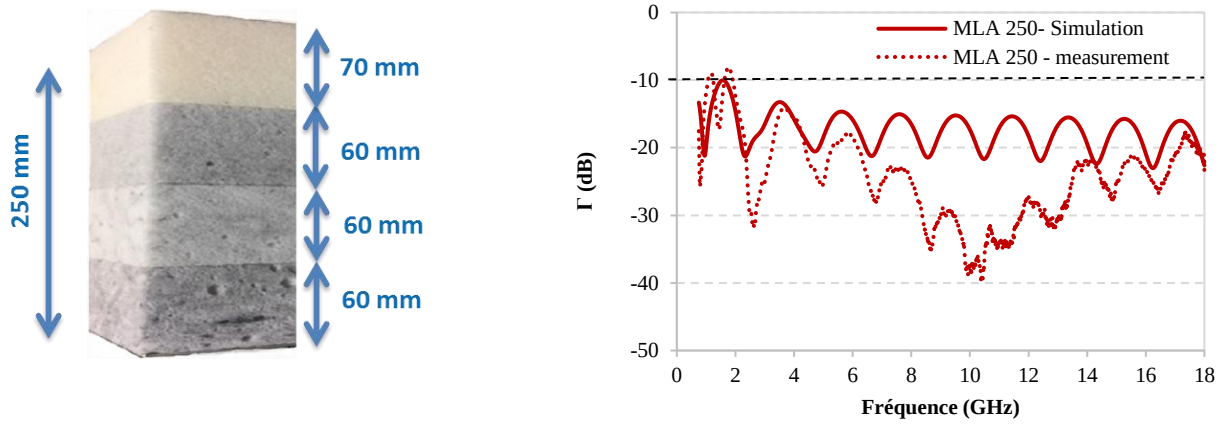

(a) *(b)*

Figure 9 : (a) Photo du prototype MLA250 réalisé et (b) simulation et mesure de son coefficient de réflexion.

La Figure 9 montre d'une part que les coefficients de réflexion obtenus sont inférieurs à -10 dB, valeur nécessaire pour considérer ce matériau comme absorbant, et d'autre part, qu'un meilleur coefficient de réflexion est obtenu pour la mesure, comparé à la simulation. Cette différence est probablement due au fait que certains matériaux présentent une forte hétérogénéité (mauvaise dispersion des fibres dans la mousse) comme on peut le voir sur la Figure 9(a), notamment sur les matériaux les plus chargés (deux dernières couches). En fait, les matériaux obtenus présentent une sorte de gradient de charge au cœur de l'échantillon ; ce gradient a été utilisé, lors de la mesure, dans le même sens que le gradient choisie pour les couches. Ceci a donc amélioré le niveau du coefficient de réflexion de l'absorbant. Néanmoins, malgré que cet absorbant montre une bonne performance d'absorption (< - 10 dB sur toute la gamme de fréquence étudiée), cette performance reste insuffisante, notamment en basses fréquences (< 8 GHz), au regard de son épaisseur relativement élevée. Ceci n'est surement pas dû au pouvoir absorbant des différentes couches, car celles-ci présentent de fortes pertes diélectriques (Figures 3(b), 4(b) et 5(b)). De même, cette performance ne peut pas être due à l'épaisseur des couches ; en effet, une la simulation d'un absorbant présentant une épaisseur réduite de moitié (125 mm) montre pratiquement le même coefficient de réflexion pour les deux designs (résultats de simulation montré dans le manuscrit de thèse). Au final, cette performance est surement due à une adaptation d'impédance insuffisante entre les différentes couches, et donc à une grande réflexion entre les couches constituant l'absorbant.

Un calcul (en pourcentage) des réflexions issues des différentes interfaces du multicouches a été réalisé ; le résultat est montré en Figure 10. Il faut noter ici que pour chaque interface, le pourcentage de réflexion est calculé en considérant que les ondes incidentes arrivant sur cette interface correspondent à 100 %.

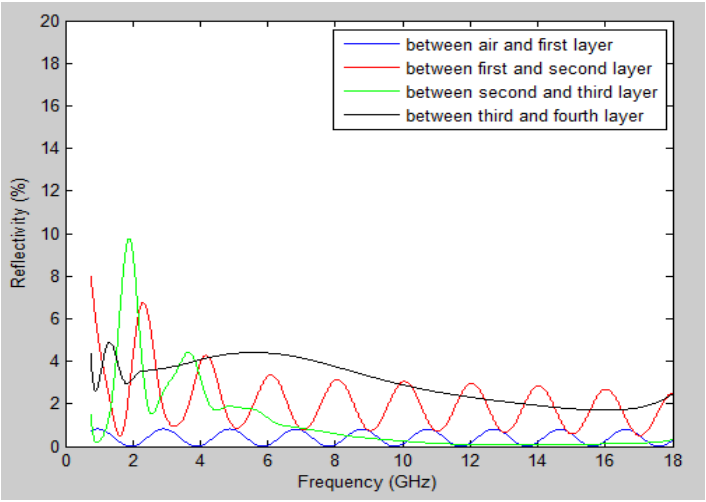

Figure 10 : Taux de réflexion calculés à chaque interface du multicouche MLA250.

A partir de la Figure 10, nous pouvons noter que la réflexion à la surface de l'absorbant (interface air/couche 1) est très faible, elle est < 1% quelque que soit la fréquence considérée. Par contre, les réflexions aux interfaces entre les couches 1 et 2, et entre les couches 2 et 3 sont élevées, notamment en basses fréquences (aux alentours de 2 GHz). La quatrième couche (la plus chargée) quant à elle, présente

une réflexion relativement élevée, et cela, sur toute la gamme de fréquence étudiée. En conclusion, ces matériaux à fortes pertes ne permettent pas d'obtenir un absorbant multicouche avec un niveau d'absorption acceptable.

Dans la suite du chapitre II, et afin d'améliorer les performances d'absorption du multicouches à base de mousses époxy chargées en fibres de carbone, de nouveaux composites ont été réalisés. Ces derniers ont été élaborés dans le cadre de la thèse de Hanadi BREISS. Pour ces nouveaux composites, des fibres longues de 12 mm avec des taux de charges très faibles (0.0125, 0.01875, 0.025, 0.05 et 0.075 wt.%) ont été choisis. Ceci permettrait d'une part, d'optimiser l'absorption en basses fréquences, et d'autre part, d'éviter les fortes réflexions grâce à une meilleure transition d'impédance.

Les permittivités, les pertes diélectriques ainsi que les impédances intrinsèques des nouveaux matériaux élaborés sont présentés en Figure 11 (a), (b) et (c), respectivement. Ces figures montrent d'une part, et comme attendu, une augmentation des propriétés diélectriques en fonction du taux de charge et d'autre part, des pertes relativement élevées associées à des permittivités faibles. Ces propriétés devraient permettre d'obtenir une meilleure performance d'absorption ; en effet, des impédances plus proches, comparées à celles des matériaux utilisés pour le premier prototype, sont ici obtenues (Figure 11(c).

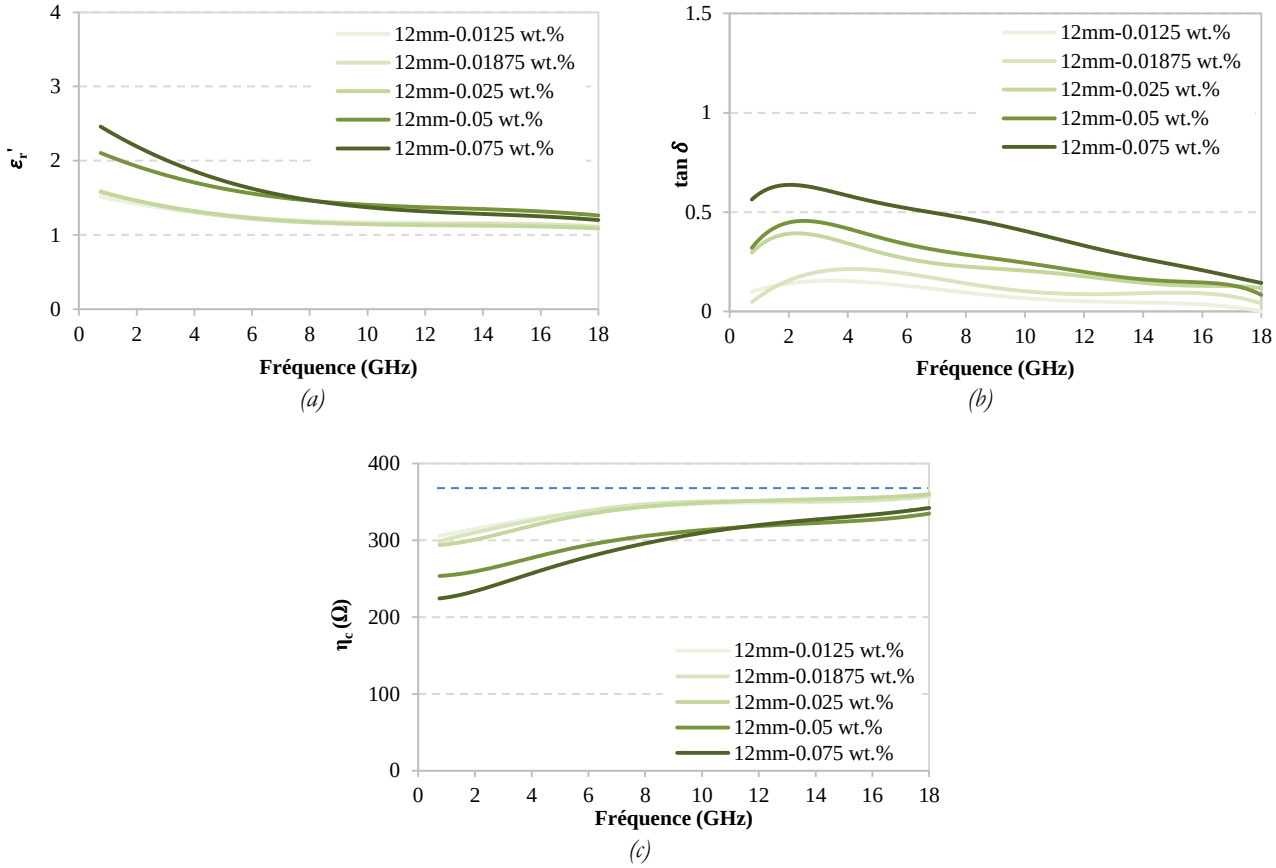

Figure 11 : Permittivités ε'_r (a), pertes diélectriques (b) et impédances (c) des composites réalisés avec des fibres de 12 mm de long.

Un nouveau prototype a été réalisé en utilisant ces différents composites. Ce nouveau prototype (appelé dans ce résumé MLA125-1) est composé de 5 couches et possède une épaisseur totale de 125 mm. Cette nouvelle épaisseur a été choisie dans le but de réduire la compacité de notre absorbant ; elle est

également largement utilisée pour les absorbants du commerce. De même, et dans ces derniers, 5 couches sont souvent utilisées ; nous avons donc fait ce choix afin d'améliorer la transition d'impédance dans l'absorbant multicouche. Par ailleurs, une épaisseur identique (25 mm) a été choisie pour toutes les couches, ceci est également souvent adopté pour les absorbants du commerce, comme par exemple l'AH 125 de SIEPEL. Le design ainsi que la photo du nouveau prototype réalisé sont montrés en Figure 12.

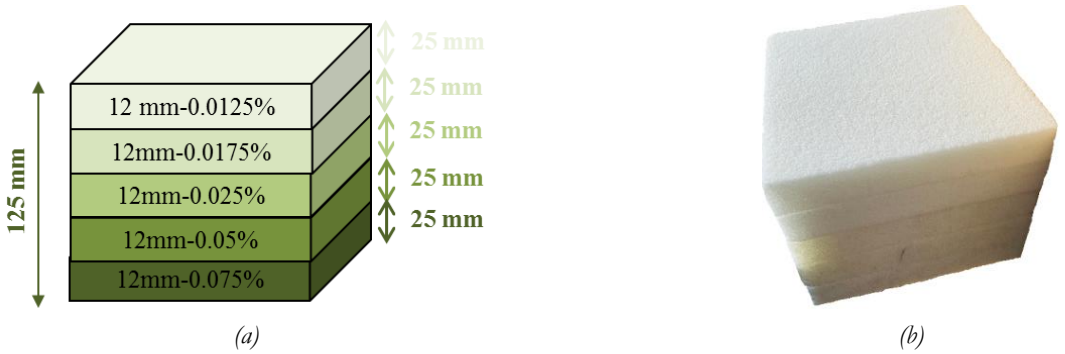

Figure 12 : Design (a) et photo (b) du prototype MLA125–1 réalisé avec les composites chargés avec des fibres de 12 mm de long.

La simulation et la mesure, en incidence normale et incidence oblique de l'onde EM de 30° (avec les modes TE et TM), du prototype élaboré sont comparées en Figure 13. Une bonne concordance est à noter entre les deux résultats. Ici, pour l'incidence normale (Figure 13 (a)), un coefficient de réflexion inférieur à -10 dB est mesuré sur pratiquement toute la bande de fréquence étudiée (entre 1.34 GHz et 18 GHz) ; ce coefficient devient inférieur à -20 dB à partir de 4.6 GHz.

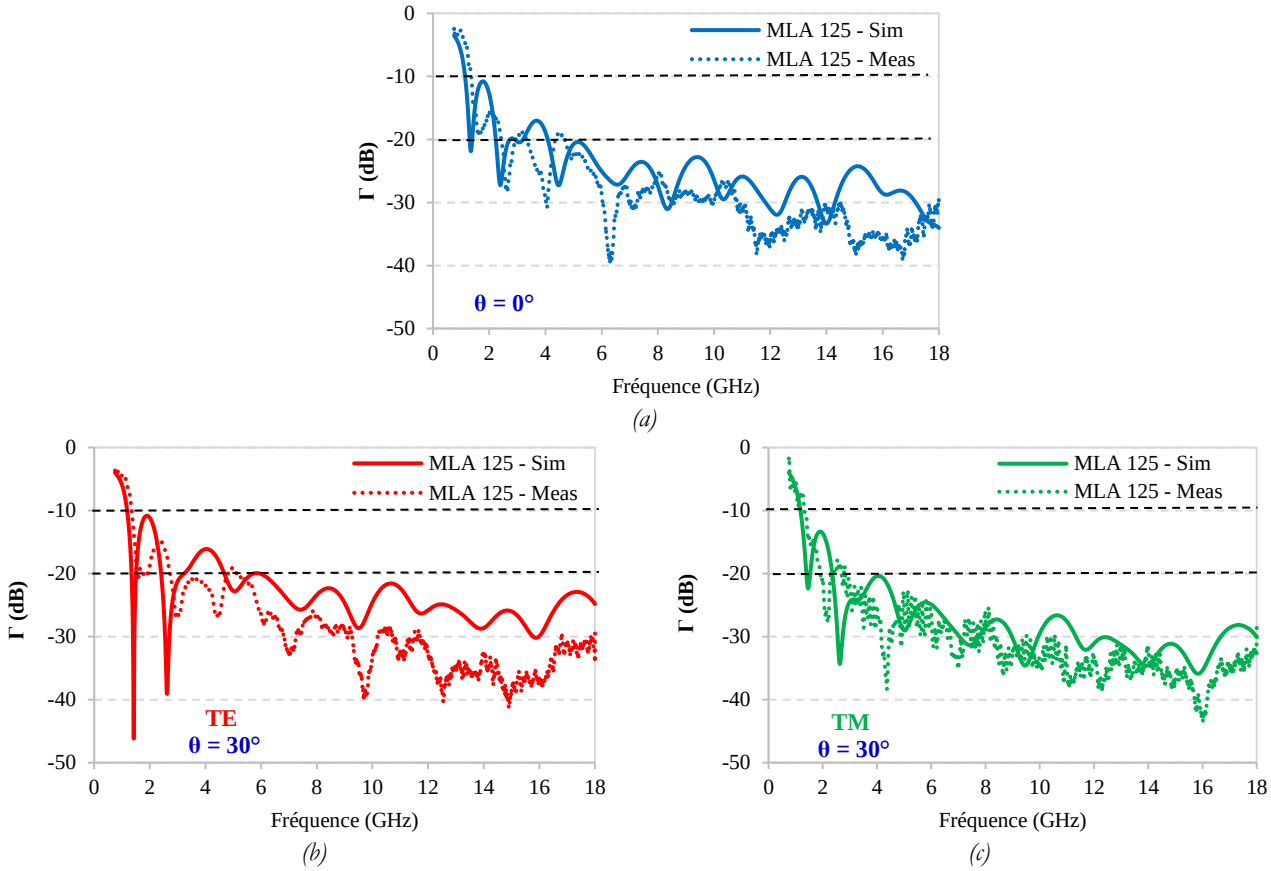

Figure 13 : Simulation et mesure des coefficients de réflexion du prototype MLA125–1 pour une incidence normale (a) et oblique de 30° pour le mode TE (b) et TM (c).

Pour l'incidence oblique, un résultat équivalent à celui de l'incidence normale est obtenu, à savoir, un coefficient de réflexion inférieur à -10 dB à partir de 1.3 GHz et qui devient inférieure à -20 dB à partir de 4.8 GHz et 2.3 GHz pour les modes TE et TM, respectivement. Une différence entre la simulation et la mesure est à noter pour le mode TE, celle-ci n'a pas pu être expliquée. Néanmoins, la mesure montre pour les différentes configurations un résultat comparable, voir meilleure, que celui obtenu par la simulation.

Un dernier prototype a été réalisé est montré en fin du chapitre II. Ce prototype est réalisé avec le même design et les mêmes compositions (taux et longueurs de fibres) que ceux utilisés pour le prototype précédent MLA125-1, mais possède une densité plus faible. En effet, dans le cadre de la thèse de Hanadi BREISS, la densité des matériaux à base de mouse a été diminuée grâce à un nouveau procédé d'élaboration. La densité est réduite de moitié ; elle est passée de 0.12 $g.cm^{-3}$ à environs 0.06 $g.cm^{-3}$. Ceci permet d'une part, de réduire la masse de l'absorbant et d'autre part, de garder un niveau de pertes important, tout en réduisant les permittivités des échantillons. En effet, grâce à la présence des grosses porosités remplies d'air dans ces nouveaux composites, leurs permittivités sont réduites comme l'atteste la Figure 14. Cette dernière montre les propriétés diélectriques de ces nouveaux composites, ainsi que leurs impédances intrinsèques ; une transition plus douce des impédances, notamment en basses fréquences, est attendue avec ces nouveaux matériaux.

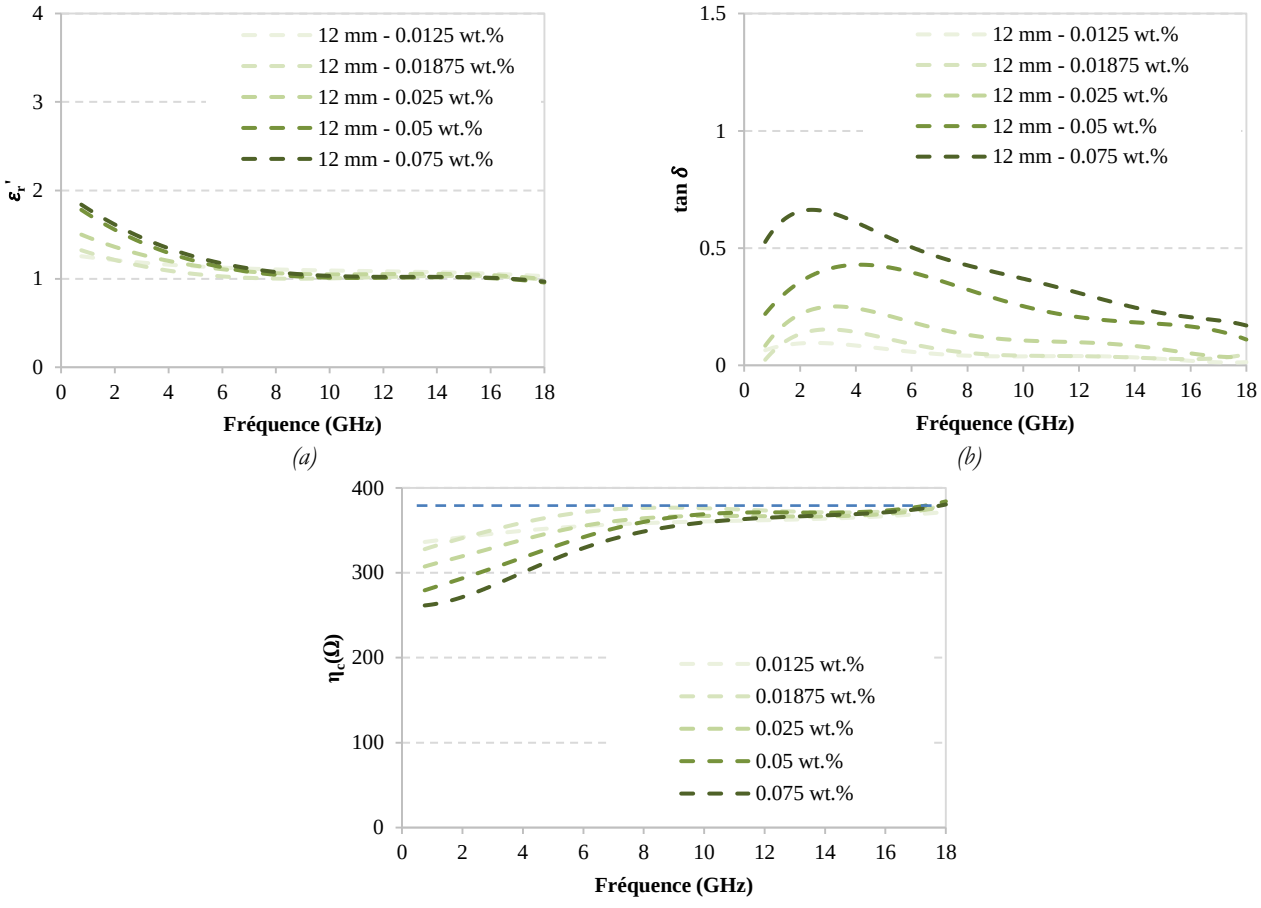

Figure 14 : Permittivités ε'_r (a), pertes diélectriques (b) et impédances (c) des composites légers réalisés avec des fibres de 12 mm de long.

La Figure 15 montre la photo du prototype réalisé (nommé LW-MLA125-1) avec une épaisseur totale de 125 mm (Figure 15 (a)) ainsi que les coefficients de réflexion simulés et mesurés pour ce prototype, pour l'incidence normale (Figure 15 (b)) et oblique de 30 ° (Figures 15 (c) et (d)) des ondes EM. Une performance comparable à celle mesurée sur le prototype précédent est également obtenue ici. Ceci a donc permit de garder une très bonne performance d'absorption, tout en réduisant la masse de cet absorbant de 50%.

En conclusion de ce second chapitre, une comparaison a été réalisée dans le manuscrit de thèse, entre les performances des différents prototypes réalisés (MLA125-1 et LW-MLA125-1) ainsi que celle de l'absorbant commercial AH 125. Ces trois absorbants montrent le même design (même nombre de couche et épaisseurs), mais aussi des performances comparables. Notre étude a montré donc la potentialité du matériau absorbant à base de mousse époxy chargée en fibres longues de carbone pour une utilisation autant qu'absorbant plan à multicouches. Rappelons que ce matériau, et contrairement à celui du commerce, est constituée d'une charge non volatile qui est, en plus, piégée dans la matrice contrairement au noir de carbone utilisé dans les absorbants du commerce. Il faut noter ici que le noir de carbone est souvent à l'origine du vieillissement prématuré de ces absorbants, mais aussi, une source de pollution nanométrique de moins en moins tolérée par les normes REACH.

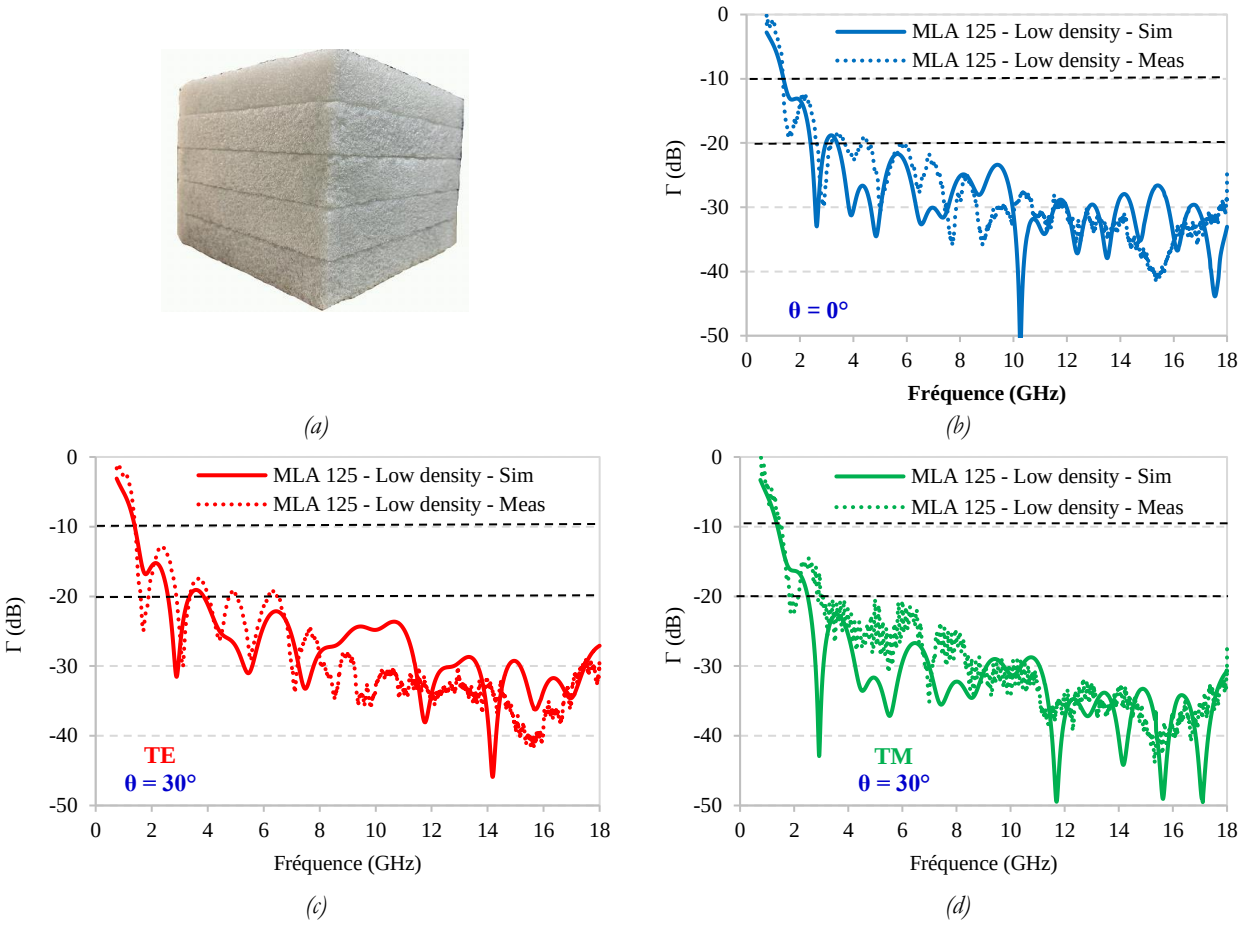

Figure 15 : Photo du prototype LW-MLA125–1 (a) et simulation et mesure de ses coefficients de réflexion pour une incidence normale (b) et oblique de 30° pour le mode TE (c) et TM (d).

Dans le chapitre III de la thèse, une optimisation des prototypes absorbants, réalisés dans le chapitre précédent, a été expérimentée. Pour cela, l'utilisation de l'algorithme génétique a été proposée. Deux optimisations ont été parallèlement testées ; la première en utilisant l'algorithme génétique implémenté dans le logiciel de simulation électromagnétique commercial CST et la seconde, en s'appuyant sur le code de calcul du coefficient de réflexion, réalisé sur MATLAB, et en utilisant l'algorithme génétique implémenté dans ce même logiciel. Le principe ainsi que la logique adoptée pour ce code sont détaillés dans la thèse.

Dans la première partie de ce chapitre, l'algorithme génétique du logiciel CST a été utilisé pour optimiser la performance d'absorption des différents prototypes multicouches. Cet algorithme nous permet de proposer une gamme d'épaisseur pour chaque couche (épaisseur min et max) et le logiciel effectue à chaque itération, le calcul de la réflexion en utilisant une épaisseur différente. Un objectif est introduit, il s'agit ici d'un coefficient de réflexion inférieur à -20 dB sur toute la gamme de fréquence étudiée (entre 0.75 GHz et 18 GHz). Il faut noter ici, que l'épaisseur totale de l'absorbant doit être imposée lors de la simulation.

Pour la première optimisation, les mêmes matériaux qui ont servi à la réalisation du MLA250 ont été utilisés. Il s'agit, dans l'ordre, de la mousse époxy non chargée, de la mousse chargée avec 0.25 wt.% de CF de 3 mm, puis chargée de 0.25 wt.% de CF de 12 mm et finalement, de la mousse chargée avec 0.75 wt.% de CF de 6 mm. Une épaisseur totale de 125 mm a été imposée pour cette première optimisation, avec des gammes d'épaisseur comprises entre 35-45 mm et 15-40 mm pour la première et deuxième couche, respectivement, et entre 25-40 mm pour les deux dernières couches. Il faut noter ici que cet absorbant est constitué que de 4 couches. La photo du prototype réalisé ainsi que la simulation et la mesure de ce prototype sont montré en Figure 16. Cette figure montre, d'une part, une très bonne concordance entre la simulation et la mesure du coefficient de réflexion et d'autre part, un coefficient inférieur à -10 dB dans toute la gamme de fréquence étudiée, et cela, quelque que soit l'incidence de l'onde ou le mode de polarisation de celle-ci. Néanmoins, le coefficient de réflexion recherché ici (< -20 dB) n'a pas pu être obtenu avec cette optimisation. Ceci confirme d'une part que le choix des matériaux utilisé n'est pas optimum, mais d'autre part, que l'optimisation par l'algorithme génétique implémenté dans le logiciel de simulation CST n'est pas suffisante. En effet, cette optimisation est limitée à l'épaisseur des différentes couches ; ici, l'épaisseur totale est imposée, les matériaux sont également imposés ainsi que leur ordre dans le multicouche. Dans le cas de notre problématique, une optimisation multi-paramètres est nécessaire afin d'atteindre l'objectif ; c'est pour cette raison, que l'algorithme génétique de MATLAB, associé au code développé au chapitre II, ont été utilisés par la suite.

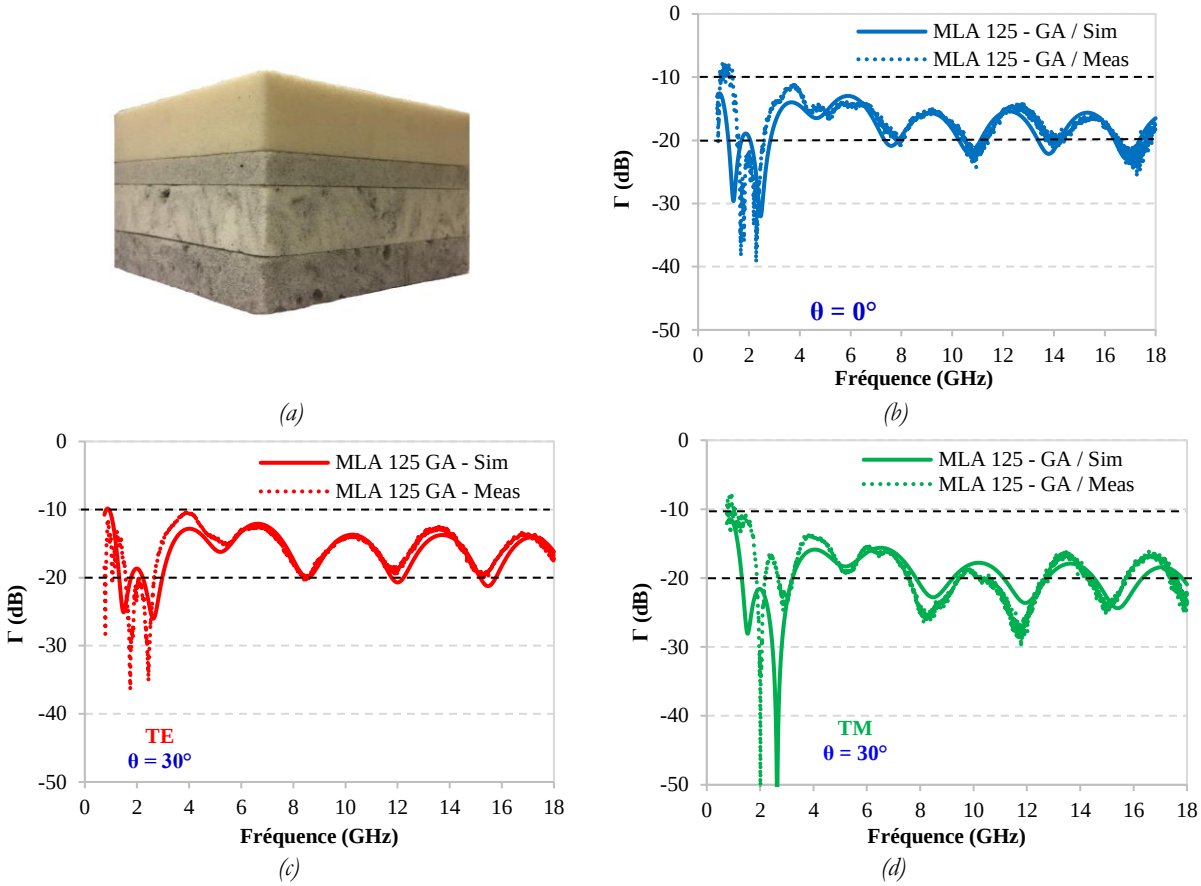

Figure 16 : Photo du prototype MLA125–GA (a) et simulation et mesure de ces coefficients de réflexion pour une incidence normale (b) et oblique de 30° pour le mode TE (c) et TM (d).

Pour la deuxième optimisation, réalisée grâce au code MATLAB, les paramètres que l'algorithme génétique va optimiser sont le choix des matériaux pour chaque couche, l'épaisseur de cette dernière et l'épaisseur totale de l'absorbant. Avec ce code, une base de données, regroupant les propriétés diélectriques des différents matériaux élaborés, est tout d'abord introduite. Par la suite, la gamme d'épaisseur pour chaque couche est fixée (épaisseur min et max), ce qui déterminera automatiquement l'épaisseur totale min et max imposées pour l'absorbant.

Pour cette partie du chapitre, un plus large panel de matériaux (24 au total) a été utilisé ; les propriétés diélectriques (les permittivités réelles et imaginaires) de ces matériaux, qui sont introduites dans le code, sont présentées dans la Figure 17. Celle-ci montre d'une part, la large gamme de propriétés possibles à obtenir en variant le taux et la longueur des fibres (entre 100 µm et 12 mm) et d'autre part, ces figures confirment l'influence de la longueur des fibres sur la gamme de fréquence du maxima des pertes. En effet, ici un shift, vers les basses fréquences, du maxima de la partie imaginaire de la permittivité est clairement observé lorsque la longueur des fibres augmente, et ceci quel que soit le pourcentage de fibres utilisé.

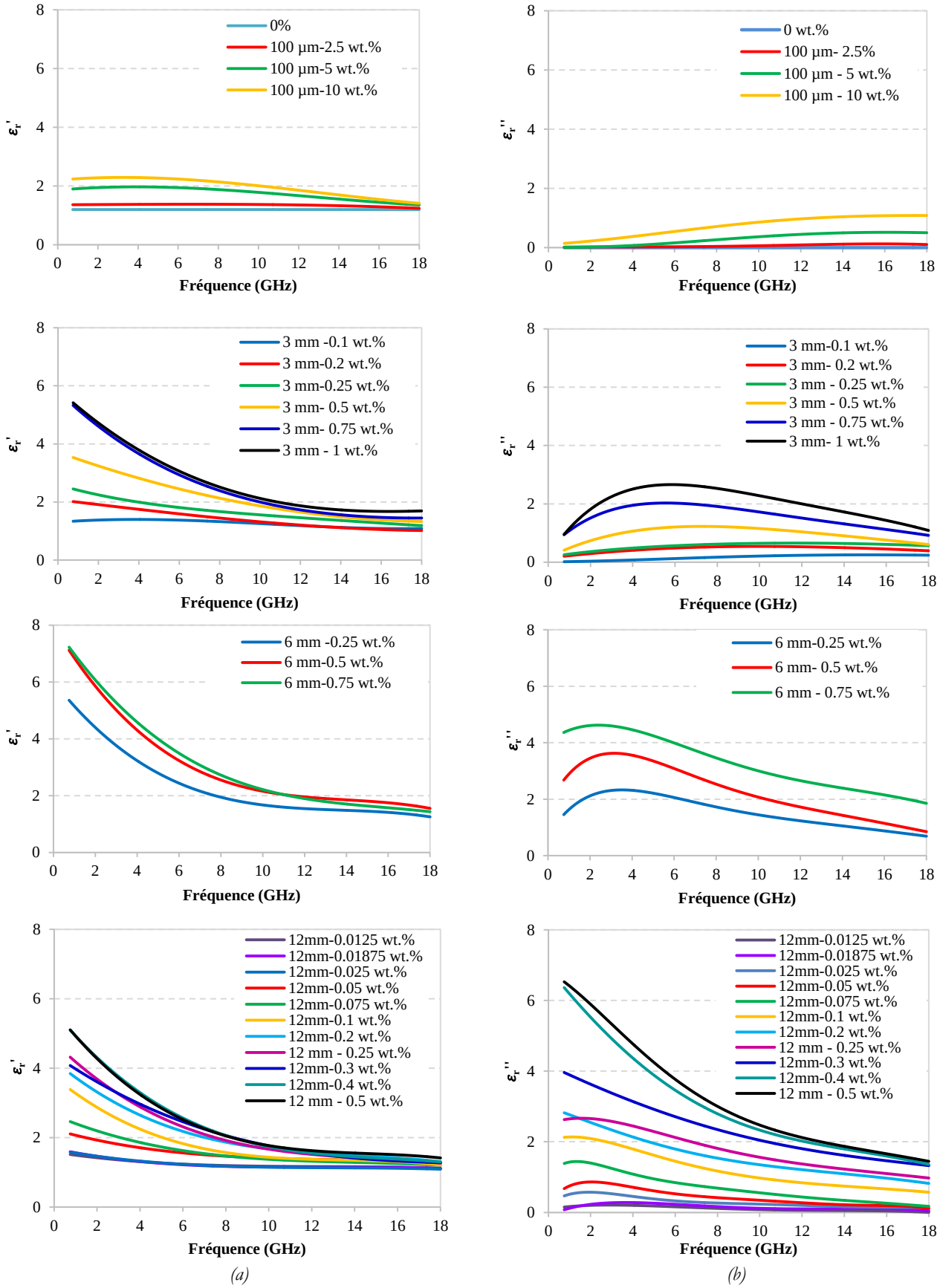

Figure 17 : Propriétés diélectriques ε_r' (a) et ε_r'' (b) des différents composites élaborés avec des fibres de carbones de différentes longueurs (100 µm, 3 mm, 6 mm et 12 mm).

Grâce à ce nouveau code et aux différents composites disponibles, plusieurs optimisations ont été menées en réduisant de plus en plus l'épaisseur maximale imposée au code MATLAB ; le but ici est de

réduire la compacité de l'absorbant multicouches, tout en gardant une performance d'absorption acceptable. Nous avons fixé une réflexion maximale de -20 dB, sur toute la bande de fréquence étudiée, pour les absorbants à plus de 100 mm d'épaisseur et de – 10 dB à ceux de moins de cette limite d'épaisseur. Certaines de ces optimisations sont présentées dans ce résumé. La première optimisation a permis d'avoir un absorbant de 98 mm d'épaisseur et qui montre un coefficient de réflexion de -20 dB sur toute la gamme de fréquence étudiée (0.75 à 18 GHz). Cette optimisation est très encourageante ; son résultat est montré dans le manuscrit. Par ailleurs, comme nous visons des absorbants plus compacts, des épaisseurs encore plus faibles ont été imposées au code, tout en réduisant l'objectif en réflexion ; ce dernier a été imposé à -10 dB, sur toute la gamme de fréquence étudiée. En effet, l'épaisseur d'un absorbant est un des éléments qui détermine sa performance d'absorption, notamment en basse fréquences. En d'autres mots, et pour un absorbant large bande, une épaisseur minimale est nécessaire pour absorber en basses fréquences quelles que soit les propriétés des matériaux choisis et la transition d'impédance réalisée.

Pour l'optimisation qui suit, un design avec 5 couches a été proposé. L'ensemble des matériaux a été introduit dans la base, une épaisseur minimale de 10 mm a été imposée pour les différentes couches. Une épaisseur maximale de 20 mm a été imposée pour les trois premières couches de l'absorbant afin d'assurer une bonne transition d'impédance, et une épaisseur maximale de 15 mm a été imposée pour les deux dernières couches. Comme vu précédemment, les premières couches servent pour assurer la transition d'impédance alors que les dernières couches servent d'absorbants ; le choix des épaisseurs imposées est basé sur ce résonnement. L'épaisseur finale de l'absorbant va donc être comprise entre 50 mm et 90 mm. Il faut noter ici que la gamme de fréquence qui a été introduite pour l'optimisation est comprise entre 0.75 et 6 GHz. En effet, ce sont ces basses fréquences qui sont les plus difficiles à absorber avec ces faibles épaisseurs d'absorbant. Quelle que soit l'épaisseur finale proposée, ou les composites choisis, le prototype permettra probablement l'absorption des ondes EM en hautes fréquences.

La Figure 18 montre le design (les épaisseurs) proposé par l'optimisation ainsi que le prototype réalisé avec ce design ; une épaisseur totale de 70 mm a été suggérée ici. Ce design se compose que de quatre couches car le même matériau a été proposé pour les deux premières couches. Les composites choisis ici sont tous élaborés à partir de fibres longues (12 mm). Ceci est dû au fait que les performances de ces fibres longues sont meilleures en basses fréquences, comme discuté précédemment (Figure 5 et 6).

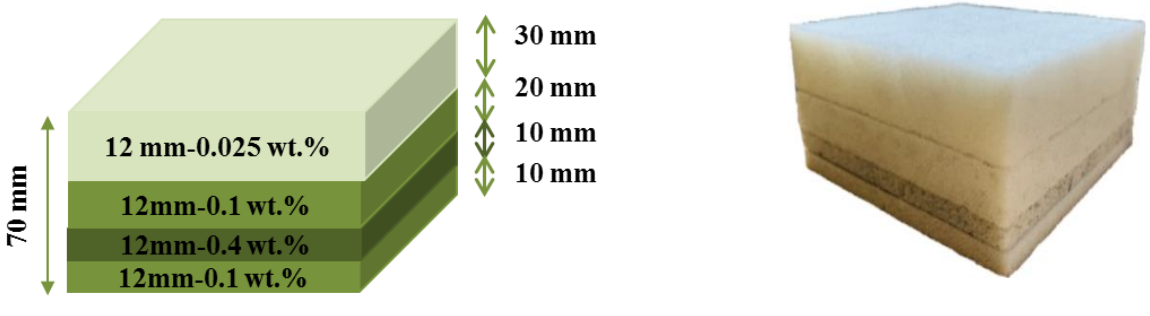

Figure 18 : Design (a) et photo (b) du prototype MLA70–GA–M réalisé.

La simulation et la mesure du prototype réalisé, dans la gamme de fréquence comprise entre 0.75 et 18 GHz sont présentées en Figure 19 pour les différentes incidences (normale et oblique de 30°). Ces figures montrent une bonne concordance entre la simulation et la mesure avec toujours une meilleure performance mesurée que simulée, notamment en hautes fréquences. Un coefficient de réflexion inférieur à –10 dB est obtenu dans toute la gamme de fréquence étudiée ; un coefficient de -20 dB est atteint à partir d'une fréquence aux alentours de 6 GHz pour les différentes incidences et polarisations des ondes EM. Ce résultat est très intéressant au regard des prototypes réalisés auparavant avec des épaisseurs plus élevées et des performances moins intéressantes.

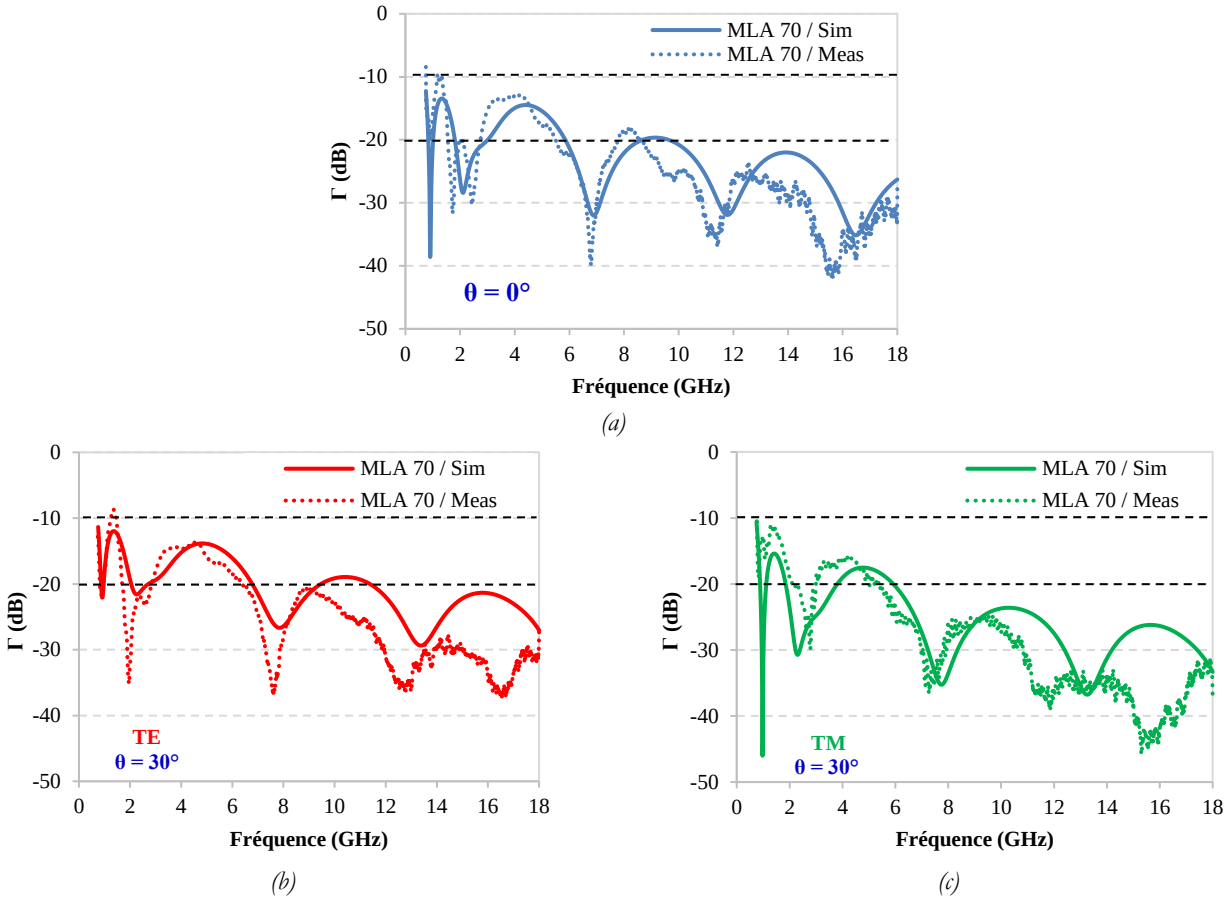

Figure 19 : Simulation et mesure des coefficients de réflexion du prototype MLA70–GA–M pour une incidence normale (a) et oblique de 30° pour le mode TE (b) et TM (c).

Une nouvelle optimisation, avec un design encore plus compact, a été menée par la suite. Ici, 3 couches seulement ont été proposées avec des épaisseurs minimales de 10 mm chacune et une épaisseur maximale allant de 15 mm (imposée pour les deux dernières couches) à 25 mm (imposée pour la première couche). Le design ainsi que la photo du prototype découlant de cette optimisation sont montrés en Figure 20. L'absorbant final, d'épaisseur totale de 50 mm, est constitué de deux couches seulement car, comme pour le précédent prototype, le même composite a été choisi pour la première et la deuxième couche. Ici aussi, les fibres longues ont été privilégiées par le code, confirment que ces fibres sont plus efficaces pour l'absorption en large bande et plus précisément, en basses fréquences.

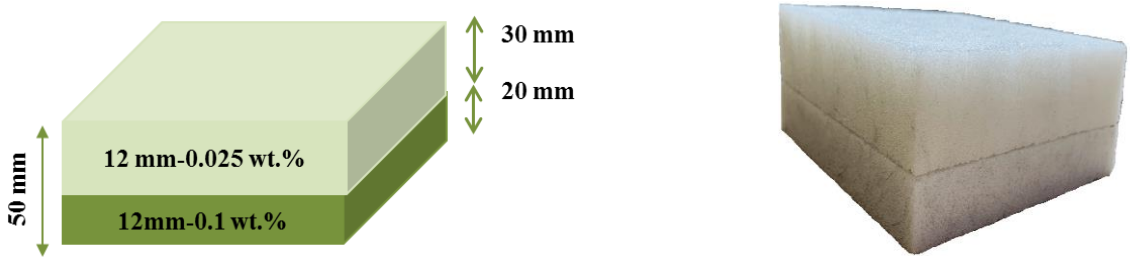

(a) (b)

Figure 20 : Design (a) et photo (b) du prototype MLA50–GA–M réalisé.

La simulation et la mesure de ce nouveau prototype sont présentées en Figure 21 pour les différentes incidences (normale et oblique de 30°) des ondes EM. Ces figures montrent une bonne concordance entre la simulation et la mesure avec toujours une meilleure performance mesurée que simulée, notamment en hautes fréquences. Le coefficient de réflexion imposé de –10 dB est obtenu ici à partir de la fréquence de 1.1 GHz pour les différentes incidences et polarisations des ondes EM. Un coefficient de -20 dB est atteint à partir d'une fréquence aux alentours de 6 GHz.

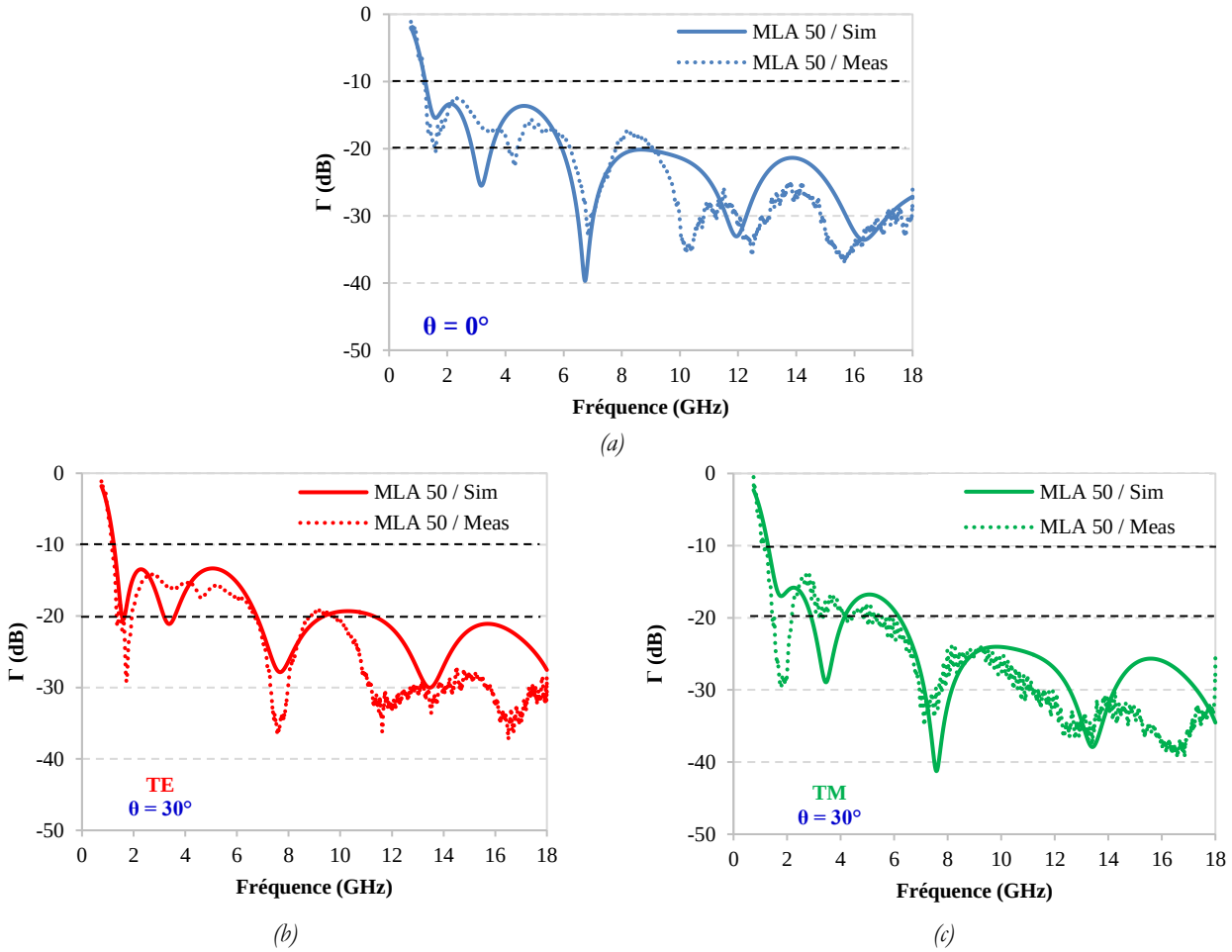

(a)

(b) (c)

Figure 21 : Simulation et mesure des coefficients de réflexion du prototype MLA50–GA–M pour une incidence normale (a) et oblique de 30° pour le mode TE (b) et TM (c).

La Figure 22 compare, pour l'incidence normale, les coefficients de réflexion mesurés sur les deux derniers prototypes (MLA70 et MLA50), optimisés par le code MATLAB, avec celui du prototype réalisé

par l'optimisation sur CST (MLA77) et celui du MLA125 (avec des épaisseurs identiques de 25 mm pour les différentes couches). Cette figure montre que la performance la moins intéressante est celle donnée par le MLA77 (optimisé par CST) ; l'optimisation avec MATLAB donne de meilleures performances d'absorption et cela avec des épaisseurs plus faibles (50 et 70 mm). Ceci confirme que l'optimisation à multi-paramètre de MATLAB est plus efficace que celle de CST qui est limitée à l'optimisation d'un seul paramètre, qui est l'épaisseur des couches. Par ailleurs, il faut noter ici que la performance d'absorption des deux prototypes réalisés grâce à MATLAB sont similaires, malgré la différence des épaisseurs, pour les fréquences aux delà de 5 GHz. Par contre, en basses fréquences, une différence d'environ 10 dB est à noter entre ces deux prototypes. Ceci confirme encore une fois que quel que soit le choix des matériaux utilisés pour les différentes couches de l'absorbant, une épaisseur minimale reste nécessaire pour garantir l'absorption en basses fréquence.

Par ailleurs, les différentes optimisations par MATLAB montrent un résultat équivalent à celui du MLA125 (notre absorbant de référence de 125 mm et avec les épaisseurs standards de 25 mm pour chaque couche) en hautes fréquences. Ceci confirme que pour ces fréquences, un bon choix des matériaux ainsi que de leur épaisseurs permet de garder une bonne performance tout en réduisant la compacité du multicouches.

Au final, un bon choix matériaux/ordre et épaisseurs des couches, réalisé avec le code MATLAB, nous a permis d'acquérir une bonne performance sur une large bande de fréquence avec le MLA70.

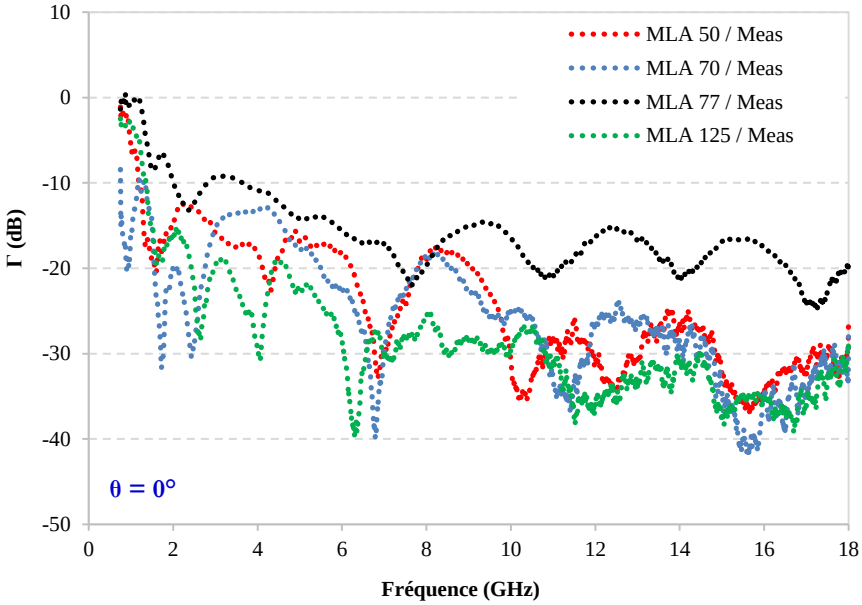

Figure 22 : Comparaison des coefficients de réflexion mesurés, pour l'incidence normale, sur les prototypes MLA77–GA, MLA70–GA–M, MLA50–GA–M et MLA125-1.

En conclusion de cette partie, nous pouvons dire que le prototype MLA70, optimisé par MATLAB, reste celui qui présente, si on prend en considération toute la gamme de fréquence étudiée, le meilleur compromis épaisseur/performance. Celui a été obtenu grâce à une optimisation réalisée par un

programme développé lors de cette thèse. Cette optimisation multi-paramètres a été réalisée dans notre cas en ne prenant en considération que l'incidence normale de l'onde électromagnétique. L'incidence oblique peut bien sûr être traitée, mais pour cela, les formules intégrant cet angle d'incidence doivent être introduites dans le programme ; cette optimisation pourrait faire l'objet de futurs travaux.

Dans le chapitre IV, les absorbants plans à métamatériaux sont abordés. Ces matériaux ont l'avantage d'être compacts mais présentent un inconvénient majeur qui est leur bande d'absorption étroite, qui découle de leur principe de fonctionnement, à savoir l'absorption à la fréquence de résonance. Le but de ce chapitre est la conception d'absorbants plans, à base de métamatériaux, fonctionnant en large bande et idéalement sur toute la gamme de fréquence comprise entre 2 et 18 GHz.

Dans la première partie de ce chapitre, un rappel des principes de fonctionnement et quelques formules relatives aux métamatériaux sont rappelés. Il faut noter ici que pour ce type d'absorbant, la géométrie et les dimensions des résonateurs, constituant le métamatériau, déterminent sa(ses) fréquence(s) de résonance(s).

Par la suite, une première étude par simulation d'un absorbant à métamatériau est présentée. Il s'agit d'un matématriau de forme « Fleur » inspiré de la littérature et pour lequel il a été montré que suivant la taille de la fleur, le pic d'absorption pouvait shifter vers les basses fréquences. Il faut noter ici que cette étude bibliographique était réalisée dans la gamme de fréquence comprise entre 12 et 18 GHz, gamme de fréquence plus haute que celle visée ici. A partir de cet exemple, j'ai proposé d'associer différentes fleurs avec différentes dimensions dans la même cellule, afin de réaliser un métamatériau multi-résonant, mais aussi, d'augmenter les dimensions des fleurs afin de shifter leurs résonances vers les fréquences visées ici (aux alentours de 2 GHz).

Une étude paramétrique a été réalisée pour cette première structure MM en variant indépendamment la distance entre les fleurs dans la même cellule *(a)*, la largeur de la cellule unitaire *L*, le rayon des fleurs constituant ainsi que l'emplacement des fleurs dans la cellule. Cette étude a permis de montrer d'une part, l'influence de chaque paramètre et a permis d'isoler les paramètres optimums pour shifter les résonances vers les basses fréquences. D'autre part, il a été montré qu'un compromis entre la fréquence de résonance et l'intensité de cette résonance (niveau du coefficient de réflexion) doit être fait. En effet, en augmentant le rayon des fleurs, un shift des pics de résonances est observé, mais celui-ci est accompagné par une augmentation de la réflexion. Au final, nos simulations ont montré que cette géométrie n'est pas adaptée aux fréquences visées par cette thèse (entre 2 et 18 GHz), mais plutôt aux fréquences au-delà de 10 GHz.

Parallèlement à cette première structure d'absorbant à métamatériau, une étude a été réalisée afin d'extraire, à partir de l'impédance, les paramètres effectifs du métamatériau. Ces propriétés ont été utilisées dans le calcul analytique (sur MATLAB) du coefficient de réflexion de la structure. Nos résultats ont

montré une très grande concordance entre la simulation et le calcul, validant ainsi notre technique d'extraction et de calcul.

Par la suite, une nouvelle conception de métamatériaux a été proposée et réalisée ; il s'agit d'un design nommé V-shape. Une première structure avec une cellule unitaire de dimensions 10x10 mm², présentant différentes résonances dans la gamme de fréquence étudiée, a été proposée. Les différentes étapes de conception, permettant d'aboutir à cette géométrie sont succinctement présentées. La géométrie du V-shape, ainsi que ces dimensions sont présentées en Figure 23 et dans le Tableau 1, respectivement.

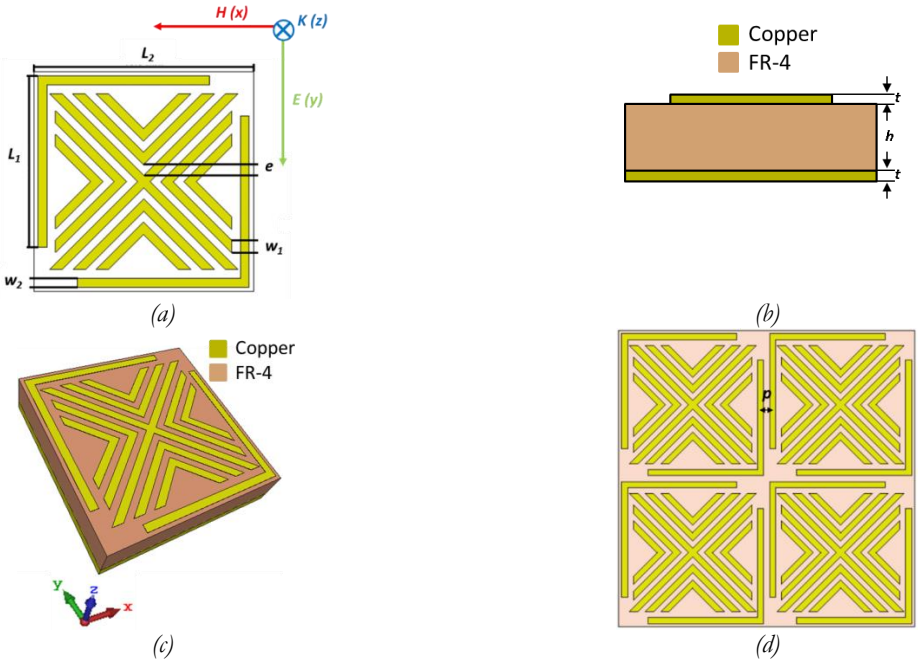

Figure 23 : Différentes vues du métamatréiau V-shape 10x10.

Paramètres	Valeur (mm)
e	0.5
h	3.2
L_1	10
L_2	7.8
p	0.4
t	0.017
w_1	0.6
w_2	0.4

Tableau 1 : Paramètres proposés pour le V-shape MM 10 × 10.

Les Figures 24 (a), (b) et (c) montrent les coefficients de réflexion simulés pour cette pour une incidence normale et oblique de 30° des ondes EM, respectivement. Différentes résonances, comprises entre 3.6 et 16.5 GHz, sont observées avec des niveaux d'absorption variables. Les principales résonances, avec un coefficient de réflexion inférieur à -10 dB, sont observées aux fréquences 3.6 GHz, 5.9 GHz, 8.6 GHz, 10.12 GHz et 16.48 GHz, pour l'incidence normale des ondes EM. Des résonances aux fréquences très similaires sont observées pour le mode TE de l'incidence oblique de 30° (Figure 24(b)) alors que pour

le mode TM, quelques résonances supplémentaires apparaissent en hautes fréquences (7.25 GHz, 13.06 GHz et 17.76 GHz).

Au final, cette géométrie simple de l'absorbant métamatériau présente plusieurs résonances dans la gamme de fréquence étudiée, mais ne présente pas d'absorption en basses fréquence (aux alentours de 2 GHz, souhaitée). Une optimisation de cette géométrie est tentée dans la suite du chapitre.

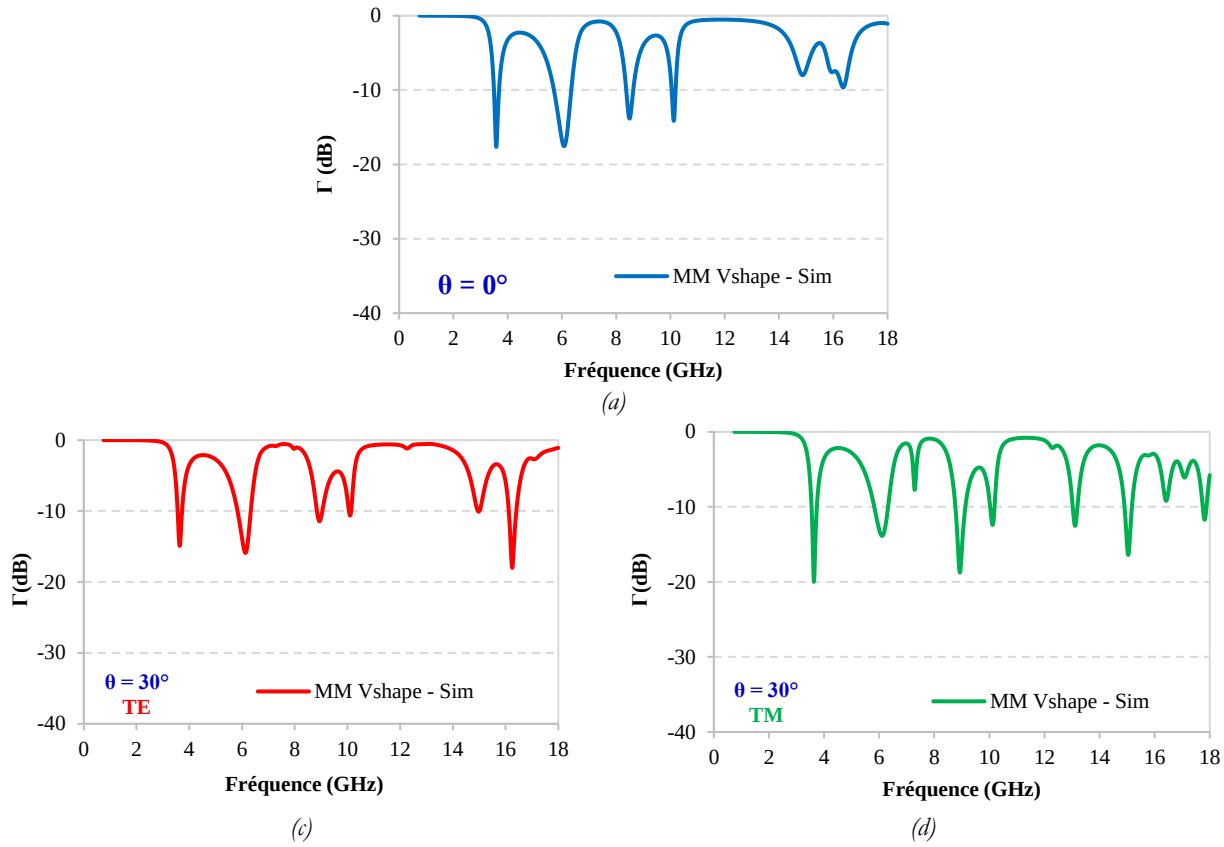

Figure 24 : Coefficient de réflexion simulés du métamatériau V-shape 10x10 pour l'incidence normale (a) et oblique de 30° pour le mode TE (b) et TM (c).

La géométrie V-shape a été optimisé afin d'augmenter le nombre de résonance, mais surtout, de créer une résonance aux alentours de 2 GHz. La taille d'une cellule unitaire a été augmentée de 10 x 10 mm² à 15 x 15 mm². Cette modification engendre l'augmentation de la longueur des différents résonateurs, mais aussi a permis de rajouter d'autres résonateurs de formes V, créant ainsi la nouvelle géométrie présentée en Figure 25. Les différentes dimensions (largeur de lignes, gaps…) ont été maintenues identiques à celle du Tableau 1.

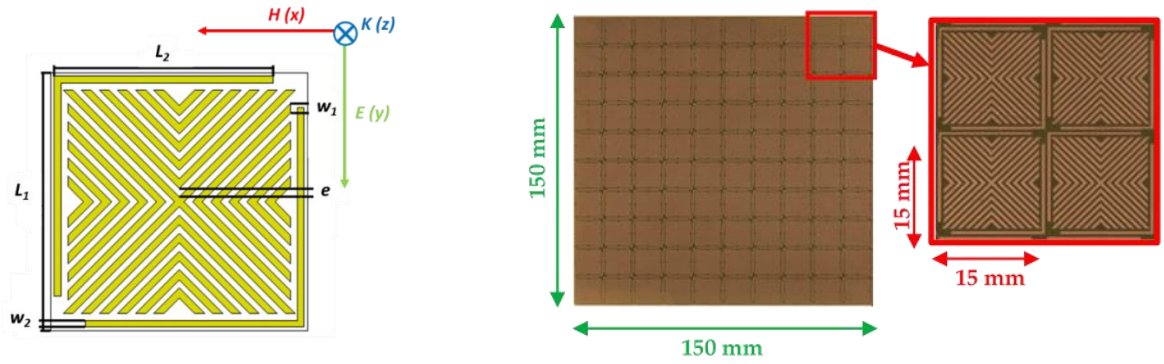

(a) (b)

Figure 25 : Design (a) et photo (b) du métamatréiau V-shape 15x15 réalisé.

Les coefficients de réflexion simulées et mesurées pour cette géométrie optimisée sont montrés en Figure 26 pour l'incidence normale et oblique de (30°) de l'onde EM. Ces résultats montrent une bonne concordance entre la simulation et la mesure, notamment sur la position des différentes résonances, même si le niveau d'absorption de ces piques de résonance n'est pas exactement identique. Ces résultats confirment par ailleurs l'augmentation du nombre de résonnance avec cette nouvelle géométrie, même si le niveau d'absorption de la résonance autour de 2 GHz n'est pas aussi important qu'attendu par la simulation. En effet, il est connu que la fréquence de résonance est inversement proportionnelle aux dimensions du résonateur, mais ceci devient au détriment de l'intensité de la résonance, lorsqu'il s'agit des basses fréquences. Néanmoins, cette structure est multi-résonante et présente des pics d'absorption sur toute la gamme de fréquence étudiée, et donc répond au cahier des charges initialement établie. Cette structure a été donc retenue pour la réalisation de l'absorbant hybride.

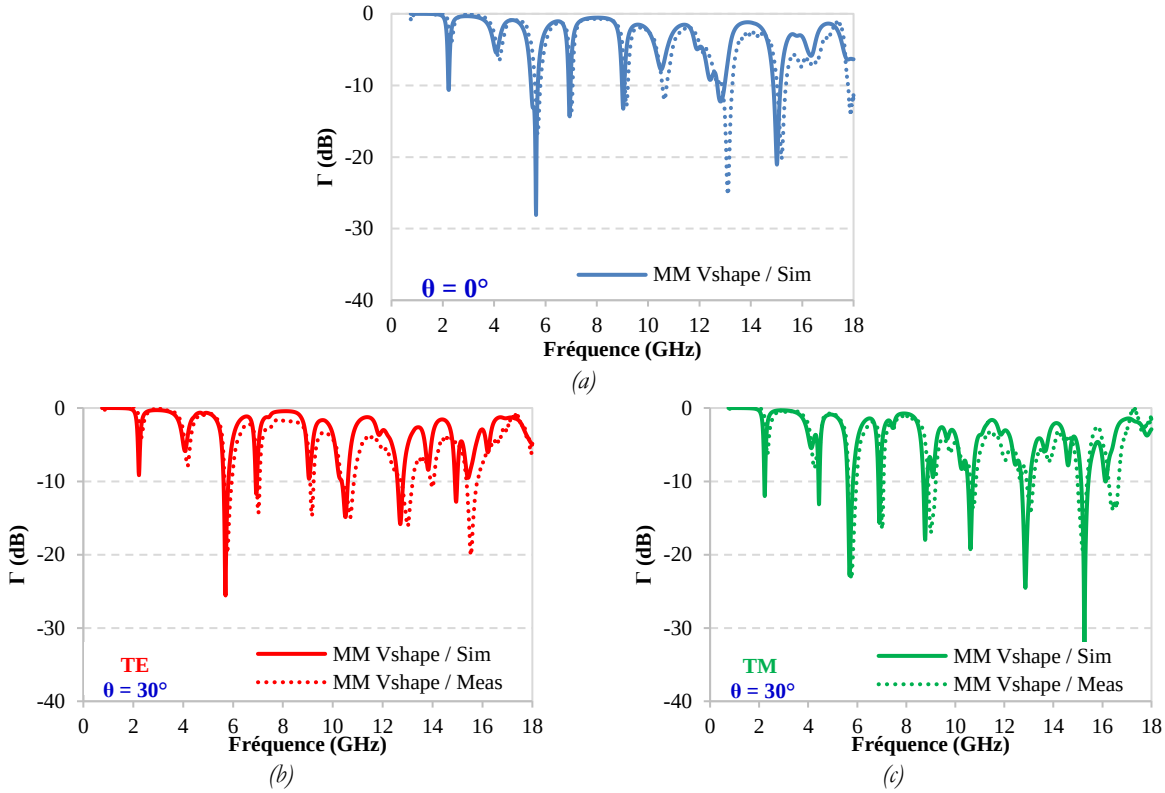

Figure 26 : Coefficient de réflexion simulés et mesurés du prototype métamatériau V-shape 15x15 réalisé pour l'incidence normale (a) et oblique de 30° pour le mode TE (b) et TM (c).

En fin de ce chapitre, une solution simple et innovante a été proposée pour élargir la bande d'absorption du métamatériau multi-résonant de la Figure 25. Cette solution de matériau hybride associe une couche d'absorbant « naturel » à l'absorbant artificiel à base de métamatériau. Une couche de mousse époxy chargée en fibres de carbone longues (12 mm) a été utilisée pour cette nouvelle conception. Cette longueur de fibre permet, comme vu précédemment, d'apporter des pertes en basses fréquences. Différents taux de charge (entre 0.025 wt.% et 0.2 wt.%) et d'épaisseurs (de 10 à 15 mm) de couche ont été d'abord testés par simulation. Une épaisseur optimum de 13 mm pour la couche époxy a été finalement retenue ; les simulations, en fonction du taux de charge sont montrées en Figure 27. Ces figures regroupent d'une part les mousses très peu chargées (Figure 27(a)) et d'autre part, ceux plus chargées (Figure 27(b)) ; le métamatériau tout seul est représenté par la courbe noir sur les deux figures. Il en découle de ces résultats de simulation que la mousse époxy chargée avec 0.075 wt.% est celle qui présente la plus large bande passante. En effet, cette couche présente le meilleur compromis ; elle apporte assez de pertes, grâce aux fibres longues, pour participer à l'absorption, tout en permettant de maintenir une bonne transition d'impédance entre l'air et l'absorbant. Ceci permettrait une absorption sur une large bande de fréquence.

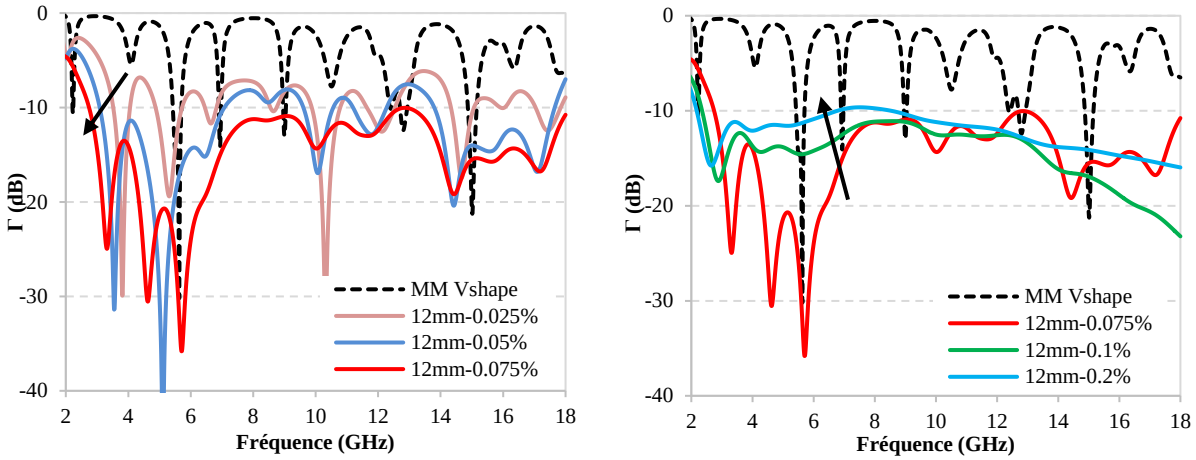

Figure 27 : Simulation de la structure hybride réalisée avec le métamatériau V-shape 15x15 associé avec des composites élaborés avec différents taux de fibres de carbone de 12 mm.

La Figure 28 (a) montre la photo du prototype absorbant hybride réalisé. Les Figures 28 (b), (c) et (d) présentent les coefficients de réflexion simulés et mesurés pour cette structure en incidence normale et oblique (30°). Ces figures ne montrent pas une parfaite concordance entre la simulation et la mesure, ceci est probablement dû à la différence des propriétés du matériau utilisé par rapport à celles utilisées en simulation. En effet, ce composite montre une légère hétérogénéité de la distribution des fibres, comme on peut le voir sur la Figure 28(a). Néanmoins, une très bonne performance est globalement obtenue par mesure pour les différentes incidences et polarisations des ondes EM. Il faut noter ici que le pic de réflexion observé aux alentours de 4 GHz est un artéfact de la mesure et est probablement dû au bruit de la chambre car il apparait sur l'ensemble des mesures qui ont été réalisées le même jour.

Nos résultats confirment donc l'obtention d'une large bande d'absorption grâce à l'association originale de l'absorbant naturel, faiblement chargé, à l'absorbant multi-résonant à métamatériaux. Une comparaison (présentée dans le manuscrit de thèse) de notre matériau a été réalisée avec les absorbants large-bande disponibles dans la littérature, en prenant en compte, l'épaisseur, la bande passante ainsi que le niveau d'absorption. Celle-ci a confirmé le très bon compromis/rapport obtenu ici et nous permet de qualifier notre absorbant hybride d'absorbant ultra large bande.

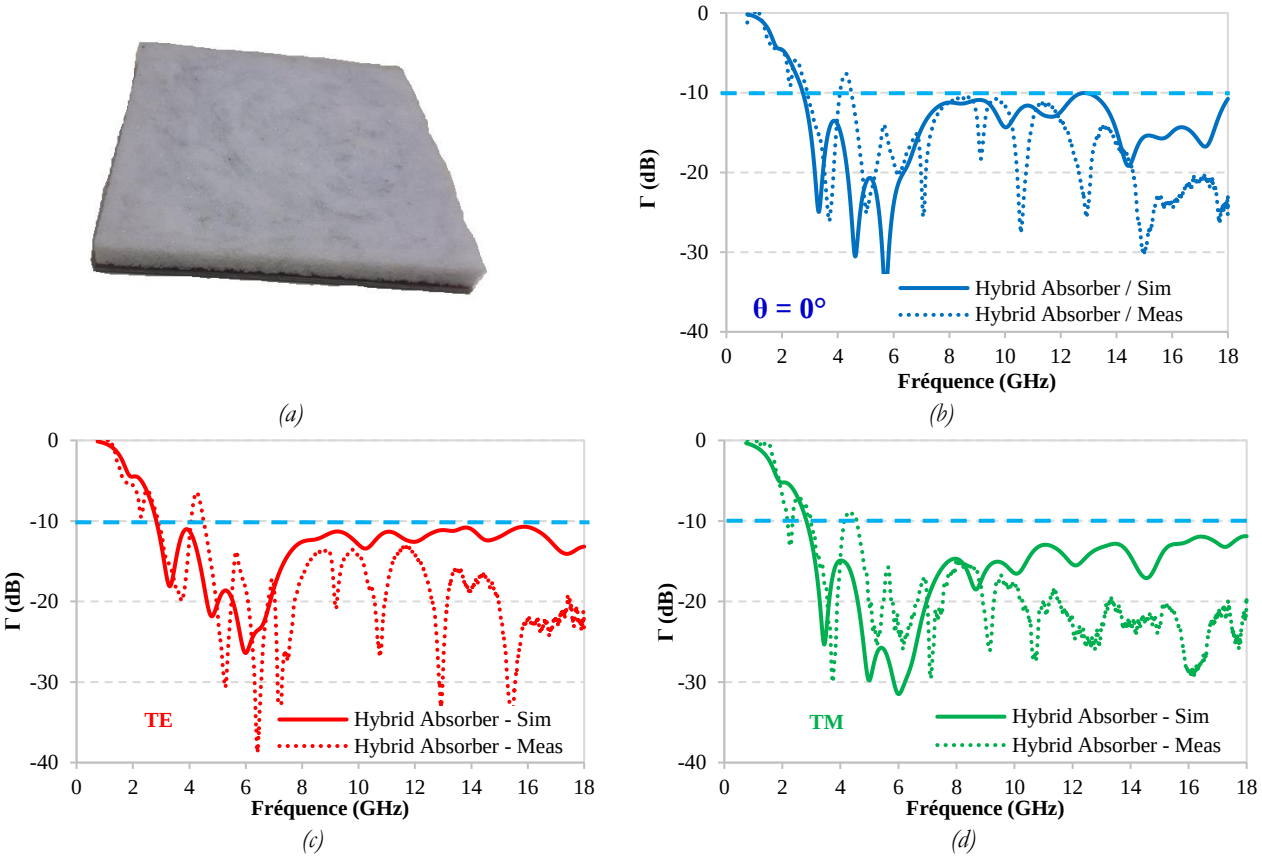

Figure 28 : Photo (a) et simulation et mesure du coefficient de réflexion pour l'incidence normale (a) et oblique de 30° pour le mode TE (b) et TM (c) de la structure finale retenue pour l'absorbant hybride.

En conclusion, mes travaux de thèse portent sur l'élaboration de matériaux absorbants plans ; de leur conception à leur réalisation et mesure. Trois types d'absorbants ont été traités, il s'agit des absorbants multicouches, des absorbants à métamatériaux multi-résonants et des absorbants hybrides. Des mousses époxy chargées en fibres de carbone (développées dans l'équipe FunMAT de l'IETR, site de St-Brieuc) ont été utilisées pour développer les absorbants « naturels » utilisés pour les absorbants à multicouches et hybrides.

Plusieurs prototypes d'absorbants plans à multicouches ont été réalisés, tout d'abord, en utilisant le principe d'adaptation d'impédance. La mesure de ces prototypes a montré d'une part, une grande réflectivité des absorbants lorsque des couches hautement chargées sont utilisées et d'autre part, la nécessité d'optimiser le choix et l'épaisseur des couches afin d'atteindre l'objectif d'absorption fixé. Par la suite, une optimisation de ces absorbants a été réalisée ; elle a été effectuée en utilisant deux méthodes. La

première fait appel à l'algorithme génétique implémenté dans le logiciel commercial de simulation électromagnétique CST. Cette optimisation permet de varier l'épaisseur des différentes couches, mais l'épaisseur totale, le choix des différents matériaux ainsi que leur séquence dans le multicouche sont fixés au préalable. Cette optimisation a permis une petite amélioration de la performance d'absorption, mais celle-ci ne répondait pas au cahier des charges imposé qui était de -20 dB pour les absorbants au-delà de 100 mm d'épaisseur, et -10 dB pour les absorbants d'épaisseur inférieure à cette limite. La seconde optimisation a été conduite en utilisant un programme développé au cours de cette thèse associé à l'algorithme génétique de MATLAB. Ce code nous a permis de réduire considérablement le temps de calcul (quelques heures contre quelques jours pour CST), mais il a aussi permis de faire une optimisation à multi-paramètres. En effet, le choix du matériau, l'ordre de ces matériau ou l'épaisseur totale de l'absorbant n'étaient plus imposés, mais plutôt optimisés lors des différentes itérations. Au final, en utilisant un large panel de matériaux (avec différents taux et longueurs de fibres), plusieurs prototypes compacts (≤ 100 mm) répondant aux objectifs de réflectivité fixés, ont été proposés. Ces résultats ont été confirmés par la mesure, en chambre anéchoïque, des prototypes réalisés.

Parallèlement, la conception d'un nouveau absorbant à métamatériau multi-résonant a été menée. Plusieurs structures ont été testées réalisées. La simulation, caractérisation et calcul de leurs coefficients de réflexion ont montré des résultats très similaires, validant ainsi l'extraction des propriétés effectif et le model analytique mis en place pour le calcul. Notre étude a également mis en avant le compromis entre géométrie / fréquence de résonance / intensité de la résonance rencontré surtout en basses fréquences.

La structure V-shape 15x15 qui présentait le plus de résonances mais aussi des résonances aux basses fréquences a été retenue pour la réalisation de l'absorbant hybride à large bande. Ce dernier a été réalisé grâce à une solution simple et innovante, associant ce métamatériau à une couche d'époxy faiblement chargée en fibre de carbone (0.075 wt.% de FC de 12 mm) de 13 mm d'épaisseur. Un absorbant large bande (entre 2.6 et 18 GHz) avec une épaisseur totale de 16.2 mm, épaisseur fine au regard des résultats présentés dans l'état de l'art, a ainsi été obtenu.

En perspective de ce travail de thèse, une optimisation des absorbants multicouche pourra également être réalisée en prenant en compte les incidences obliques des ondes EM. Celle-ci pourra être effectuée en optimisant le code MATLAB développé. La conception et la réalisation de matériaux absorbants hybrides avec une couche de très faible épaisseur pourront également être envisagées grâce à une optimisation avec le code MATLAB développé. Pour cela, les propriétés effectives extraites du métamatériau seront utilisées pour simulé le MM autant que monocouche ; la couche naturelle sera optimisé grâce au algorithme génétique.

Contents

Acronyms....1

General Introducion....3

Chapter I: Bibliography

List of Figures....10

1. Introduction....13

2. Microwave frequency ranges....13

3. Theory and principles of an absorbing material....14

3.1 Absorption condition....14

3.2 Permittivity and permeability of an absorbing material....15

3.3 Skin depth....16

4. Classification of the microwave absorbers as function of their bandwidth....17

4.1 Resonant microwave absorbers....17

4.2 Broadband microwave absorbers....22

5. Classification of the microwave absorbers as function of their compositions....31

5.1 Absorbers based on magnetic losses....31

5.2 Absorbers based on dielectric losses....35

5.3 Absorbers based on dielectric and magnetic losses....42

6. Motivations for epoxy loaded foams as absorbing materials....43

6.1 Absorbers used in the anechoic chambers....43

6.2 Absorbers used in this thesis....45

7. Conclusion....47

8. References....48

Chapter II: Multilayer Absorbers

List of Figures....64

1. Introduction....66

2. Reflection coefficient of planar electromagnetic absorbers....66

2.1 Monolayer absorbers 66

2.2 Multilayer absorbers 70

3. Carbon fiber loaded epoxy foam composites 77

3.1 Elaboration steps 77

3.2 Characterization technique 79

3.3 Dielectric properties and module of the characteristic impedance of the elaborated samples 82

4. Microwave multilayer absorber based on loaded epoxy foams 85

5. Improved reflection coefficient using lower CF rates 88

6. CF loaded lightweight epoxy foams 93

7. Conclusion 96

8. References 97

Chapter III: Optimizations of the Multilayer Absorbers

List of Figures 102

List of Tables 104

1. Introduction 105

2. MLA optimization using genetic algorithm of CST 105

2.1 Optimization results 106

2.2 Experimental results 109

2.3 Conclusion 111

3. Analytical solution and optimization technique using the GA of MATLAB 112

3.1 Reflection coefficient optimization by GA-MATLAB 112

3.2 Elaborated composites used for the optimization by GA-MATLAB 114

3.3 Optimization results 116

4. Conclusion 129

Chapter IV: Hybrid Metamaterial Absorber

List of Figures 134

List of Tables 136

1. Introduction 137

2. Metamaterial fundamentals....137
3. Flower shape metamaterial absorber....138
3.1 Simulation results of the first proposed MM absorber....138
3.2 Normalized input impedance and effective permittivity and permeability....147
4. The novel proposed symmetrical V-shape MM....150
4.1 Multi-resonance V-shape 10 × 10 MM....150
4.2 Multi-resonance V-shape 15 × 15 MM....153
5. Hybrid MM absorber....158
5.1 Simulation results....158
5.2 Measurement results....162
5.3 Comparison with other works....163
6. Conclusion....165
7. References....167

General Conclusion....169
List of communications....175

Acronyms

EM	Electromagnetic
IEEE	Institute of Electrical and Electronics Engineers
ITU	International Telecommunication Union
PEC	Perfect Electric Conductor
SiC	Silicon Carbide
HIS	High Impedance Surface
MM	Metamaterial
ERR	Electric Ring Resonator
CNT	Carbon NanoTube
SRR	Split Ring Resonator
RSR	Ring-Shaped Resonator
HMSR	Half-Moon-Shaped Resonator
WAIM	Wide-Angle Impedance Matching Layers
3D	Three dimensional
SCR	Split Circle Ring
CIP	Carbonyl-Iron Powder
CPE	Chlorinated Polyethylene
PVC	Polyvinylchloride
SiCNW	SiC NanoWire
CB	Carbon Black
SWCNT	Single-Walled Carbon Nanotubes
MWNTs	Multi-Walled Carbon Nanotubes
CF	Carbon Fiber
SCF	Short Carbon Fibers
PANI	Polyaniline
PPy	Polypyrrole
MCCFs	Magnetite Coated Carbon Fibers
EMC	Electromagnetic Compatibility
EMI	Electromagnetic Interference
PU	Polyurethane
MLA	Multilayer Absorber
TE	Transverse Electric

TM	Transverse Magnetic
MUT	Material Under Test
NRW	Nicolson - Ross – Weir
LW	Lightweight
GA	Genetic Algorithm
FoM	Factor of merit
MM	Metamaterial

General introduction

General introduction

In the last quarter century, and due to the rapid increase in telecommunication, microwave absorbing materials are becoming an important topic in most technologies and environments where the main goal is to reduce the electromagnetic pollution. Absorbers are therefore employed in electromagnetic interference, radar signature, telecommunication, medical systems and in electromagnetic characterization environments. In addition to that, researchers are always concentrated on developing new absorbing materials with a good absorption performance over a wide frequency band, presenting a lightweight and compactness.

A wide variety of absorbing materials was studied through the years. These materials can be classified by their geometries such as pyramidal geometry, multilayer absorbers and metamaterial absorbers or by their loads where absorbers based on dielectric, conductive and/or magnetic loads are used. In order to ensure the maximum absorption of the electromagnetic waves by an absorber, reflections of the waves at the first interface (between air and absorber) must be firstly minimized, ensuring an impedance matching and a smooth transition of the electromagnetic waves between the air and the absorber. This could be realized by adjusting either the geometry of the material, providing a geometrical transition, or the compositions of multiple stacked layers, providing a gradient of composition. In both cases, the waves will be gradually dissipated in the material and thus, being absorbed along its depth.

Due to the great progress in both electronic and telecommunication fields, new microwave absorbing materials that meet the new requirements were required. From here, an electromagnetic absorbing material based on the loaded epoxy foam composite with carbon fibers was previously developed by our team. This absorbing material was used in previous works for pyramidal and complex geometries, showing a very interesting absorption performance compared to that of the commercial pyramidal absorber of the same height. In this thesis, the objective is to use the same absorbing material in order to develop a broadband planar multilayer absorber with the minimum thickness and that operates over a wide band of frequency.

On the other hand, metamaterials are also widely used as electromagnetic absorbers. This type of absorbers usually provides a narrowband absorption bandwidth. Consequently, many efforts were made in order to broaden their absorption bandwidth. In this thesis, there is another goal dedicated to the elaboration of a novel multiband metamaterial absorber from one hand, and to broaden the absorption bandwidth of this metamaterial absorber, keeping a thin thickness, from the other hand.

Finally, it should be noted that the work of this thesis was in parallel with another thesis of Ms. Hanadi Breiss, which is devoted to the optimization of the absorbing material; some of these material will be used here in order to achieve the aforementioned goals.

This thesis manuscript is organized as following:

Chapter I is a chapter of the state of art. In this chapter, theory and principles of an absorbing material are first explained. Different examples of resonant, multiband and broadband absorbers are then presented. Finally, the absorbing material that will be used in this thesis is introduced and compared to that of commercial absorbers. Here, some previous work, using this material, will be also presented.

In **chapter II**, first of all, the theory of the calculation of the reflection coefficient of both monolayer and multilayer absorbers are detailed. These equations are used to elaborate a MATLAB code that calculates the total reflection coefficient. This code will help us to rapidly compute the total reflection coefficient of any multilayer absorber. In this chapter, the importance of using a smooth gradual impedance was also emphasized and verified by elaboration of three prototypes.

In **chapter III**, a genetic algorithm is proposed to enhance the absorption performance of the planar multilayer absorber. Here, the algorithm will use the code that we have elaborated in chapter II in order to compute the total reflection coefficient at each iteration. The purpose of this study is to find a set of layers with the smallest reflection coefficient associated with a thin total thickness in a specific frequency range. The optimized design of the multilayer absorber in this study discusses only the case of normal incidence of the EM waves. The oblique incidence can also be used in the optimization process and could be discussed in future studies.

In **chapter IV**, different multi-resonance MM absorbers have been proposed. The normalized input impedance, effective permittivity and effective permeability of these MMs will be extracted. To broaden the absorption bandwidth of the best of them, a thin dielectric composite based on CF low-loaded epoxy foam is used forming an ultra-wideband hybrid absorber.

Chapter I:

Bibliography

Table of Contents

List of Figures 10

1. Introduction 13

2. Microwave frequency ranges 13

3. Theory and principles of an absorbing material 14

   3.1 Absorption condition 14

   3.2 Permittivity and permeability of an absorbing material 15

   3.3 Skin depth 16

4. Classification of the microwave absorbers as function of their bandwidth 17

   4.1 Resonant microwave absorbers 17

   4.2 Broadband microwave absorbers 22

5. Classification of the microwave absorbers as function of their compositions 31

   5.1 Absorbers based on magnetic losses 31

   5.2 Absorbers based on dielectric losses 35

   5.3 Absorbers based on dielectric and magnetic losses 42

6. Motivations for epoxy loaded foams as absorbing materials 43

   6.1 Absorbers used in the anechoic chambers 43

   6.2 Absorbers used in this thesis 45

7. Conclusion 47

8. References 48

List of Figures

Figure I.1. Electromagnetic radiation spectrum [2]. 14
Figure I.2. The different frequency band designations proposed by IEEE radar designations, by the international standard bands and by the military standard bands [2]. 14
Figure I.3. Absorption mechanism of a monolayer absorber. 15
Figure I.4. The attenuation of a sinusoidal wave before and after its penetration in an absorbing material [9]. 17
Figure I.5. (a) Salisbury screen, (b) Jaumann layers and (c) Dällenbach layer. 18
Figure I.6. First Salisbury screen [10]. 18
Figure I.7. Reflection coefficient S11 (in dB) for (a) 1 layer (Salisbury screen) and Jaumann layers of (b) 2 layers and (c) 3 layers [12]. 19
Figure I.8. Absorber based on Dällenbach principle (a) and its simulated and measured reflection coefficients (b) [13]. 20
Figure I.9. (a) Top view, (b) Perspective view and (c) cross-section of the high-impedance surface of Sivenpiper [14]. 20
Figure I.10. (a) Proposed HIS and (b) its reflection coefficient [15]. 21
Figure I.11. Simulated reflection coefficient (green line), absorption coefficient (red line) and transmission coefficient (blue line) of the MM perfect absorber [17]. 21
Figure I.12. (a) proposed multi-resonance MM and (b) its simulated reflection coefficient [46]. 22
Figure I.13. Impedance matching applying (a) a geometric transition using the pyramidal shape and (b) multilayer configuration. 23
Figure I.14. (a) Pyramidal absorber APM by SIEPEL and (b) its guaranteed reflectivity at normal incidence[48]. 23
Figure I.15. A multilayered foam of poly (ε-caprolactone) with gradual concentrations of CNTs (a) and its simulated reflection coefficients (b) [50]. 24
Figure I.16. Reflection coefficients of the tri-layer absorbers with two different gradients of the dielectric and magnetic properties varying them from the lowest to the highest (a) and from the highest to the lowest (b) [51]. 25
Figure I.17. Reflection coefficient of the proposed multilayer [73]. 25
Figure I.18. (a) A multilayered polyurethane foams loaded with carbon particles and (b) guaranteed reflection coefficients for the AH absorbers from SIEPEL at normal incidence [48]. 26
Figure I.19. The design (a) and the absorption performance of MM with single ring resonator (b) and with several rings (c) [53]. 27
Figure I.20. The MM design (a) and reflection coefficients of three MMs with three different dimensions of a single SRR resonator (SRR1, SRR2 and SRR3) (b) and multilayer SRRs (c) [69]. 28

Figure I.21. The design (a) and absorption performance of (b) multilayer MM using (HMSR and RSR resonators [58]. 28
Figure I.22. The design (a) and the reflection coefficient of (b) the proposed multilayer structure [72].29
Figure I.23. The design (a) and absorption performance of (b) 3D Pyramidal MMs [56]. 29
Figure I.24. The design (a) and absorption performance (b) of 3D cylindrical MMs [57]. 30
Figure I.25. The design (a) and absorption performance of (b) SCR resonator using lumped elements [65]. 30
Figure I.26. (a) Design of the proposed MM and (b) the simulated reflection coefficients with and without lumped elements in [76]. 31
Figure I.27. Reflection coefficients of the rubber matrix containing iron flakes of different initial particle sizes (2 μm, 7μm and 70 μm) [85]. 32
Figure I.28. Reflection coefficients of epoxy resin composites loaded with 50 vol% Fe nanowires using different thicknesses [80]. 32
Figure I.29. Reflection coefficients of the samples (a) with the same thickness (1 mm) and different weight ratios (CIP:CPE) (b) with the weight ratio (CIP:CPE) of 16:1 using different thicknesses [88]. 33
Figure I.30. Reflection coefficients of prepared composites for different (a) particle sizes, (b) concentrations, and (c) fraction ratios of the double MnZn/NiZn ferrite fillers [90]. 34
Figure I.31. Reflection coefficient of the single-layer absorber using NiZn ferrite (a) and (b) α-Fe and a double layer absorber (c) using both layers [92]. 35
Figure I.32. Reflection coefficients of the epoxy resin, composite with 15 wt.% microparticles, and composites with 15, 25, and 35 wt.% of SiCNWs at 2-18 GHz [95]. 36
Figure I.33. (a) SiC/epoxy monolayer and (b) its reflection coefficient [94]. 36
Figure I.34. Dielectric losses of the tungsten-Teflon composite as a function of metal volume fraction p (solid lines are the fit of the data) [98]. 37
Figure I.35. Simulated reflection loss (a) using different carbon black wt.% (composite thickness = 2 mm) and (b) using different thicknesses of the composite loaded with 10 wt.% CB [103]. 38
Figure I.36. Reflection coefficient of the double layer absorber based on glass fiber /epoxy composites loaded with CB [100]. 38
Figure I.37. Reflection coefficients of the SWNTs loaded polyurethane composites of 2 mm thickness using different wt.% of SWNTs (0-25 wt.%) [105]. 39
Figure I.38. Reflection coefficients of polymer composite, using the MWNTs [106]. 39
Figure I.39. (a) MWCNTs based and (c) Graphite based multilayer absorbers and (b) and (d) their corresponding reflection coefficients [108]. 40
Figure I.40. Reflection coefficients of prepared composites loaded with different wt.% of the SCF (a) 0 wt.%, (b) 20 wt.%, (c) 25 wt.%, (d) 30 wt.%, (e) 35 wt.%, and (f) 40 wt.% [115]. 41
Figure I.41. Reflection coefficients of 30 wt.% hybrids for different thicknesses[118]. 41

Figure I.42. The calculated reflection coefficient of the epoxy-PANI/CB composites at 2-18 GHz [102]. 42
Figure I.43. Reflection coefficient of different wt.% of the absorbing loads based on (1-5): 10 wt.%, 20 wt. %, 30 wt.%, 40 wt.% and 50 wt.%..... 43
Figure I.44. (a) SEM images of a carbon fiber coated with Fe_3O_4 film and (b) the reflection coefficients of the achieved composites using different thicknesses [129]. 43
Figure I.45. SEM of a pyramidal absorber [143]..... 45
Figure I.46. SEM of CFs embedded in the composite [144]. 45
Figure I.47. Photos of the elaborated prototype and the commercial absorber APM 12 (a) and measurement results of these two prototypes at normal incidence (b) and oblique incidence of 30° (c) [143]. 46
Figure I.48. Photos of the elaborated prototype and the commercial absorber APM 12 (a) and measurement results of these two prototypes at normal incidence (b) and oblique incidence of 30° (c) [142]. 47

1. Introduction

Electromagnetic (EM) wave absorbers' researches were investigated in the mid 1930's where the first patent was deposited in 1936 in the Netherlands [1]. The earliest record involves a simple resonant absorber that was designed for a 2 GHz antenna in order to improve its front-to-back ratio [1]. This absorber was using carbon black as a lossy material for energy dissipation and titanium dioxide for its high dielectric constant in order to reduce the thickness [1].

Then, during the Second World War, the use of absorbing materials became necessary in order to reduce, or to eliminate, the signal of military equipment (planes and submarines) from the first radar detectors. During this period, German submarines had their periscopes coated with a layer of 'Wesch' material, which resonates around 3 GHz, made up of a rubber substrate loaded with carbonyl iron powder; this layer served to dissipate radar energy into the substrate material [1].

Since the middle of the 20th century, whether for civil or military domains, the variety of applications requiring EM absorbers has been increased rapidly. Therefore, new materials had to be developed in order to meet the requirements of the different applications.

In the following sections of this chapter, firstly, the electromagnetic principles of absorbing materials, absorbers' types and absorption mechanism are presented. Then, absorbers are classified according to their loads and their absorbing bandwidth. After that, absorbers used in the anechoic chamber are presented. And finally, an introduction to the absorbing material used in this thesis is done.

2. Microwave frequency ranges

Microwaves are the electromagnetic waves situated between radio and infrared waves [2]. The microwave range is between a few hundred of MHz and a few hundred of GHz (Figure I.1) [2]. A letter-based nomenclature was proposed by the Institute of Electrical and Electronics Engineers (IEEE) radar designations, another one was proposed by the International Telecommunication Union (ITU) and a third one was proposed by the military standard bands (Figure I.2) [2]. Since the designations of the IEEE are more widely used in most scientific articles than those of the ITU, we adopt the same nomenclature as the IEEE in this thesis.

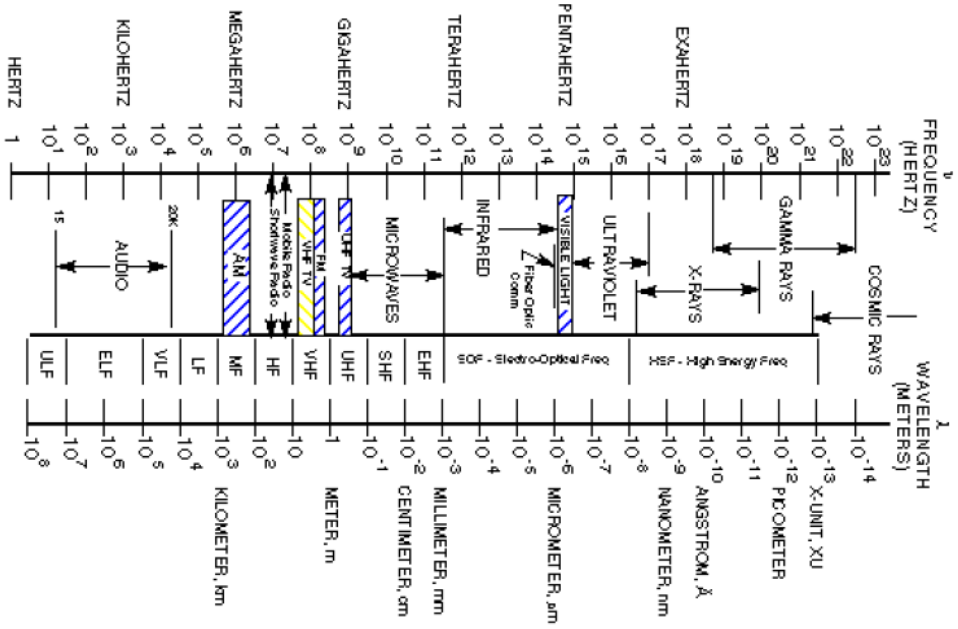

Figure I.1. Electromagnetic radiation spectrum [2].

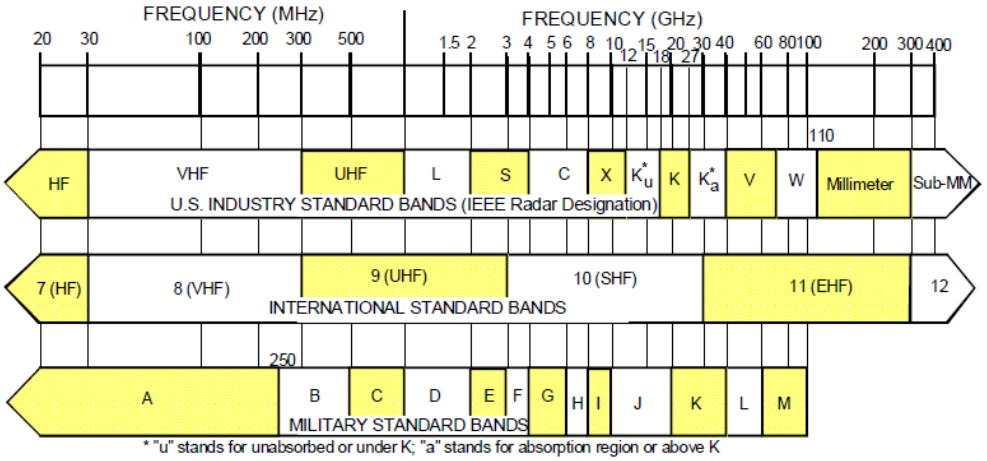

Figure I.2. The different frequency band designations proposed by IEEE radar designations, by the international standard bands and by the military standard bands [2].

3. Theory and principles of an absorbing material

The interaction of an EM wave with a microwave absorbing material can be described as the transformation of the EM energy into thermal energy. According to the principle of energy conservation, when the EM wave arrives at the surface of a material, it will be reflected, attenuated or transmitted through the material. The response of the material to the wave depends on its electromagnetic properties.

3.1 Absorption condition

When an EM wave arrives at the surface of an absorbing material (Figure I.3), a part of this wave (**r**) is reflected, a second part is transmitted inside the material. This transmited wave will partially absorbed in the material or reflected several times inside it by the metallic plate (Figure I.3). However, no transmission to other medium will occur since the metallic plate (or Perfect Electric Conductor (PEC)) acts as a reflector

that blocks the transmission of the EM waves; in other words, the PEC will reflect the EM waves that arrives at the back preventing them to be transmitted. Therefore, the total reflection is composed of the different partial internal reflections r_1 , r_2, r_3,…. , and the reflection r that occurs at the first air/material interface due to impedance mismatching between the two media. Thereby, the absorbing material should firstly, ensure an impedance matching at this air/material interface, to avoid the reflection at the surface, and secondly, to ensure a good absorption, thanks to the lossy layer, in order to attenuate the EM waves inside it.

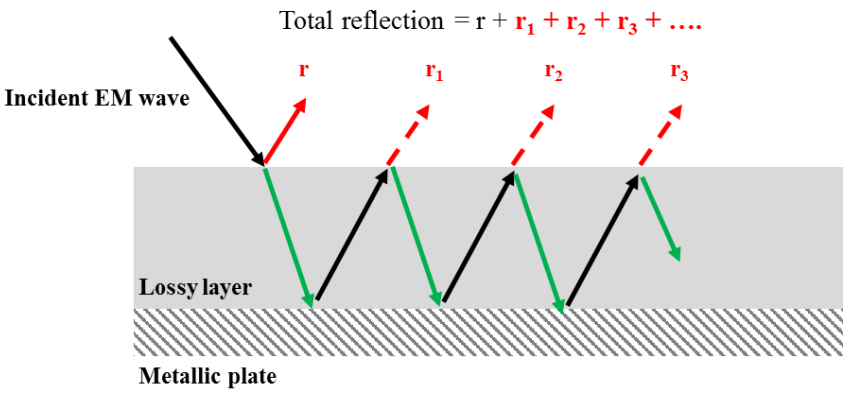

Figure I.3. Absorption mechanism of a monolayer absorber.

3.2 Permittivity and permeability of an absorbing material

The dielectric losses of a material result mainly from two mechanisms: polarization and conduction. When a dielectric material (non-conductive), whose dominant charges (negative and positive charges) are not capable of moving, is subjected to an electric field $\vec{E}$, these charges will be set in motion under the effect of this field. This will result in an alignment of the dipoles as a function of the direction of the electric field and thus creates the electric displacement $\vec{D}$ [3]. The displacement of current induced by the variation of the electric field direction is accompanied by energy losses. However, when a conductive material, is subjected to the electric field $\vec{E}$, the free charges are set in motion and the displacement of these charges is also accompanied by energy losses by the Joule effect [4].

On the other hand, the magnetic losses of a material result also from several mechanisms. When a magnetic material, represented by magnetic dipoles oriented in a random fashion, is subjected to a magnetic field, these magnetic dipoles will tend to align in the direction of the magnetic flux $\vec{B}$ by alignment and rotation of the magnetization spin [3]. The change that occured in this case will lead to the transformation of the EM waves energy into thermal energy and hence, causing the absorption of the microwaves. Magnetic losses could also come from eddy currents (also called Foucault's currents), which are loops of electrical current that are induced within conductors by the variation of the magnetic field in the conductor [5]. Ferromagnetic resonance phenomena is also an absorption mechanism and depends on the orientation of the material and the intensity of the magnetic field [6]. The energy dissipated by these different mechanisms will also be transformed into heat.

The electromagnetic absorption mechanism depends on the relative dielectric permittivity **($\tilde{\varepsilon}$)** and the relative magnetic permeability **($\tilde{\mu}$)** of the material. The dielectric permittivity holds information about the polarization and the conduction mechanisms of a dielectric material in response to an applied electric field [7]; whereas, the magnetic permeability holds information about the magnetization capacity and the eddy currents mechanisms in a material in response to an applied magnetic field [7, 8]. These quantities are complex, the real part is associated to the ability of the material to store energy, while the imaginary part is associated to its ability to dissipate the energy, in the presence of external electric and magnetic fields. $\tilde{\boldsymbol{\varepsilon}}$ and $\tilde{\boldsymbol{\mu}}$ are give in equations (1) and (2).

$$\tilde{\varepsilon} = \varepsilon_0(\varepsilon_r' - j\,\varepsilon_r'') \tag{1}$$

$$\tilde{\mu} = \mu_0(\mu_r' - j\,\mu'_r) \tag{2}$$

Here, ε_0 is the permittivity of the vacuum which is equal to 8.85 pF/m and μ_0 the permeability of the vacuum which is equal to $4\pi.10^{-7}$ H/m. The dielectric and magnetic losses are defined in equations (3) and (4).

$$\tan\delta_e = \frac{\varepsilon_r''}{\varepsilon_r'} \tag{3}$$

$$\tan\delta_m = \frac{\mu_r''}{\mu_r'} \tag{4}$$

3.3 Skin depth

When an EM waves propagate into a lossy material, their electric fields are attenuated exponentially in depth of the material. Figure I.4 shows the attenuation factor of a wave before and after its penetration in the absorbing material [9]. For this example, the interface that seperates both media (air and absorber) is situated at position x = 200. From this interface, the wave started to be attenuated exponentially in the form $e^{-\alpha x}$ where x is the traveled distance by the wave and α is the attenuation of the wave during its propagation. The skin depth of the material is the distance at which the power of the waves is reduced to 1/e = 37% of the incident power and it is inversly proportional to α (equation (5)). The skin depth δ of an absorbing lossy material is inversely proportional to the dielectric and magnetic properties, the frequency ($\omega = 2\pi f$) and to the conductivity of the absorbing material as shown in equation (6).

$$\delta = \frac{1}{\alpha} \tag{5}$$

Where

$$\alpha = \omega\sqrt{\varepsilon\mu}\left[\frac{1}{2}\left(-1+\sqrt{1+\left(\frac{\sigma}{\omega\varepsilon}\right)^2}\right)\right]^2 \tag{6}$$

With

ω: pulsation of the EM wave

ε: permittivity of the material

μ: permeability of the material

σ: conductivity of the material (S/m)

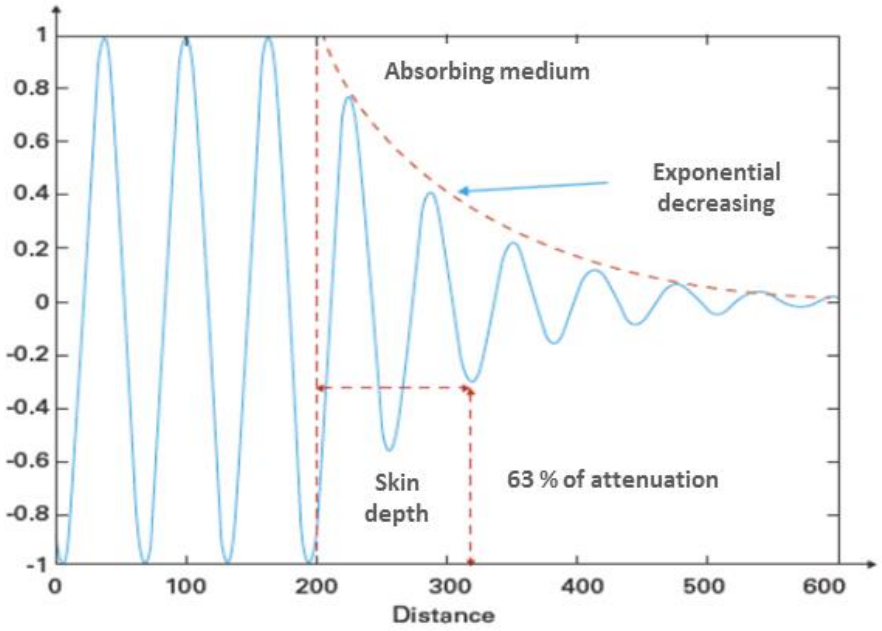

Figure I.4. The attenuation of a sinusoidal wave before and after its penetration in an absorbing material [9].

4. Classification of the microwave absorbers as function of their bandwidth

4.1 Resonant microwave absorbers

Electromagnetic absorbers could be narrowband or broadband. Absorbers, such as Salisbury screens, Dällenbach layers, Jaumann layers, as well as, metamaterial absorbers [9], are narrowband absorbers.

4.1.1 Salisbury screens, Dällenbach layers and Jaumann layers

Figure I.5 presents the design principle of Salisbury screens (Figure I.5 (a)), of the Dällenbach layers (Figure I.5 (b)) and of Jaumann layers (Figure I.5 (c)). The Salisbury screen is one of the oldest and simplest absorbing screens which is inherently narrowband. As shown in Figure I.5 (a), it is constituted by placing a single thin resistive layer (blue colored layer), followed by a spacer (a lossless dielectric layer) of a thickness equal to a quarter wavelength (of the desired frequency) above a perfect electrically conducting plane. The incident EM wave will be reflected twice; the first time is occurred by the resistive sheet and the second time by the metallic plate. At the resonant frequency, these two reflected waves are out of phase of 180°, so they cancel each other, leading to a zero reflection. The thickness of the dielectric layer determines the frequency of resonance, where the spacer has an odd quarter wavelength thickness (n λ/4). However, the impedance matching is ensured when $\frac{1}{r\sigma}$ is equal to the impedance of air (377 Ω) as shown in equation (7), where r is the thickness of the resistive layer and σ is its conductivity [9]. The first Salisbury screen was invented by W. W. Salisbury (Figure I.6) [10]. It consists of a canvas layer coated with colloidal solution of graphite, followed by a wood layer as a spacer which is backed by a metallic plate.

$$Z_0 = 377\ \Omega = \frac{1}{r\sigma} \tag{7}$$

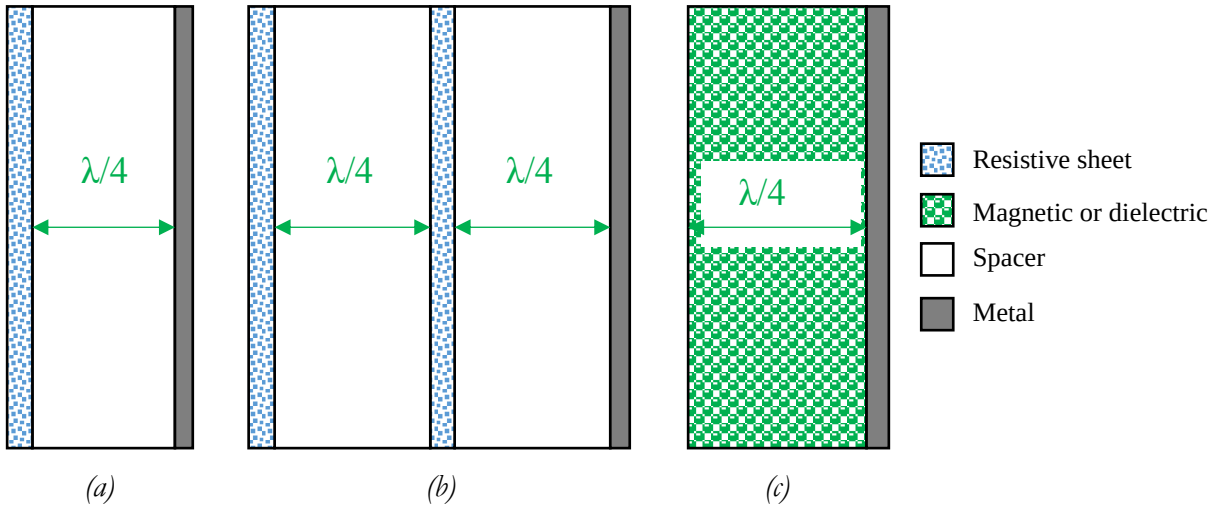

Figure I.5. (a) Salisbury screen, (b) Jaumann layers and (c) Dällenbach layer.

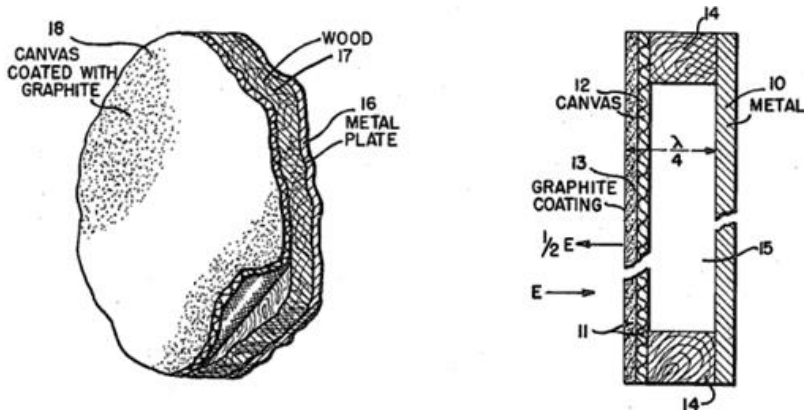

Figure I.6. First Salisbury screen [10].

Jaumann layers [11] are the extension of Salisbury screens that consist of two or more resistive films sandwiched between several spacers of λ/4 thicknesses (Figure I.5 (b)) where sheets are designed to operate at distinct frequencies. This will provide resonances over multiple wavelengths depending on the number of sheets used and the spacer thickness. The bandwidth will be increased by each added layer, but by this way the absorber will be thick and bulky. An example of the simulated reflection coefficient S_{11} of Jaumann layers is presented in Figure I.7.

In this figure, absorbers with increased number of resistive layers from one to three sheets are shown [12]; the dielectric material used here is vacuum ($\varepsilon_r = 1$ and $\mu_r = 1$) with a thickness of λ/4 of the desired frequency (10 GHz). When using a single sheet (Salisbury screen), a single resonance at 10 GHz has been obtained (Figure I.7 (a)). For Jaumann absorber of two layers (Figure I.7 (b)), with two resistive sheets of resistance R_1=250 Ω, two resonances have been obtained with a reflection coefficient less than -20 dB between 6.4 GHz and 13.7 GHz. For Jaumann absorber of three layers (Figure I.7 (c)), with three resistive sheets of resistances R_1=320 Ω, R_2=670 Ω and R_3=1560 Ω; three resonances have been obtained with a reflection coefficient less than -20 dB between 4 GHz and 16 GHz. Note that the thickness of the spacer

is λ/4 of the desired frequency of resonance. From here, it can be deduced that increasing the number of layers, with increasing resistances, will increase the bandwidth, as well as, the thickness of the absorber.

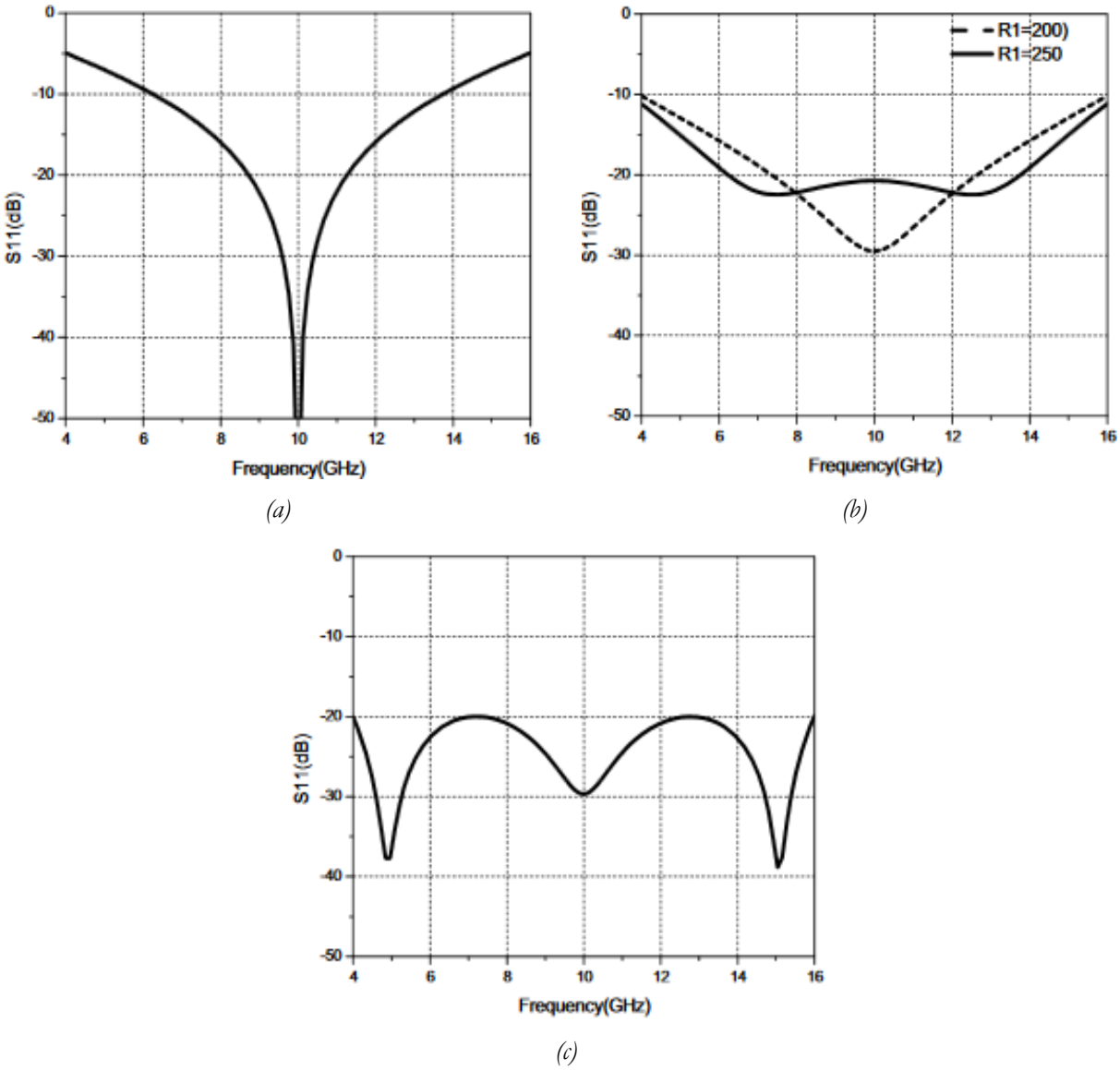

Figure I.7. Reflection coefficient S11 (in dB) for (a) 1 layer (Salisbury screen) and Jaumann layers of (b) 2 layers and (c) 3 layers [12].

Dällenbach layers (shown in Figure I.5 (c)) are made of a dielectric or magnetic lossy material (green colored layer) backed with a metallic plate [13]. The thickness, permittivity and permeability of this material could be adjusted to minimize the reflectivity at the desired frequency. In fact, for Salisbury screen and Jaumann layers, the absorption occurs in the thin sheets while it occurs in the dielectric/magnetic layer for the Dällenbach layer. An example of using the principle of the Dällenbach layer is presented by *Kwon and al.* [13]. The proposed monolayer absorber is composed of the integration of the glass/epoxy composite into SiC fibers network that is arranged as shown in Figure I.8 (a). They have used the dielectric and magnetic properties of the absorbing material to calculate the needed thickness which is of quarter wavelength of the desired frequency of resonance. Here, the optimal thickness was found between 3 and 3.1 mm and a thickness of 3.12 mm was chosen to achieve the monolayer absorber. As a result, a reflection coefficient resonance of -39 dB was obtained at 9.87 GHz; reflection coefficient less than -10 dB was achieved between 8.25–11.83 GHz (Figure I.8).

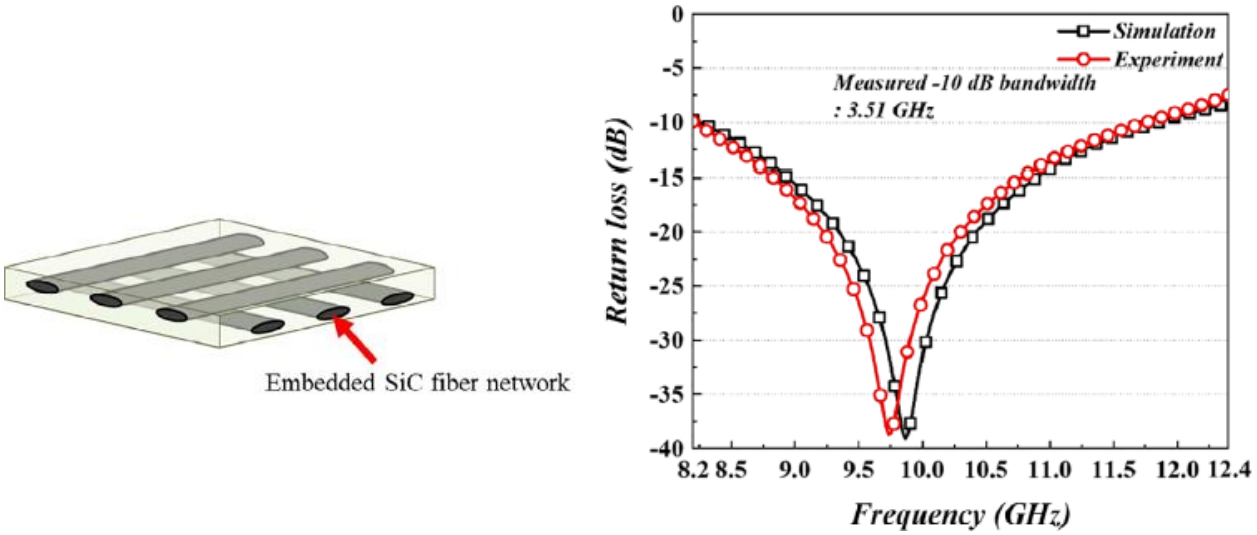

(a) *(b)*

Figure I.8. Absorber based on Dällenbach principle (a) and its simulated and measured reflection coefficients (b) [13].

4.1.2 Metamaterial absorbers

In the first steps towards metamaterial absorbers, *D. Sievenpiper*, in his doctoral thesis in 1999, has proposed a compact surface called a High Impedance mushroom-type Surface (HIS) [14], which is composed of an array of 2D metal fine cell patches that have the geometry of hexagon and looks like thumbtacks or mushrooms. These cells are attached to the ground plane by a metallized hole to make a continuous metal structure (Figure I.9).

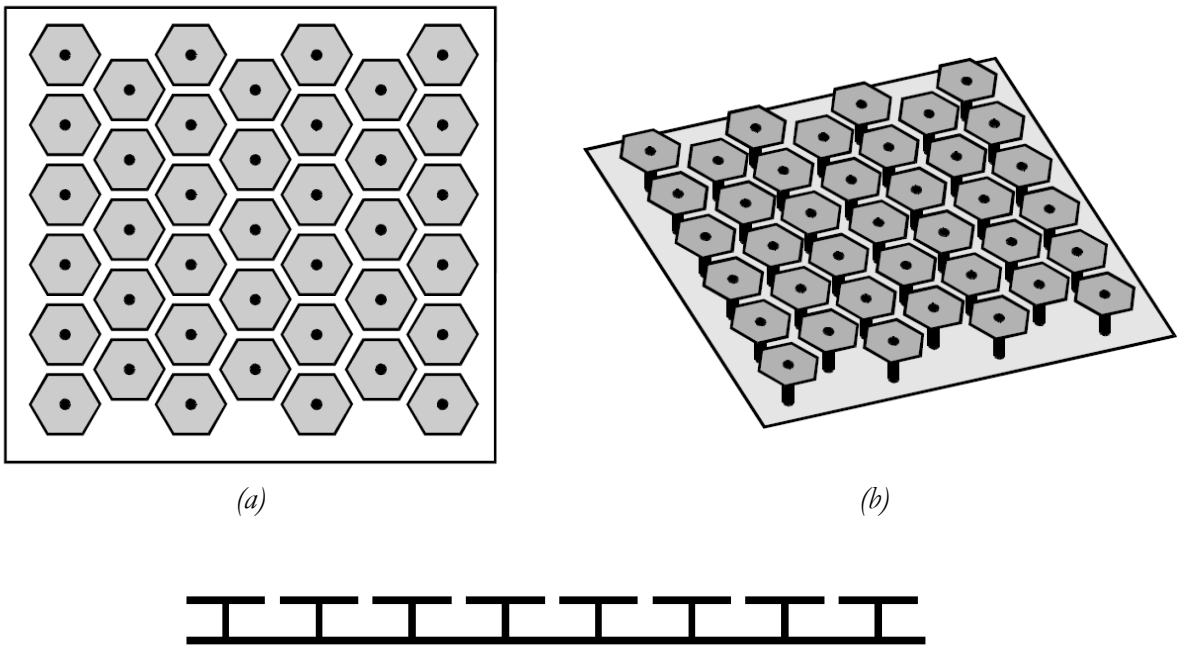

(a) *(b)*

(c)

Figure I.9. (a) Top view, (b) Perspective view and (c) cross-section of the high-impedance surface of Sivenpiper [14].

The principle of Sievenpiper was later used by *Tretyakov and al.* as an alternative design strategy to reduce the thickness of a Salisbury screen absorber with a HIS that has metallic patches instead of the thumbtacks (Figure I.10 (a)) [15]. Here, the HIS is composed of a dielectric layer of 3 mm thickness where on the top

of this latter, a square patch array is printed. An absorption peak at 2.3 GHz has been obtained with a layer thickness of only λ/50.

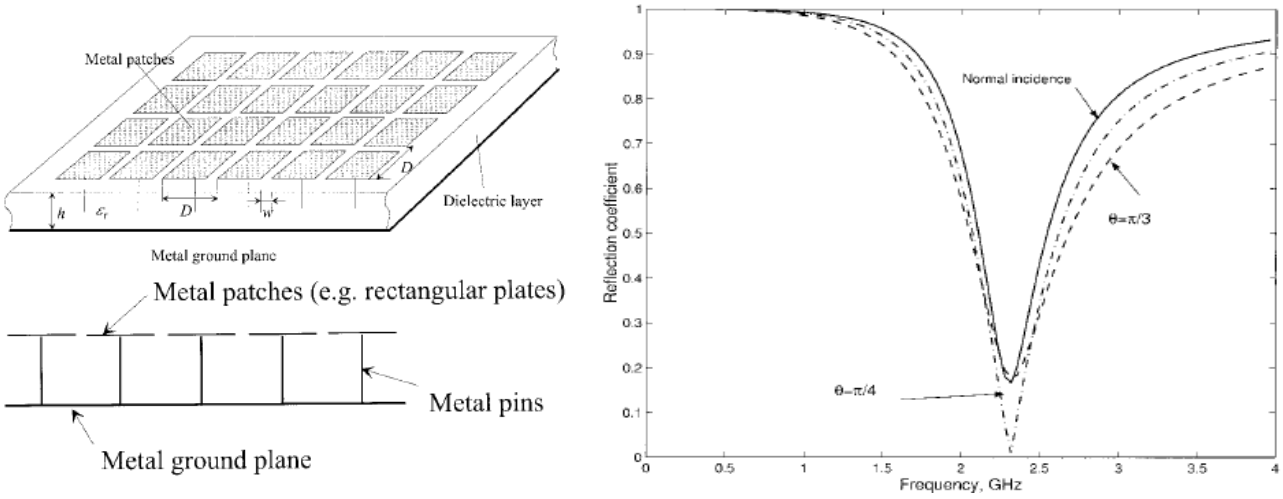

(a) *(b)*

Figure I.10. (a) Proposed HIS and (b) its reflection coefficient [15].

Before this, the idea of a metamaterial (MM) as an absorber, based on the HIS principle, was firstly proposed by *Engheta* [16] in 2002, and the first MM was realized after that by *Landy and al.*, in 2005, in the gigahertz (GHz) domain [17]. Since then, many studies have been conducted concerning metamaterials for electromagnetic wave absorption in various frequency ranges, such as microwave [18–20], terahertz [21, 22], infrared [23] and visible spectral region [24, 25]. Metamaterials (MM) have found their applications in radar cross section reduction [26], military target stealth missions [27], human exposure to electromagnetic fields protection [28], frequency tuning [29] and antenna gain enhancement [30].

Common MMs mainly consist of printed arrays of a conductive pattern (a periodic unit cell), on a thin dielectric substrate which is metallized at the back. The resonances that occur in this case depend on the size, shape and arrangement of the patterns. Figure I.11 shows the first metamaterial based absorber proposed by *Landy and al.* [17]. It consists of three layers: an electric ring resonator (ERR) pattern at the top layer, a substrate and a cut wire at the back layer as shown in Figure I.11 (a). A simulated absorption peak of around 99% has been obtained at 11.48 GHz, as shown in Figure I.11 (b).

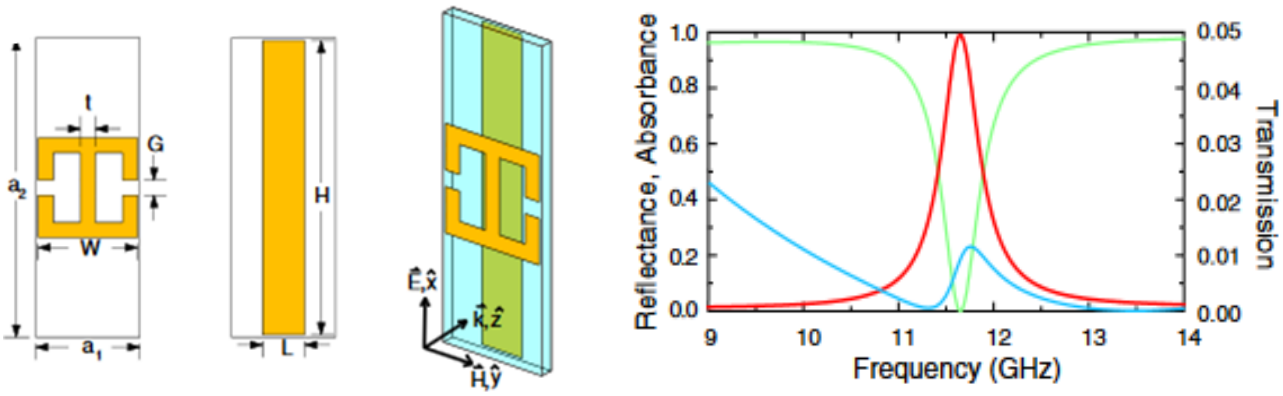

(a) *(b)*

Figure I.11. Simulated reflection coefficient (green line), absorption coefficient (red line) and transmission coefficient (blue line) of the MM perfect absorber [17].

Generally, as the MM absorption occurs only at the resonant frequency, the absorption bandwidth is considered as narrowband as in [31–36]. However, it could be considered as a multi-resonance absorber when it resonates at different frequencies [37–46]. An example of a multi-resonance MM over multiple bands is shown in Figure I.12 (a). The proposed MM is composed of a unit cell of 10 mm x 10 mm made of copper with thickness t_1 = 0.018 mm and a substrate dielectric layer, with permittivity ε_r' = 4, tangent loss tanδ = 0.02 and a thickness of t_2 = 0.78 mm [46]. The simulation results of the absorption of the proposed MM are shown in Figure I.12 (b). Three absorption peaks at frequencies 4.06 GHz, 6.73 GHz and 9.22 GHz have been obtained with an absorption of 0.99, 0.93, and 0.95, respectively [46].

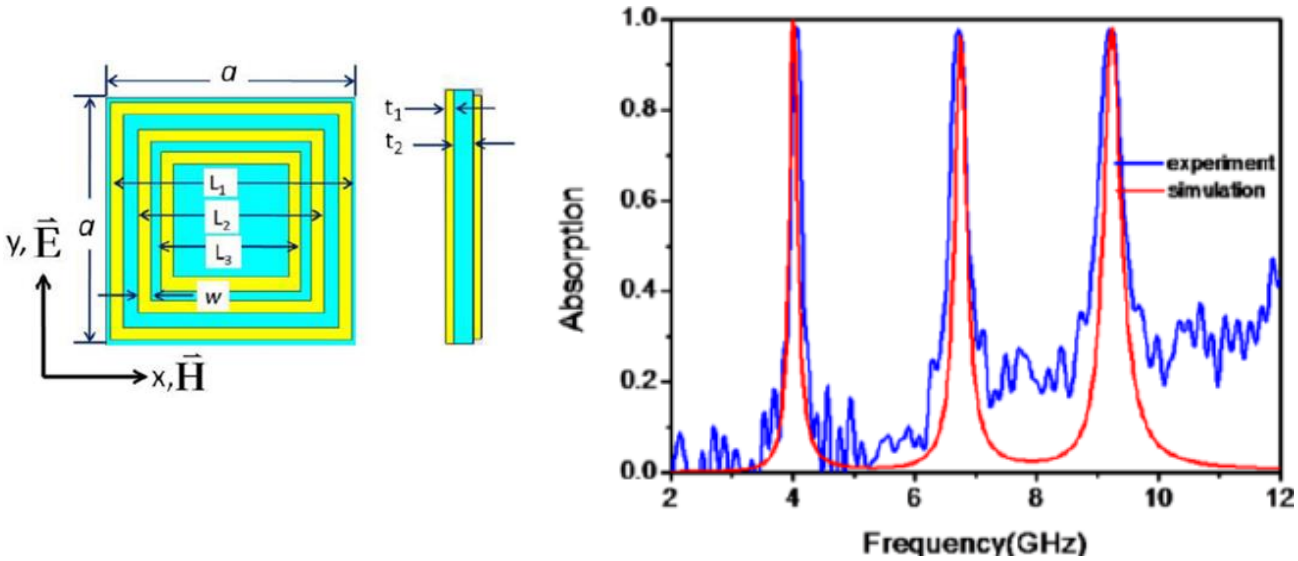

(a) *(b)*

Figure I.12. (a) proposed multi-resonance MM and (b) its simulated reflection coefficient [46].

4.2 Broadband microwave absorbers

4.2.1 Pyramidal and multilayer absorbers

Broadband absorbers are materials that absorb over a wide frequency range. These absorbers are generally very thick. In fact, the thickness becomes more important when the frequencies to be absorbed are low. This is directly related to the skin depth which is inversely proportional to the frequency.

To broaden the absorption bandwidth of an absorbing material, a gradient of impedance should be realized. The front face of the absorber should have close impedance to that of air (377 Ω); then the impedance decreases gradually in depth till reaching the back layer where a PEC (0 Ω) is placed. Consequently, we have two methods that could be applied here to obtain a gradual impedance. The first one is realized by changing the shape of the material, ensuring a geometrical transition of the EM waves [47] (Figure I.13 (a)), while the second method is realized by tapering multiple layers ensuring a gradient of impedance and forming a multilayer absorber (Figure I.13 (b)). The idea behind this gradient is to create a slowly varying transition from free space into a lossy material using gradual shapes or loads. Consequently, the waves are gradually absorbed in the depth and the total reflection is minimized.

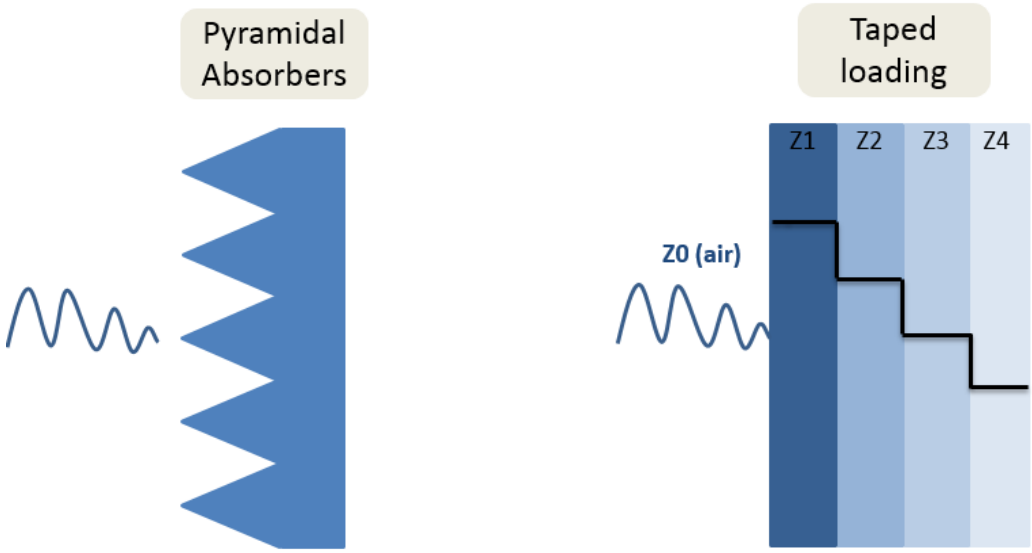

(a) (b)

Figure I.13. Impedance matching applying (a) a geometric transition using the pyramidal shape and (b) multilayer configuration.

For the first method, several standard shapes such as pyramidal, truncated pyramid, wedge, convoluted and others, have been tested. The most common shape is the pyramid (Figure I.14 (a)), that is usually used in anechoic chambers, because it ensures the best geometrical transition among all geometries. In addition to that, the EM waves will be trapped between the pyramids, contributing to the minimization of the total reflection of the waves. This type of absorbers become huge when are used for low frequencies at normal incidence (Figure I.14 (b))) [48].

GUARANTEED REFLECTIVITY PERFORMANCES (dB) OF APM ABSORBERS (normal incidence)

TYPE	Total overall height		80 MHz	200 MHz	300 MHz	500 MHz	1 GHz	2 GHz	4 GHz	8 GHz	12 GHz	18 GHz	40 GHz
	mm	in											
APM 3	28	1.1							-17	-17	-23	-23	-30
APM 5	55	2.2						-20	-21	-25	-31	-35	-38
APM 9	89	3.5					-16	-20	-29	-35	-40	-43	-40
APM 12	115	4.5					-19	-20	-33	-40	-45	-50	-40
APM 20	210	8.3				-13	-25	-36	-45	-46	-52	-51	-44
APM 30	305	12				-25	-36	-40	-48	-52	-52	-51	-45
APM 45	455	18				-27	-40	-42	-50	-52	-52	-51	-45
APM 55	550	21.6			-26	-36	-44	-44	-50	-52	-52	-51	-45
APM 66	660	26	-6	-21	-26	-37	-45	-47	-52	-52	-52	-51	-45
APM 85	850	33.5	-10	-25	-28	-42	-49	-50	-52	-52	-52	-51	-45
APM 100	1000	39.4	-11	-26	-36	-45	-50	-52	-52	-52	-52	-51	-45
APM 115	1150	43.7	-16	-26	-36	-45	-50	-52	-52	-52	-52	-51	-45

(a) (b)

Figure I.14. (a) Pyramidal absorber APM by SIEPEL and (b) its guaranteed reflectivity at normal incidence[48].

For the multilayer configuration [49], the absorber is composed of several flat sheets or layers (Figure I.13 (b)) where the electrical parameters within the sheets will vary continuously with depth, in order to have the minimum discontinuity of the impedance with the free space. Thus, the EM waves will penetrate into

the core of the material that is gradually charged, they are thus gradually dissipated inside it. By this configuration, a gradual impedance, from front to back, will be ensured as shown schematically in Figure I.13 (b). However, wherever there is a mismatch of impedance between layers, reflections will occur. The calculation of the impedances of the materials to be used to compose a multilayer absorber could serve in choosing the sequence of the material in the multilayer absorber; this point will be presented later in this manuscript.

An example that shows the advantageous use of the multilayer absorbers over the monolayer absorbers is presented in [50], where a multilayer absorber based on carbon nanotubes dispersed in a poly (ε-caprolactone) polymer foam with graded concentration of CNTs has been developed. The multilayer absorber was composed of three foaming layers with concentrations of 0.5 wt.%, 1 wt.% and 2 wt.%, respectively for the first, second and third layers (Figure I.15 (a)). The proposed multilayer absorber shows a better reflection coefficient than the monolayers of each composite alone in the X-band (Figure I.15 (b).

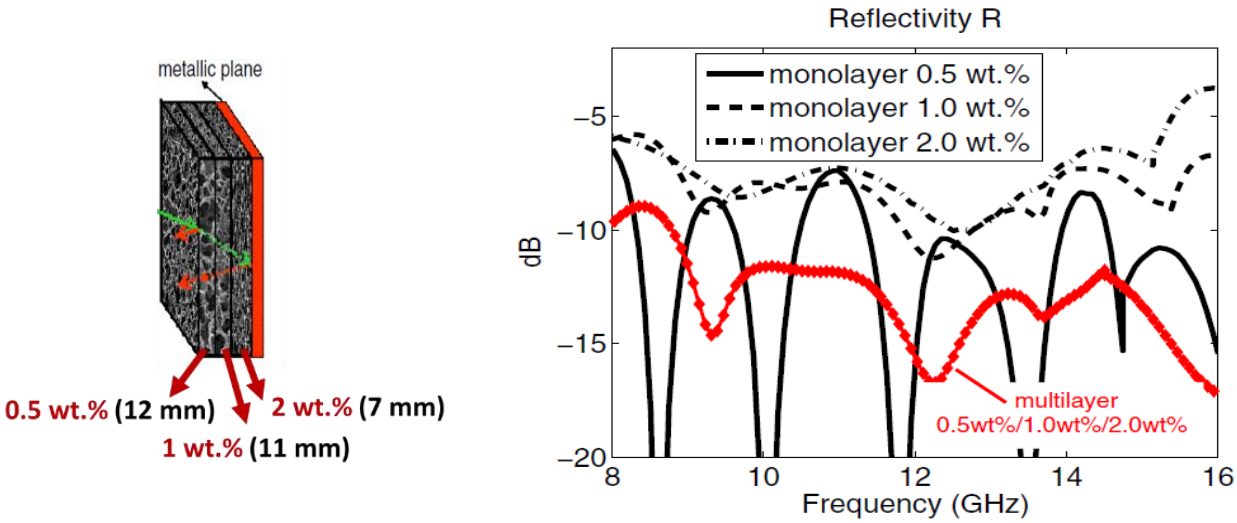

(a) *(b)*

Figure I.15. A multilayered foam of poly (ε-caprolactone) with gradual concentrations of CNTs (a) and its simulated reflection coefficients (b) [50].

Another example that shows the effect of the gradual concentrations from the lowest to the highest and from the highest to the lowest loads is presented in [51], where Ni nanoparticles are used as magnetic fillers for the multilayer absorbers. To achieve an effective absorber, tri-layer structure based on paraffin loaded with 30 wt.%, 50 wt.% and 60 wt.% of Ni nanoparticles was realized (Figure I.16). Two cases were tested: in the first case, the composites are stacked as following from back to front: metallic plate / 60 wt.% / 50 wt.% / 30 w.t% (Figure I.16 (a)), while in the second case, the layers were reversed as metallic plate /30 wt.% / 50 wt.% / 60 wt.% (Figure I.16 (b)). As expected, the absorption properties for the first case are more effective than the second case in the whole frequency range with a reflection coefficient less than -20 dB at some frequencies. This verifies that the impedance matching at the interfaces (between the layers) occurred when the gradient of the dielectric and magnetic properties is achieved from the lowest (ε_{r1} and μ_{r1}) to the highest (ε_{r3} and μ_{r3}).

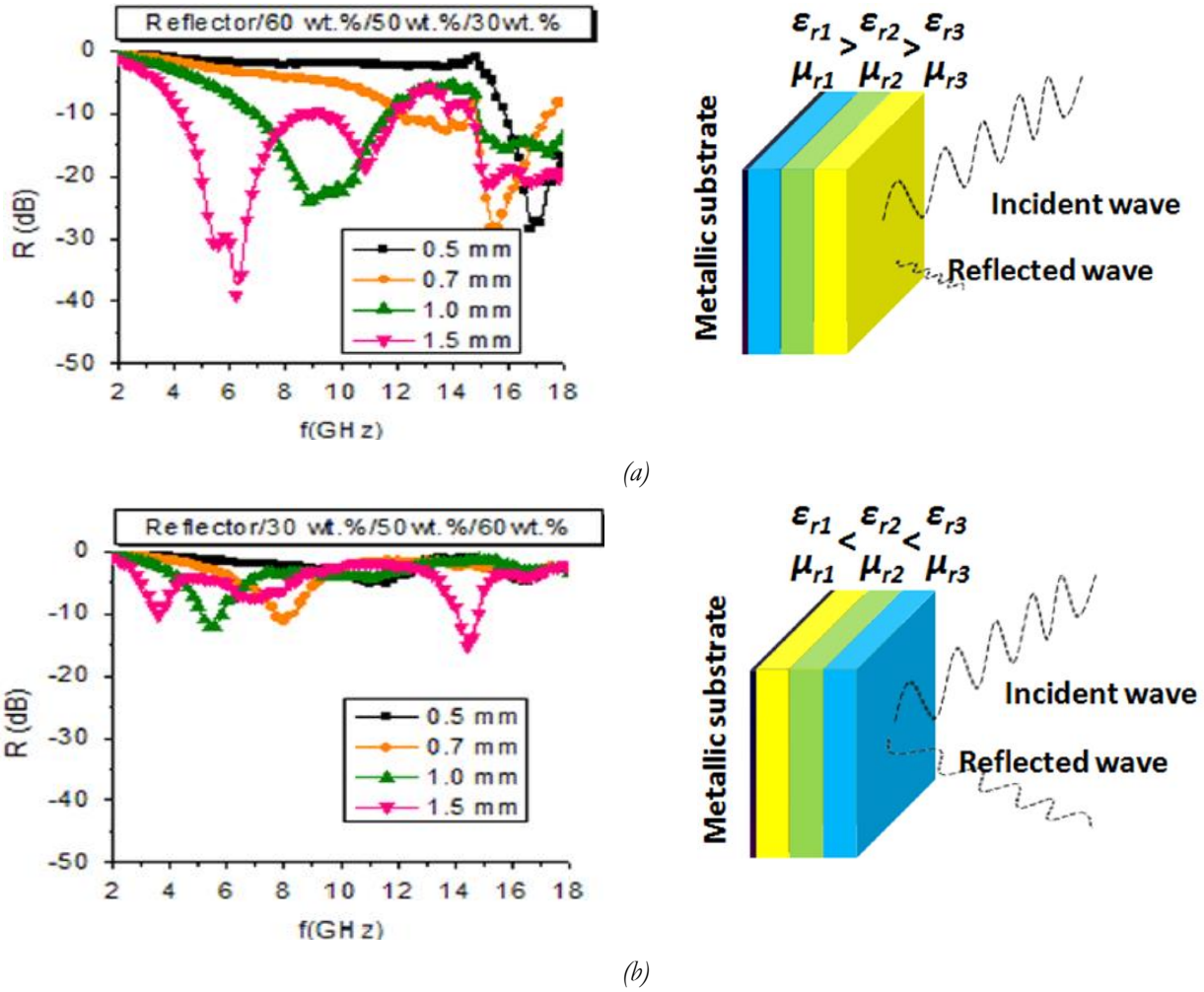

Figure I.16. Reflection coefficients of the tri-layer absorbers with two different gradients of the dielectric and magnetic properties varying them from the lowest to the highest (a) and from the highest to the lowest (b) [51].

Recently, and in the same concept, *Vong and al.* have proposed a multilayer absorber with a total thickness of 10 mm [52]; this multilayer absorber is composed of 17 layers. The simulated reflection coefficients for three tested types of charge (charge 1, charge 2 and charge 3) are shown in Figure I.17; a reflection coefficient less than -17 dB was obtained between 8.5 GHz and 18 GHz when charge 1 was used.

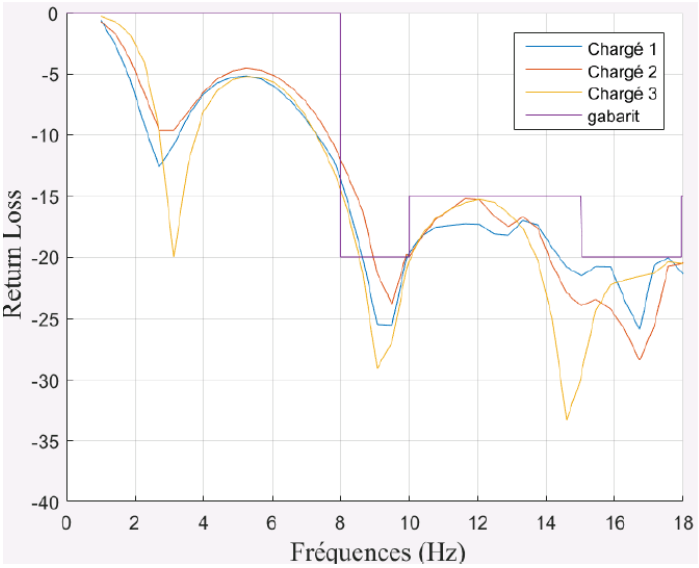

Figure I.17. Reflection coefficient of the proposed multilayer [52].

The last example of multilayer absorber presented here is one of the commercial multilayer absorbers, AH from SIEPEL. This type of absorbers has a typical reflectivity of -20 dB in a wide band depending on the total thickness (Figure I.18 (b)) [48].

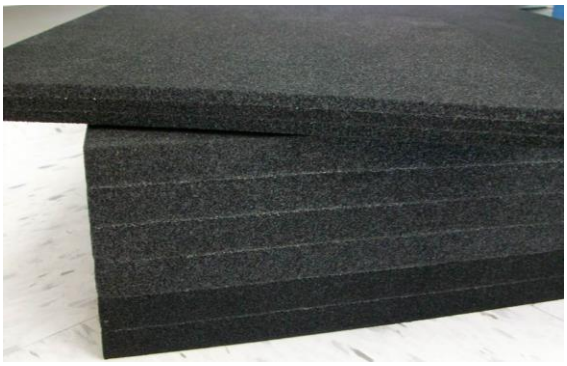

Type	e Thickness of one layer	E Total thickness	Frequency in GHz	Weight in kg
AH 25	5 mm	25 mm	9 to 100	0.56
AH 30	6 mm	30 mm	5 to 100	0.67
AH 40	8 mm	40 mm	2.4 to 100	0.89
AH 75	15 mm	75 mm	0.95 to 100	1.65
AH100	20 mm	100 mm	0.8 to 100	2.22
AH 125	25 mm	125 mm	0.6 to 100	2.78
AH 250	50 mm	250 mm	0.45 to 100	5.55

Typical reflectivity: - 20 dB, at mentioned frequencies.

(a) *(b)*

Figure I.18. (a) A multilayered polyurethane foams loaded with carbon particles and (b) guaranteed reflection coefficients for the AH absorbers from SIEPEL at normal incidence [48].

4.2.2 Metamaterial absorbers

Generally, metamaterials are considered as resonant absorbers, but many efforts have been made in the literature in order to achieve multiband, broadband, or ultra-wideband microwave MM absorbers. In fact, there are many effective solutions that have been proposed in the literature for enhancing the absorption bandwidth of MM absorbers; for instance, combining various absorption peaks by combining multiple resonating structures with different sizes or shapes [53]–[55]. Stacking different MM structures [56] or stacking multiple metallic/dielectric layers, forming a pyramid [21, 56] or a cylinder [58], were also tested. Sometimes, layers composing the multilayer MM absorber are separated by a spacer (such as air) [58, 59]. Incorporating lumped elements into the MM resonators [61]–[66] is also another useful method that broaden the absorption bandwidth. As one of the aims of this thesis is to broaden the metamaterial absorption bandwidth, different examples of the cited methods are detailed below; here, bandwidth of MM absorbers, with an absorption of 90 %, corresponding to -10 dB of reflection coefficient will be presented.

a) MM absorbers combining different resonators

A first method of broadening the absorption bandwidth is based on the combination of various absorption peaks by combining multiple resonating structures with different sizes or shapes [53]–[55], [67]–[69]. As a result, multiple close resonances will appear in the absorption spectrum. If these frequency resonances are very close to each other, they will form a broadband absorption, if not, they will form a multi-resonance absorber. In [54], for example, a unit cell of 8 mm x 8 mm, with a ring resonator of a radius R = 1.3 mm deposited on FR-4 substrate with a total thickness of 0.4 mm was used (Figure I.19 (a)); this structure resonates at 16 GHz (Figure I.19 (b)). To broaden the absorption bandwidth, the same ring

resonator has been used nine times with different sizes (with radii that ranges from 1.5 mm to 2.14 mm) in the same unit cell of 30 mm x 30 mm and with the same total thickness as the single ring resonator structure. A 2 GHz absorption bandwidth, between 10.5 and 12.7 GHz, has been obtained using this method (Figure I.19 (c)).

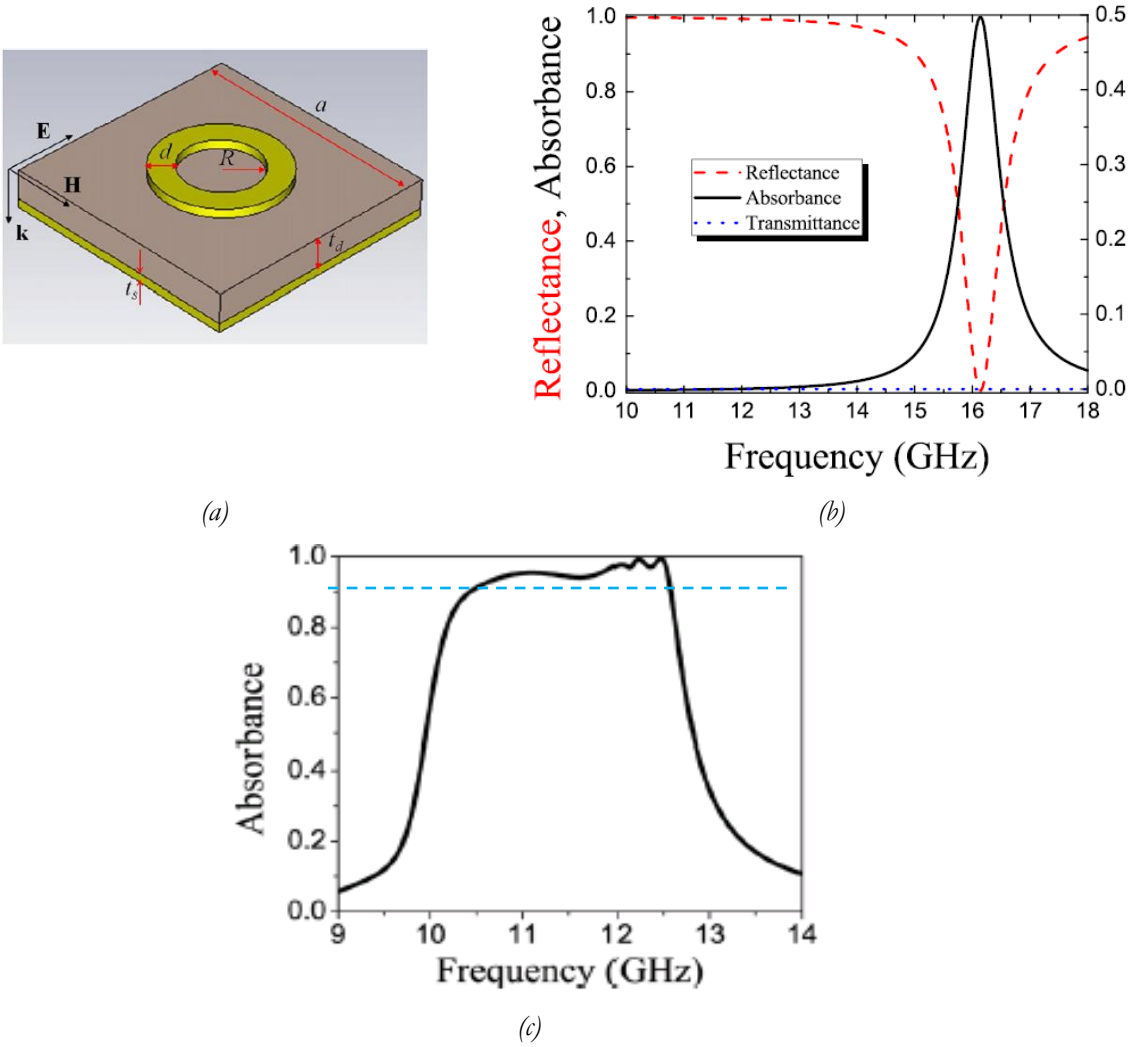

Figure I.19. The design (a) and the absorption performance of MM with single ring resonator (b) and with several rings (c) [54].

b) Multilayer and/or 3D MM absorbers

A second method was used in literatures to broaden the absorption bandwidth, it is about stacking multiple layers [55, 58, 59, 69–71]. In [70] for example, three MM absorbers (SRR1, SRR2 and SRR3), with different dimensions of the Split Ring Resonator (SRR) and a lossy substrate at the front surface of each proposed MM (Figure I.20 (a)), present three different resonances in the range [2-8 GHz] (Figure I.20 (b)) depending on the dimensions of the SRR. Metamaterial of multilayered SRRs structure with 4.25 mm total thickness, by combining the three MM absorbers (SRR1, SRR2 and SRR3) in a multilayer structure where a substrate of a thickness d_4 = 2.25 mm is placed at the front surface of the MM absorber, was proposed (Figure I.20 (c)). As a result, an absorption bandwidth of 20 GHz, between 10 and 30 GHz, has been obtained (green curve in Figure I.20 (d)). By this way, they have broadened the absorption bandwidth of the SRR MM absorber.

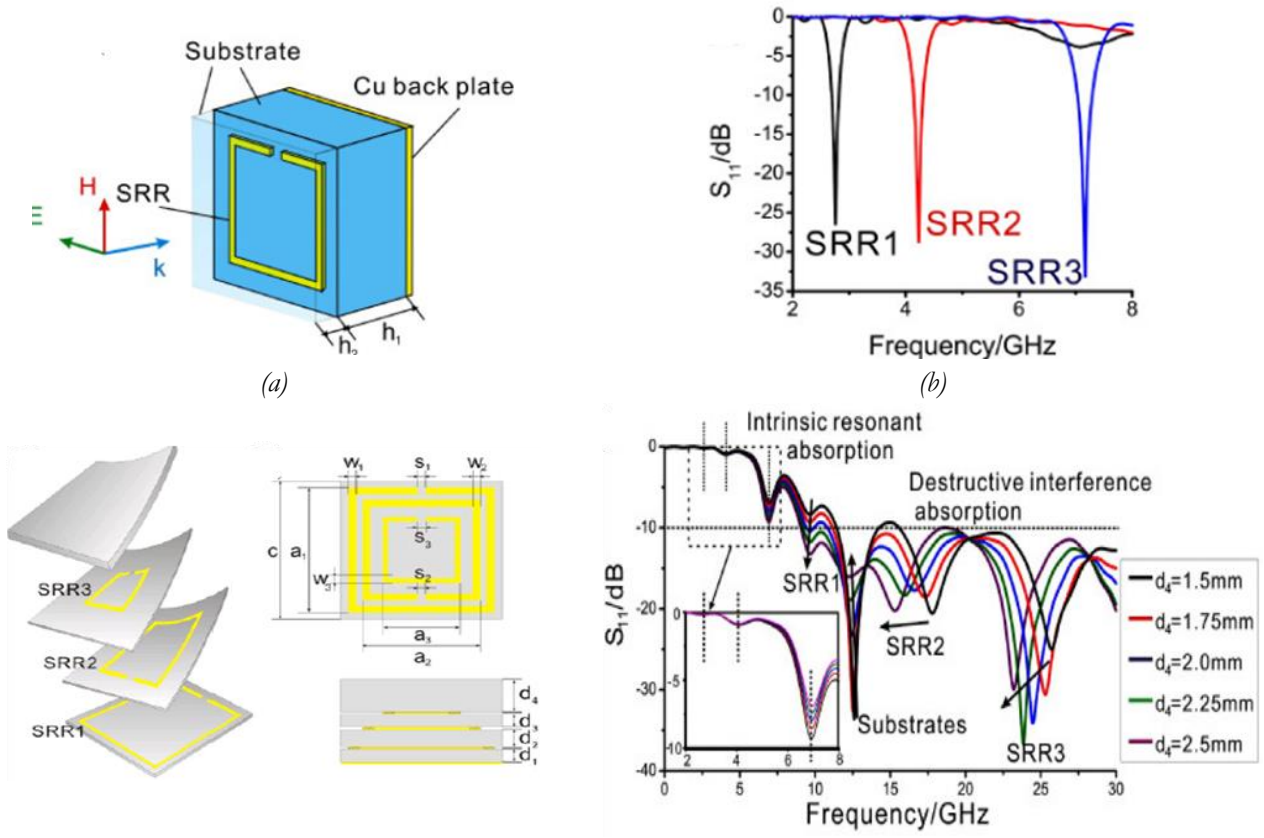

Figure I.20. The MM design (a) and reflection coefficients of three MMs with three different dimensions of a single SRR resonator (SRR1, SRR2 and SRR3) (b) and multilayer SRRs (c) [70].

In [59], two dielectric layers, separated by an air gap of 1.5 mm, with two different resonator shapes, half-moon-shaped resonator (HMSR) in the first layer and a ring-shaped resonator (RSR) in the second layer, were used to compose a multilayer MM absorber (Figure I.21 (a)). In case 'b' where only the first layer (HMSR), backed with a metallic plate was tested, three resonances have been obtained (blue line in Figure I.21 (b)). To broaden the absorption bandwidth, a second layer (RSR) was placed 1.5 mm away from the first layer, at the top, with a total thickness of 5.2 mm of the proposed MM absorber (red line in Figure I.21 (b)). As a result, a dual absorption bandwidth have been obtained between 4.8 and 7.2 GHz and between 8 and 11.1 GHz (red line Figure I.21 (b)) and a broad absorption bandwidth was realized.

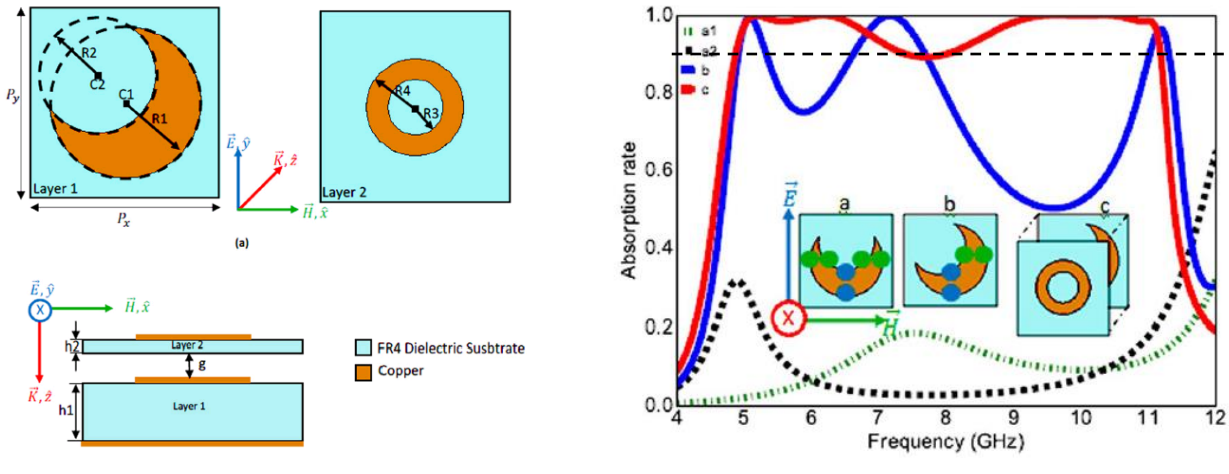

Figure I.21. The design (a) and absorption performance of (b) multilayer MM using (HMSR and RSR resonators [59].

In [73], the multilayer structure is composed of dielectric layers, metasurfaces and wide-angle impedance matching layers (WAIM) in order to minimize the impedance discontinuity between the absorber and free space, improving by that the absorption performance. The proposed multilayer absorber has a total thickness of 11.5 mm and it is presented in Figure I.22 (a); the simulated and measured reflection coefficients are presented in Figure I.22 (b). At normal incidence, a reflection coefficient less than -10 dB has been obtained, by simulation and measurement, between 3.7 GHz and 17.5 GHz. This bandwidth ratio is slightly reduced at oblique incidence for the TE and TM polarizations, but the proposed MM absorber remains very broadband.

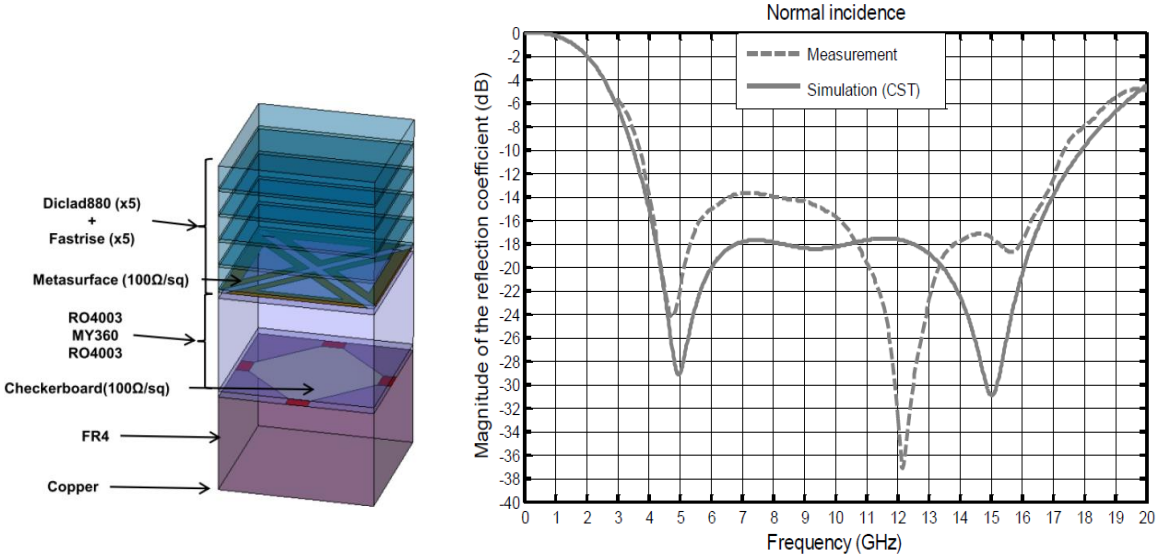

(a) *(b)*

Figure I.22. The design (a) and the reflection coefficient of (b) the proposed multilayer structure [73].

To broaden the absorption bandwidth, dielectric substrates were also stacked in a multilayer structure and separated by metallic layers forming a 3D MM absorber in pyramidal [57], [74] or cylindrical [58] geometries. For example, in the case of pyramidal shape (Figure I.23 (a)) [57], the absorber is composed of 20 metallic patches with their width increasing linearly from the top to the bottom where every two adjacent metallic patches are separated by a dielectric substrate (FR-4). Below these layers, a copper film and a FR-4 substrate were added (Figure I.23 (a)). A thickness of 0.05 mm for each copper layer and 0.2 mm for each FR-4 layer, with a total thickness of 5 mm, were used for this prototype. As a result, an absorption bandwidth of 6 GHz has been achieved in the range of frequency 8-14 GHz (Figure I.23 (b)).

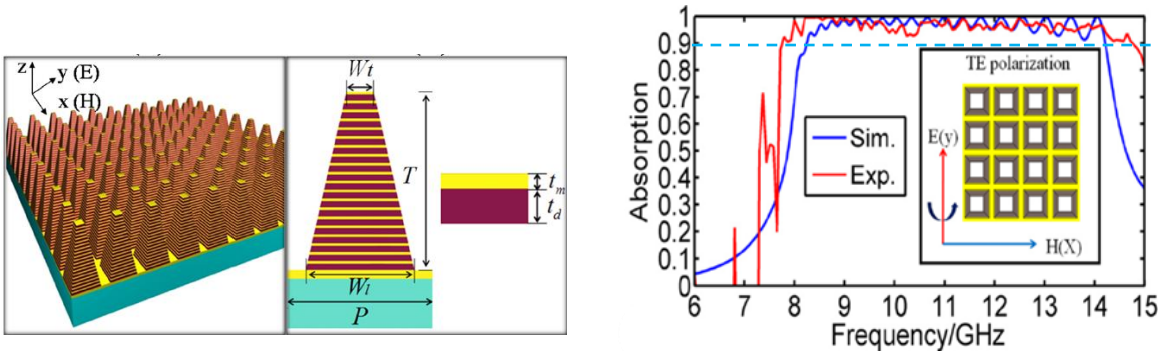

(a) *(b)*

Figure I.23. The design (a) and absorption performance of (b) 3D Pyramidal MMs [57].

The same principle was used to develop a microwave MM in a 3D cylindrical structure ; here, 29 metallic and dielectric pair-layers with a total thickness of 6.3 mm (Figure I.24 (a)) were stacked [58]. A dual broadband absorption bandwidth, of 2 GHz, was achieved by this cylindrical shape in the frequency bands [4-6 GHz] and [12-14 GHz] (Figure I.24 (b)).

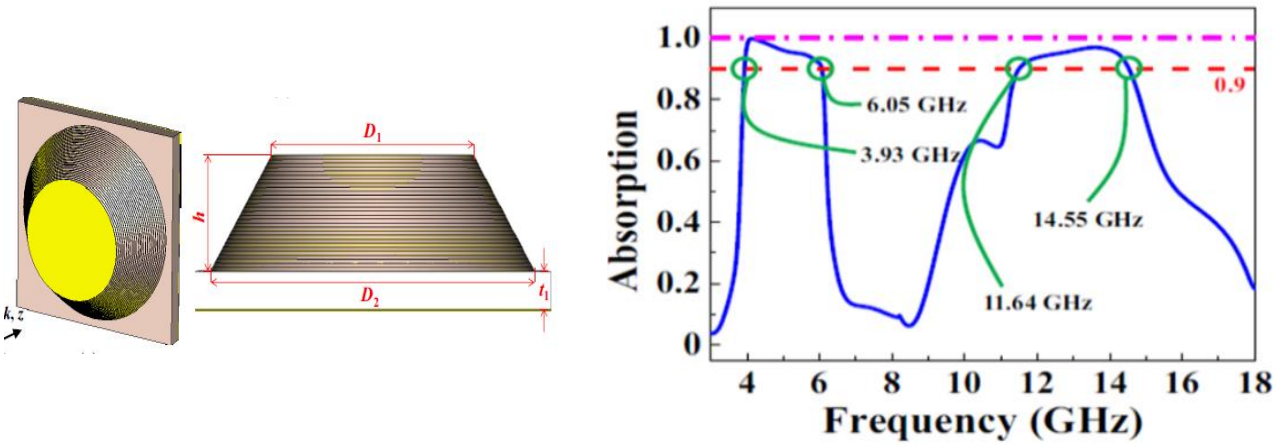

(a) *(b)*

Figure I.24. The design (a) and absorption performance (b) of 3D cylindrical MMs [58].

c) MM absorbers incorporating lumped elements

Another approach has been used to realize a broadband MM absorber by incorporating lumped elements into the MM resonators [65, 64, 63, 61, 62, 60, 75–79]. It aims to match the input impedance with that of free space over a wide frequency range. In [66], for example, a split circle ring (SCR) loaded with four lumped resistors, with R = 250 Ω, was proposed for X-band applications (Figure I.25 (a)). MM without lumped resistors provides one absorption peak at 12.5 GHz, while incorporating four lumped resistors in the same MM absorber exhibits a broadband absorption performance in the frequency range between 7.8 GHz and 12.6 GHz (Figure I.25 (b)).

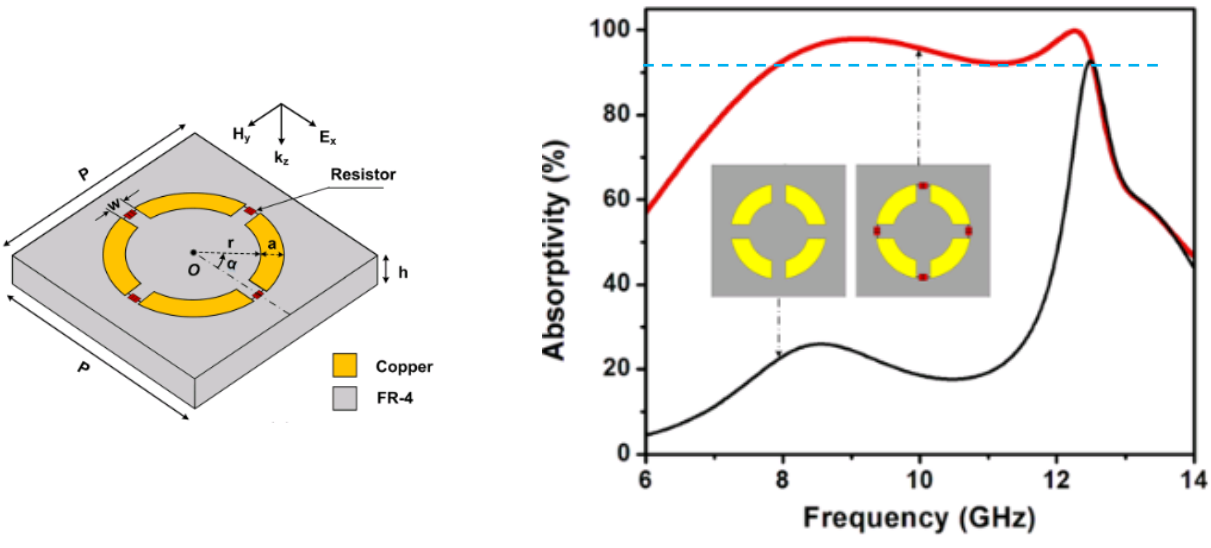

(a) *(b)*

Figure I.25. The design (a) and absorption performance of (b) SCR resonator using lumped elements [66].

Figure I.26 (a) shows the design of the proposed broadband absorber in [76], based on a multilayer MM loaded with lumped elements. It consists of two layers, each one with a metal (patch) printed on dielectric layers, separated by a spacer. The top and bottom metal patches are loaded with lumped resistors at the center of each of the four edges of the squares as shown in Figure I.26 (a). Here, an air spacer of 3 mm has been used between the two layers, and the overall structure has been backed by a metallic plate. Simulated reflection coefficients of the proposed wideband absorber with and without the lumped resistors are presented in Figure I.26 (b). Without lumped resistors, simulation of the proposed MM shows small peaks at 4.40, 10.46, and 18.40 GHz, with reflection coefficients of −5.85 dB, −1.15 dB and −5.08 dB, respectively. However, when resistors are used in the designed absorber, the reflection coefficient becomes less than −10 dB in the frequency range of 4.96–18.22 GHz with three main resonances at 5.76 GHz, 11 GHz and 17.28 GHz with reflection coefficients of −16.81 dB, −18.88 dB and −12.29 dB, respectively.

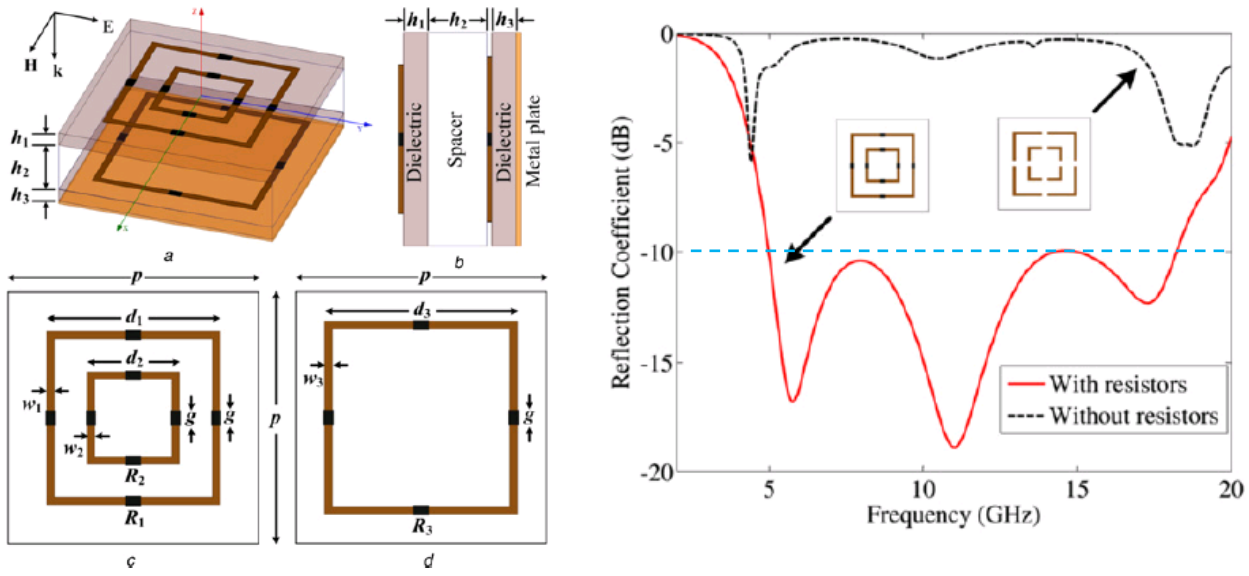

(a) (b)

Figure I.26. (a) Design of the proposed MM and (b) the simulated reflection coefficients with and without lumped elements in [76].

5. Classification of the microwave absorbers as function of their compositions

5.1 Absorbers based on magnetic losses

The magnetic absorbing materials are usually composed of metallic or ferrite powder loaded matrix. This type of absorbers ensures an important absorption performance associated with a thin thickness; they have acquired particular interest because of their absorption performance not only at frequencies below 2 GHz [80–82], but also at frequencies above 2 GHz [83, 84]. However, this important absorption is counterbalanced by their important densities due to the mass of the atoms constituting them (such as iron), which limits their applications [9]. These materials also present a dielectric permittivity greater than 1, so they are not purely magnetic; they can thus exhibit impedance close to that of air, especially when μ_r is close to ε_r. In this part, some examples of magnetic materials that are used to make absorbers for different (wide or narrow) frequency ranges are presented.

a) Metallic particles:

Kim and al. have proposed a rubber matrix with a thickness of 1 mm loaded with 65 vol % iron flake (thin plate) particles, obtained by a milling process from different initial particle size (2 μm, 7μm and 70 μm) [85]. A resonance was obtained between 3 and 4 GHz, with a reflection coefficient less than −10 dB, for the composite containing an initial particle size of 2 μm (Figure I.27). The absorbing bandwidth shifts to lower frequencies, between 1 and 2 GHz, with a reflection coefficient less than −5 dB (Figure I.27) when flakes from particle size of 7 μm were used. However, when flakes achieved from particles of 70 μm are used, a bad reflection coefficient (about −1 dB) was obtained in the studied frequency range.

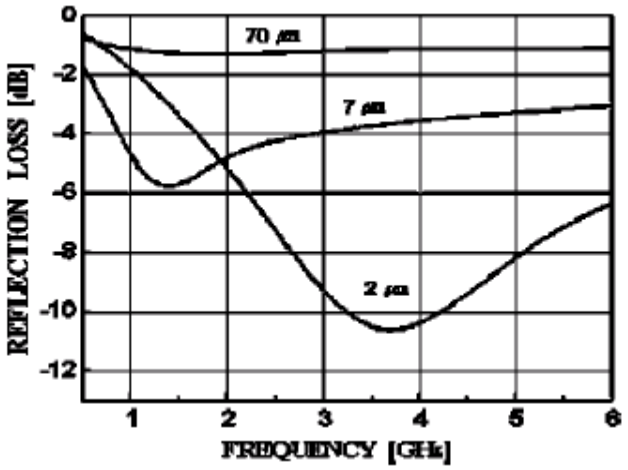

Figure I.27. Reflection coefficients of the rubber matrix containing iron flakes of different initial particle sizes (2 μm, 7μm and 70 μm) [85].

In [80], *Li and al.* have developed monolayer epoxy resin composites with 50 vol% Fe nanowires using different thicknesses. Resonant reflection coefficients less than -10 dB for frequencies between 0.8 GHz and 2.1 GHz, depending on the thickness of the absorber (between 2 mm and 4 mm), have been obtained ensuring by that the absorption at the L-band, as shown in Figure I.28 [80]. The reflection loss peak shifts toward a lower frequency as the absorber thickness increases. From here, it can be verified that not only the filler type, but also the thickness of the absorber have an influence on the absorption peak and its intensity. However, the thickness of these absorbers is very low, but their weights are always very high.

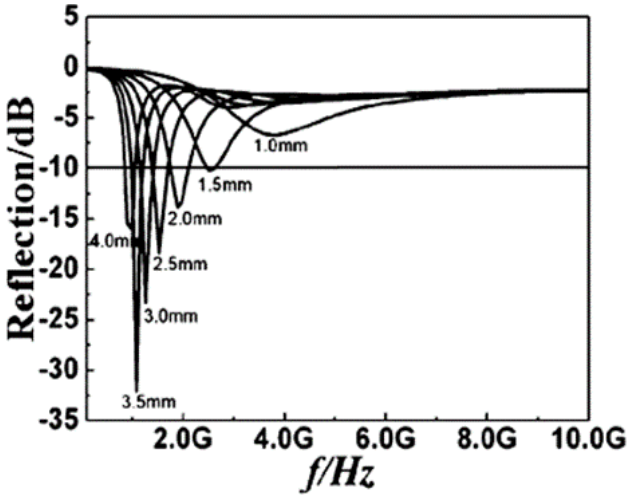

Figure I.28. Reflection coefficients of epoxy resin composites loaded with 50 vol% Fe nanowires using different thicknesses [80].

b) Carbonyl iron:

Carbonyl iron is one of the widely used materials in the magnetic microwave absorbing materials. It is an iron based material, which possesses both electric and magnetic properties [86]. In a dielectric matrix, carbonyl iron particles can be added until the percolation threshold is reached. In [87], *Wang and al.* have achieved a carbonyl iron/epoxy resin composite with a reflection coefficient less than -10 dB between 5.5 and 18 GHz for a thickness of 1.4 mm. This performance was obtained by orienting the petals of carbonyl iron in the matrix using a magnetic field. In [88], *Liu and al.* have used a thin microwave absorbing sheet loaded with carbonyl-iron powder (CIP) matrix, with an average particle diameter of 3.46 μm in chlorinated polyethylene (CPE). Reflection coefficients of 1#, 2#, 3#, 5#, 8# samples, with the same thickness (1mm) with the weight ratio (CIP:CPE) 10:1, 12:1, 14:1, 16:1, 17:1, are shown in Figure I.29 (a).

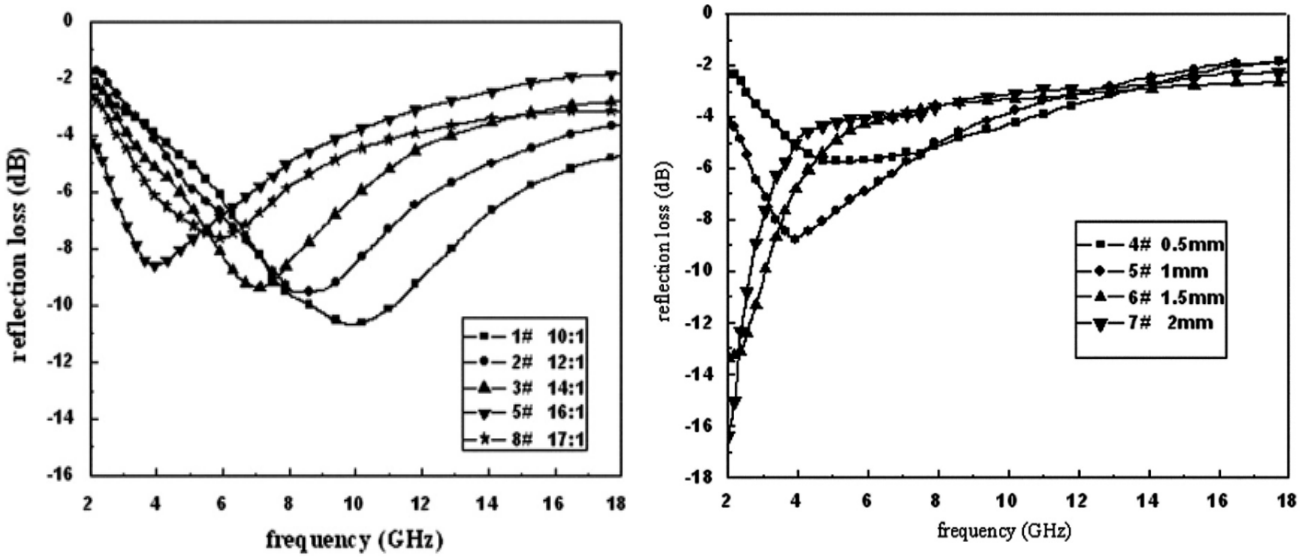

(a) *(b)*

Figure I.29. Reflection coefficients of the samples (a) with the same thickness (1 mm) and different weight ratios (CIP:CPE) (b) with the weight ratio (CIP:CPE) of 16:1 using different thicknesses [88].

In Figure I.29, the frequency of absorption peak shifts toward lower frequency when increasing the weight ratio up to 16:1. However, when the raising ratio is over 16:1, the frequency of absorption peak moves to higher frequency (sample 8# in Figure I.29 (a)). Reflection coefficient less than -10 dB was attained between 2–3.1 GHz, with a minimum reflection coefficient of -13.2 dB at 2.2 GHz with sample 6# (ratio 16:1) of 1.5 mm thickness, as shown in Figure I.29 (b).

c) Ferrites:

Absorbing materials based on ferrites (iron oxides) and other metal oxides [9] such as nickel and cobalt, are generally thin (few millimeters) so they remain very attractive materials. Many researches were carried out using the ferrite as a filler in polymers such as polyvinylchloride (PVC) [89, 90] and polyurethane [91]. In [90], for example, *Dosoudil and al.* have used both $Mn_{0.52}Zn_{0.43}Fe_{2.05}O_4$ and $Ni_{0.33}Zn_{0.67}Fe_2O_4$ ferrites as dual magnetic fillers in PVC polymer matrix. Different resonances with reflection coefficients less than -20 dB

are obtained in the frequency band of 0.6–3 GHz for the three tested sets (A, B and C) as a function of particle sizes (Figure I.30 (a)), concentrations (Figure I.30 (b)) and fraction ratios of the MnZn/NiZn ferrite fillers (Figure I.30 (c)). The absorption frequency peak shifts toward lower frequency when increasing filler particle size (Figure I.30 (a)) and concentration (Figure I.30 (b)).

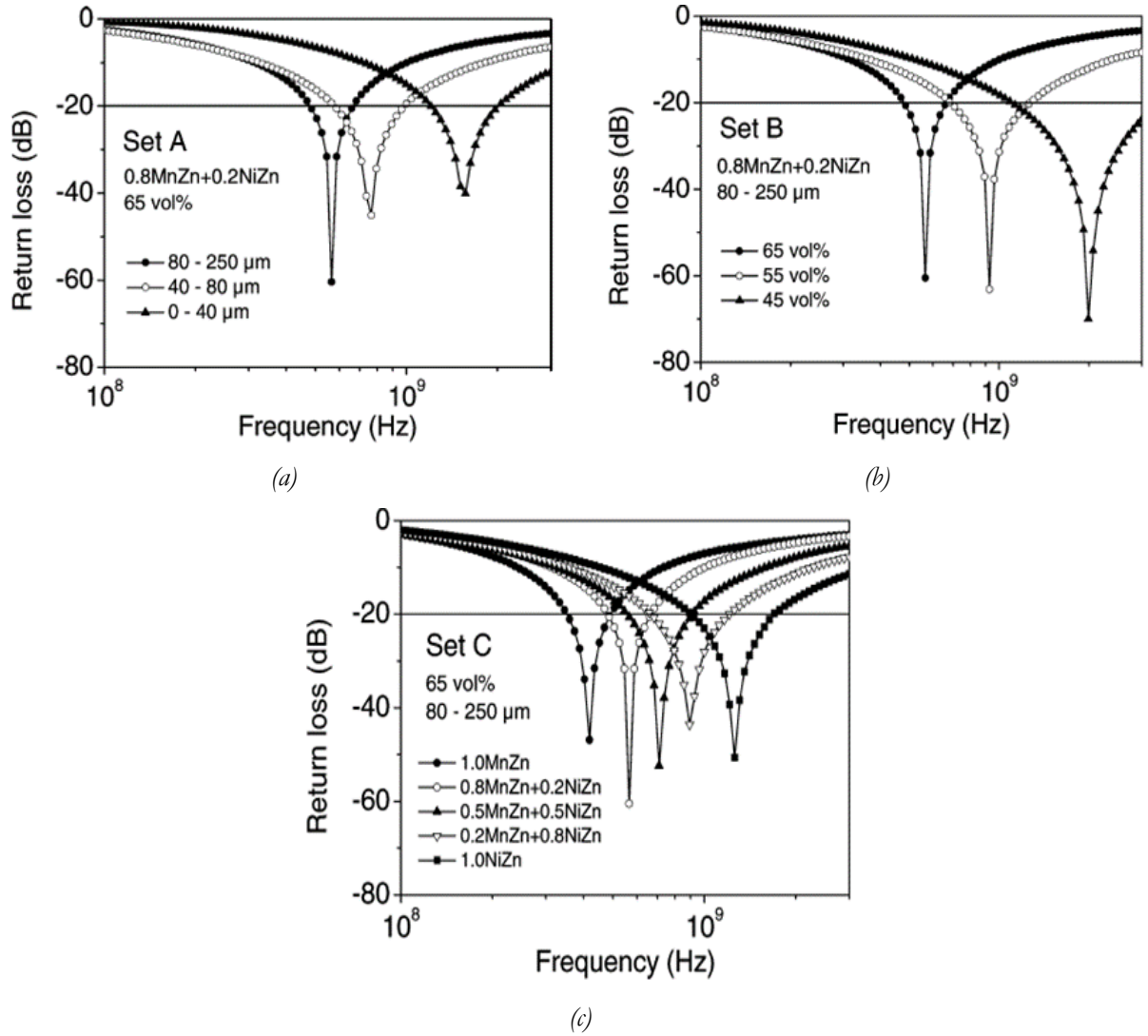

Figure I.30. Reflection coefficients of prepared composites for different (a) particle sizes, (b) concentrations, and (c) fraction ratios of the double MnZn/NiZn ferrite fillers [90].

Ferrites have been also used to form a double layer microwave absorbers. For example, in [92], when a single-layer absorber composed of nanocrystalline NiZn ferrite with 67 wt.% of ($Zn_{0.5}Ni_{0.5}Fe_2O_4$) microfibers and 33 wt.% wax was used, a reflection coefficient less than -10 dB has been obtained from 2.9 to 11.8 GHz with a thickness of 4.5 mm (Figure I.31 (a)). When another single-layer, which is composed of 50 wt.% of nanocrystalline iron (α-Fe) microfibers and 50 wt.% wax is used, a reflection coefficient less than -10 dB has been obtained in the range of 15–18 GHz for a thickness of 0.7 mm (Figure I.31 (b)). However, when a double-layer absorber, based on both layers with a thickness of 0.2 mm for the first layer based on α-Fe ferrite and a thickness of 1.8 mm for the second layer based on NiZn ferrite, was elaborated, a reflection coefficient less than -10 dB was achieved in a large bandwidth (7.8 –18 GHz) with a minimal reflection coefficient of -73 dB at 13.8 GHz (Figure I.31 (c)).

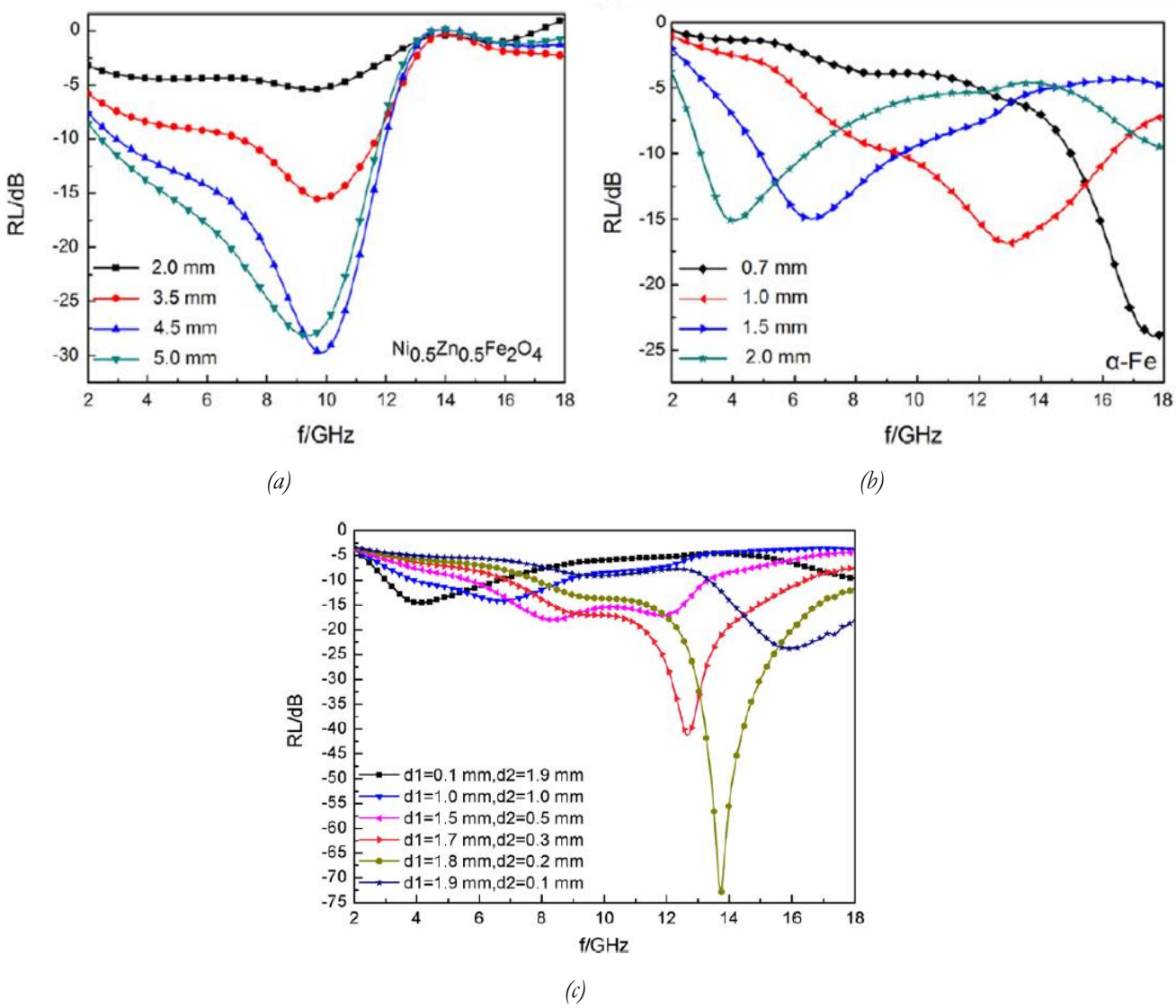

Figure I.31. Reflection coefficient of the single-layer absorber using NiZn ferrite (a) and (b) α-Fe and a double layer absorber (c) using both layers [92].

5.2 Absorbers based on dielectric losses

Generally, the dielectric absorbers are lower in density than the magnetic absorbers, but often present higher thickness. Materials based on dielectric losses are composed of either conductive polymers or dielectric matrices in which dielectric or conductive inclusions are added. Dielectric matrices are mainly resins, plastics or foams and conductive inclusions could be metallic particles or carbon loads (carbon black, carbon fibers, nanotubes with single or multiple walls and graphene). The conductive fillers are used to control only the complex permittivity and their weight percentages are very low compared to those of the magnetic fillers. Below, are presented the most frequently used inclusions and conductive polymers to develop dielectric microwave absorbers.

5.2.1 Dielectric matrices associated with dielectric inclusions

Dielectric inclusions, such as Silicon Carbide (SiC), are sometimes used as a filler in absorbing composites [93]–[96]. SiC presents a lightweight and high-temperature resistance, and adjustable electrical conductivity; an example, using this filler, is shown in [95] where SiC nanowire (SiCNW) loaded epoxy

composites of 2 mm thickness were elaborated and studied in the range of 2-18 GHz. The effect of adding SiC could not be seen until the concentration in the composite reaches 35 wt.% with a reflection loss of -31.7 dB at 8.3 GHz (Figure I.32).

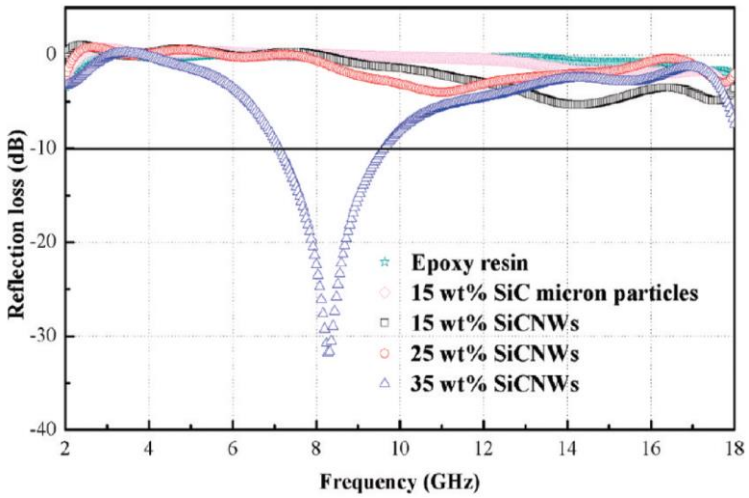

Figure I.32. Reflection coefficients of the epoxy resin, composite with 15 wt.% microparticles, and composites with 15, 25, and 35 wt.% of SiCNWs at 2-18 GHz [95].

In addition to that, SiC fiber was also used in the epoxy resin to form a monolayer [94]. Here, they have ensured an impedance matching between the air and the absorber in order to achieve an important absorption bandwidth. For this monolayer made of SiC/epoxy composite of 2 mm thickness (Figure I.33 (a)), a 3.2 GHz absorption bandwidth (-10 dB) was obtained; the minimum attained reflection coefficient is −26.0 dB at 10.1 GHz (Figure I.33 (b)) [94].

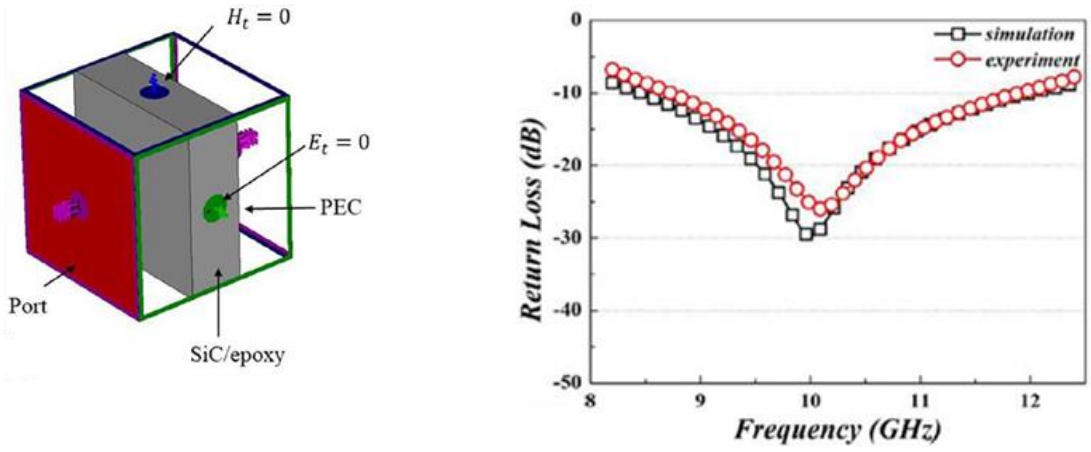

(a) *(b)*

Figure I.33. (a) SiC / epoxy monolayer and (b) its reflection coefficient [94].

5.2.2 Dielectric matrices associated with conductive inclusions

a) Metallic particles

Metallic particles such as copper and tungsten are non-ferromagnetic metals and are used as loads in the insulator in order to induce dielectric losses [97, 98]. For example, in [97], it was seen that the microwave absorption, at 2.45 GHz, by a pure copper powder depends on the particle size. Tungsten was also used as

a metallic inclusion to compose the tungsten-Teflon composite, for the microwave absorption at 2.45 GHz [98]. Here also, the particle size, as well as, the volume fraction of the tungsten particles have an effect on the dielectric losses and thus, on the absorption performance [98]. Figure I.34 presents the dielectric losses of three different particle sizes (from left to right: 0.7, 2.3 and 9.1 μm) of tungsten, as a function of their volume fraction p, in Teflon matrix. Results showed that when the particle size increases, the volume fraction p where the maximum of the losses tanδ is obtained also increases. For example, when the particle size is 0.7 μm, the maximum of the losses occur with a volume fraction p of 0.1 while for the particle size of 9.1 μm, a volume fraction of 0.4 is needed to get the maximum losses. In addition to that, the dielectric losses increase with the decrease of the particle size. For example, the maximum losses (tanδ ~ 0.34) are obtained for the particle size of 0.7 μm while the maximum losses of tanδ ~ 0.05 are obtained for the particle size of 9.1 μm.

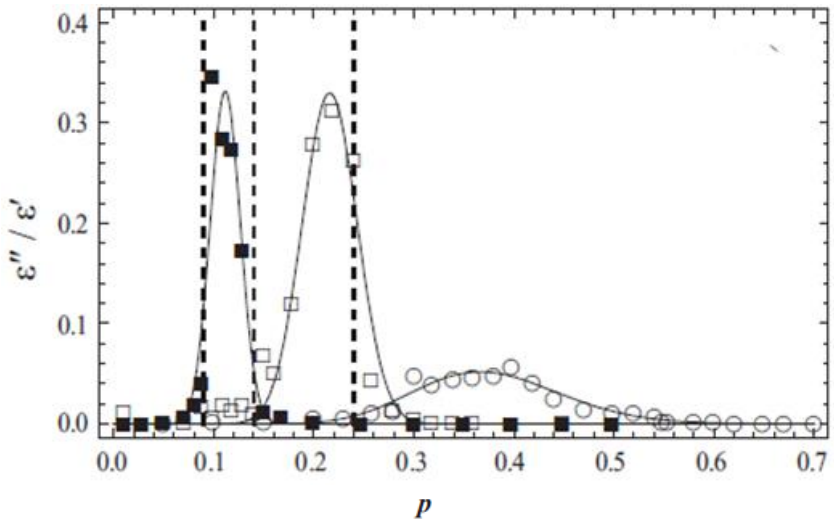

Figure I.34. Dielectric losses of the tungsten-Teflon composite as a function of metal volume fraction p (solid lines are the fit of the data) [98].

b) Carbon loads

1) Carbon black

Carbon black (CB) filled polymers have been widely employed for the last decades [99] in many applications, and particularly for absorbers used in anechoic chambers, because of their electrical conductivity, their absorption performance over a wide frequency range and their low cost [100–103]. In [103], carbon black loaded silicone rubber were prepared and investigated in 2-18 GHz frequency range; different CB weight percentages (wt.%) (Figure I.35 (a)) and different sample thicknesses (Figure I.35 (b)) were tested. The reflection coefficient decreases when CB wt.% increases from 0 wt.% to 10 wt.%, but above 20 wt.%, the reflection coefficient increases compared to the composite loaded with 10 wt.% (Figure I.35 (a)). This is because an impedance mismatching has occurred for composites loaded with high wt.% of CB (20 wt.% and 30 w.%). However, for the best composite loaded with 10 wt.% CB, the frequency of absorption, where the impedance matching has occurred, is shifted to lower frequencies with lower intensities when varying the sample thickness between 2 and 4 mm (Figure I.35 (b)).

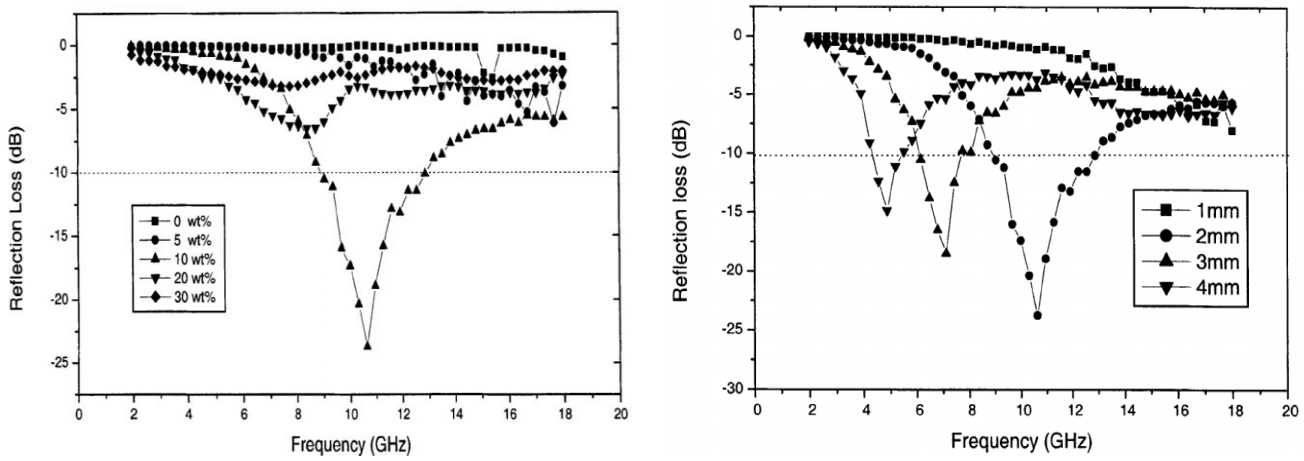

(a) *(b)*

Figure I.35. Simulated reflection loss (a) using different carbon black wt.% (composite thickness = 2 mm) and (b) using different thicknesses of the composite loaded with 10 wt.% CB [103].

CB was also used to elaborate multilayer absorbers; for example, *Jung-Hoon Oh and al.* have elaborated a double layer absorber made of glass fiber /epoxy composites loaded with carbon black (CB) with 7 wt.% for the first layer (0.65 mm thickness) and with 5 wt.% for the second layer (1.9 mm thickness) [100]. Reflection coefficient less than -10 dB with 2.4 GHz bandwidth, in the X-band, has been obtained (Figure I.36) with this double layer absorber.

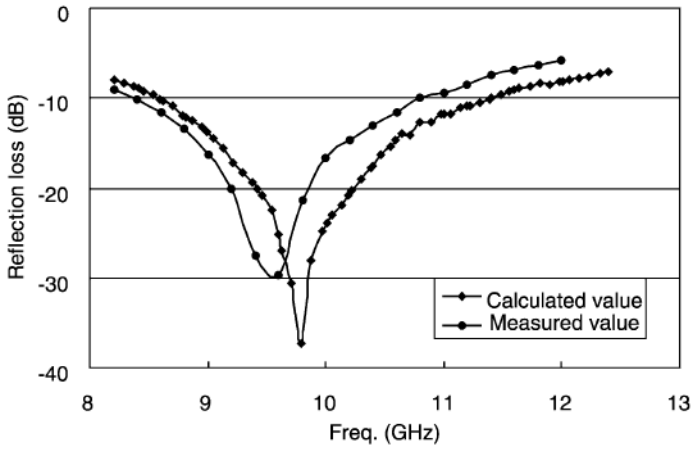

Figure I.36. Reflection coefficient of the double layer absorber based on glass fiber /epoxy composites loaded with CB [100].

2) Carbon nanotubes

Carbon nanotubes (CNTs) have been also widely studied as conductive fillers for microwave absorbing materials due to their physical and chemical properties [104]–[107]. Good absorbing materials with low concentrations could be elaborated due to the high form factor of CNTs associated with their excellent electrical conductivity. However, the use of CNTs is limited today due to their high cost.

CNTs exist in single-walled (SWNTs) and in multi-walled (MWNTs) carbon nanotubes. The electrical properties of SWNTs are different from the MWNT; thus, their EM absorbing properties are totally different.

In [105], composites of polyurethane of 2 mm thickness were elaborated with different weight percentages of SWNTs (0-25 wt.%). The composite loaded with 5 wt.% of SWNTs shows the best reflection coefficient peak of -22 dB at 8.8 GHz. The resonant frequency shifts to lower frequencies when increasing SWNT rates, but with lower performance (Figure I.37). Note that for 25 wt.% of SWNTs, the composite absorption performance becomes very low.

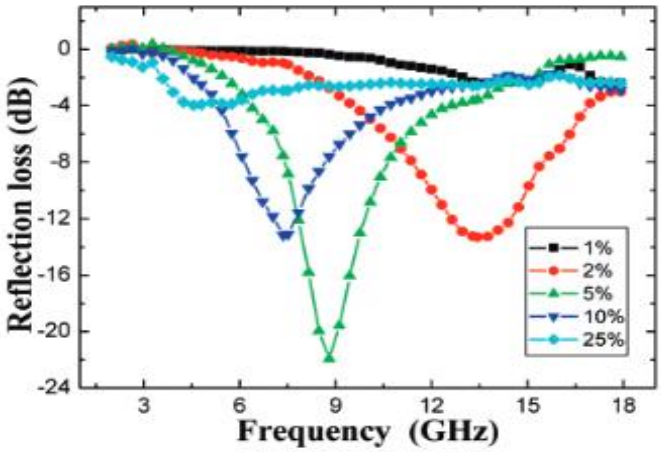

Figure I.37. Reflection coefficients of the SWNTs loaded polyurethane composites of 2 mm thickness using different wt.% of SWNTs (0-25 wt.%) [105].

MWNTs were used to elaborate different polymer based composites as microwave absorbing materials in [106]. In this example, the best resonances have occurred for 4 wt.% MWNTs/PET (2 mm thickness) and 8 wt.% MWNTs/varnish (1 mm thickness) composites at 7.6 GHz (-17.61 dB) and at 15.3 GHz (-24.27 dB), respectively (Figure I.38).

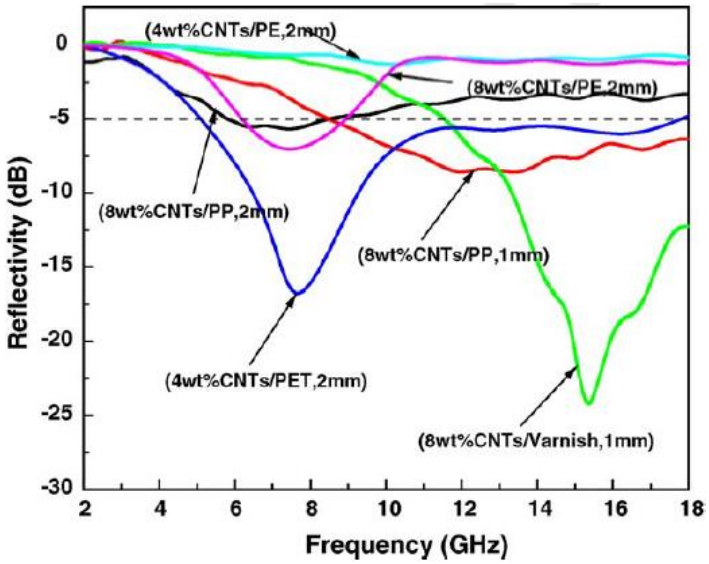

Figure I.38. Reflection coefficients of polymer composite, using the MWNTs [106].

MWNTs were also used to form multilayer absorbers [108]–[112]. In [108] for example, two multilayer absorbers were compared: a MWCNT-based multilayer absorber (Figure I.39 (a)) with a total thickness about ~ 10 mm and a graphite-based multilayer absorber (Figure I. 39 (c)) with a total thickness about ~ 11 mm. A broadband absorption was obtained by the MWCNT-based multilayer absorber in the X-band (8.2–

12.4 GHz), with a reflection coefficient less than -10 dB (Figure I. 39 (b)). It also shows a better reflection coefficient than the graphite-based multilayer absorber (Figure I. 39 (d)); for the latter absorber, the reflection coefficient is higher than -10 dB in all the studied frequency range. This result shows the poor performance of graphite with respect to carbon nanotubes [108]. From here, it can be seen that using low weights of CNTs, absorbers are more performant than those loaded with higher weights of graphite.

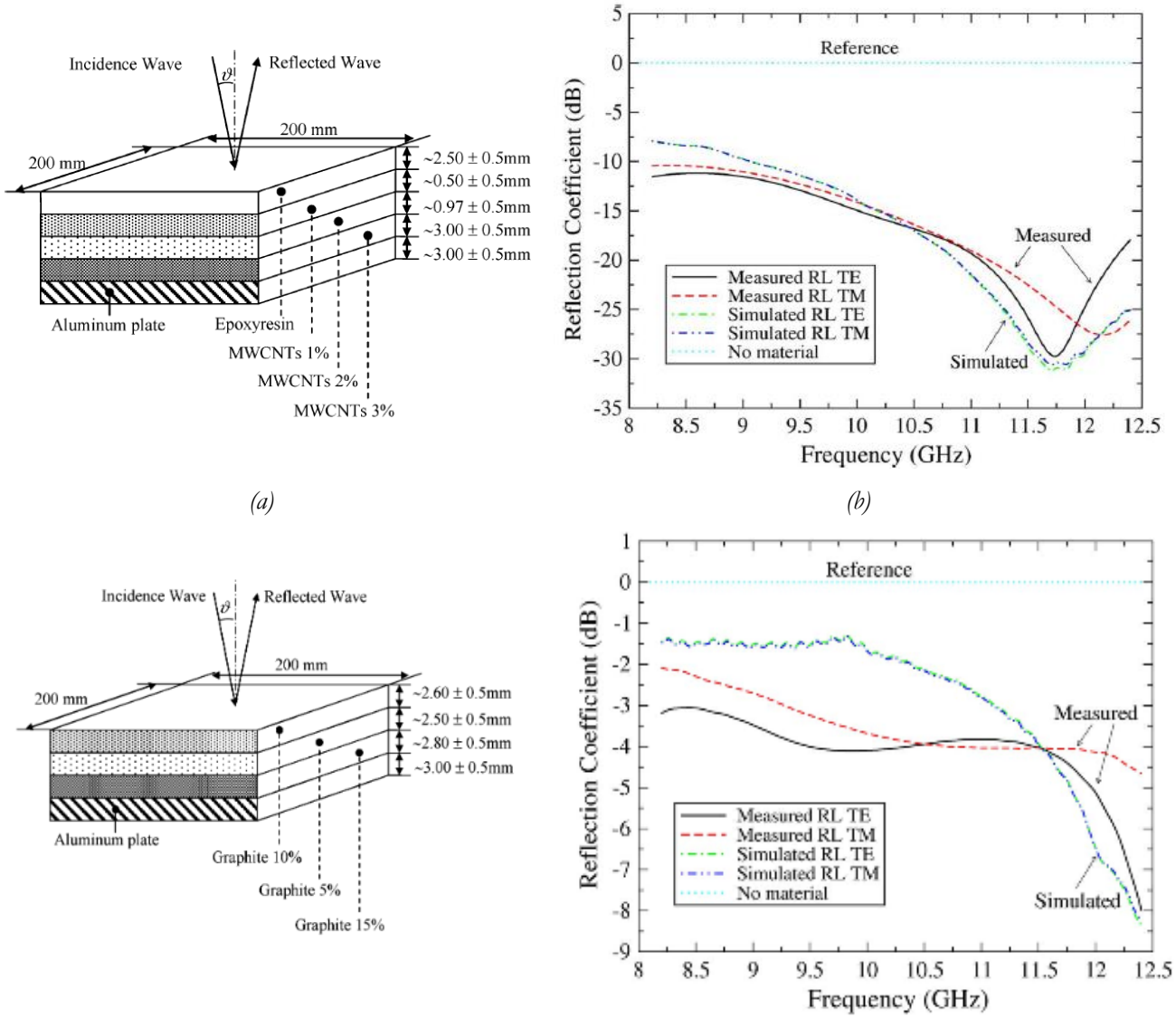

Figure I.39. (a) MWCNTs based and (c) Graphite based multilayer absorbers and (b) and (d) their corresponding reflection coefficients [108].

3) Carbon fibers

Carbon fiber (CF) is a conductive material that is widely used as a filler in absorbing materials due to its low density, high electrical conductivity, thermal stability and high mechanical strength [113, 114]. Several studies using the CF as a filler in microwave absorbers were conducted [113, 115–117]. In [115], for example, polyethylene and Ethylene–octene composites loaded with different contents (from 0 to 40 wt.%) of short carbon fibers (SCF) were prepared. The results show that the resonance is shifted to lower frequencies when the SCF weight increases and the bandwidth becomes wider. For example, the composite loaded with 20

wt.% shows a very weak absorption (Figure I.40) where the maximum achieved reflection loss is −4.15 dB at 13.2 GHz. However, the absorption peak of the sample loaded with 25 wt.% is shifted to lower frequency (6.8 GHz) with a reflection coefficient of −11.29 dB, and the reflection loss is below −10 dB in the range of 6.3–7.3 GHz. When increasing the load to 30 wt.% , two absorbing peaks at 4.6 GHz and 16.4 GHz of −15.66 dB and−17.37 dB, respectively, have appeared. In contrast, when the composites are loaded with 35 wt.% and 40 wt.%, no reflection coefficient lower than -10 dB is obtained.

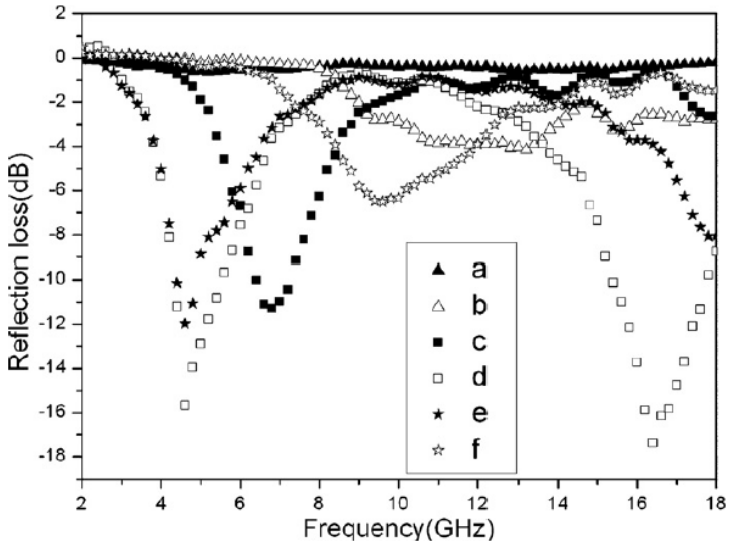

Figure I.40. Reflection coefficients of prepared composites loaded with different wt.% of the SCF (a) 0 wt.%, (b) 20 wt.%, (c) 25 wt.%, (d) 30 wt.%, (e) 35 wt.%, and (f) 40 wt.% [115].

5.2.3 Conductive polymers

Conductive polymers are widely studied because they have several advantages such as their low density. Polyaniline (PANI) and polypyrrole (PPy) are the most widely used conductive polymers for electromagnetic absorption [118]–[123]. However, conductive polymers are not used alone, they are often combined with magnetic materials, such as ferrites, to enhance their microwave absorption performance [124]. *Sun and al.* [118], for example, have prepared Fe_3O_4@SiO_2@PPy composite absorbers. The results demonstrated that the composite loaded with 30 wt.%, with a thickness of 3.7 mm, has a minimum reflection coefficient of -56.90 dB at 10.41 GHz and the widest effective absorbing bandwidth is 6.38 GHz with 3 mm thickness (Figure I.41).

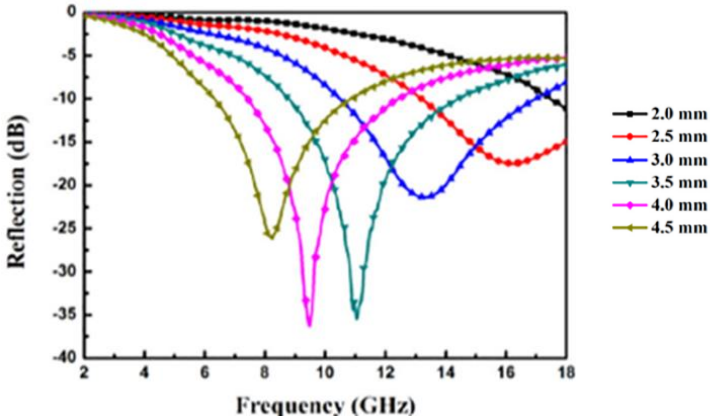

Figure I.41. Reflection coefficients of 30 wt.% hybrids for different thicknesses[118].

Conductive polymers were also used with carbon loads such as CB [102]. For this example, the mixture of the powders from PANI and CB (with different weight percentages of CB between 10 and 30 wt.%) and the epoxy resin were prepared for microwave absorbers; the mixing ratio of the powders to epoxy resin is 2: 1 by weight [102]. At 2-18 GHz, the resonance shifts toward relative lower frequencies with the increase of CB weight percentages, and its intensity increases as well (Figure I.42). Epoxy-PANI/CB(30) composite, loaded with 30 wt.% of CB, showed the best absorption between 9 and 13 GHz (X-band) among all elaborated composites.

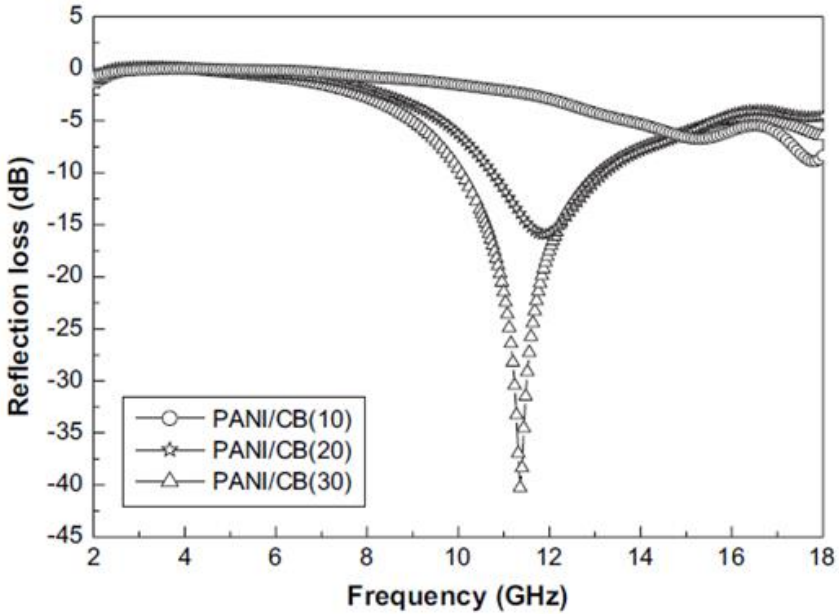

Figure I.42. The calculated reflection coefficient of the epoxy-PANI/CB composites at 2-18 GHz [102].

5.3 Absorbers based on dielectric and magnetic losses

Another way to improve the absorption performance of the absorbing materials is to combine dielectric loss materials with magnetic loss materials [125–128]. This combination allows the elaboration of an absorber whose impedance is close to air if and only if the magnetic and the dielectric properties are very close. Here are some examples of those materials.

In [125], the combination of copper-cobalt-nickel ferrite, polyaniline (conductive polymer) and graphene oxide was used as the absorbing load in polyurethane matrix; this mixture was used as coating on cotton fabric to prepare a flexible absorbing material. Compared to polyaniline and graphene oxide, the microwave absorption of the tri-composite was significantly enhanced with an achieved reflection coefficient of -33 dB at 10.8 GHz when a 40 wt.% coat is used and the thickness of the coated fabric is 2 mm [125] (Figure I.43). In addition to that, the resonance peak of the reflection coefficient shifts to lower frequencies when the wt.% increases (Figure I.43).

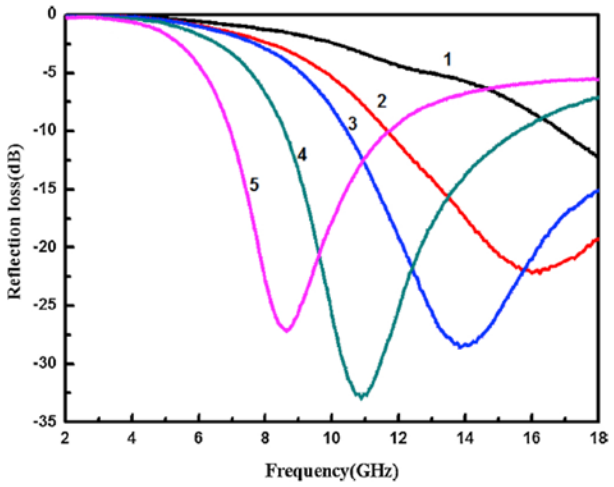

Figure I.43. Reflection coefficient of different wt.% of the absorbing loads based on (1-5): 10 wt.%, 20 wt. %, 30 wt.%, 40 wt.% and 50 wt.%.

Other works have been carried out by incorporating carbon fibers coated by magnetic materials, in absorber composites [129]. Figure I.44 (a) shows SEM image of a carbon fiber coated with Fe_3O_4 films [129]. Magnetite coated carbon fibers (MCCFs) /paraffin composite (50 wt.% of MCCFs) was prepared and a minimum reflection coefficient of −30 dB at 3.2 GHz, in a 4 mm layer thickness of, has been obtained (Figure I.44 (b)) [129].

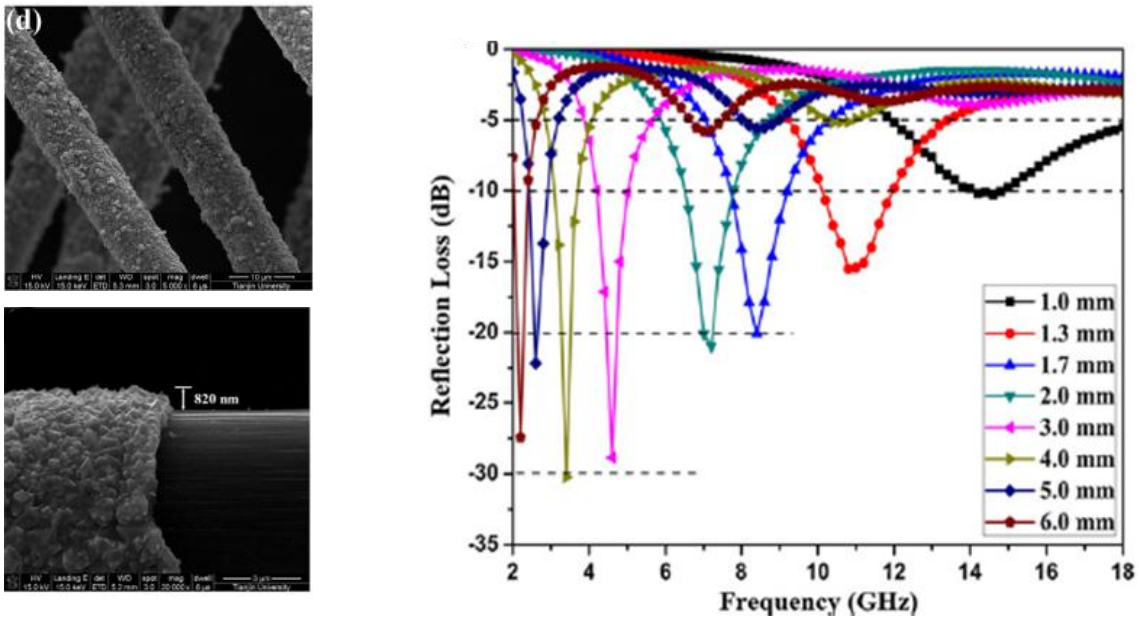

(a) *(b)*

Figure I.44. (a) SEM images of a carbon fiber coated with Fe_3O_4 film and (b) the reflection coefficients of the achieved composites using different thicknesses [129].

6. Motivations for epoxy loaded foams as absorbing materials

6.1 Absorbing materials used in the anechoic chambers

A non-reflective (echo-free) environment is used when the measurement of systems are needed. In fact, we are surrounded by several EM waves such as WIFI (at 2.4 GHz and 5 GHz), 3G (between 1.8 GHz and

2.5 GHz), 4G (between 2 GHz and 8 GHz), Bluetooth (at 2.4 GHz), etc…, and these operating frequencies may interfere with the operating frequency range of the systems we tend to measure. Therefore, it is necessary to build a measurement environment that prevents any external interference. To ensure this environment, the measurement room is placed in a Faraday cage, a shielded room, where walls, ceiling and floor are covered with large steel plates that prevent any EM transfer from outside [130]. Then, to remove the internal echoes that come from the multi-reflections caused by the metallic plates, absorbers will cover all surfaces, thus producing an anechoic environment.

One of the work at "Radiation Laboratory" during the 2nd war years was to invent a way to improve the accuracy of indoor measurements by Neher in 1945 [131]. His objective was to prevent or to reduce reflection of electromagnetic radiations from the inner and outer surfaces of the testing chamber. Therefore, he covered the inner surfaces with a pyramidal shaped absorber and he has demonstrated that the energy of the EM waves will be reflected several times between the pyramids and being reduced in magnitude with each reflection [131].

In 1953, the work on the production of the first commercial microwave absorbers has started, and in the same year, the first anechoic chamber was under investigation to be used for antenna measurements [1]. After this, anechoic chambers become dedicated for the measurements of electromagnetic compatibility (EMC) tests, electromagnetic interference (EMI) measurements and for variety of antenna measurements and microwave tests such as antenna radiation patterns.

Several shapes of microwave absorbers exist for anechoic chamber application such as the pyramids [48, 132], multilayers [48], [132]–[134], wedges [48, 132], honeycomb [135], the egg box (convoluted shape) [48, 132, 136], multi-layer pyramidal absorber [137], walk on absorbers (pyramidal box) [48, 132, 136], truncated pyramidal [132, 138], triangular pyramidal [139], cylinder pyramidal [140], double pyramidal [141], etc….

Most of the used absorbers in anechoic chambers are made of Polyurethane (PU) foam, with open cells, impregnated with carbon particles (carbon black). These absorbers have different advantages, such as their low density thanks to the presence of air bubbles. This will not only facilitate the installation of the absorbers on the walls and ceiling of the anechoic chambers, but also ensure a safety of the person who is doing a measurement. In fact, if a light absorber fall down, from the ceiling of the anechoic chamber, on someone performing a test, it will be less dangerous than an absorber of high density.

On the other hand, these foaming absorbers show several disadvantages. First of all, the flexibility of the PU foam does not allow the fabrication of complex shapes in the aim of enhancing the absorption [142]. Furthermore, the impregnation method, which is used to introduce the carbon particles in the pyramids, induces an inhomogeneous distribution of the load in the pyramids. In addition to that, the used elaboration method does not trap the carbon particles, which are volatile loads, inside the material. This will let the carbon particles easily escape from the matrix inducing a premature aging of the absorbers. This premature aging was observed by SEM photos of the commercial pyramidal absorber that are shown in Figure I.45

[143]. In this figure, one can clearly observe the absence of the load at the tip of the pyramidal absorber and its presence at its base. However, the escaped carbon particles from these absorbers are in the form of fine particles that may constitute a real danger to human health. From here, the need for a new material becomes necessary.

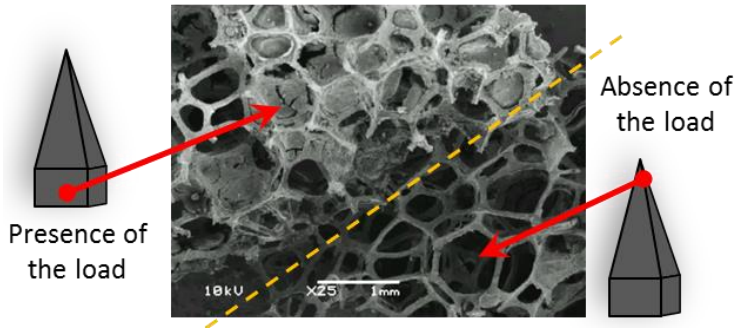

Figure I.45. SEM of a pyramidal absorber [143].

6.2 Absorbers used in this thesis

The Functional Materials team (FunMAT) of the 'Institut d'Electronique et des Technologies du numéRique' (IETR) from St-Brieuc has developed epoxy foam loaded with carbon fibers to overcome the disadvantages of the conventional used PU material [143]. The epoxy foam is characterized, like all polymer foams, by the low values of ε_r' and tanδ [143]. Carbon fibers, which are used as fillers inside the epoxy foam matrix, are nonvolatile loads and their use provide high dielectric losses for very low concentrations [144].

The elaboration technique of this composite material absorber will be detailed in chapter II; here, the carbon fibers (CFs) are dispersed in the epoxy foam during the elaboration process which makes them trapped inside the material. Like this, loads are situated on the walls of the foam as shown in Figure I.46, unlike the CB load used with the PU foam that are situated on the surface of the pores. By that, we are able to overcome the problem of the premature aging of the absorber and the danger obtained by the volatile carbon particles.

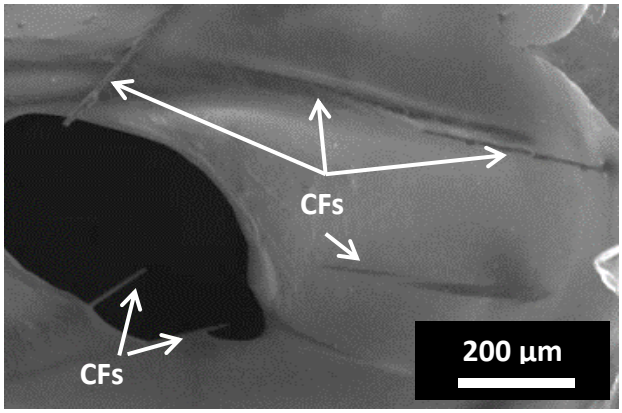

Figure I.46. SEM of CFs embedded in the composite [144].

In previous work of our team, the loaded epoxy foam composite was used for the elaboration of absorber prototypes (Figure I.47 and Figure I.48). In [143], a pyramidal absorber based on loaded epoxy

foam with 0.5 wt.% CF of 3 mm length was elaborated with the same dimensions of the commercial absorber APM 12 of SIEPEL. Photos of the elaborated prototype and the commercial absorber APM 12 are shown in Figure I.47 (a) and measurement results of these two prototypes are shown in Figure I.47 (b) and (c) for normal and oblique incidences (30°), respectively [143]. The elaborated absorber has a good absorption performance with a reflection coefficient Γ less than -20 dB, from 3 GHz, for both normal and oblique incidences. A better performance of the elaborated absorber has been obtained between 3 GHz and 7.5 GHz at normal incidence and from 3 GHz to 7 GHz at oblique incidence of 30°. Beyond that, both absorbers have the same performance.

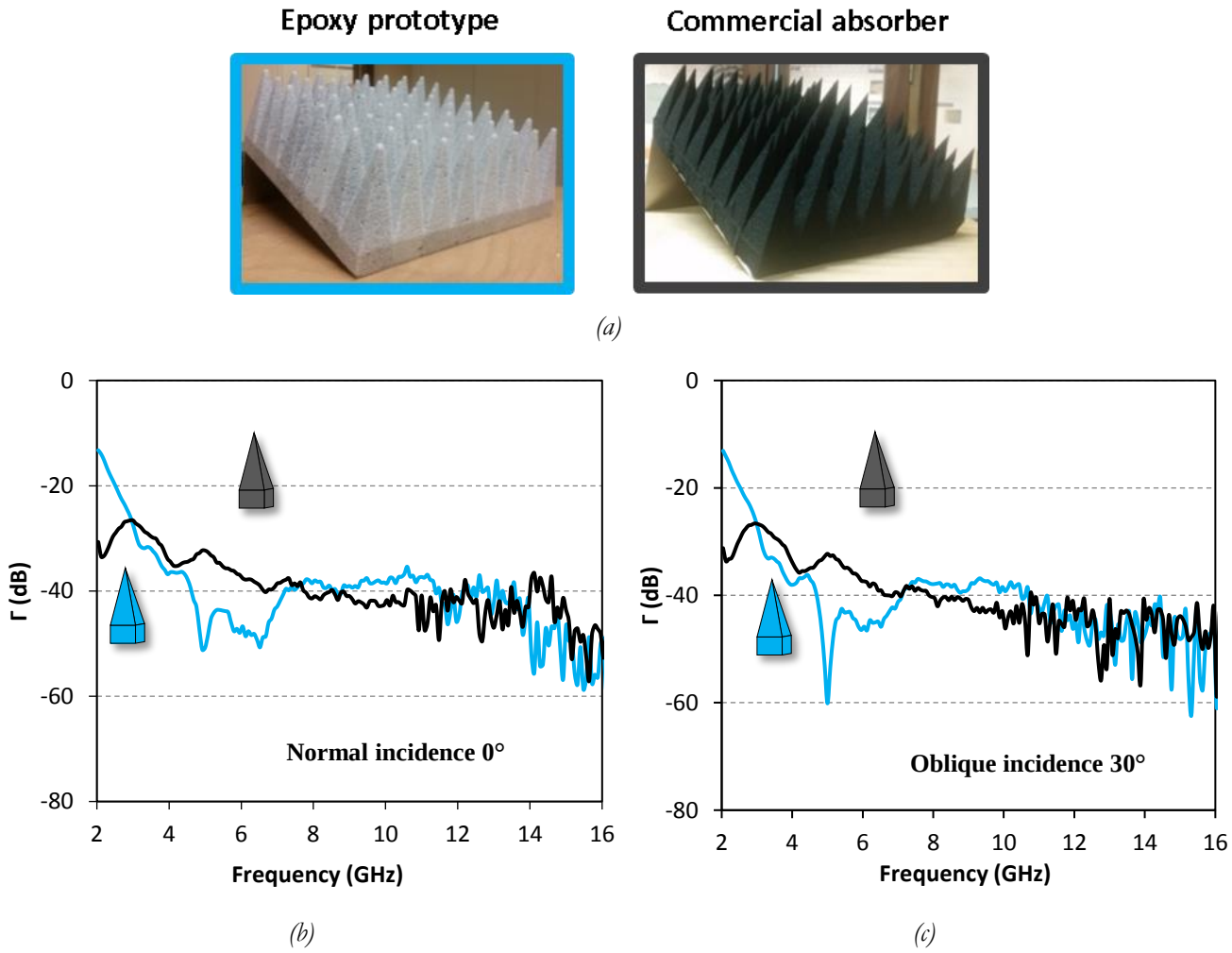

Figure I.47. Photos of the elaborated prototype and the commercial absorber APM 12 (a) and measurement results of these two prototypes at normal incidence (b) and oblique incidence of 30° (c) [143].

Otherwise, the epoxy foam has close cells which makes it more rigid than the PU foam. Consequently, more complex forms could be achieved [142]. An example of a previously realized absorber, using the same material as before (3 mm - 0.5 wt.%) and the same height as the commercial absorber AMP 12 of SIEPEL, but with a complex geometry is presented here [142]. Photos of the elaborated prototype and the commercial absorber APM 12 are shown in Figure I.48 (a). The new elaborated prototype shows an excellent absorption performance with reflection coefficient less than -20 dB over the entire studied frequency range and for both normal and oblique incidences with an average improvement of about 10 dB compared to the commercial absorber (Figure I.48 (b) and (c)). A better performance has been obtained by the proposed

absorber from 2.35 GHz to 16 GHz at normal incidence and from 2.43 GHz to 16 GHz at the oblique incidence of 30°.

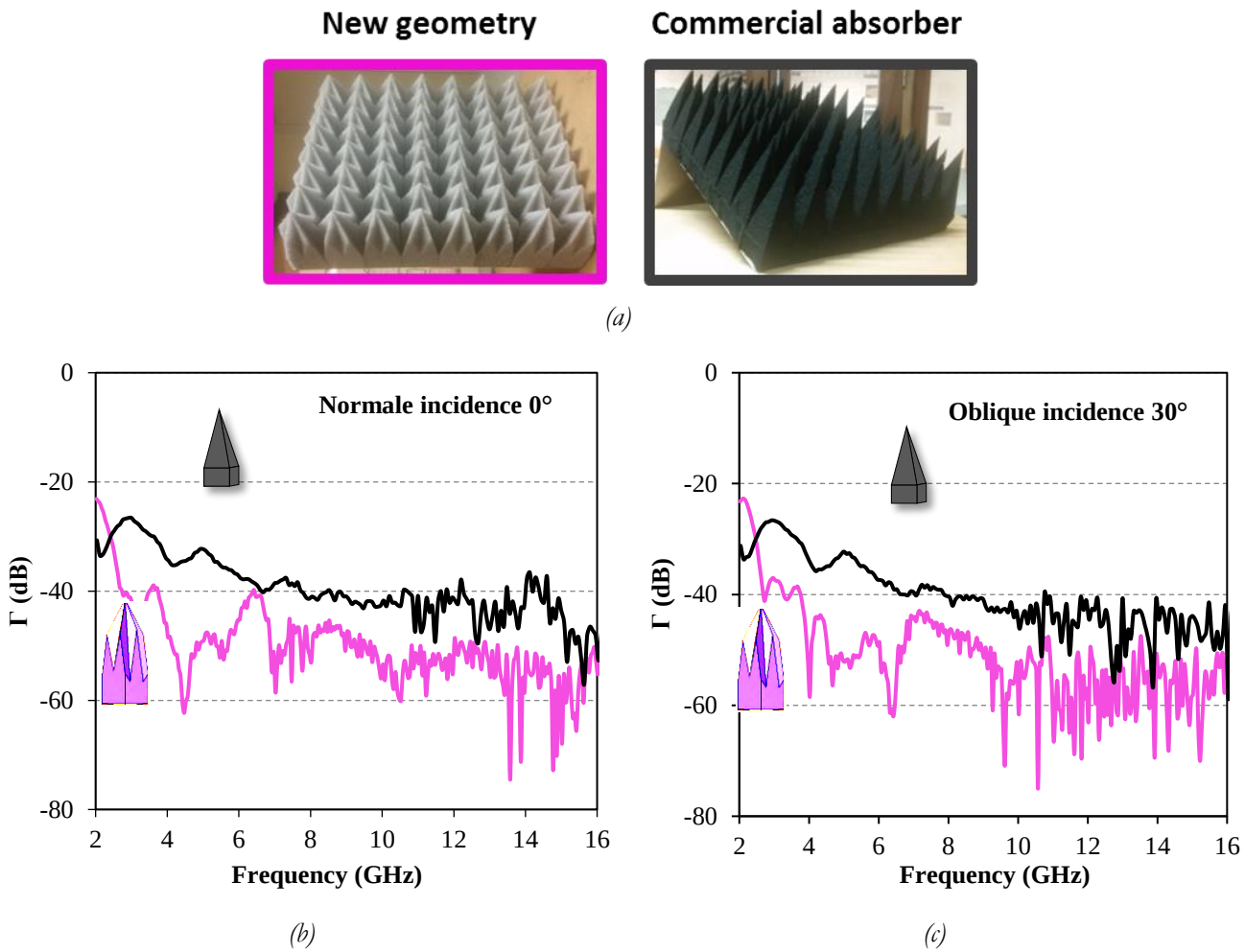

Figure I.48. Photos of the elaborated prototype and the commercial absorber APM 12 (a) and measurement results of these two prototypes at normal incidence (b) and oblique incidence of 30° (c) [142].

7. Conclusion

In this first chapter, the mechanism and the principles of electromagnetic absorption, as well as, the basic equations to be used in the following chapters of this thesis have been presented. The absorbers were also classified basing on the absorption bandwidth (resonant, multiband or broadband). The different types of the loads used for the dielectric and/or magnetic microwave absorbers were also presented. Then, the absorbers used in the anechoic chambers were introduced. Finally, the absorbing material that will be used during this thesis were presented with their advantage compared to the commercial absorbers. This material is going to be used to elaborate planar absorbers that are of our interest, especially planar multilayer and metamaterial absorbers. For multilayer absorbers, a compromise between thickness and absorption should be done; the aim is to ensure a good absorption performance over a wide frequency range with the minimum thickness. This will be discussed in chapter II and chapter III. In addition to that, a simple method to broaden the absorption bandwidth of a new elaborated metamaterial absorber, with also the minimal possible thickness, will be proposed in chapter IV.

8. References

[1] W. Emerson, "Electromagnetic wave absorbers and anechoic chambers through the years," *IEEE Trans. Antennas Propag.*, vol. 21, no. 4, pp. 484–490, Jul. 1973, doi: 10.1109/TAP.1973.1140517.

[2] Naval Air Warfare Center Weapons Division, *Electronic Warfare and Radar Systems Engineering Handbook*, Fourth edition. California: Technical Communication Office, 2013.

[3] C. A. Balanis, *Advanced engineering electromagnetics*. New York: Wiley, 1989.

[4] D. Micheli, C. Apollo, R. Pastore, and M. Marchetti, "X-Band microwave characterization of carbon-based nanocomposite material, absorption capability comparison and RAS design simulation," *Compos. Sci. Technol.*, vol. 70, no. 2, pp. 400–409, Feb. 2010, doi: 10.1016/j.compscitech.2009.11.015.

[5] W. Hong, P. Xiao, and H. Luo, "Structural magnetic loss of vertical aligned carbon fibres," *J Appl Phys*, vol. 113, no. 22, p. 224901, Jun. 2013, doi: 10.1063/1.4810856.

[6] Y. Iijima, Y. Houjou, and R. Sato, "Millimeter wave absorber using M-type hexagonal ferrite," in *IEEE International Symposium on Electromagnetic Compatibility. Symposium Record (Cat. No.00CH37016)*, Washington, DC, USA, 2000, vol. 2, pp. 547–549, doi: 10.1109/ISEMC.2000.874679.

[7] R. Zamorano Ulloa, M. Guadalupe Hernandez Santiago, and V. L. Villegas Rueda, "The Interaction of Microwaves with Materials of Different Properties," in *Electromagnetic Fields and Waves*, K. Ho Yeap and K. Hirasawa, Eds. IntechOpen, 2019.

[8] M.-S. Cao, W.-L. Song, Z.-L. Hou, B. Wen, and J. Yuan, "The effects of temperature and frequency on the dielectric properties, electromagnetic interference shielding and microwave-absorption of short carbon fiber/silica composites," *Carbon*, vol. 48, no. 3, pp. 788–796, Mar. 2010, doi: 10.1016/j.carbon.2009.10.028.

[9] A. D. Lustrac, "Matériaux composites en électromagnétisme - Matériaux absorbants radar." Techniques de l'ingénieur, 2018.

[10] W. W. Salisbury, "Absorbent body for electromagnetic waves," Patent US2599944A, Jun. 10, 1952.

[11] L. J. Du Toit, "The design of Jauman absorbers," *IEEE Antennas Propag. Mag.*, vol. 36, no. 6, pp. 17–25, Dec. 1994, doi: 10.1109/74.370526.

[12] L. Ke, Z. Xin, H. Xinyu, and Z. Peng, "Analysis and Design of Multilayer Jaumann Absorbers," in *2011 IEEE International Conference on Microwave Technology & Computational Electromagnetics*, May 2011, p. 4.

[13] H. Kwon *et al.*, "Design and verification of simultaneously self-sensing and microwave-absorbing composite structures based on embedded SiC fiber network," *Compos. Struct.*, p. 113286, Nov. 2020, doi: 10.1016/j.compstruct.2020.113286.

[14] D. Sievenpiper, "High-Impedance Electromagnetic Surfaces," PhD, University of California, Los Angeles, 1999.

[15] S. A. Tretyakov and S. I. Maslovski, "Thin absorbing structure for all incidence angles based on the use of a high-impedance surface," *Microw. Opt. Technol. Lett.*, vol. 38, no. 3, pp. 175–178, Aug. 2003, doi: 10.1002/mop.11006.

[16] N. Engheta, "Thin absorbing screens using metamaterial surfaces," in *IEEE Antennas and Propagation Society International Symposium (IEEE Cat. No.02CH37313)*, San Antonio, TX, USA, 2002, pp. 392–395, doi: 10.1109/APS.2002.1016106.

[17] N. I. Landy, S. Sajuyigbe, J. J. Mock, D. R. Smith, and W. J. Padilla, "Perfect Metamaterial Absorber," *Phys. Rev. Lett.*, vol. 100, no. 20, May 2008, doi: 10.1103/PhysRevLett.100.207402.

[18] Z. Zhang *et al.*, "Broadband metamaterial absorber for low-frequency microwave absorption in the S-band and C-band," *J. Magn. Magn. Mater.*, vol. 497, p. 166075, Mar. 2020, doi: 10.1016/j.jmmm.2019.166075.

[19] S. Ghosh, K. V. Srivastava, D. Chaurasiya, and S. Bhattacharyya, "Wide-angle broadband microwave metamaterial absorber with octave bandwidth," *IET Microw. Antennas Propag.*, vol. 9, no. 11, pp. 1160–1166, Aug. 2015, doi: 10.1049/iet-map.2014.0632.

[20] D. Sood and C. C. Tripathi, "A Compact Ultrathin Ultra-wideband Metamaterial Microwave Absorber," *J. Microw. Optoelectron. Electromagn. Appl.*, vol. 16, no. 2, pp. 514–528, Apr. 2017, doi: 10.1590/2179-10742017v16i2797.

[21] Z. Ma, "Ultra-broadband metamaterial absorber in Terahertz regime," p. 3, 2012.

[22] M. Labidi and F. Choubani, "Performances enhancement of metamaterial loop antenna for terahertz applications," *Opt. Mater.*, vol. 82, pp. 116–122, Aug. 2018, doi: 10.1016/j.optmat.2018.05.050.

[23] F. Ding, J. Dai, Y. Chen, J. Zhu, Y. Jin, and S. I. Bozhevolnyi, "Broadband near-infrared metamaterial absorbers utilizing highly lossy metals," *Sci. Rep.*, vol. 6, no. 1, Dec. 2016, doi: 10.1038/srep39445.

[24] Z. Y. Yang, M. Zhao, and P. X. Lu, "A Numerical Study on Helix Nanowire Metamaterials as Optical Circular Polarizers in the Visible Region," *IEEE Photonics Technol. Lett.*, vol. 22, no. 17, pp. 1303–1305, Sep. 2010, doi: 10.1109/LPT.2010.2054073.

[25] T. Cao, C. Wei, R. E. Simpson, L. Zhang, and M. J. Cryan, "Broadband Polarization-Independent Perfect Absorber Using a Phase-Change Metamaterial at Visible Frequencies," *Sci. Rep.*, vol. 4, no. 1, May 2015, doi: 10.1038/srep03955.

[26] W. Pan, C. Huang, P. Chen, X. Ma, C. Hu, and X. Luo, "A Low-RCS and High-Gain Partially Reflecting Surface Antenna," *IEEE Trans. Antennas Propag.*, vol. 62, no. 2, pp. 945–949, Feb. 2014, doi: 10.1109/TAP.2013.2291008.

[27] W. Xu *et al.*, "An ultra-thin broadband active frequency selective surface absorber for ultrahigh-frequency applications," *J. Appl. Phys.*, vol. 118, no. 18, p. 184903, Nov. 2015, doi: 10.1063/1.4934683.

[28] M. R. I. Faruque, M. T. Islam, and N. Misran, "Analysis of Electromagnetic Absorption in Mobile Phones Using Metamaterials," *Electromagnetics*, vol. 31, no. 3, pp. 215–232, Apr. 2011, doi: 10.1080/02726343.2011.558457.

[29] M. Odit, P. Kapitanova, A. Andryieuski, P. Belov, and A. V. Lavrinenko, "Experimental demonstration of water based tunable metasurface," *Appl. Phys. Lett.*, vol. 109, no. 1, p. 011901, Jul. 2016, doi: 10.1063/1.4955272.

[30] B. Ma *et al.*, "Gain enhancement of transmitting antenna incorporated with double-cross-shaped electromagnetic metamaterial for wireless power transmission," *Optik*, vol. 127, no. 16, pp. 6754–6762, Aug. 2016, doi: 10.1016/j.ijleo.2016.04.107.

[31] B. X. Khuyen *et al.*, "Size-efficient metamaterial absorber at low frequencies: Design, fabrication, and characterization," *J. Appl. Phys.*, vol. 117, no. 24, p. 243105, Jun. 2015, doi: 10.1063/1.4923053.

[32] Y. J. Yoo *et al.*, "Flexible and elastic metamaterial absorber for low frequency, based on small-size unit cell," *Appl. Phys. Lett.*, vol. 105, no. 4, p. 041902, Jul. 2014, doi: 10.1063/1.4885095.

[33] P. V. Tuong, V. D. Lam, J. W. Park, E. H. Choi, S. A. Nikitov, and Y. P. Lee, "Perfect-absorber metamaterial based on flower-shaped structure," *Photonics Nanostructures - Fundam. Appl.*, vol. 11, no. 1, pp. 89–94, Feb. 2013, doi: 10.1016/j.photonics.2012.09.002.

[34] C. Sabah, F. Dincer, M. Karaaslan, E. Unal, O. Akgol, and E. Demirel, "Perfect metamaterial absorber with polarization and incident angle independencies based on ring and cross-wire resonators for shielding and a sensor application," *Opt. Commun.*, vol. 322, pp. 137–142, Jul. 2014, doi: 10.1016/j.optcom.2014.02.036.

[35] K. P. Kaur, T. Upadhyaya, and M. Palandoken, "Ultrathin wideband polarization independent compact metamaterial microwave absorber," in *2018 28th International Conference Radioelektronika (Radioelektronika)*, Prague, Apr. 2018, pp. 1–6, doi: 10.1109/RADIOELEK.2018.8376395.

[36] M. Amiri, F. Tofigh, N. Shariati, J. Lipman, and M. Abolhasan, "Wide-angle metamaterial absorber with highly insensitive absorption for TE and TM modes," *Sci. Rep.*, vol. 10, no. 1, Dec. 2020, doi: 10.1038/s41598-020-70519-8.

[37] J. Wang, X. Ding, X. Huang, J. Wu, Y. Li, and H. Yang, "Metamaterials absorber for multiple frequency points within 1 GHz," *Phys. Scr.*, vol. 95, no. 6, p. 065505, Jun. 2020, doi: 10.1088/1402-4896/ab7f49.

[38] K. P. Kaur, T. K. Upadhyaya, and M. Palandoken, "Dual-band polarization-insensitive metamaterial inspired microwave absorber for LTE-band applications," *Prog. Electromagn. Res. C*, vol. 77, pp. 91–100, 2017, doi: 10.2528/PIERC17060502.

[39] S. Ji, C. Jiang, J. Zhao, X. Zhang, and Q. He, "Design of a polarization-insensitive triple-band metamaterial absorber," *Opt. Commun.*, vol. 432, pp. 65–70, Feb. 2019, doi: 10.1016/j.optcom.2018.09.040.

[40] D. Sood and C. C. Tripathi, "A polarization insensitive ultrathin compact triple band metamaterial absorber," *APPL PHYS*, vol. 56, p. 9, 2018.

[41] S. R. Thummaluru, N. Mishra, and R. K. Chaudhary, "Design and analysis of an ultrathin triple-band polarization independent metamaterial absorber," *AEU - Int. J. Electron. Commun.*, vol. 82, pp. 508–515, Dec. 2017, doi: 10.1016/j.aeue.2017.10.024.

[42] Q. Ye, Y. Liu, H. Lin, M. Li, and H. Yang, "Multi-band metamaterial absorber made of multi-gap SRRs structure," *Appl. Phys. A*, vol. 107, no. 1, pp. 155–160, Apr. 2012, doi: 10.1007/s00339-012-6796-7.

[43] Z. Yu, S. Liu, C. Fang, X. Huang, and H. Yang, "Design, simulation, and fabrication of single-/dual-/triple band metamaterial absorber," *Phys. Scr.*, vol. 90, no. 6, p. 065501, Jun. 2015, doi: 10.1088/0031-8949/90/6/065501.

[44] S. Bhattacharyya and K. Vaibhav Srivastava, "Triple band polarization-independent ultra-thin metamaterial absorber using electric field-driven LC resonator," *J. Appl. Phys.*, vol. 115, no. 6, p. 064508, Feb. 2014, doi: 10.1063/1.4865273.

[45] J. W. Park *et al.*, "Multi-band metamaterial absorber based on the arrangement of donut-type resonators," *Opt. Express*, vol. 21, no. 8, p. 9691, Apr. 2013, doi: 10.1364/OE.21.009691.

[46] X. Shen, T. J. Cui, J. Zhao, H. F. Ma, W. X. Jiang, and H. Li, "Polarization-independent wide-angle triple-band metamaterial absorber," *Opt. Express*, vol. 19, no. 10, p. 9401, May 2011, doi: 10.1364/OE.19.009401.

[47] E. F. Knott, J. F. Shaeffer, and M. T. Tuley, *Radar cross section*, 2nd ed., corr. Reprinting. Raleigh, NC: SciTech Pub, 2004.

[48] "Microwave Absorbers," *Siepel.* https://siepel.asia/products/rf-microwave/microwave-absorbers/ (accessed Nov. 02, 2020).

[49] Y. Duan and H. Guan, *Microwave absorbing materials*. 2017.

[50] I. Huynen, L. Bednarz, J.-M. Thomassin, C. Pagnoulle, R. Jerome, and C. Detrembleur, "Microwave absorbers based on foamed nanocomposites with graded concentration of carbon nanotubes," in *2008 38th European Microwave Conference*, Amsterdam, Netherlands, Oct. 2008, pp. 5–8, doi: 10.1109/EUMC.2008.4751372.

[51] X. F. Zhang and G. P. Zhou, "Broadband asymmetric electromagnetic wave absorption tailored by impedance gradation: To construct diode-like absorbers," *Mater. Lett.*, vol. 149, pp. 29–32, Jun. 2015, doi: 10.1016/j.matlet.2015.02.099.

[52] C. Vong, A. Chevalier, M. Azar, J. Ville, J.-F. Rosnarho, and V. Laur, "Optimisation de surfaces absorbantes multicouches fabriquées par impression 3D," *JCMM 2020*, Nov. 2020.

[53] D. Q. Vu *et al.*, "Broadening the absorption bandwidth of metamaterial absorber by coupling three dipole resonances," *Phys. B Condens. Matter*, vol. 532, pp. 90–94, Mar. 2018, doi: 10.1016/j.physb.2017.03.046.

[54] T. Hien Nguyen *et al.*, "Metamaterial-based perfect absorber: polarization insensitivity and broadband," *Adv. Nat. Sci. Nanosci. Nanotechnol.*, vol. 5, no. 2, p. 025013, May 2014, doi: 10.1088/2043-6262/5/2/025013.

[55] J. B. O. de Araujo, G. L. Siqueira, E. Kemptner, M. Weber, C. Junqueira, and M. M. Mosso, "An Ultrathin and Ultrawideband Metamaterial Absorber and an Equivalent-Circuit Parameter Retrieval

Method," *IEEE Trans. Antennas Propag.*, vol. 68, no. 5, pp. 3739–3746, May 2020, doi: 10.1109/TAP.2020.2963900.

[56] H. Xiong, J.-S. Hong, C.-M. Luo, and L.-L. Zhong, "An ultrathin and broadband metamaterial absorber using multi-layer structures," *J. Appl. Phys.*, vol. 114, no. 6, p. 064109, Aug. 2013, doi: 10.1063/1.4818318.

[57] F. Ding, Y. Cui, X. Ge, Y. Jin, and S. He, "Ultra-broadband microwave metamaterial absorber," *Appl. Phys. Lett.*, vol. 100, no. 10, p. 103506, Mar. 2012, doi: 10.1063/1.3692178.

[58] Y. Kim, Y. J. Yoo, W. Kim, J. Y. Rhee, Y. H. Kim, and Y. Lee, "Dual broadband metamaterial absorber," *Opt. EXPRESS*, 2015.

[59] T. Beeharry, R. Yahiaoui, K. Selemani, and H. H. Ouslimani, "A dual layer broadband radar absorber to minimize electromagnetic interference in radomes," *Sci. Rep.*, vol. 8, no. 1, Dec. 2018, doi: 10.1038/s41598-017-18859-w.

[60] M. Cao and Q. Zhang, "Design of broadband multi-layer metamaterial absorber," in *2018 IEEE MTT-S International Wireless Symposium (IWS)*, Chengdu, May 2018, pp. 1–3, doi: 10.1109/IEEE-IWS.2018.8400804.

[61] W. Wang, H. Huang, B. Sima, B. Zhu, and Y. Feng, "A Broadband Metamaterial Microwave Absorber Utilizing Both Magnetic and Electric Resonances," in *2018 Cross Strait Quad-Regional Radio Science and Wireless Technology Conference (CSQRWC)*, Xuzhou, Jul. 2018, pp. 1–3, doi: 10.1109/CSQRWC.2018.8455549.

[62] S. Ghosh, T. T. Nguyen, and S. Lim, "Recent progress in angle-insensitive narrowband and broadband metamaterial absorbers," *EPJ Appl. Metamaterials*, vol. 6, p. 12, 2019, doi: 10.1051/epjam/2019010.

[63] T. T. Nguyen and S. Lim, "Angle- and polarization-insensitive broadband metamaterial absorber using resistive fan-shaped resonators," *Appl. Phys. Lett.*, vol. 112, no. 2, p. 021605, Jan. 2018, doi: 10.1063/1.5004211.

[64] W. Yuan and Y. Cheng, "Low-frequency and broadband metamaterial absorber based on lumped elements: design, characterization and experiment," *Appl. Phys. A*, vol. 117, no. 4, pp. 1915–1921, Dec. 2014, doi: 10.1007/s00339-014-8637-3.

[65] J. Chen *et al.*, "Polarization-Independent, Thin, Broadband Metamaterial Absorber Using Double-Circle Rings Loaded with Lumped Resistances," *J. Electron. Mater.*, vol. 44, no. 11, pp. 4269–4274, Nov. 2015, doi: 10.1007/s11664-015-3951-x.

[66] T. Q. H. Nguyen, T. K. T. Nguyen, T. N. Cao, H. Nguyen, and L. G. Bach, "Numerical study of a broadband metamaterial absorber using a single split circle ring and lumped resistors for X-band applications," *AIP Adv.*, vol. 10, no. 3, p. 035326, Mar. 2020, doi: 10.1063/1.5143915.

[67] D. T. Viet *et al.*, "Perfect absorber metamaterials: Peak, multi-peak and broadband absorption," *Opt. Commun.*, vol. 322, pp. 209–213, Jul. 2014, doi: 10.1016/j.optcom.2014.02.037.

[68] X.-R. Guo, Z. Zhang, J.-H. Wang, and J.-J. Zhang, "The design of a triple-band wide-angle metamaterial absorber based on regular pentagon close-ring," *J. Electromagn. Waves Appl.*, vol. 27, no. 5, pp. 629–637, Mar. 2013, doi: 10.1080/09205071.2013.758317.

[69] D.-E. Wen, Q. Zhang, X. Huang, F. Ding, and X. Huang, "A bandwidth-enhanced metamaterial absorber based on dual-band sub-cells," *Optik*, vol. 127, no. 14, pp. 5585–5590, Jul. 2016, doi: 10.1016/j.ijleo.2016.03.063.

[70] J. Sun, L. Liu, G. Dong, and J. Zhou, "An extremely broad band metamaterial absorber based on destructive interference," *Opt. Express*, vol. 19, no. 22, p. 21155, Oct. 2011, doi: 10.1364/OE.19.021155.

[71] M. R. Soheilifar and R. A. Sadeghzadeh, "Design, fabrication and characterization of stacked layers planar broadband metamaterial absorber at microwave frequency," *AEU - Int. J. Electron. Commun.*, vol. 69, no. 1, pp. 126–132, Jan. 2015, doi: 10.1016/j.aeue.2014.08.005.

[72] D. Wen, H. Yang, Q. Ye, M. Li, L. Guo, and J. Zhang, "Broadband metamaterial absorber based on a multi-layer structure," *Phys. Scr.*, vol. 88, no. 1, p. 015402, Jul. 2013, doi: 10.1088/0031-8949/88/01/015402.

[73] X. Begaud, A. C. Lepage, S. Varault, M. Soiron, and A. Barka, "Ultra-Wideband and Wide-Angle Microwave Metamaterial Absorber," *Materials*, vol. 11, no. 10, p. 2045, Oct. 2018, doi: 10.3390/ma11102045.

[74] T. Q. V. Hoang, B. Loiseaux, and T. Research, "Ultra-broadband Multilayer Microwave Absorber by Multimaterial 3D Printing," p. 4.

[75] Z. Yao, S. Xiao, Z. Jiang, L. Yan, and B.-Z. Wang, "On the Design of Ultrawideband Circuit Analog Absorber Based on Quasi-Single-Layer FSS," *IEEE Antennas Wirel. Propag. Lett.*, vol. 19, no. 4, pp. 591–595, Apr. 2020, doi: 10.1109/LAWP.2020.2972919.

[76] K. V. Srivastava, S. Ghosh, and S. Bhattacharyya, "Design, characterisation and fabrication of a broadband polarisation-insensitive multi-layer circuit analogue absorber," *IET Microw. Antennas Propag.*, vol. 10, no. 8, pp. 850–855, Jun. 2016, doi: 10.1049/iet-map.2015.0653.

[77] H. Chen *et al.*, "Flexible and conformable broadband metamaterial absorber with wide-angle and polarization stability for radar application," *Mater. Res. Express*, vol. 5, no. 1, p. 015804, Jan. 2018, doi: 10.1088/2053-1591/aaa7ab.

[78] S. Fan and Y. Song, "Ultra-Wideband Flexible Absorber in Microwave Frequency Band," *Materials*, vol. 13, no. 21, p. 4883, Oct. 2020, doi: 10.3390/ma13214883.

[79] S.-J. Li *et al.*, "Ultra-wideband and Polarization-Insensitive Perfect Absorber Using Multilayer Metamaterials, Lumped Resistors, and Strong Coupling Effects," *Nanoscale Res. Lett.*, vol. 13, no. 1, Dec. 2018, doi: 10.1186/s11671-018-2810-0.

[80] X. Li, X. Guo, T. Liu, X. Zheng, and J. Bai, "Shape-controlled synthesis of Fe nanostructures and their enhanced microwave absorption properties at L-band," *Mater. Res. Bull.*, vol. 59, pp. 137–141, Nov. 2014, doi: 10.1016/j.materresbull.2014.07.016.

[81] T. Kasagi, T. Tsutaoka, and K. Hatakeyama, "Complex permeability spectra of permendur composite materials," *J. Phys. Conf. Ser.*, vol. 200, no. 8, p. 082012, Jan. 2010, doi: 10.1088/1742-6596/200/8/082012.

[82] E. H. Min, M. S. Kim, and J. G. Ko, "Microwave Absorption Properties in Absorbers for Mobile Phones," *J. Korean Phys. Soc.*, vol. 52, no. 6, pp. 1850–1853, Jun. 2008, doi: 10.3938/jkps.52.1850.

[83] Z. Wang *et al.*, "Magnetic and microwave absorption properties of Ni microcrystals with hierarchical branch-like and flowers-like shapes," *Mater. Chem. Phys.*, vol. 142, no. 1, pp. 119–123, Oct. 2013, doi: 10.1016/j.matchemphys.2013.07.003.

[84] Y. Liu, X. Liu, and X. Wang, "Double-layer microwave absorber based on CoFe2O4 ferrite and carbonyl iron composites," *J. Alloys Compd.*, vol. 584, pp. 249–253, Jan. 2014, doi: 10.1016/j.jallcom.2013.09.049.

[85] S.-S. Kim, S.-T. Kim, Y.-C. Yoon, and K.-S. Lee, "Magnetic, dielectric, and microwave absorbing properties of iron particles dispersed in rubber matrix in gigahertz frequencies," *J. Appl. Phys.*, vol. 97, no. 10, p. 10F905, May 2005, doi: 10.1063/1.1852371.

[86] K. S. Sista, S. Dwarapudi, D. Kumar, G. R. Sinha, and A. P. Moon, "Carbonyl iron powders as absorption material for microwave interference shielding: A review," *J. Alloys Compd.*, vol. 853, p. 157251, Feb. 2021, doi: 10.1016/j.jallcom.2020.157251.

[87] D. Min, W. Zhou, Y. Qing, F. Luo, and D. Zhu, "Greatly enhanced microwave absorption properties of highly oriented flake carbonyl iron/epoxy resin composites under applied magnetic field," *J. Mater. Sci.*, vol. 52, no. 4, pp. 2373–2383, Feb. 2017, doi: 10.1007/s10853-016-0532-1.

[88] L. Liu, Y. Duan, S. Liu, L. Chen, and J. Guo, "Microwave absorption properties of one thin sheet employing carbonyl–iron powder and chlorinated polyethylene," *J. Magn. Magn. Mater.*, vol. 322, no. 13, pp. 1736–1740, Jul. 2010, doi: 10.1016/j.jmmm.2009.12.017.

[89] R. Dosoudil, M. Ušáková, J. Franek, J. Sláma, and V. Olah, "RF electromagnetic wave absorbing properties of ferrite polymer composite materials," *J. Magn. Magn. Mater.*, vol. 304, no. 2, pp. e755–e757, Sep. 2006, doi: 10.1016/j.jmmm.2006.02.216.

[90] R. Dosoudil, M. Usakova, J. Franek, J. Slama, and A. Gruskova, "Particle Size and Concentration Effect on Permeability and EM-Wave Absorption Properties of Hybrid Ferrite Polymer Composites," *IEEE Trans. Magn.*, vol. 46, no. 2, pp. 436–439, Feb. 2010, doi: 10.1109/TMAG.2009.2033347.

[91] S. M. Abbas, A. K. Dixit, R. Chatterjee, and T. C. Goel, "Complex permittivity, complex permeability and microwave absorption properties of ferrite–polymer composites," *J. Magn. Magn. Mater.*, vol. 309, no. 1, pp. 20–24, Feb. 2007, doi: 10.1016/j.jmmm.2006.06.006.

[92] C. Wei, X. Shen, F. Song, Y. Zhu, and Y. Wang, "Double-layer microwave absorber based on nanocrystalline Zn0.5Ni0.5Fe2O4/α-Fe microfibers," *Mater. Des.*, vol. 35, pp. 363–368, Mar. 2012, doi: 10.1016/j.matdes.2011.09.018.

[93] X. Liu, Z. Zhang, and Y. Wu, "Absorption properties of carbon black/silicon carbide microwave absorbers," *Compos. Part B Eng.*, vol. 42, no. 2, pp. 326–329, Mar. 2011, doi: 10.1016/j.compositesb.2010.11.009.

[94] J.-H. Choi, Y.-W. Nam, M.-S. Jang, and C.-G. Kim, "Characteristics of silicon carbide fiber-reinforced composite for microwave absorbing structures," *Compos. Struct.*, vol. 202, pp. 290–295, Oct. 2018, doi: 10.1016/j.compstruct.2018.01.081.

[95] S.-C. Chiu, H.-C. Yu, and Y.-Y. Li, "High Electromagnetic Wave Absorption Performance of Silicon Carbide Nanowires in the Gigahertz Range," *J. Phys. Chem. C*, vol. 114, no. 4, pp. 1947–1952, Feb. 2010, doi: 10.1021/jp905127t.

[96] Z. Chu, H. Cheng, Y. Zhou, Q. Wang, and J. Wang, "Anisotropic microwave absorbing properties of oriented SiC short fiber sheets," *Mater. Des.*, vol. 31, no. 6, pp. 3140–3145, Jun. 2010, doi: 10.1016/j.matdes.2009.12.026.

[97] J. Ma *et al.*, "Systematic study of microwave absorption, heating, and microstructure evolution of porous copper powder metal compacts," *J. Appl. Phys.*, vol. 101, no. 7, p. 074906, Apr. 2007, doi: 10.1063/1.2713087.

[98] D. T. Zimmerman, J. D. Cardellino, K. T. Cravener, K. R. Feather, N. M. Miskovsky, and G. J. Weisel, "Microwave absorption in percolating metal-insulator composites," *Appl. Phys. Lett.*, vol. 93, no. 21, p. 214103, Nov. 2008, doi: 10.1063/1.3036900.

[99] R. H. Norman, *Conductive rubbers and plastics: their production, application and test methods*. Amsterdam, New York: Elsevier Pub. Co, 1970.

[100] J.-H. Oh, K.-S. Oh, C.-G. Kim, and C.-S. Hong, "Design of radar absorbing structures using glass/epoxy composite containing carbon black in X-band frequency ranges," *Compos. Part B Eng.*, vol. 35, no. 1, pp. 49–56, Jan. 2004, doi: 10.1016/j.compositesb.2003.08.011.

[101] W. S. Chin and D. G. Lee, "Development of the composite RAS (radar absorbing structure) for the X-band frequency range," *Compos. Struct.*, vol. 77, no. 4, pp. 457–465, Feb. 2007, doi: 10.1016/j.compstruct.2005.07.021.

[102] K. H. Wu, T. H. Ting, G. P. Wang, W. D. Ho, and C. C. Shih, "Effect of carbon black content on electrical and microwave absorbing properties of polyaniline/carbon black nanocomposites," *Polym. Degrad. Stab.*, vol. 93, no. 2, pp. 483–488, Feb. 2008, doi: 10.1016/j.polymdegradstab.2007.11.009.

[103] S. K. Kwon, J. M. Ahn, G. H. Kim, C. H. Chun, J. S. Hwang, and J. H. Lee, "Microwave absorbing properties of carbon black/silicone rubber blend," *Polym. Eng. Sci.*, vol. 42, no. 11, pp. 2165–2171, Nov. 2002, doi: 10.1002/pen.11106.

[104] J.-H. Shin, H.-K. Jang, W.-H. Choi, T.-H. Song, C.-G. Kim, and W.-Y. Lee, "Design and verification of a single slab RAS through mass production of glass/MWNT added epoxy composite prepreg," *J. Appl. Polym. Sci.*, vol. 132, no. 22, p. n/a-n/a, Jun. 2015, doi: 10.1002/app.42019.

[105] Z. Liu *et al.*, "Microwave Absorption of Single-Walled Carbon Nanotubes/Soluble Cross-Linked Polyurethane Composites," *J. Phys. Chem. C*, vol. 111, no. 37, pp. 13696–13700, Sep. 2007, doi: 10.1021/jp0731396.

[106] Z. Fan, G. Luo, Z. Zhang, L. Zhou, and F. Wei, "Electromagnetic and microwave absorbing properties of multi-walled carbon nanotubes/polymer composites," *Mater. Sci. Eng. B*, vol. 132, no. 1–2, pp. 85–89, Jul. 2006, doi: 10.1016/j.mseb.2006.02.045.

[107] A. Saib *et al.*, "Carbon nanotube composites for broadband microwave absorbing materials," *IEEE Trans. Microw. Theory Tech.*, vol. 54, no. 6, pp. 2745–2754, Jun. 2006, doi: 10.1109/TMTT.2006.874889.

[108] D. Micheli, C. Apollo, R. Pastore, R. Bueno Morles, S. Laurenzi, and M. Marchetti, "Nanostructured composite materials for electromagnetic interference shielding applications," *Acta Astronaut.*, vol. 69, no. 9–10, pp. 747–757, Nov. 2011, doi: 10.1016/j.actaastro.2011.06.004.

[109] X. Gao, J. Li, Y. Gao, S. Guo, H. Wu, and R. Chen, "Microwave absorbing properties of alternating multilayer composites consisting of poly (vinyl chloride) and multi-walled carbon nanotube filled poly (vinyl chloride) layers," *Compos. Sci. Technol.*, vol. 130, pp. 10–19, Jun. 2016, doi: 10.1016/j.compscitech.2016.03.004.

[110] M. Chen, Y. Zhu, Y. Pan, H. Kou, H. Xu, and J. Guo, "Gradient multilayer structural design of CNTs/SiO2 composites for improving microwave absorbing properties," *Mater. Des.*, vol. 32, no. 5, pp. 3013–3016, May 2011, doi: 10.1016/j.matdes.2010.12.043.

[111] Y. Danlée, I. Huynen, and C. Bailly, "Thin smart multilayer microwave absorber based on hybrid structure of polymer and carbon nanotubes," *Appl. Phys. Lett.*, vol. 100, no. 21, p. 213105, May 2012, doi: 10.1063/1.4717993.

[112] S.-E. Lee, J.-H. Kang, and C.-G. Kim, "Fabrication and design of multi-layered radar absorbing structures of MWNT-filled glass/epoxy plain-weave composites," *Compos. Struct.*, vol. 76, no. 4, pp. 397–405, Dec. 2006, doi: 10.1016/j.compstruct.2005.11.036.

[113] Z. Chu, H. Cheng, W. Xie, and L. Sun, "Effects of diameter and hollow structure on the microwave absorption properties of short carbon fibers," *Ceram. Int.*, vol. 38, no. 6, pp. 4867–4873, Aug. 2012, doi: 10.1016/j.ceramint.2012.02.077.

[114] G. Dupupet, "Fibres de carbone." Techniques de l'Ingénieur, 2008.

[115] Q. Ling, J. Sun, Q. Zhao, and Q. Zhou, "Microwave absorbing properties of linear low density polyethylene/ethylene–octene copolymer composites filled with short carbon fiber," *Mater. Sci. Eng. B*, vol. 162, no. 3, pp. 162–166, Jun. 2009, doi: 10.1016/j.mseb.2009.03.023.

[116] C. P. Neo and V. K. Varadan, "Optimization of Carbon Fiber Composite for Microwave Absorber," *IEEE Trans. Electromagn. Compat.*, vol. 46, no. 1, pp. 102–106, Feb. 2004, doi: 10.1109/TEMC.2004.823618.

[117] F. Nanni, P. Travaglia, and M. Valentini, "Effect of carbon nanofibres dispersion on the microwave absorbing properties of CNF/epoxy composites," *Compos. Sci. Technol.*, vol. 69, no. 3–4, pp. 485–490, Mar. 2009, doi: 10.1016/j.compscitech.2008.11.026.

[118] X. Sun, X. Lv, X. Li, X. Yuan, L. Li, and G. Gu, "Fe3O4@SiO2 nanoparticles wrapped with polypyrrole (PPy) aerogel: A highly performance material as excellent electromagnetic absorber," *Mater. Lett.*, vol. 221, pp. 93–96, Jun. 2018, doi: 10.1016/j.matlet.2018.03.079.

[119] N. N. Ali, Y. Atassi, A. Salloum, A. Charba, A. Malki, and M. Jafarian, "Comparative study of microwave absorption characteristics of (Polyaniline/NiZn ferrite) nanocomposites with different ferrite percentages," *Mater. Chem. Phys.*, vol. 211, pp. 79–87, Jun. 2018, doi: 10.1016/j.matchemphys.2018.02.017.

[120] F. Wu *et al.*, "A self-assembly method for the fabrication of a three-dimensional (3D) polypyrrole (PPy)/poly(3,4-ethylenedioxythiophene) (PEDOT) hybrid composite with excellent absorption performance against electromagnetic pollution," *J. Mater. Chem. C*, vol. 4, no. 1, pp. 82–88, 2016, doi: 10.1039/C5TC02887F.

[121] A. Xie *et al.*, "Self-assembled ultralight three-dimensional polypyrrole aerogel for effective electromagnetic absorption," *Appl. Phys. Lett.*, vol. 106, no. 22, p. 222902, Jun. 2015, doi: 10.1063/1.4921180.

[122] P. Chandrasekhar and K. Naishadham, "Broadband microwave absorption and shielding properties of a poly žaniline/," p. 6, 1999.

[123] K. Lakshmi, H. John, K. T. Mathew, R. Joseph, and K. E. George, "Microwave absorption, reflection and EMI shielding of PU–PANI composite," *Acta Mater.*, vol. 57, no. 2, pp. 371–375, Jan. 2009, doi: 10.1016/j.actamat.2008.09.018.

[124] Y. Wang, Y. Du, P. Xu, R. Qiang, and X. Han, "Recent Advances in Conjugated Polymer-Based Microwave Absorbing Materials," *Polymers*, vol. 9, no. 12, p. 29, Jan. 2017, doi: 10.3390/polym9010029.

[125] J. Sun, L. Wang, Q. Yang, Y. Shen, and X. Zhang, "Preparation of copper-cobalt-nickel ferrite/graphene oxide/polyaniline composite and its applications in microwave absorption coating," *Prog. Org. Coat.*, vol. 141, p. 105552, Apr. 2020, doi: 10.1016/j.porgcoat.2020.105552.

[126] L. Liu, Y. Duan, L. Ma, S. Liu, and Z. Yu, "Microwave absorption properties of a wave-absorbing coating employing carbonyl-iron powder and carbon black," *Appl. Surf. Sci.*, vol. 257, no. 3, pp. 842–846, Nov. 2010, doi: 10.1016/j.apsusc.2010.07.078.

[127] S.-H. Kim, Y.-G. Park, and S.-S. Kim, "Double-layered microwave absorbers composed of ferrite and carbon fiber composite laminates," *Phys. Status Solidi C*, vol. 4, no. 12, pp. 4602–4605, Dec. 2007, doi: 10.1002/pssc.200777374.

[128] G. Shen, M. Xu, and Z. Xu, "Double-layer microwave absorber based on ferrite and short carbon fiber composites," *Mater. Chem. Phys.*, vol. 105, no. 2–3, pp. 268–272, Oct. 2007, doi: 10.1016/j.matchemphys.2007.04.056.

[129] X. Meng, Y. Wan, Q. Li, J. Wang, and H. Luo, "The electrochemical preparation and microwave absorption properties of magnetic carbon fibers coated with Fe3O4 films," *Appl. Surf. Sci.*, vol. 257, no. 24, pp. 10808–10814, Oct. 2011, doi: 10.1016/j.apsusc.2011.07.108.

[130] "Cages de Faraday," *Siepel*. https://www.siepel.com/fr/cem/cages-de-faraday/ (accessed Nov. 02, 2020).

[131] L. k Neher, "Nonreflecting background for testing microwave equipment," US609244A, 1945.

[132] "Emerson & Cuming Anechoic Chambers." https://www.ecanechoicchambers.com/ (accessed Nov. 17, 2020).

[133] "Laird Technologies EMI | RF/IF and RFID." https://www.digikey.com/en/products/detail/laird-technologies-emi/78089099/4360298?s=N4IgjCBcoLQdIDGUAuAnArgUwDQgPZQDaIAnAAwDMIAugL514BMxIA7ABzkcWmm10gA (accessed Nov. 02, 2020).

[134] "Cuming Microwave C-RAM LF and LF-W Flexible Foam Sheet Broadband Radar Absorber - The EMC Shop." https://www.theemcshop.com/truncated-pyramidal-microwave-absorber/2193-cuming-microwave-c-ram-lf-and-lf-w-flexible-foam-sheet-broadband-radar-absorber.html (accessed Nov. 02, 2020).

[135] "Honeycomb Absorber." http://www.unetop.com.cn/e_productshow/?17-Honeycomb-Microwave-Absorber-17.html (accessed Nov. 03, 2020).

[136] "Sltmicrowave | Products." https://www.sltmicrowave.com/portfolio.html (accessed Nov. 03, 2020).

[137] "SIEPEL MI Multi-Layer Pyramidal Absorber," *GOmeasure*. https://www.gomeasure.dk/butik/emc-test/absorbers/siepel-mimulti-layer-pyramidal-absorber/ (accessed Nov. 03, 2020).

[138] "Broadband absorbers," *Siepel*. https://www.siepel.com/en/broadband-absorbers/ (accessed Nov. 03, 2020).

[139] H. Nornikman, F. Malek, P. J. Soh, A. A. H. Azremi, and A. Ismahayati, "Reflection Loss Performance of Triangular Microwave Absorber," in *International Symposium on Antennas and Propagation (ISAP 2010)*, 2010, p. 4.

[140] H. Nornikman, P. J. Soh, and A. A. H. Azremi, "Performance of Different Polygonal Microwave Absorber Designs Using Novel Material," in *International Symposium on antennas and propagation (ISAP 2009)*, Bangkok, Thailand, Oct. 2009, p. 4.

[141] F. Malek, Z. Liyana, F. H. Wee, and H. Nornikman, "Reflection loss performance of double pyramidal microwave absorber," in *2012 International Symposium on Telecommunication Technologies*, Kuala Lumpur, Malaysia, Nov. 2012, pp. 6–10, doi: 10.1109/ISTT.2012.6481555.

[142] L. Pometcu, "Matériaux et forme innovants pour l'atténuation en Hyper Fréquences," PhD, University of Rennes 1, Rennes, 2016.

[143] C. Méjean, "Élaboration de Nouveaux Matériaux absorbants : Application en Chambres anéchoïques," PhD, University of Rennes 1, Saint Brieuc, 2017.

[144] H. Breiss, A. El Assal, R. Benzerga, C. Méjean, and A. Sharaiha, "Long Carbon Fibers for Microwave Absorption: Effect of Fiber Length on Absorption Frequency Band," *Micromachines*, vol. 11, no. 12, p. 1081, Dec. 2020, doi: 10.3390/mi11121081.

Chapter II:

Multilayer Absorbers

Table of Contents

List of Figures 64

1. Introduction 66

2. Reflection coefficient of planar electromagnetic absorbers 66

2.1 Monolayer absorbers 66

2.2 Multilayer absorbers 70

3. Carbon fiber loaded epoxy foam composites 77

3.1 Elaboration steps 77

3.2 Characterization technique 79

3.3 Dielectric properties and module of the characteristic impedance of the elaborated samples 82

4. Microwave multilayer absorber based on loaded epoxy foams 85

5. Improved reflection coefficient using lower CF rates 88

6. CF loaded lightweight epoxy foams 93

7. Conclusion 96

8. References 97

List of Figures

Figure II.1. Impedances and reflection coefficients of a monolayer absorber.....67
Figure II.2. The reflection and transmission coefficients for a monolayer absorber.....69
Figure II.3. Reflection coefficients of the multilayer absorber.....70
Figure II.4. The five layers of the commercial absorber AH 125(a) and the extracted dielectric properties $\varepsilon r'$ (b) and tanδ (c) using the coaxial probe measurement. 72
Figure II.5. Comparison between computed (by MATLAB code) and simulated (by CST) reflection coefficients of AH 125. 72
Figure II.6. Setup under (a) TE and (b) TM polarizations at normal and oblique incidences.....73
Figure II.7. Configuration used to form a gradual multilayer absorber. 75
Figure II.8. Example of (a) a gradual multilayer structure, (b) of the gradient of impedance for each layer and (c) the impedance profile of an ideal absorber. 76
Figure II.9. Calculated impedances of epoxy resin composites loaded with five different types of carbon and different wt.%: (a) 1wt.%, (b) 3wt.% and (c) 5 wt.% [4]. 76
Figure II.10. (a) Proposed multilayer absorber and (b) its simulated reflection coefficient [12]. ...77
Figure II.11. Photos of the CFs with lengths of (a) 100μm, (b) 1 mm, (c) 3 mm, (d) 6 mm and (e) 12 mm. 78
Figure II.12. Elaboration steps of the CF loaded epoxy foam composites.....78
Figure II.13. Configuration used in the anechoic chamber to measure the reflection coefficient. 79
Figure II.14. Measurement (a) at normal incidence and (b) at oblique incidence of 30° in the anechoic chamber of INSA of Rennes. 80
Figure II.15. Four measurements required for the extraction of the dielectric properties.....80
Figure II.16. The extracted dielectric properties and their smooth equivalence $\varepsilon r'$ (a) and tanδ (b) of a loaded epoxy foam composite with respect to frequency.....81
Figure II.17. The fit of the extracted dielectric properties $\varepsilon r'$ (a) and tanδ (b) of a loaded epoxy foam composite with respect to frequency.....82
Figure II.18. The dielectric properties $\varepsilon r'$ (a) and tanδ (b) of the elaborated composites loaded with 3 mm CFs using different wt.% with respect to frequency.....82
Figure II.19. The dielectric properties $\varepsilon r'$ (a) and tanδ (b) of the elaborated composites loaded with 6 mm CFs using different wt.% with respect to frequency.....83
Figure II.20. The dielectric properties $\varepsilon r'$ (a) and (b) tanδ of the elaborated composites loaded with 12 mm CFs using different wt.% with respect to frequency.....83
Figure II.21. Dielectric losses of epoxy foams loaded with 0.25 wt.% of 3, 6 and 12mm-CFs. 84
Figure II.22. Calculated module of the intrinsic impedances of the elaborated epoxy foam composites. 84

Figure II.23. Design of MLA250 prototype (a) and the module of the intrinsic impedances of the epoxy foam composites that are used for this prototype (b). (Impedance of air is represented by a cyan dashed line). 85
Figure II.24. The calculated module of the intrinsic impedance of the four layers composing the first prototype MLA250 at (a) 2 GHz, (b) 4 GHz, (c) 10 GHz and (d) 16 GHz with respect to depth.86
Figure II.25. (a) Photo of the MLA250 realized prototype and (b) its simulated (by CST) and measured reflection coefficients for normal incidence. 87
Figure II.26. (a) MLA125-1 and (b) comparison between simulated reflection coefficients of MLA250 and MLA125-1. 87
Figure II.27. Reflectivity rate with respect to frequency between each two consecutive layers of (a) MLA250 and (b) MLA125-1....88
Figure II.28. Dielectric permittivity $\varepsilon r'$ (a) and dielectric losses (b) of low-loaded epoxy foam composites with 12 mm CFs. 89
Figure II.29. Dielectric permittivity $\varepsilon r'$ (a) and dielectric losses (b) of 3 mm- 0.25 wt.% and 12 mm - 0.075 wt.%....89
Figure II.30. Design of MLA125-2 (a) and the module of the intrinsic impedances of the loaded epoxy foam composites with 12 mm- low weight percentages (b). 90
Figure II.31. The calculated module of the intrinsic impedances of the five chosen layers for MLA125-2 at (a) 2 GHz, (b) 4 GHz, (c) 10 GHz and (d) 16 GHz. 91
Figure II.32. Simulated reflection coefficient of MLA125-2 for (a) normal incidence and (b) oblique incidence of θ=30° for TE and TM polarizations. 92
Figure II.33. MLA125-2 achieved prototype (a) and simulated and measured reflection coefficients for normal incidence (b), and oblique incidence θ=30° for TE (c) and TM (d) polarizations. 92
Figure II.34. (a) Dielectric permittivity $\varepsilon r'$ and (b) dielectric losses of the unloaded and low-loaded lightweight epoxy foam composites with 12 mm CFs. 93
Figure II.35. (a) Design of lightweight LW-MLA125-1 and (b) the module of the intrinsic impedances of the low-density loaded epoxy foam composites with 12 mm- low weight percentages. 94
Figure II.36. Lightweight realized LW-MLA125-1 (a) and its simulated and measured reflection coefficients for normal incidence (b), and oblique incidence θ=30° for TE (c) and TM (d) modes. 95
Figure II.37. Comparison between measured reflection coefficients of MLA125-2 and LW-MLA125-1 and with the commercial multilayer absorber AH 125....95

1. Introduction

Absorbing materials are the key items for the anechoic chamber since they absorb the EM waves to provide a non-reflecting environment. The efficient absorbers allow the incoming EM waves, firstly, to penetrate into the material with minimal reflections at the air/material interface, and secondly, to be dissipated inside it and to be transformed into thermal energy, due to the dielectric and/or magnetic losses. The thickness of the material determinates the absorption level and the operating range of the absorber. Likewise, the thickness is inversely proportional to the desired frequency of absorption, the lower the frequency of absorption, the higher the thickness of the absorbing material. However, for a planar absorber to achieve low reflections and a broadband absorption, especially in low frequencies, a smooth gradual impedance should be satisfied; for this purpose, multilayers were proposed.

In this chapter, the goal is to elaborate a multilayer absorber with a broadband absorption using the Carbon Fiber (CF) loaded epoxy foam composites. First of all, the reflection coefficient of the monolayer and the multilayer absorbers will be detailed. In this section, the way of choosing the composite of each layer of the multilayer absorber will be presented. After that, the elaboration steps and the characterization technique, as well as, the dielectric properties of the loaded epoxy foam composites, are presented. Finally, different broadband multilayer absorbers will be proposed and their simulation and measurement results will be presented.

2. Reflection coefficient of planar electromagnetic absorbers

2.1 Monolayer absorbers

For an absorbing material, a low reflection, a low transmission and a high absorption of the EM wave are needed. For any single layer absorber, the incoming EM waves will be partially reflected by the front surface of the material while the other part is transmitted into the material under test (MUT), and being dissipated in it. For this type of absorbers, the thickness of the layer is not the only considered parameter for a planar broadband absorber material; the impedance matching at the first interface between the air and the material has to be taken also into consideration; this impedance of the material is related to its complex magnetic and dielectric properties ($\tilde{\varepsilon}_r$ and $\tilde{\mu}_r$).

The total reflection coefficient of a monolayer absorber could be calculated using the transmission line theory [5]; in the following, normal incident EM waves that hits the monolayer absorber with a thickness l and backed with metallic plate (PEC), will be considered as shown in Figure II.1. In this figure, only one reflection coefficient at each boundary has been defined.

The reflection coefficient Γ at the air/material interface is calculated (as a linear magnitude) using equation (1) and in dB using equation (2).

$$\Gamma = \frac{Z_{in} - Z_0}{Z_{in} + Z_0} \tag{1}$$

$$\Gamma_{dB} = 20\, Log_{10} \left|\frac{Z_{in}-Z_0}{Z_{in}+Z_0}\right| \quad (2)$$

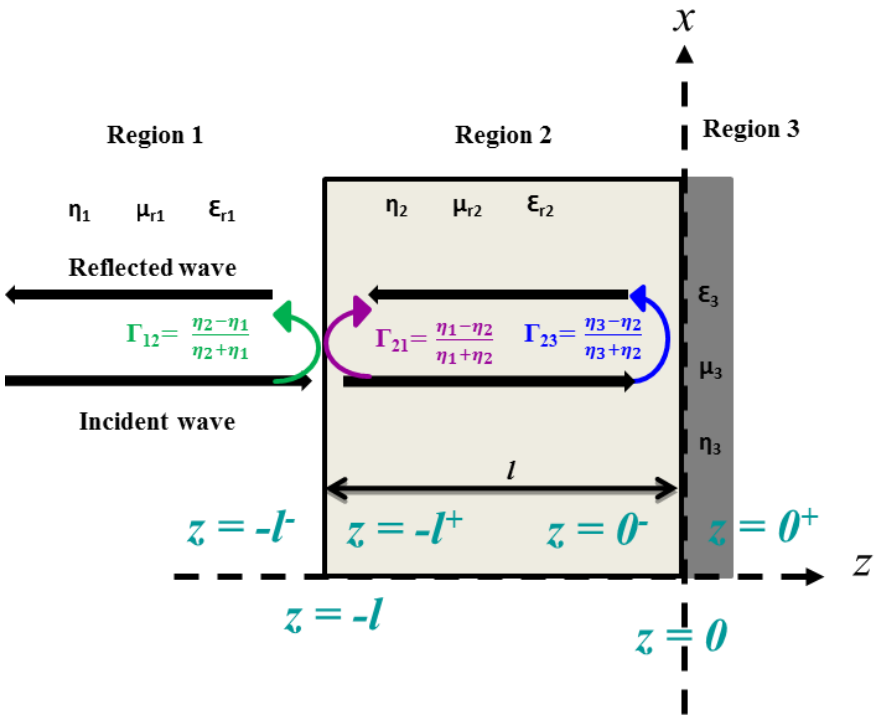

Figure II.1. Impedances and reflection coefficients of a monolayer absorber.

Z_{in} is the input impedance at the air / material interface and it depends on both electric and magnetic fields (incident (E^i *and* H^i) and reflected (E^r *and* E^r) ones) that occur in region 2 (Figure II.1); Z_{in} is calculated using equation (3):

$$Z_{in}|_{Z=-l} = \left.\frac{E^{Total}}{H^{Total}}\right|_{Z=-l} = \frac{(E^i+E^r)|_{Z=-l}}{(H^i+H^r)|_{Z=-l}} \quad (3)$$

The incident and reflected electric fields are written using equations (4) and (5) respectively, where E_0 is the magnitude of the incident electric field, and the magnetic field amplitudes can be written in terms of the electric field amplitudes as equation (6) and (7). Here, the reflection Γ^b at the first boundary interface of the single layer absorber is given by equation (8) where η_1 and η_2 are the characteristic impedances of region 1 and 2, respectively; here, $\eta_1 = \eta_0 = 377\ \Omega$ since region 1 is the air and η_2 is given in equation (9). Γ^b is used to calculate the amplitudes of the reflected electric and magnetic fields as shown in equations (5) and (7).

$$E^i = E_0\, e^{-j\beta_1 z} \quad (4)$$

$$E^r = \Gamma^b E_0\, e^{+j\beta_1 z} \quad (5)$$

$$H^i = \frac{1}{\eta_1} E^i = \frac{E_0}{\eta_1}\, e^{-j\beta_1 z} \quad (6)$$

$$H^r = -\frac{1}{\eta_1} E^r = -\frac{E_0}{\eta_1}\Gamma^b\, e^{+j\beta_1 z} \quad (7)$$

$$\Gamma^b = \frac{\eta_2 - \eta_1}{\eta_2 + \eta_1} \tag{8}$$

$$\eta_2 = \eta_1 \sqrt{\tilde{\mu}_r / \tilde{\varepsilon}_r} \tag{9}$$

Replacing the incident and reflected electric and magnetic field amplitudes in equation (3), we get:

$$Z_{in}|_{Z=-l} = \frac{E_0\, e^{+j\beta_1 l} + \Gamma^b E_0\, e^{-j\beta_1 l}}{\frac{E_0}{\eta_1} e^{+j\beta_1 l} - \frac{E_0}{\eta_1}\Gamma^b e^{-j\beta_1 l}} = \frac{E_0\, e^{+j\beta_1 l}\left[1 + \Gamma^b\, e^{-j2\beta_1 l}\right]}{\frac{E_0\, e^{+j\beta_1 l}}{\eta_1}\left[1 - \Gamma^b e^{-j2\beta_1 l}\right]} = \eta_1 \left(\frac{1 + \Gamma^b\, e^{-j2\beta_1 l}}{1 - \Gamma^b\, e^{-j2\beta_1 l}}\right) \tag{10}$$

$$Z_{in}|_{Z=-l} = \eta_1 \left(\frac{\eta_2 + j\,\eta_1 \tan(\beta_1 l)}{\eta_1 + j\,\eta_2 \tan(\beta_1 l)}\right) \tag{11}$$

With

$$\beta = 2\pi f \sqrt{\mu_0 \epsilon_0} \sqrt{\tilde{\boldsymbol{\varepsilon}}_{\boldsymbol{r}} \tilde{\mu}_{\boldsymbol{r}}} = \frac{2\pi f \sqrt{\tilde{\varepsilon}_r \tilde{\mu}_r}}{c} \tag{12}$$

Where

l: the thickness of the single layer absorber, ***(thickness of region 2)***

β_1: wave propagation number of ***regions 1****.*

f: frequency of the incident EM wave (Hz)

μ_0: relative permeability of air ***(region 1)***

$\mathcal{E}_0$: relative permittivity of air ***(region 1)***

$\tilde{\mu}_r$: complex relative permeability of the absorbing material ***(region 2)***

$\tilde{\varepsilon}_r$: complex relative permittivity of the absorbing material ***(region 2)***

Equation (11) is the well-known impedance transfer equation that is widely used in transmission line theory [1]. Using the same procedure, the reflection coefficient can be derived for the other interfaces. The input impedance at z = 0^+ (Figure II.1) is equal to the intrinsic impedance η_3 of region 3, as shown in equation (13). The input reflection coefficient at the same interface is then written as equation (14). So, using equation (10), the input impedance at z = - l^+ (Figure II.1) can be written as in equation (15).

$$Z_{in}(z = 0^+) = \eta_3 \tag{13}$$

$$\Gamma_{in}(z = 0^-) = \frac{Z_{in}(z=0^+) - Z_0}{Z_{in}(z=0^+) + Z_0} = \frac{\eta_3 - \eta_2}{\eta_3 + \eta_2} \tag{14}$$

$$Z_{in}(z = -l^+) = \eta_2 \left(\frac{1 + \Gamma_{in}(z=0^-) e^{-j2\beta_2 l}}{1 - \Gamma_{in}(z=0^-)\, e^{-j2\beta_2 l}}\right) = \eta_2 \left(\frac{(\eta_3 + \eta_2) + (\eta_3 - \eta_2) e^{-j2\beta_2 l}}{(\eta_3 + \eta_2) - (\eta_3 - \eta_2) e^{-j2\beta_2 l}}\right) \tag{15}$$

The input reflection at z = - *l* (Figure II.1) can be expressed, using the input impedance at -l^+, to obtain equation (16).

$$\Gamma_{total}\,(z=-l^{-}) = \frac{Z_{in}(z=-l^{+})-\eta_1}{Z_{in}(z=-l^{+})+\eta_1} = \frac{\eta_2\,[(\eta_3+\eta_2)+(\eta_3-\eta_2)e^{-j2\beta_2 l}]-\eta_1\,[(\eta_3+\eta_2)-(\eta_3-\eta_2)e^{-j2\beta_2 l}]}{\eta_2\,[(\eta_3+\eta_2)+(\eta_3-\eta_2)e^{-j2\beta_2 l}]+\eta_1\,[(\eta_3+\eta_2)-(\eta_3-\eta_2)e^{-j2\beta_2 l}]} \quad (16)$$

Using the reflection coefficients defined in Figure II.1, the total reflection coefficient of equation (16) can also be written as in equation (17) where β_2 is the wavenumber propagation in region 2.

$$\Gamma_{total}\,(z=-l^{-}) = \frac{\Gamma_{12}+\Gamma_{23}e^{-j2\beta_2 l}}{1+\Gamma_{12}\,\Gamma_{23}\,e^{-j2\beta_2 l}} \quad (17)$$

In fact, there are multiple internal reflections that occur inside the lossy layer, between this layer and the air from one hand, and between this layer and the baked metallic plate from the other hand. These internal reflections are presented in Figure II.2. In this figure, Γ_{12} is the reflection coefficient of the initial reflection at the air/material interface and $T_{12}\Gamma_{23}T_{21}e^{-j2\theta}$, $T_{12}\Gamma_{21}\Gamma_{23}^2T_{21}e^{-j4\theta}$, etc…, are the contributions to the total reflection coefficient that come from the multiple reflections that occur in region 2. So, using the same procedures done above, the total reflection coefficient can be written in a geometric series that takes the form of equation (18) with $\theta = \beta_2 l$. However T_{12}, Γ_{23} *and* T_{21} could be written as equations (19), (20) and (21). Replacing these quantities by their values in equation (18), the total reflection coefficient of equation (17) could be obtained again.

$$\Gamma_{total}\,(z=-l^{-}) = \Gamma_{12} + \frac{T_{12}\Gamma_{23}T_{21}e^{-j2\theta}}{1-\Gamma_{21}\,\Gamma_{23}\,e^{-j2\theta}} \quad (18)$$

$$\Gamma_{12} = -\,\Gamma_{21} \quad (19)$$

$$T_{12} = 1 + \Gamma_{12} \quad (20)$$

$$T_{21} = 1 + \Gamma_{21} = 1 - \Gamma_{12} \quad (21)$$

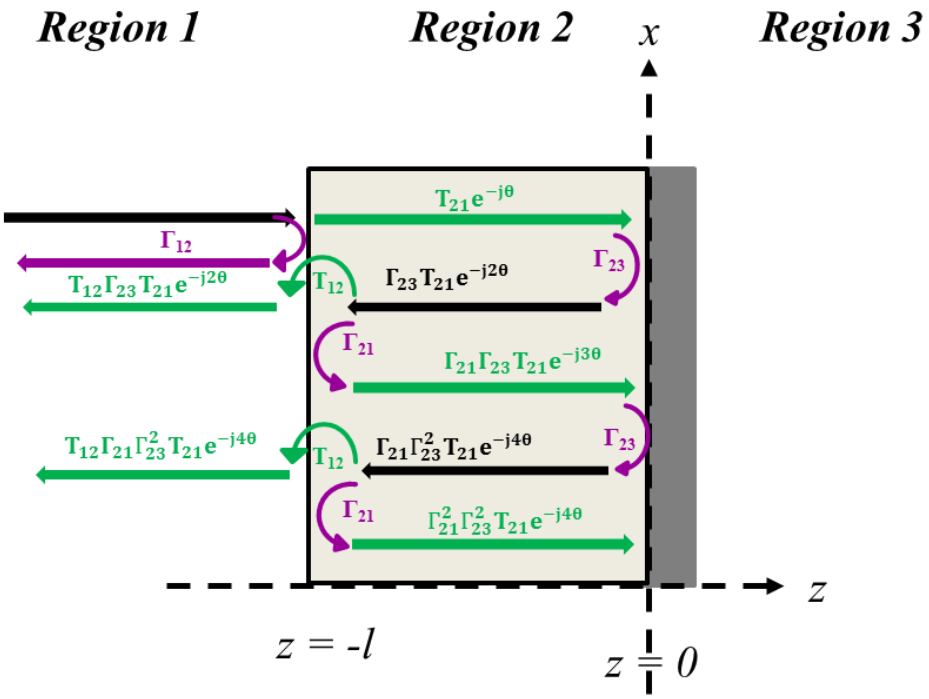

Figure II.2. The reflection and transmission coefficients for a monolayer absorber.

Furthermore, if the magnitudes of the intrinsic reflection coefficients $|\Gamma_{12}|$ and $|\Gamma_{23}|$ are very low compared to unity ($|\Gamma_{12}| \ll 1$ and $|\Gamma_{23}| \ll 1$), an approximation of equation (17) could be performed in order to get the calculation of the total reflection coefficient Γ_{total} (equation (22)); the error of this approximation is less than or equal to 4% when $|\Gamma_{12}| = |\Gamma_{23}| \leq 0.2$ according to [1].

$$\Gamma_{total}\,(z = -l^{-}) \approx \Gamma_{12} + \Gamma_{23} e^{-j2\beta_2 l} \tag{22}$$

2.2 Multilayer absorbers

2.2.1 Calculation of the reflection coefficient at normal incidence

As mentioned in the previous section, the monolayer absorbers are of narrowband. To increase the absorption bandwidth, multilayers, with different characteristics (dielectric and/or magnetic properties), must be used. When N layers, are installed successively to form a multilayer absorber as shown in Figure II.3, the computation of the total reflection and transmission coefficients becomes cumbersome. This is because of the multiple reflections and transmissions that occur at each boundary. However, an approximation could be made to obtain the total reflection coefficient Γ given in equation (23) [1]. The total reflection coefficient Γ, for a normal incidence, is computed by adding all the single reflection coefficients ($\Gamma_0, \Gamma_1, \ldots, \Gamma_N$) that are given by equations (24) to (27), multiplying each one by its phase; note that the phase will evolve in depth. This approximation could be considered accurate because the multiple reflection coefficients at each boundary of the multilayer absorber are small compared to unity (<<1).

$$\boldsymbol{\Gamma_{Total} = \Gamma_0 + \Gamma_1 e^{-j2\beta_1 d_1} + \Gamma_2 e^{-j2(\beta_1 d_1 + \beta_2 d_2)} + \ldots + \Gamma_N e^{-j2(\beta_1 d_1 + \beta_2 d_2 + \cdots + \beta_N d_N)}} \tag{23}$$

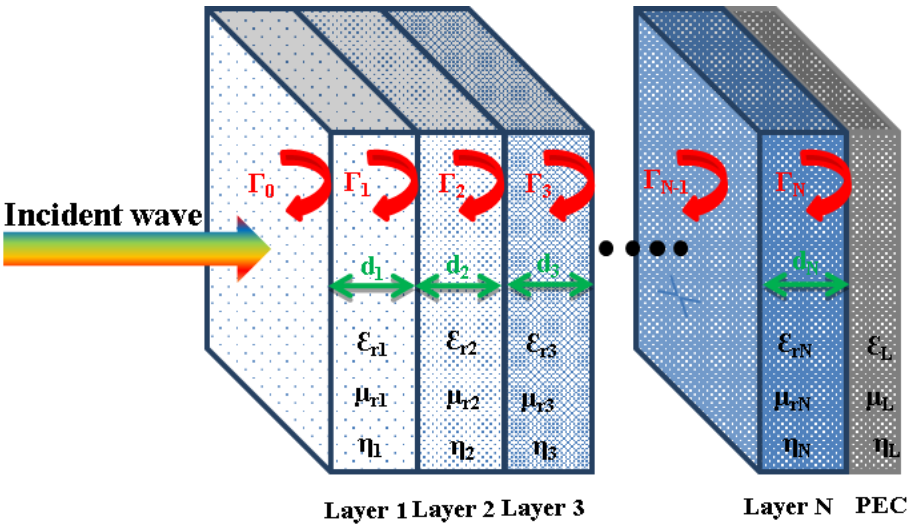

Figure II.3. Reflection coefficients of the multilayer absorber.

$$\Gamma_0 = \frac{\eta_1 - \eta_0}{\eta_1 + \eta_0} \quad (24)$$

$$\Gamma_1 = \frac{\eta_2 - \eta_1}{\eta_2 + \eta_1} \qquad \beta_1 = \frac{2\pi f}{c}\sqrt{\varepsilon_{r1}\mu_{r1}} \quad (25)$$

$$\Gamma_2 = \frac{\eta_3 - \eta_2}{\eta_3 + \eta_2} \qquad \beta_2 = \frac{2\pi f}{c}\sqrt{\varepsilon_{r2}\mu_{r2}} \quad (26)$$

$$\Gamma_N = \frac{\eta_L - \eta_N}{\eta_L + \eta_N} \qquad \beta_L = \frac{2\pi f}{c}\sqrt{\varepsilon_{rL}\mu_{rL}} \quad (27)$$

In this work, commercial electromagnetic software CST Microwave studio was used for the simulation of the reflection coefficient of the multilayer absorbers (MLA), by the frequency domain solver for all simulations in this manuscript. At the same time, a MATLAB code that computes the total reflection coefficient of any multilayer absorber based on the approximation, detailed above, has been developed. For example, if the MLA is composed of three layers, the total reflection coefficient will be computed using Γ_0, Γ_1, Γ_2 and Γ_3. In our case, only the complex permittivity will be used since our materials are dielectric ($\mu_r = 1$). This code will help us to rapidly (about 3 seconds) compute the total reflection coefficient of any multilayer absorber, unlike CST which requires several hours. This code could also use the permeabilities, if needed, to calculate the total reflection coefficient of magnetic absorbers; this could be easily done by replacing $\mu_r = 1$ by the values of the complex permeability in this code. In addition to that, this code gives us the possibility to observe the reflections between each two consecutive layers in order to define the source of the highest reflection in the multilayer absorber.

A verification of the elaborated MATLAB code is done using the commercial multilayer absorber AH 125. This multilayer absorber is composed of five layers with equal thicknesses of 25 mm (Figure II.4 (a)), each one with a 25 mm thickness. The dielectric properties (real part of permittivity and dielectric losses), of the different layers composing AH 125, measured using the coaxial probe method [2], are presented in Figure II.4 (b) and (c).

Using the dielectric properties of the different layers of AH 125, the reflection coefficient of this absorber was simulated using CST and calculated using the developed MATLAB code in order to validate the efficiency of the latter. A comparison between the two reflection coefficients is presented in Figure II.5. The same reflection coefficient has been obtained by the simulation and the computation, which validates the efficiency of the developed MATLAB code. We note weaker intensities of the reflection coefficients, calculated by the GA MATLAB, at the first three resonances; this is due to the number of used points (frequencies). Indeed, 51 points between 2 and 18 GHz (the number of points obtained by the coaxial probe) are used for the GA MATLAB, versus more points (1005 points) that are generated by simulation (using CST) between 2 and 18 GHz; therefore, the obtained result by CST is more accurate. However, our composite materials will be measured using free space method where 3451 points, between 2 GHz and 18

GHz, will be obtained. This will approach the calculated and simulated reflection coefficients from each other.

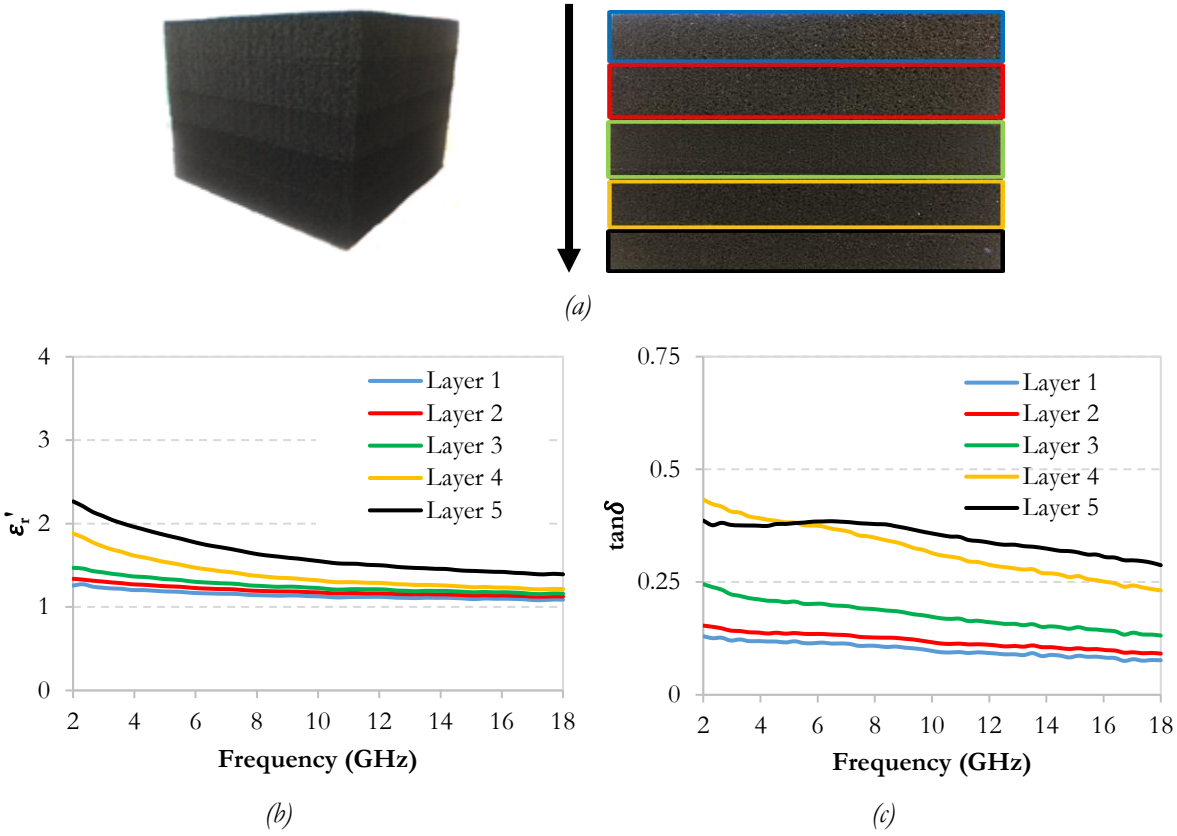

Figure II.4. The five layers of the commercial absorber AH 125(a) and the extracted dielectric properties ε_r' (b) and tanδ (c) using the coaxial probe measurement.

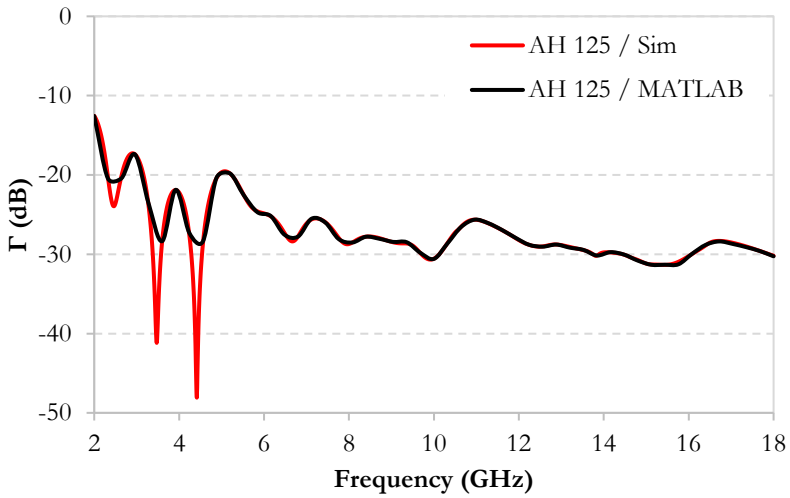

Figure II.5. Comparison between computed (by MATLAB code) and simulated (by CST) reflection coefficients of AH 125.

2.2.2 Calculation of the reflection coefficient at oblique incidence

When an EM wave arrives at the boundary with any angle (measured from the normal to the boundary surface), we refer to it as an oblique incidence. Here, we may classify two modes: TE and TM, as shown in Figure II.6 (a) and (b). For TE polarization, the electric fields are aligned towards y-axis, the magnetic fields are aligned towards x-axis and the wave propagation is always aligned towards the z-axis (Figure II.6 (a)) while for TM mode, the electric fields are aligned towards x-axis and the magnetic fields are aligned towards

y-axis (Figure II.6 (b)). Moreover, in the case of TE polarization, the incident electric field $\vec{E}_i$ is perpendicular to the plane of incidence, as shown in Figure II.6 (a) while in the case of TM polarization, the incident magnetic field $\vec{H}_i$ is perpendicular to the plane of incidence, as shown in Figure II.6 (b). In our case (for planar and isotropic material), TE and TM modes are identical for normal incidence ($\theta = 0°$); but when an incident EM wave with an angle of incidence θ_i arrives at the boundary between medium 1 and medium 2, a part is reflected with an angle of reflection θ_r and another part is transmitted through the medium 2 with an angle of transmission θ_t as illustrated in Figure II.6. In this case ($\theta \neq 0°$), and for both modes, the directions of the electric fields (for TM) or magnetic fields (for TE) and wave propagation are varied simultaneously by an angle θ with respect to x (for TM) or y (for TE) and z directions, respectively (Figure II.6 (a) and (b)).

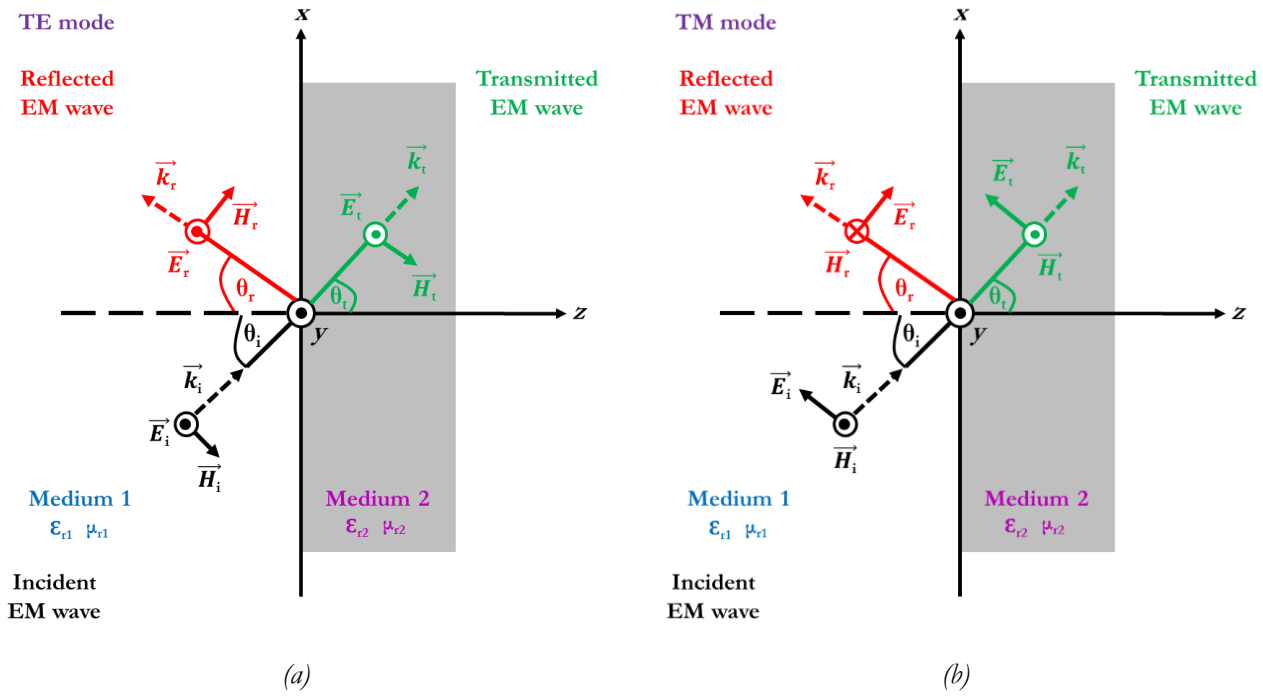

(a) *(b)*

Figure II.6. Setup under (a) TE and (b) TM polarizations at normal and oblique incidences.

The overall reflection and transmission coefficients for TE and TM modes can be written as equations (28) to (31) [1].

For TE Mode:

$$\Gamma_{TE} = \frac{E^r}{E^i} = \frac{B_j}{A_j} \tag{28}$$

$$T_{TE} = \frac{E^t}{E^i} = \frac{1}{A_j} \tag{29}$$

For TM Mode:

$$\Gamma_{TM} = \frac{E^r}{E^i} = \frac{C_j}{D_j} \tag{30}$$

$$T_{TM} = \frac{E^t}{E^i} = \frac{1}{D_j} \tag{31}$$

Where A_j, B_j, C_j and D_j are found using the recursive formulas as following:

$$A_j = \frac{e^{\psi_j}}{2}\left[A_{j+1}\left(1 + Y_{j+1}\right) + B_{j+1}\left(1 - Y_{j+1}\right)\right] \quad (32)$$

$$B_j = \frac{e^{-\psi_j}}{2}\left[A_{j+1}\left(1 - Y_{j+1}\right) + B_{j+1}\left(1 + Y_{j+1}\right)\right] \quad (33)$$

$$C_j = \frac{e^{\psi_j}}{2}\left[C_{j+1}\left(1 + Z_{j+1}\right) + D_{j+1}\left(1 - Z_{j+1}\right)\right] \quad (34)$$

$$D_j = \frac{e^{-\psi_j}}{2}\left[C_{j+1}\left(1 - Z_{j+1}\right) + D_{j+1}\left(1 + Z_{j+1}\right)\right] \quad (35)$$

$$A_{N+1} = C_{N+1} = 1 \quad (36)$$

$$B_{N+1} = D_{N+1} = 0 \quad (37)$$

$$Y_{j+1} = \frac{cos\theta_{j+1}}{cos\theta_j}\sqrt{\frac{\varepsilon_{j+1}\left(1-j\ tan\ \delta_{j+1}\right)}{\varepsilon_j\left(1-j\ tan\delta_j\right)}} \quad (38)$$

$$Z_{j+1} = \frac{cos\theta_{j+1}}{cos\theta_j}\sqrt{\frac{\varepsilon_j\left(1-j\ tan\ \delta_j\right)}{\varepsilon_{j+1}\left(1-j\ tan\ \delta_{j+1}\right)}} \quad (39)$$

$$\psi_j = d_j\gamma_j cos\theta_j \quad (40)$$

$$\gamma_j = \pm\sqrt{j\omega\mu_j(\sigma_j + j\omega\varepsilon_j)} \quad (41)$$

Where θ_j = complex angle of refraction in the ith layer.

In this manuscript, the developed code for the computation of the reflection coefficient has only treated the normal incidence.

2.2.3 Choice of the compositions of the different layers

To obtain a good absorption, we have to minimize the reflections between air and absorber and also at the interfaces between the different layers. Thus, the composition of each layer of the multilayer absorber should be chosen carefully. Indeed, if the incoming EM wave arrives at a medium with very different dielectric properties, the medium will act as a reflector due to the impedance mismatching. Thus, in the case of the multilayer absorber, if there is an impedance discontinuity between the layers, reflections will occur not only at the first interface, but also between the different layers, with a reflection level proportional to the amount of the impedance discontinuity.

A smooth gradual impedance could be ensured by following the configuration shown in Figure II.7. In this configuration, the first layer possesses the lowest losses among all layers in order to ensure a smooth transition, of the EM waves, between air and absorber. This first layer is followed by a layer, or several layers, with medium losses that ensure impedance continuity (for a smooth transition of the EM waves) and

a gradual absorption. The last layer, or several layers, is the one with the highest losses in order to ensure the total absorption of the EM waves. By this way, the EM waves will be transmitted from one layer to another with the minimal reflections between the interfaces, and these waves will be absorbed gradually in consecutive layers.

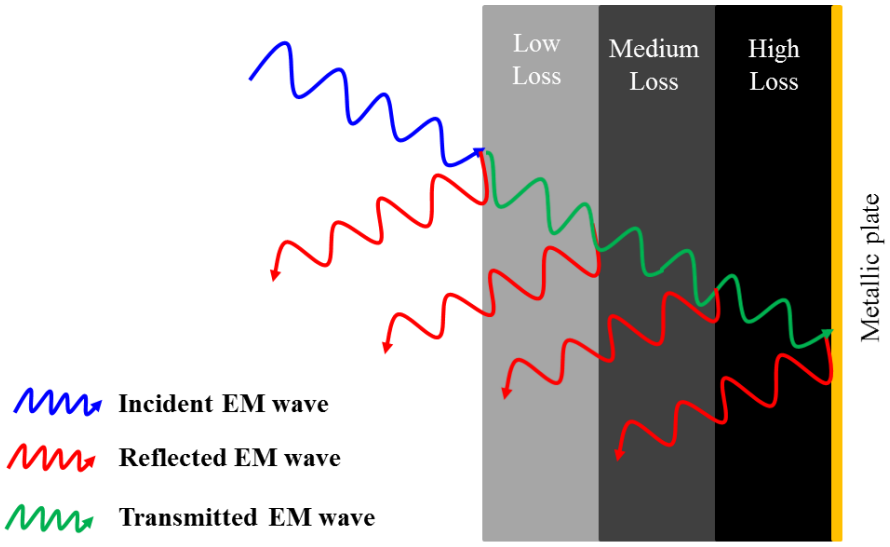

Figure II.7. Configuration used to form a gradual multilayer absorber.

By another way, one could observe the impedance of each layer in order to investigate the impedance discontinuity. Indeed, the closer the values of the impedances of two materials that composes two adjacent layers are, the less the reflectivity that will occur at their boundaries. For this reason, the characteristic impedances of the different composites are calculated; these impedances, related to the dielectric and magnetic properties of the material, can be calculated using equation (42). In our case, where pure dielectric composites will be used, the magnetic properties are equal to 1; therefore, the impedances of all composites that will be used for the multilayer absorber should be calculated using the dielectric properties of these composites.

$$\eta_c = \eta_0 \sqrt{\widetilde{\mu_r}/\widetilde{\varepsilon_r}} = \sqrt{\mu_0/\varepsilon_0} \sqrt{\widetilde{\mu_r}/\widetilde{\varepsilon_r}} = 377 \sqrt{1/\widetilde{\varepsilon_r}} \tag{42}$$

The gradual impedance, which should be realized for any microwave multilayer absorber, could be also observed by plotting the impedance of each layer at each frequency with respect to the depth. In Figure II.8 (a), an example of a dielectric multilayer structure with gradual impedance from Z_1 to Z_4 is presented. Here the green color of the layers, which becomes lighter with depth, corresponds to the impedance of each layer. On the other hand, the module of the characteristic impedance $|Z|$ of each layer with respect to depth is presented in Figure II.8 (b). This impedance starts from an impedance near to that of air (Z_0) and decreases gradually with depth to Z_4, the lowest impedance. However, for an ideal absorber, the impedance should decrease exponentially in depth [3], as shown in Figure II.8 (c), in order to absorb all the incident EM waves. Therefore, the nearest the gradual impedance to the ideal behavior, the better the performance of the multilayer absorber.

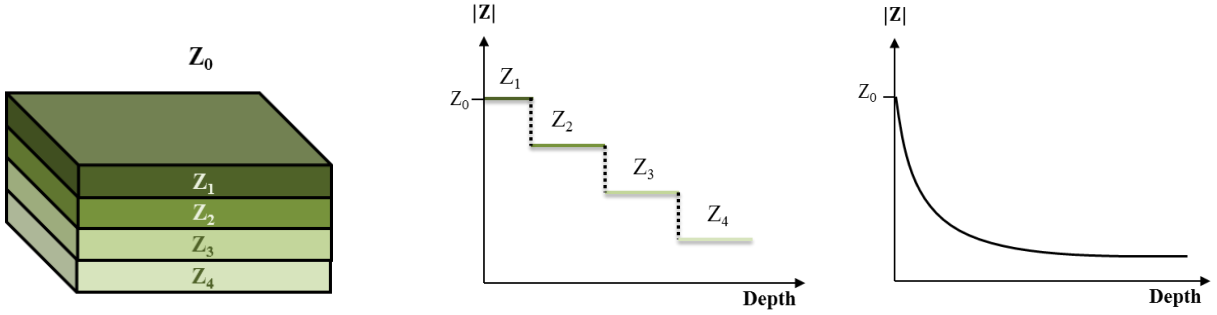

(a) (b) (c)

Figure II.8. Example of (a) a gradual multilayer structure, (b) of the gradient of impedance for each layer and (c) the impedance profile of an ideal absorber.

An example of how to build a multilayer absorber is presented in [4]. Here, *Micheli and al.* have calculated the modules of the intrinsic impedances, in the X-Band, of the epoxy resin composites loaded with five different types of carbon (graphite, fullerene, SWCNT, MWCNT and CNF) and different weight percentages (1, 3 and 5 wt.%). The modules of the calculated intrinsic impedances of their composites, using the material properties and equation (42), are presented in Figure II.9. Based on these calculated impedances, they achieved a multilayer absorber of 10 mm total thickness (Figure II.10 (a)) which is composed of two types of carbon: graphite (1 wt.% and 3 wt.%) for the first two layers and fibers (3 wt.% and 5 wt.%) for the last two layers. They have chosen the composite with the highest impedance (graphite 1 wt.%) for the first layer and the composite with the lowest impedance (CNF 5 wt.%) for the last layer. For the layers in between, they have chosen two composites with intermediate impedances. By this, a reflection coefficient less than -10 dB in the X-band and less than -20 dB between 8.3 GHz and 11.5 GHz are obtained (Figure II.10 (b)).

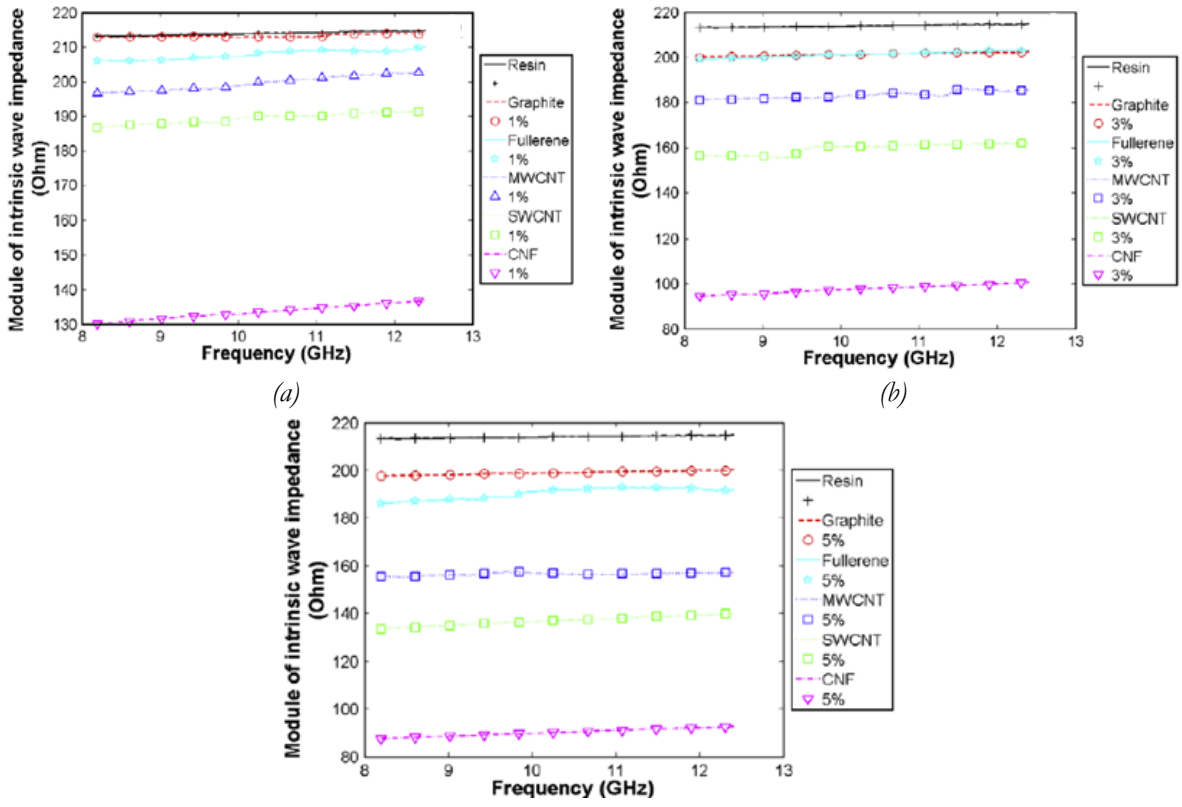

(a) (b) (c)

Figure II.9. Calculated impedances of epoxy resin composites loaded with five different types of carbon and different wt.%: (a) 1wt.%, (b) 3wt.% and (c) 5 wt.% [4].

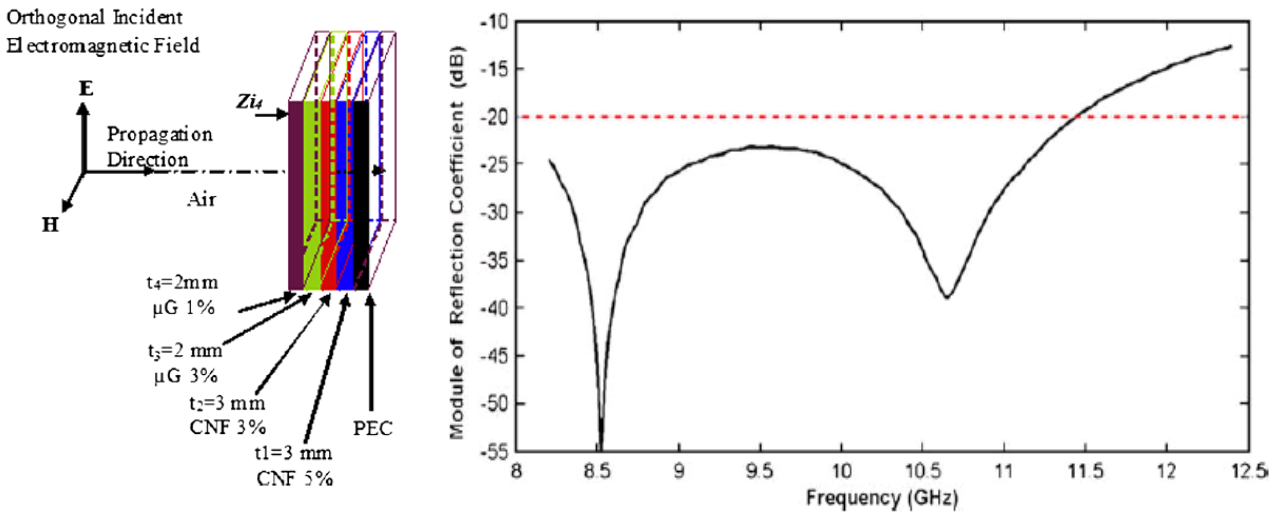

(a) *(b)*

Figure II.10. (a) Proposed multilayer absorber and (b) its simulated reflection coefficient [12].

3. Carbon fiber loaded epoxy foam composites

The carbon fiber (CF) loaded epoxy foam composites, elaborated by our team [2], will be used in this section to develop planar multilayer absorbers. In this section, the elaboration technique of these composites is explained in the first part, and followed by the characterization technique in the second part. In this work, different carbon fiber lengths and weight percentages will be used in order to obtain a large panel of dielectric properties that will be used after this to build an efficient multilayer absorber over a large band.

3.1 Elaboration steps

The epoxy resin (PB 170) and hardener (DM02), purchased from SICOMIN, and carbon fibers (fibers exPAN), provided by Apply Carbon SA, are used for the elaboration of our composites. CFs have a density of 1.7, a diameter of 7 µm and different lengths of 100 µm, 1 mm, 3mm, 6 mm and 12 mm; these CFs are shown in Figure II.11. Different CF weight percentages, from 0.0125 wt.% to 1 wt.%, are used in this thesis.

Figure II.12 summarizes the different steps of the elaboration method: the CFs (with the chosen length and wt.%) were dispersed in the acetone (60 ml) using the chemical surfactant SDS (Sodium Dodecyl Sulfate) and ultra-sonication methods; this step is detailed in [5]. Then, ¼ of the epoxy resin quantity is added to the mixture that was exposed to a temperature of 50°C to evaporate the acetone. After that, the rest of the epoxy resin quantity was added to the mixture, as well as, the hardener with the proportions Resin:Hardener of 10:3.6. Finally, the mixture was placed into a large mold for foaming and polymerization steps, during 6 hours at room temperature. Subsequently, the mold was placed in the oven (at 60°C for 6 hours) to finalize the polymerization of the epoxy foam and thus obtaining the final rigid composite. The samples were finally cut to the dimensions of 15 cm x 15 cm x 6 cm, needed for the characterization in anechoic chamber.

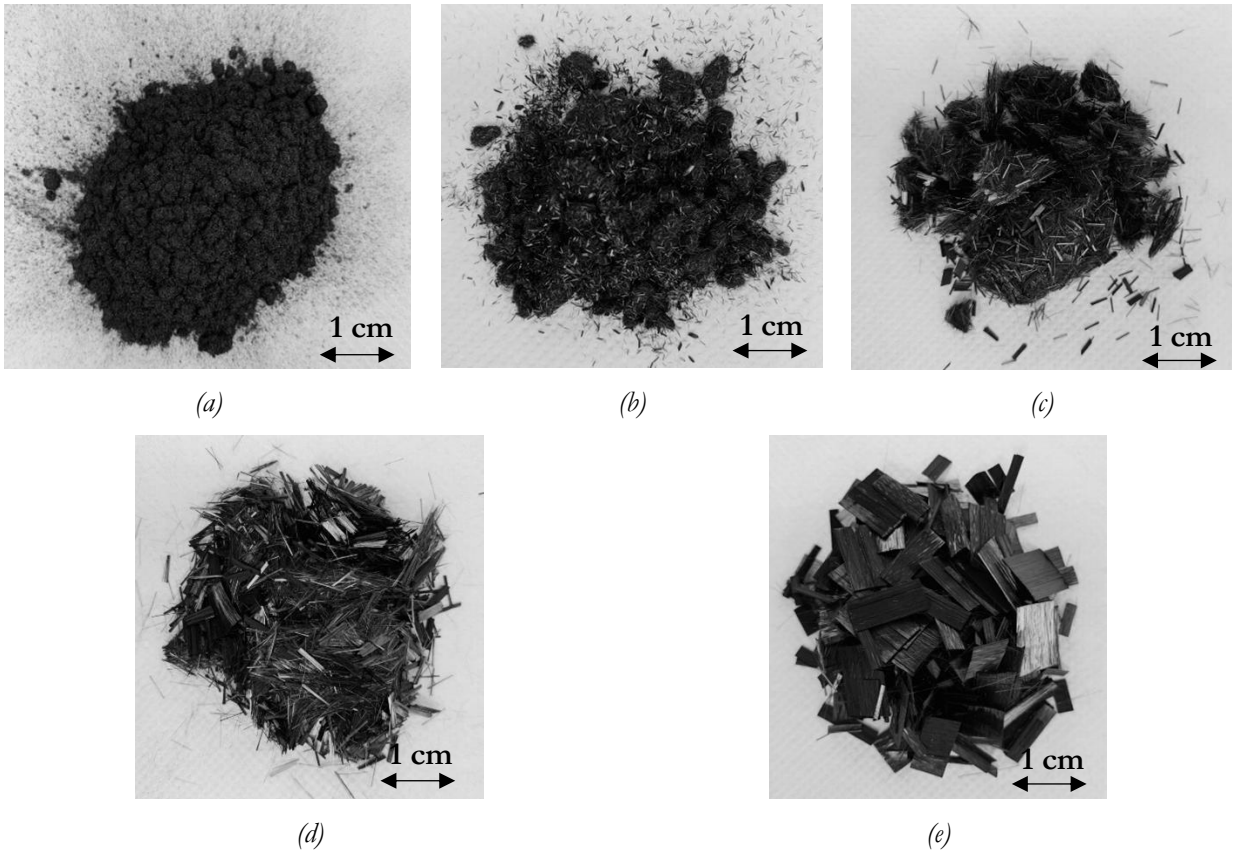

Figure II.11. Photos of the CFs with lengths of (a) 100µm, (b) 1 mm, (c) 3 mm, (d) 6 mm and (e) 12 mm.

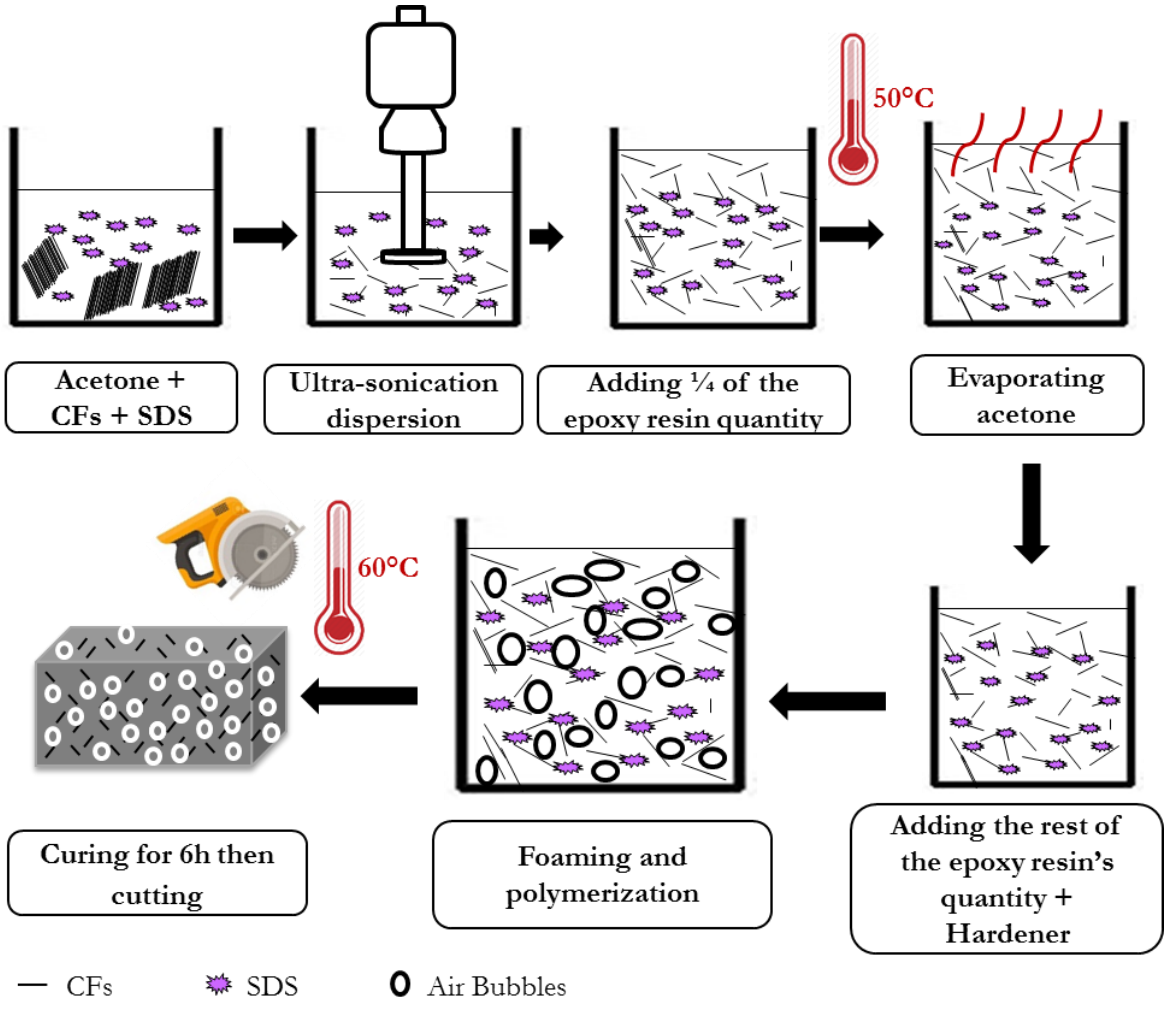

Figure II.12. Elaboration steps of the CF loaded epoxy foam composites.

3.2 Characterization technique

The complex permittivity of the elaborated composites was extracted from the measurement using free space method detailed in [6]. For this measurement, a quasi-monostatic configuration was used (as shown in Figure II.13). Thus, two horn antennas (3115 Ets-Lindgren Model, one transmitter and one receiver), that operates in the range 0.75-18 GHz, were placed side by side in the anechoic chamber. Antennas were connected to a vector network analyzer with a wave's power of -8 dBm (0.15 mW). Each sample of the elaborated composites was placed in front of the two antennas at a distance d from the antennas, ensuring the far field condition (equation (43)), where D is the antenna aperture diameter and λ is the highest measured wavelength [6].

$$d \geq \frac{2D^2}{\lambda} \tag{43}$$

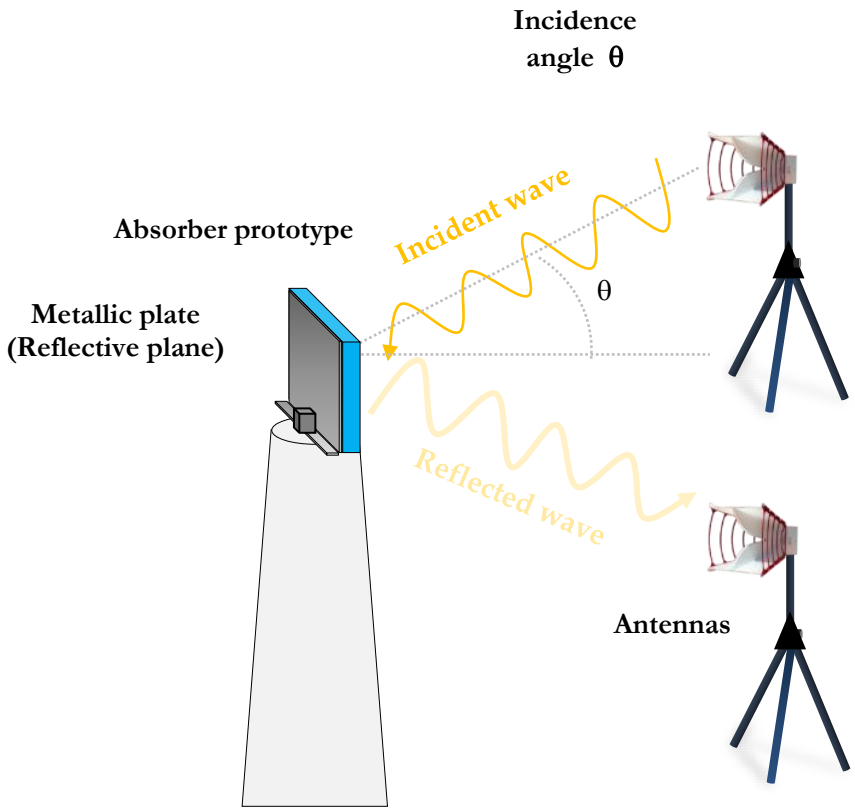

Figure II.13. Configuration used in the anechoic chamber to measure the reflection coefficient.

For this measurement method, conducted in the anechoic chamber, the reflection (S_{11} & S_{22}) and transmission (S_{21} & S_{12}) coefficients of the different elaborated composites were measured. These coefficients were used to extract the dielectric properties of the composites (material under test / MUT) using NRW method [6]. The same configuration was also used for the measurement of the reflection coefficient of the prototypes. For a normal incidence (Figure II.14 (a)), the two antennas are placed side by side with a small negligible angle of incidence. For an oblique incidence θ, the two antennas are separated

by a distance in order to form the required angle of incidence; Figure II.14 (b) shows the configuration of the two antennas with an angle of incidence of 30°.

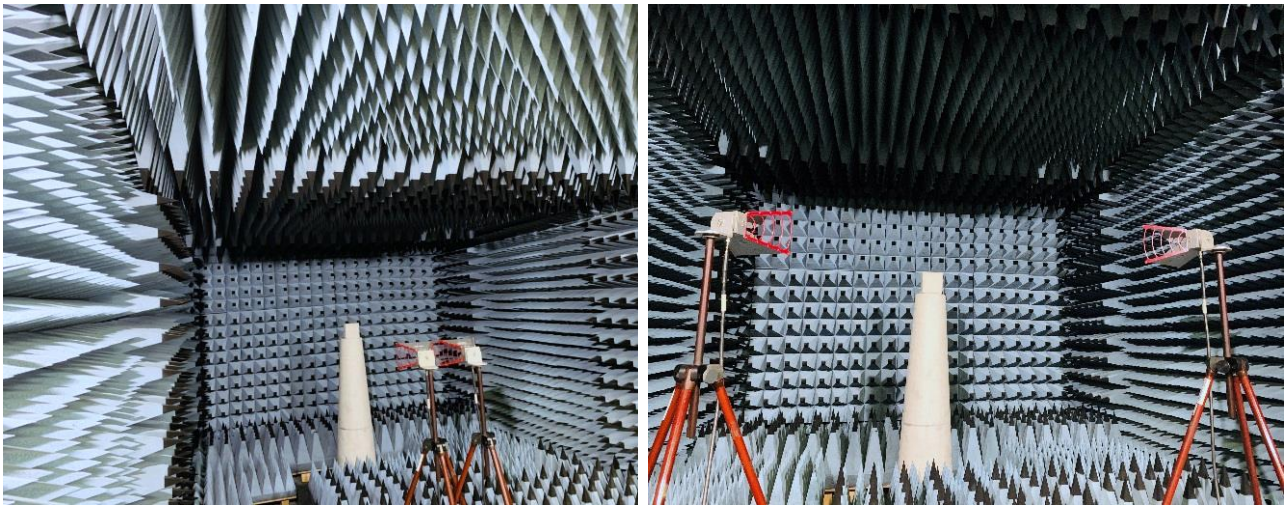

(a) (b)

Figure II.14. Measurement (a) at normal incidence and (b) at oblique incidence of 30° in the anechoic chamber of INSA of Rennes.

For the extraction of the dielectric properties of our materials, the reflection and transmission coefficients were measured at normal incidence and for four different configurations as illustrated in Figure II.15: absorber alone, absorber backed with metallic plate, metallic plate alone and the environment alone. For the absorber, measurements of each face with four orientations were done.

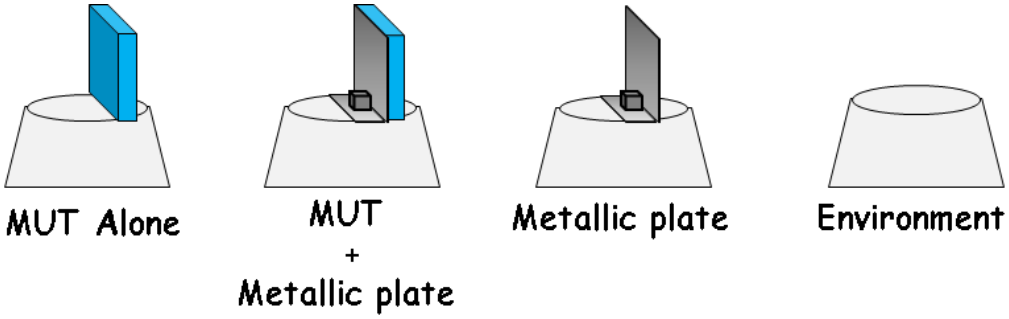

Figure II.15. Four measurements required for the extraction of the dielectric properties.

For the calculation of the reflection coefficient of a material with metallic plate (MUT + MP) or without it (MUT), we use the following equations (44) and (45):

$$S_{11}^{MUT} = \frac{S_{21}^{MUT} - S_{21}^{env}}{S_{21}^{env} - S_{21}^{metal}} \tag{44}$$

$$S_{11}^{MUT+MP} = \frac{S_{21}^{MUT+MP} - S_{21}^{env}}{S_{21}^{env} - S_{21}^{metal}} \tag{45}$$

To extract the complex permittivity, first we have to calculate Z using equation (46) where Z^2 is the transverse impedance and Z^A and Z^B are the impedances of the sample backed with the metallic plate (MUT + MP) and alone (MUT), respectively. Since the measurements were done in free space, the wave impedance is Z_0 = 377 Ω and Z^A and Z^B are calculated using equations (47) and (48).

$$Z^2 = \frac{Z_0 Z^A Z^B}{Z_0 + Z^A - Z^B} \quad (46)$$

$$Z^A = Z_0 \frac{1+S_{11}^{MUT+MP}}{1-S_{11}^{MUT+MP}} \quad (47)$$

$$Z^B = Z_0 \frac{1+S_{11}^{MUT}}{1-S_{11}^{MUT}} \quad (48)$$

Now, the complex permittivity can be extracted using equation (49) where θ is the very small angle between the two antennas that can be calculated mathematically. Dielectric losses are calculated by equation (50).

$$\tilde{\varepsilon}_r = \frac{Z_0^2}{Z^2} + sin^2\theta \quad (49)$$

$$\tan\delta = \frac{\varepsilon_r''}{\varepsilon_r'} \quad (50)$$

The measured reflection coefficient, as well as, the extracted dielectric properties have little noise and are not smooth. For the measured reflection coefficient of the prototypes and the extracted dielectric properties of the elaborated samples, the noise could be reduced by smoothing the resulting curves in MATLAB. However, for the extracted dielectric properties, where the measure uncertainty appears the most at the beginning of the curves, a fit tool (with a degree) is applied after the smooth in order to fit the real behavior of the measured composite. An example of the extracted dielectric properties (blue curve), and their smooth equivalence (black curve), are shown in Figure II.16 (a) and (b).

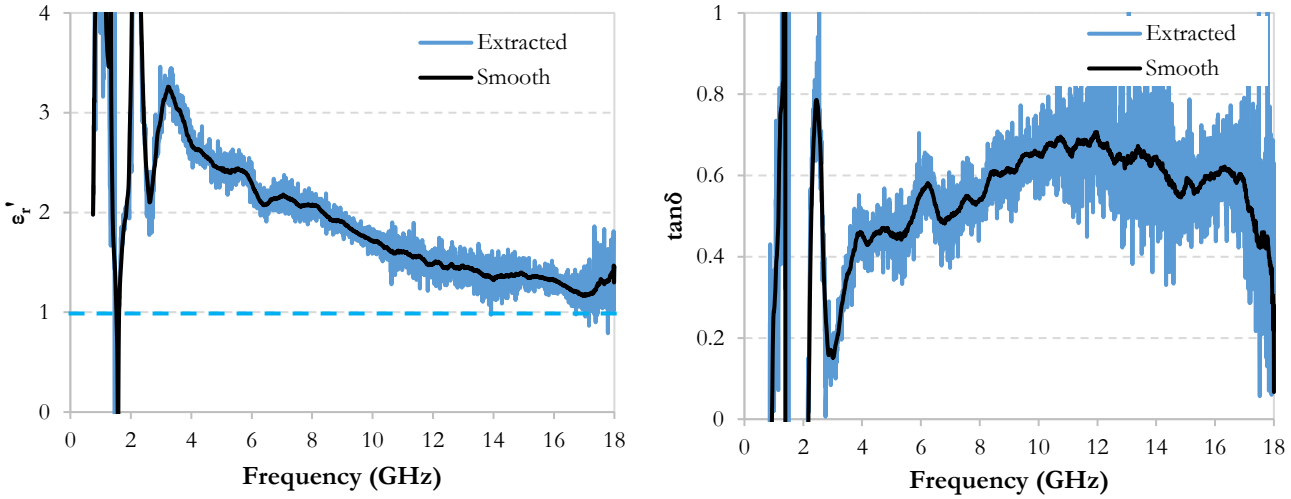

Figure II.16. The extracted dielectric properties and their smooth equivalence ε_r' (a) and tanδ (b) of a loaded epoxy foam composite with respect to frequency.

Figure II.17 (a) and (b) present the dielectric properties of the same measurement for the smoothed (black curve) and the fitted (red curve) using "cftool" in MATLAB. After doing the fit for the eight measurements, a mean value of the eight is calculated and is considered as the dielectric properties of the measured composite.

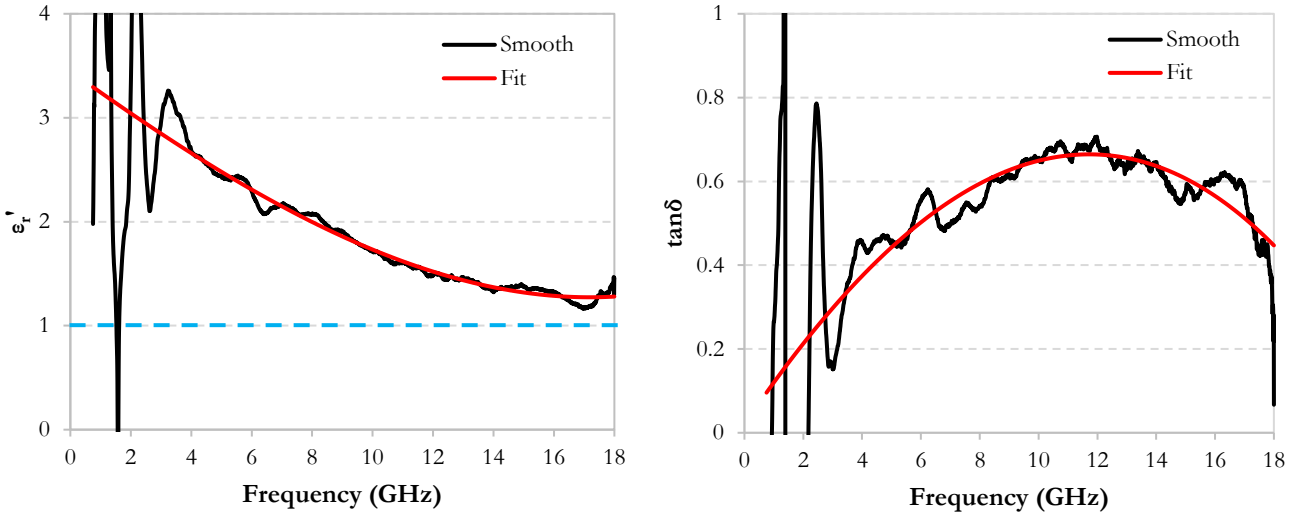

Figure II.17. The fit of the extracted dielectric properties ε_r' (a) and tanδ (b) of a loaded epoxy foam composite with respect to frequency.

3.3 Dielectric properties and module of the characteristic impedance of the elaborated samples

In this part, several samples (15 cm x 15 cm x 6 cm) of epoxy foam composites, with a density equal to 0.12 g/cm^3, loaded with different weight percentages ≤ 1 wt.% and three CF lengths (3 mm, 6 mm and 12 mm), were elaborated. For long fibers, the used weight percentages are limited to 0.5 wt.% and 1 wt.% for CFs of 12 mm and 6 mm lengths respectively; this is due to the percolation threshold that is achieved in these cases. The dielectric properties ε_r' and tanδ of the elaborated composites are shown in Figure II.18, Figure II.19 and Figure II.20, respectively for 3 mm, 6 mm and 12 mm CF lengths. We note an increase of ε_r' associated with an increase of the dielectric losses with respect to the weight percentage and for all CF lengths.

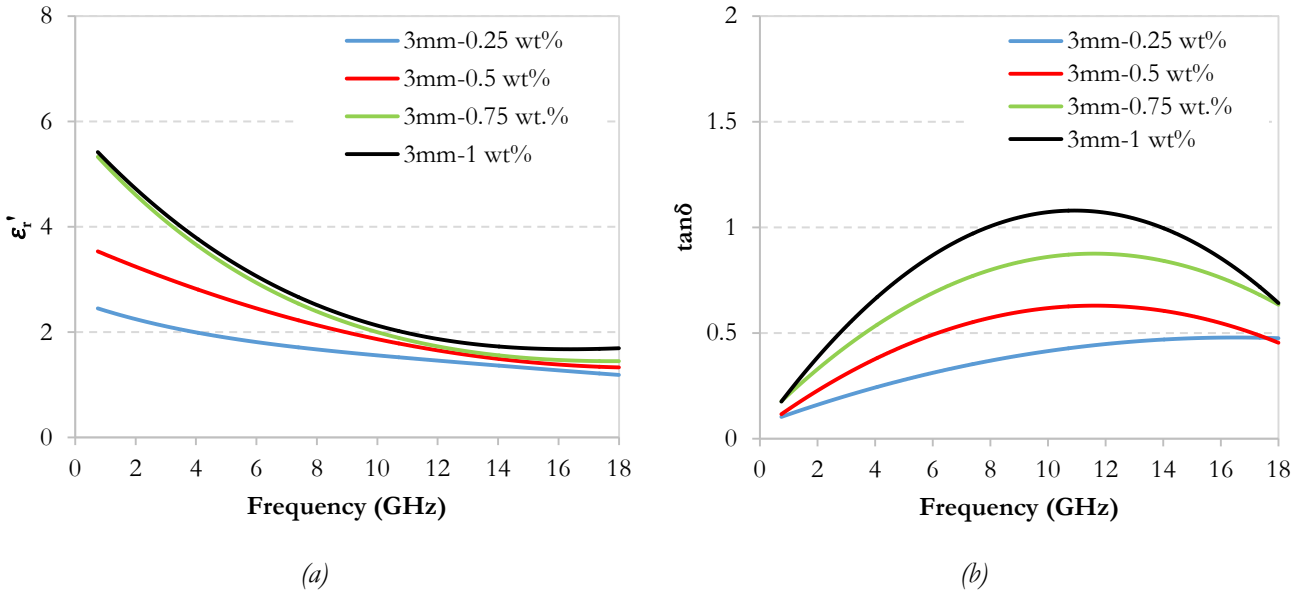

Figure II.18. The dielectric properties ε_r' (a) and tanδ (b) of the elaborated composites loaded with 3 mm CFs using different wt.% with respect to frequency.

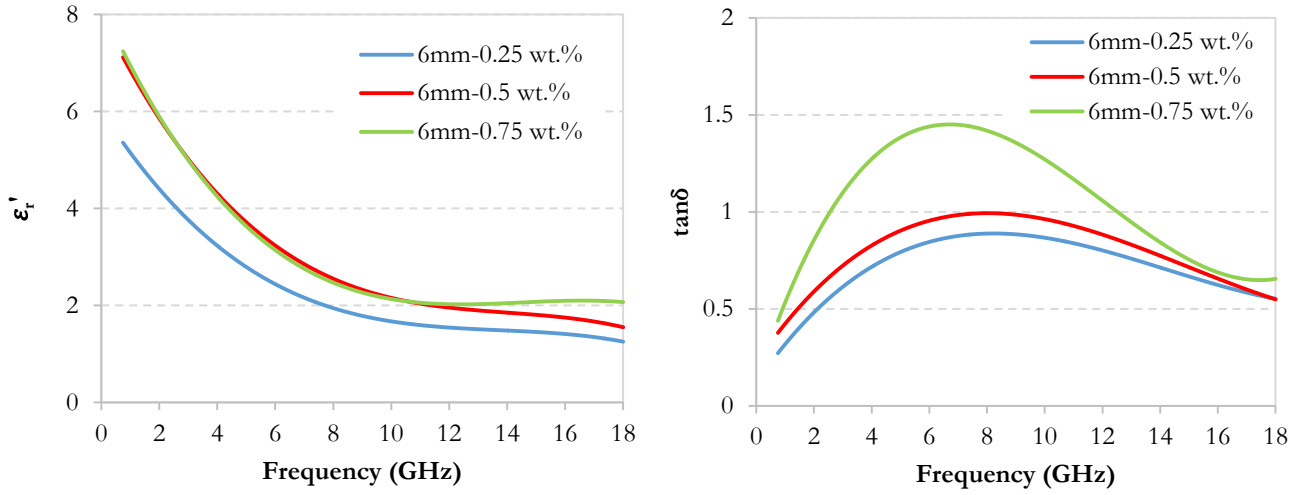

(a) (b)

Figure II.19. The dielectric properties ε'_r (a) and tanδ (b) of the elaborated composites loaded with 6 mm CFs using different wt.% with respect to frequency.

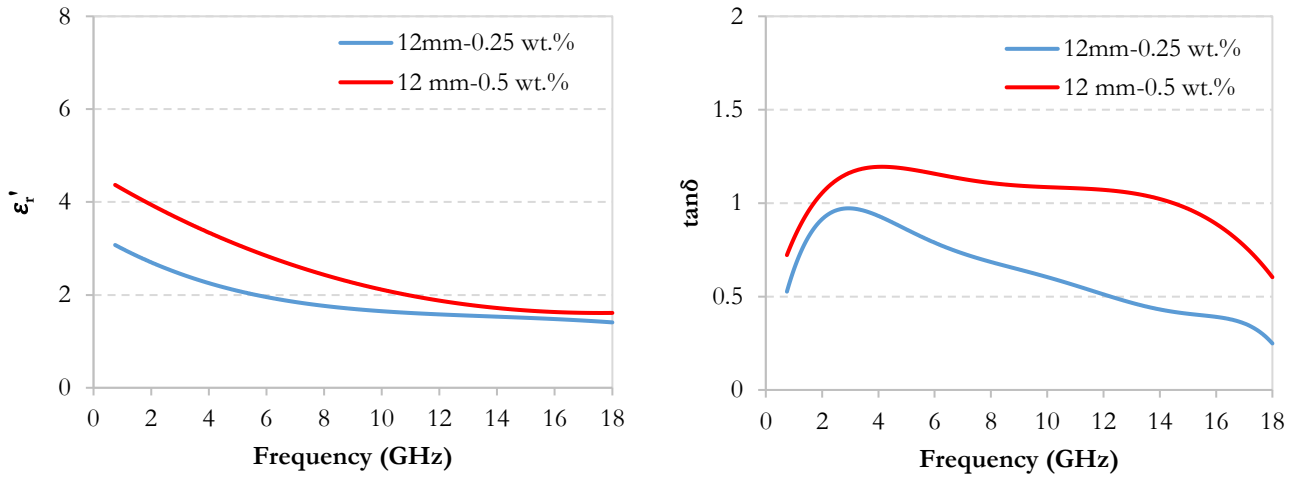

(a) (b)

Figure II.20. The dielectric properties ε'_r (a) and (b) tanδ of the elaborated composites loaded with 12 mm CFs using different wt.% with respect to frequency.

The decreasing behavior of ε'_r versus frequency is typical of carbon loads, whereas for the tanδ, we firstly observe a gradual increase to a maximum around 11 GHz for the CF length of 3 mm, around 6 GHz for CF length of 6 mm and around 3 GHz for the CF length of 12 mm; this behavior was observed in previous work [5]. For a clear observation of this phenomena, the dielectric losses of samples loaded with 0.25 wt.% of 3, 6 and 12mm-CFs are plotted in Figure II.21. From the latter, it is clearly visible that the maximum of the dielectric losses is obtained at low frequencies for material loaded with 12mm-CFs ($\tan\delta_{max}$ = 0.97 at 2.8 GHz) and at high frequencies for material loaded with 3mm-CFs ($\tan\delta_{max}$ = 0.55 at 18 GHz). The material loaded with 6 mm-CFs shows maximum losses at the central frequencies, $\tan\delta_{max}$ = 0.89 at 8 GHz. Consequently, these results confirm the effect of the CF length on the absorption frequency range, represented here by the dielectric losses. Therefore, it seems that long CFs are more interesting for absorption at low frequencies while short CFs (3 mm) are more interesting for absorption at high frequencies.

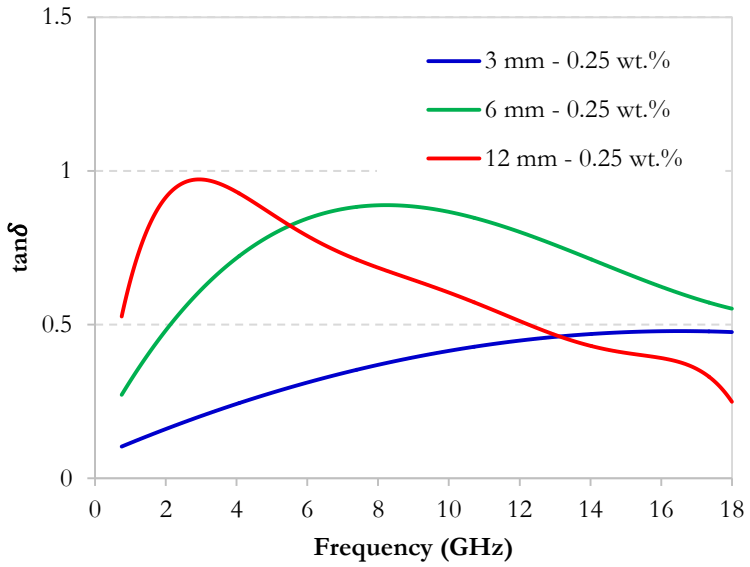

Figure II.21. Dielectric losses of epoxy foams loaded with 0.25 wt.% of 3, 6 and 12mm-CFs.

The module of the intrinsic impedances of all the elaborated composites are calculated by equation (42) and presented in Figure II.22. The impedance of the same CF length, using different rates, decreases with the increase of the weight percentage. For example, at 10 GHz, for the loaded epoxy foams with 3 mm CFs, the impedance decreases from 290 Ω (for 0.25 wt.%) to 203 Ω (for 1 wt.%); for the epoxy loaded foam with 6 mm CFs, the impedance decreases from 254 Ω (for 0.25 wt.%) to 213 Ω (for 0.75 wt.%) and for the epoxy loaded foam with 12 mm CFs, the impedance decreases from 271 Ω (for 0.25 wt.%) to 213 Ω (for 0.5 wt.%). Note that there is a big gap (Figure II.22) between the unloaded epoxy foam and the first loaded epoxy foam composites (between 344 Ω and 262 Ω at 4 GHz, for example). This gap should be reduced in order to have a better gradient of impedance and consequently, improve the absorber performance.

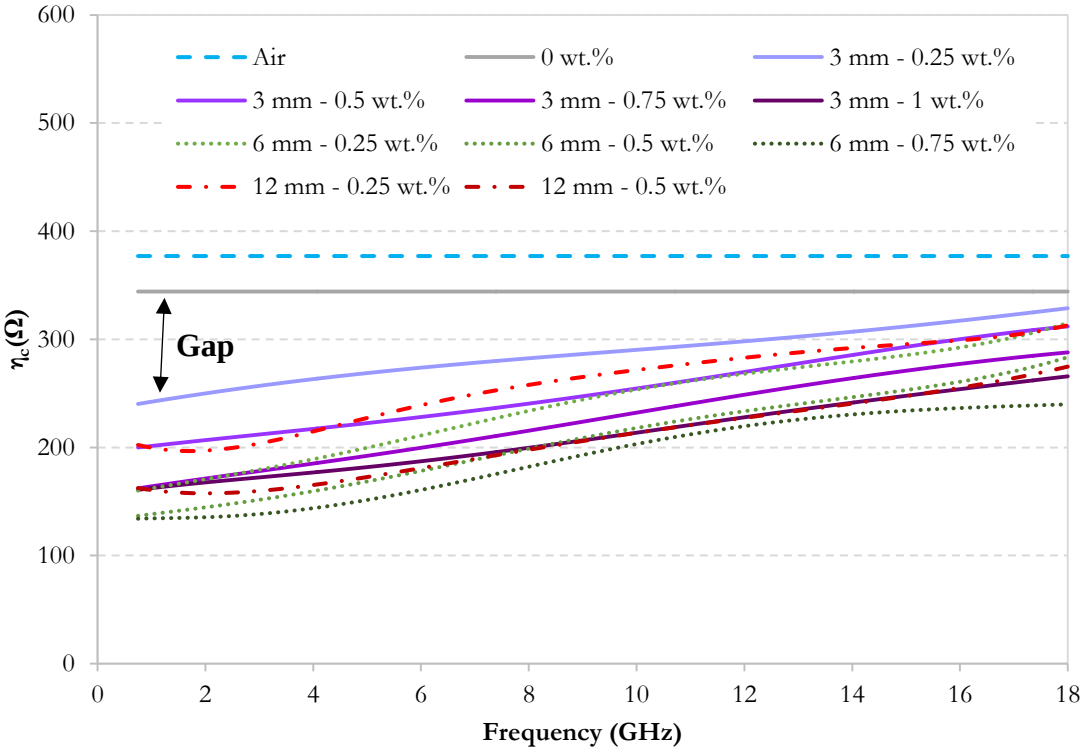

Figure II.22. Calculated module of the intrinsic impedances of the elaborated epoxy foam composites.

4. Microwave multilayer absorber based on loaded epoxy foams

A first prototype of multilayer absorber (with 4 layers) has been realized using the elaborated composites presented in the previous section. The proposed prototype MLA250 (with 250 mm total thickness) is shown in Figure II.23 (a); this thickness is often used for commercial multilayer absorbers (such as SIEPEL). For the choice of the compositions of the different layers and to ensure and impedance matching, as well as, a smooth transition of the EM waves, we referred to the example cited before (Figure II. 9). Indeed, to ensure an impedance matching between the air and the absorber interface, the first layer must have the closest impedance to that of the air. Here, the unloaded epoxy foam (0 wt.%), that has an impedance equal to 344 Ω, was chosen for this first layer. Then, epoxy foam loaded with 6 mm-0.75 wt. %, which has the lowest impedance among all elaborated composites, was chosen for the last layer of the absorber. After this, and in order to guarantee the impedance matching between the different layers, the impedance of the intermediate layers must be between the impedances of the first and the last layer. For this reason, the 3mm-0.25 wt.% and the 12mm-0.25 wt.% composites, with intermediate characteristic impedances, were respectively chosen for the second and the third layers. The chosen impedances of the proposed prototype are shown in Figure II.23 (b). It should be noted here that the thickness of the first layer is chosen higher than the three other layers in order to guarantee a good transition of the EM waves between the air and the multilayer absorber.

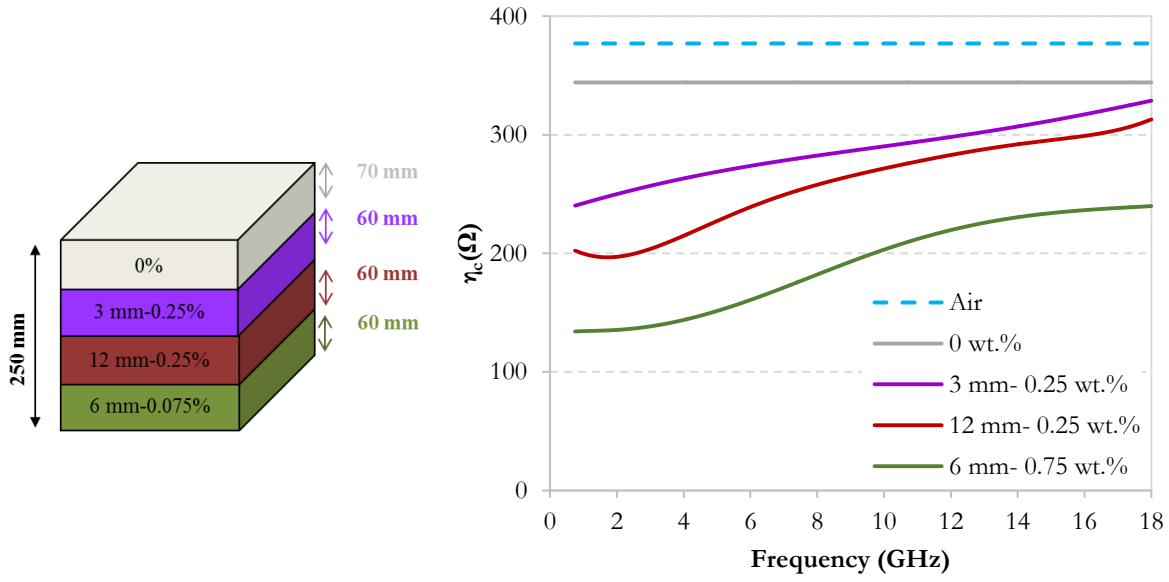

(a) *(b)*

Figure II.23. Design of MLA250 prototype (a) and the module of the intrinsic impedances of the epoxy foam composites that are used for this prototype (b). (Impedance of air is represented by a cyan dashed line).

A plot of the calculated module of the intrinsic impedances of this prototype, with respect to the depth, is shown in Figure II.24 (a), (b), (c) and (d), respectively for 2 GHz, 4 GHz, 10 GHz and 16 GHz. It could be observed from these figures that the gradual impedance principle is well applied here for all the presented frequencies with respect to depth. In addition to that, the impedance discontinuity becomes smaller for high

frequencies than at low frequencies. For example, at 2 GHz, the impedance of the first layer (Layer 1), which is 344.1 Ω, decreases progressively to 134 Ω at the last layer (Layer 4); here, the difference is about 210.1 Ω, while at 16 GHz, the impedance of the first layer, which is 344.1 Ω, decreases to 236.4 Ω at the last layer; here, the difference is about 107.6 Ω.

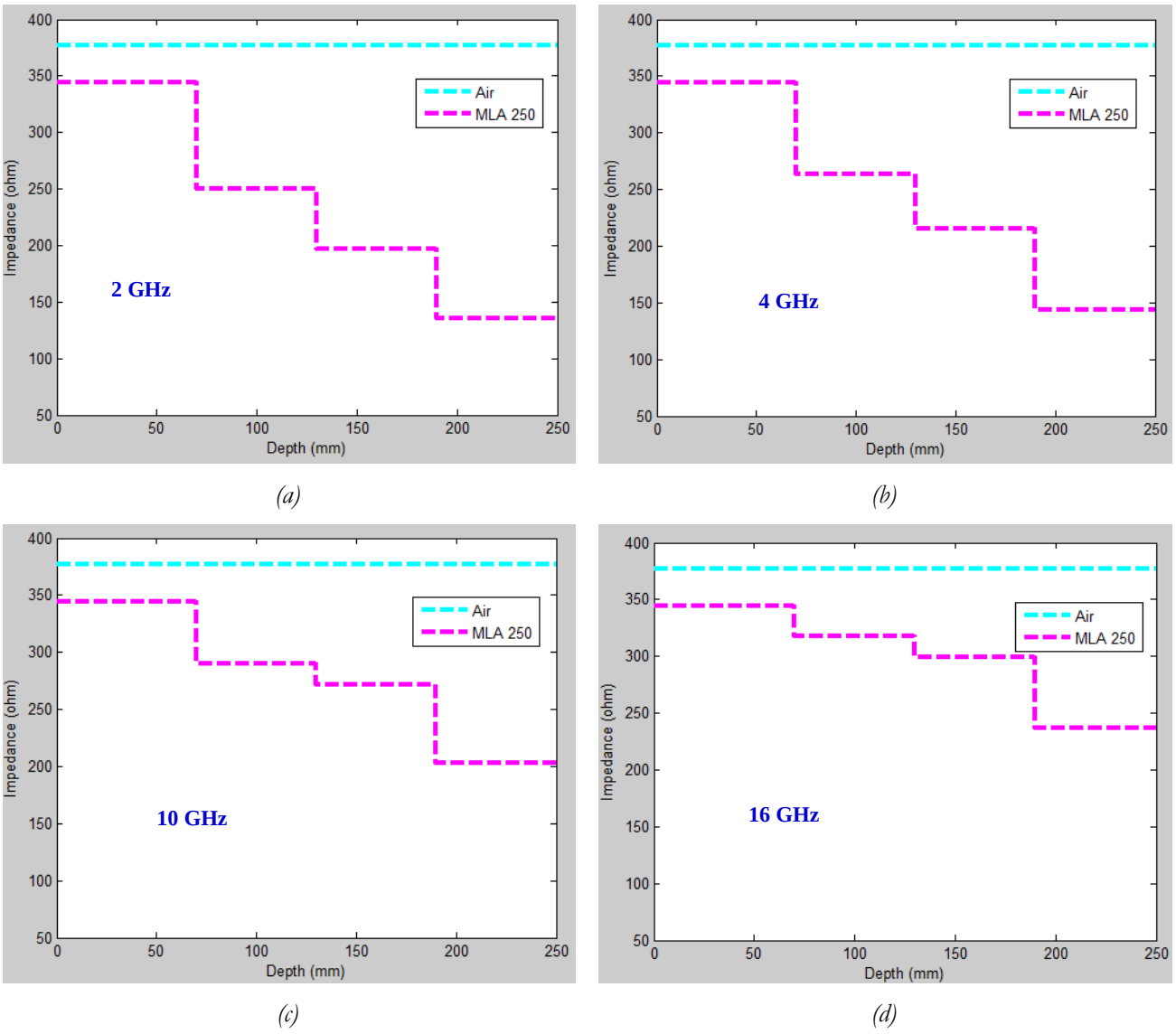

Figure II.24. The calculated module of the intrinsic impedance of the four layers composing the first prototype MLA250 at (a) 2 GHz, (b) 4 GHz, (c) 10 GHz and (d) 16 GHz with respect to depth.

The realized prototype MLA250 is presented in Figure II.25 (a). The simulated and the measured reflection coefficients of this first prototype are presented in Figure II.25 (b). A simulated reflection coefficient less than -10 dB has been predicted in the overall studied frequency range between 0.75 GHz and 18 GHz. This performance is confirmed by the measurement result. A difference between the measured and the simulated performances is observed above 4 GHz. This is probably due to inhomogeneous elaborated composites, especially those loaded with long CFs (6 and 12 mm). In fact, these two composites present a gradient of the load, this inhomogeneity (gradient load) was used to our advantage during the measurement by placing the inhomogeneous layers (with their gradient load) in the direction of our gradual multilayer. This is why a better measured performance is obtained.

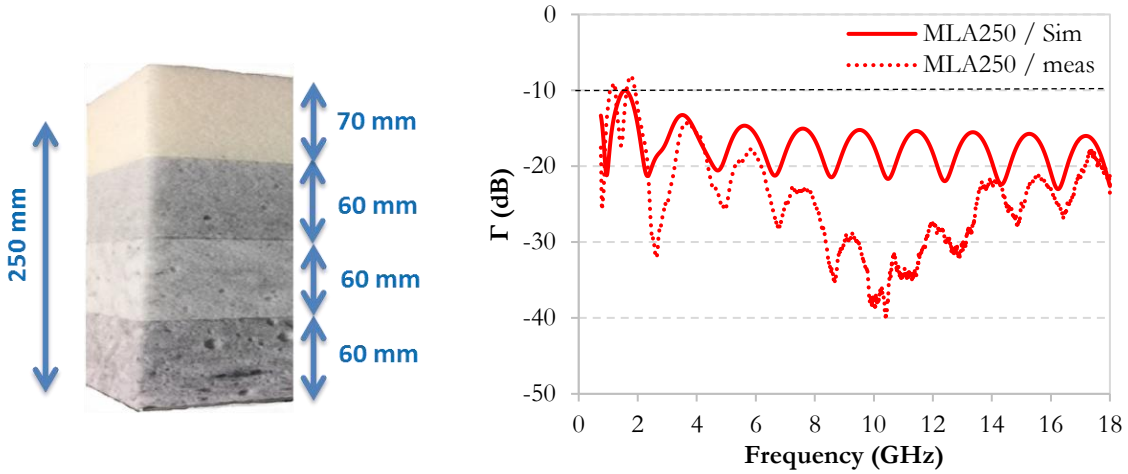

(a) (b)

Figure II.25. (a) Photo of the MLA250 realized prototype and (b) its simulated (by CST) and measured reflection coefficients for normal incidence.

Although the measurement of our first prototype shows an interesting result, the simulation of this latter predicts a relative high reflection (between -10 and -20 dB) with regard to the thickness of this absorber. The problem in this case is not the properties of the absorbing layers or their thicknesses, but the reflections that occur between each two consecutive layers. In fact, the used composite layers exhibit high losses, so their absorption capacities cannot be at the origin of the high observed reflection coefficient. In addition, the used thickness of 250 mm cannot also justify this performance. This is confirmed by the simulation of a 125 mm prototype MLA125-1 (Figure II.26 (a)) where each layer of MLA250 is reduced to the half, and conducted with the same materials. The reflection coefficients of this absorber are very close to that of MLA250 (Figure II.26 (b)) with a small difference at the lowest frequencies. Indeed, the high ε_r' and tanδ that have the different layers could be the responsible of the high reflection coefficient.

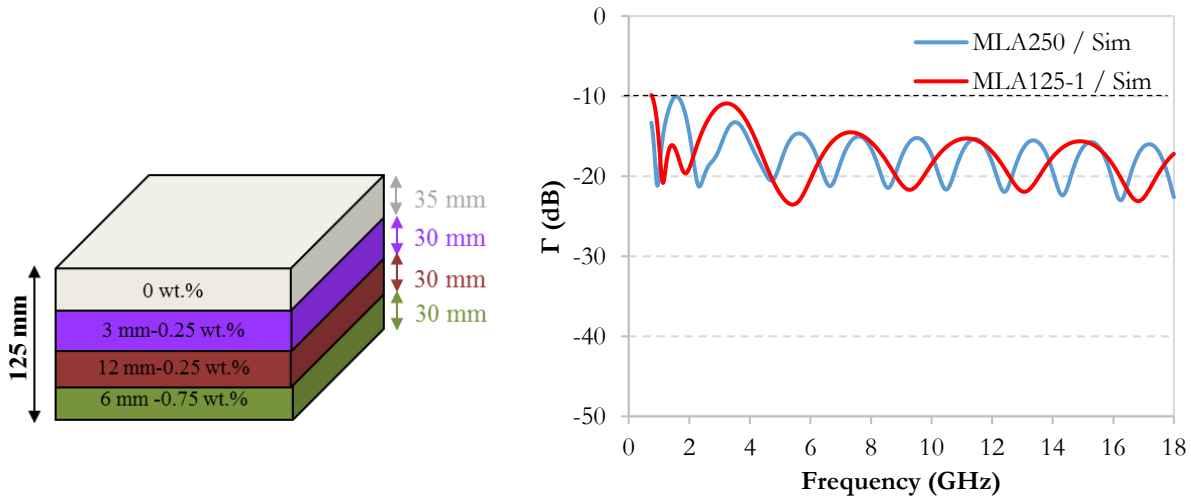

(a) (b)

Figure II.26. (a) MLA125-1 and (b) comparison between simulated reflection coefficients of MLA250 and MLA125-1.

In fact, the chosen layers seem to create an unsmooth gradient of impedance (impedance discontinuity), and induces high reflections at the interfaces of each two successive layers. To confirm this, the reflectivities between each two consecutive layers, for both MLA250 and MLA125-1, were calculated (in %), and the

results are presented in Figure II.27. Here, the presented reflectivity (in %) corresponds to the percentage of the reflected waves, at the interface between two adjacent layers, calculated from the waves which arrive at this interface; so, 100% corresponds to a total reflection of the waves while 0% corresponds to a zero reflection. The reflections seem to be identical for both prototypes, they mainly come from the interfaces between the first and the second layers and between the second and the third layers for the low frequencies, and between the third and the fourth layers interface for the other frequencies > 4 GHz. A slight difference between the levels of the reflections is noted between the two prototypes at the lowest frequencies, this is due to the effect of the thickness of the absorbing layers. Once again, the problem of this prototype lies on the reflectivities between the different layers and not on the thickness or the efficient absorption of the layers.

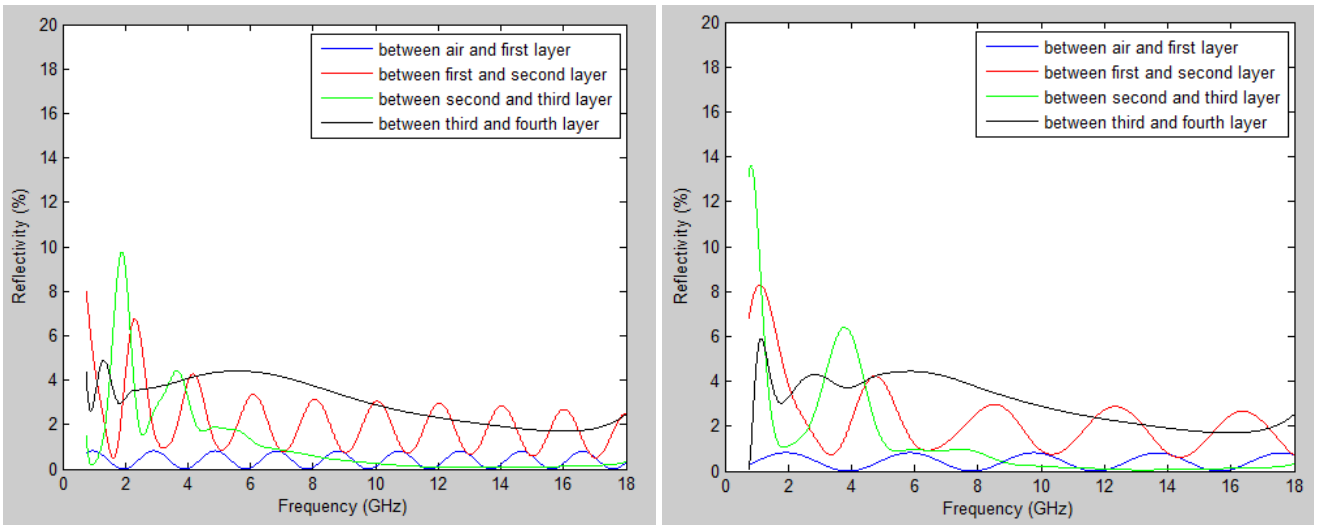

(a) *(b)*

Figure II.27. Reflectivity rate with respect to frequency between each two consecutive layers of (a) MLA250 and (b) MLA125-1.

5. Improved reflection coefficient using lower CF rates

From the previous presented dielectric properties (Figures II.18 to II.20), it could be noticed that the epoxy foam composites loaded with 12 mm CF length have the lowest real permittivity values, even if with high CF rates (> 0.25 wt.%). These low permitivitties are associated with important values of dielectric losses tanδ. In addition to that, it was shown, in a previous work of our team [7], that the use of long CFs makes it possible to obtain high dielectric losses with very low wt.%. For these reasons, composites with low CF rates of the 12 mm CF length were elaborated. The dielectric properties of the five elaborated composites with 0.0125 wt.%, 0.01875 wt.%, 0.025 wt.%, 0.05 wt.% and 0.075 wt.% are shown in Figure II.28. The real permittivity values of the lowest three weights (0.0125 wt.%, 0.01875 wt.% and 0.025 wt.%) are very close to each other; for example, at 10 GHz, the real permittivity ε'_r is equal to 1.17, 1.15 and 1.14 for 0.0125 wt.%, 0.01875 wt.% and 0.025 wt.% respectively. Whereas an increase of permittivities has been noted for both composites loaded with 0.05 wt.% and 0.075 wt.%; for example, the real permittivity ε'_r is equal to 1.37 for both 0.05 wt.% and 0.075 wt.% at the frequency of 10 GHz.

On the other hand, an increase of the dielectric losses is noted with the increase of the CF rate for the five used weight percentages. For example, at 10 GHz, the dielectric loss has increased from 0.06 for 0.0125 wt.% to 0.4 for 0.075 wt.%. The highest dielectric losses (tan δ_{max} = 0.64) are obtained at 2 GHz, associated with ε'_r = 2.19, with the 0.075 wt.% CFs rate. In addition to that, Figure II.28 confirms the importance of using these epoxy foam composites with the 12 mm CF length, which present for low loads, low permittivity values and high losses.

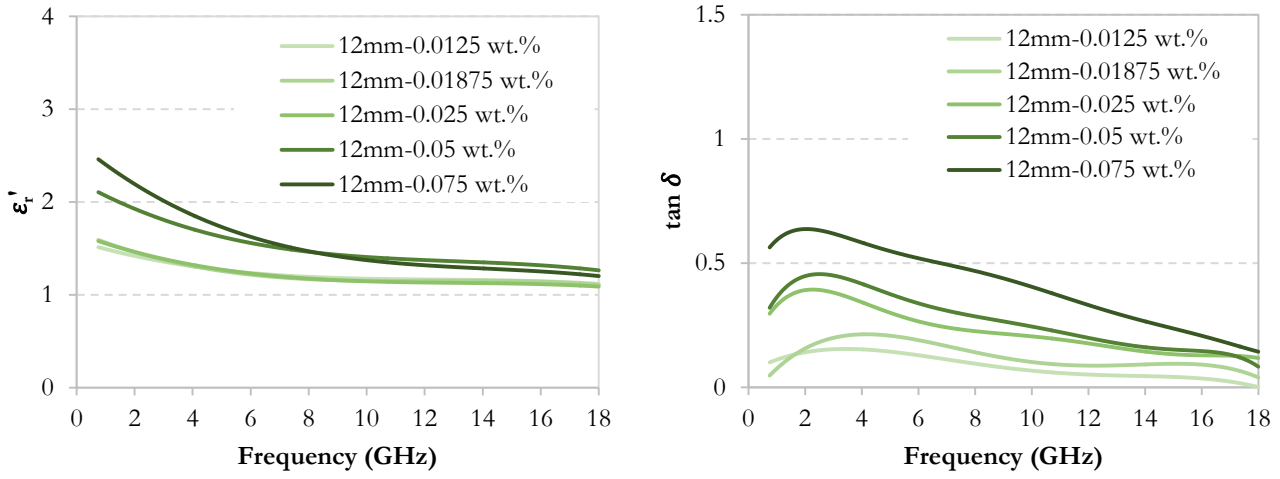

(a) *(b)*

Figure II.28. Dielectric permittivity ε'_r (a) and dielectric losses (b) of low-loaded epoxy foam composites with 12 mm CFs.

Dielectric properties of the composites loaded with 3 mm - 0.25 wt.% and 12 mm - 0.075 wt.% are compared in Figure II.29 (a) and (b). The importance of this comparison is to emphasize the benefit of using the 12 mm CF length. Note that using the 12 mm CF length, with a small weight percentage (0.075 wt.%), induces high dielectric losses, especially at low frequencies, than when using the 3 mm CF length with high weight percentage (0.25 wt.%), associated with very close values of ε'_r. For example, at 4 GHz, the loaded epoxy foam with 0.25 wt.% of 3mm-CFs presents dielectric losses (tanδ) value around 0.24 while the loaded epoxy foam with 0.075 wt.% of 12mm-CFs shows tanδ of 0.58 (practically three times higher).

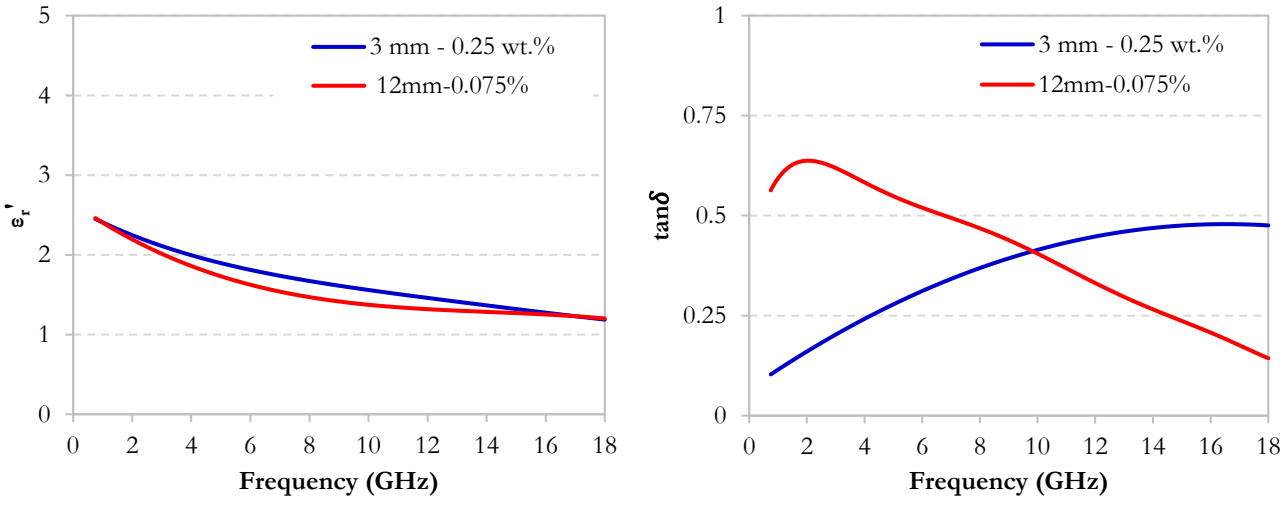

(a) *(b)*

Figure II.29. Dielectric permittivity ε'_r (a) and dielectric losses (b) of 3 mm- 0.25 wt.% and 12 mm - 0.075 wt.%.

The new proposed multilayer absorber MLA125-2 is composed of five layers, contrary to the first realized prototype (with only 4 layers); this fifth layer was added in order to ameliorate the impedance gradient of the multilayer absorber. In addition to that, the commercial absorbers, of the same thickness, are composed of five layers. The module of the intrinsic impedances of the elaborated composites used for this prototype are calculated using equation (42) and the extracted dielectric properties (Figure II.28). The layers ordering, of the proposed prototype, are presented in Figure II.30 (a) and the impedances of each layer are shown in Figure II.30 (b). The latter shows that the impedance decreases with the increase of the weight percentage. For example, at 2 GHz, the highest impedance is equal to 315 Ω for the composite loaded with 12 mm-0.0125 wt.% and the lowest is equal to 212.7 Ω for the composite loaded with 12 mm-0.075 wt.%. For these composites, a better smooth gradual impedance is obtained by the first three layers of the proposed multilayer absorber.

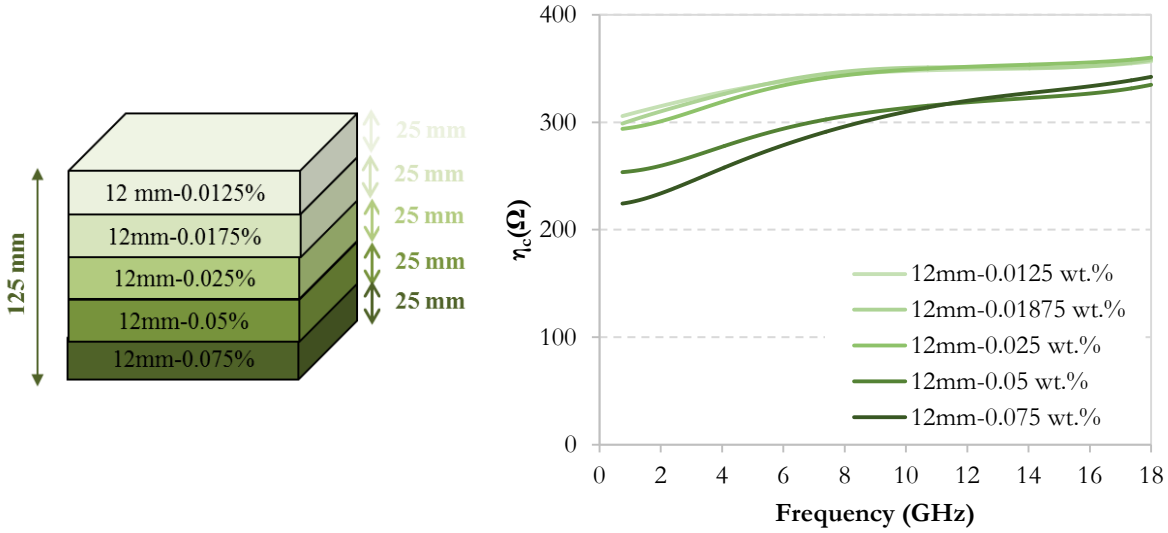

(a) *(b)*

Figure II.30. Design of MLA125-2 (a) and the module of the intrinsic impedances of the loaded epoxy foam composites with 12 mm-low weight percentages (b).

A better view of the smooth gradual impedance is presented in Figure II.31 for several frequencies (2 GHz, 4 GHz, 10 GHz and 16 GHz) and with respect to depth. For example, at 2 GHz (Figure II.31 (a)), the first layer has an impedance of 314.95 Ω which decreases in depth to 310.05 Ω, when achieving the second layer. Then, it decreases to 300.84 Ω at the third layer, to 259.4 Ω at the fourth layer and to 212.7 Ω at the last layer before the metallic plate. Here, a smoother gradient of impedance is obtained, especially for the first three layers. This was done in order to reduce the reflection as much as possible between the first layers. However, the EM waves will be absorbed inside the last two layers which are more loaded than the first three layers.

At the highest frequencies, the impedances of the first three layers are very close to each other, and so the last two layers. For example at 16 GHz (Figure II.31 (d)), the first three layers have very near impedances around 353 Ω. Then the last 2 layers have impedances around 324 Ω.In fact, the ε'_r of all the composites are very close at the high frequencies, due to uncertainty in the measurement; moreover, in the calculation

of the impedances, the variation of the permittivity will impact the obtained values more than the losses; therefore, the impedances look very close.

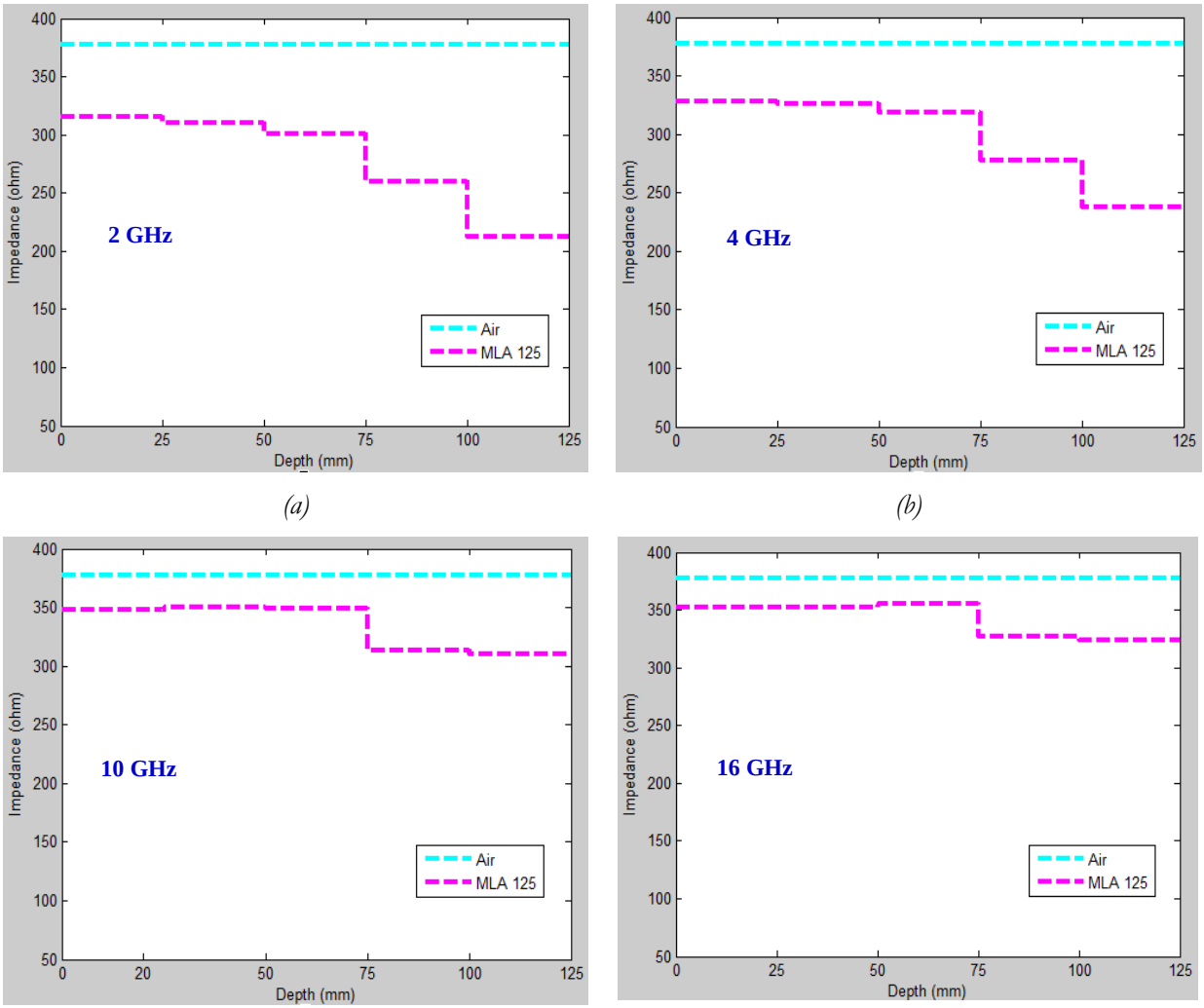

Figure II.31. The calculated module of the intrinsic impedances of the five chosen layers for MLA125-2 at (a) 2 GHz, (b) 4 GHz, (c) 10 GHz and (d) 16 GHz.

The second prototype is simulated using the measured dielectric properties of the elaborated composites (Figure II.28) based on loaded epoxy foams with different weight percentages (from 0.0125 wt.% to 0.075 wt.%) of 12 mm-CFs. The thickness of each layer is 25 mm with a total thickness of 125 mm. This prototype has the same dimensions as the commercial polyurethane foam based multilayer absorber used in the anechoic chamber for the same frequency bandwidth [21].

The simulated reflection coefficients of the proposed MLA125-2, for normal incidence and oblique incidence of 30° are presented in Figure II.32. For normal incidence (Figure II.32 (a)), a reflection coefficient less than -10 dB has been obtained in the whole interval from 1.13 GHz to 18 GHz and a reflection coefficient less than -20 dB has been obtained from 4 to 18 GHz. For oblique incidence of 30° (Figure II.32 (b)), a reflection coefficient less than -10 dB has been obtained from 1.17 GHz and is ensured in the whole interval for both TE and TM modes. A reflection coefficient less than -20 dB has been obtained from 4.2 to 18 GHz for TE mode and from 2.13 to 18 GHz for TM mode.

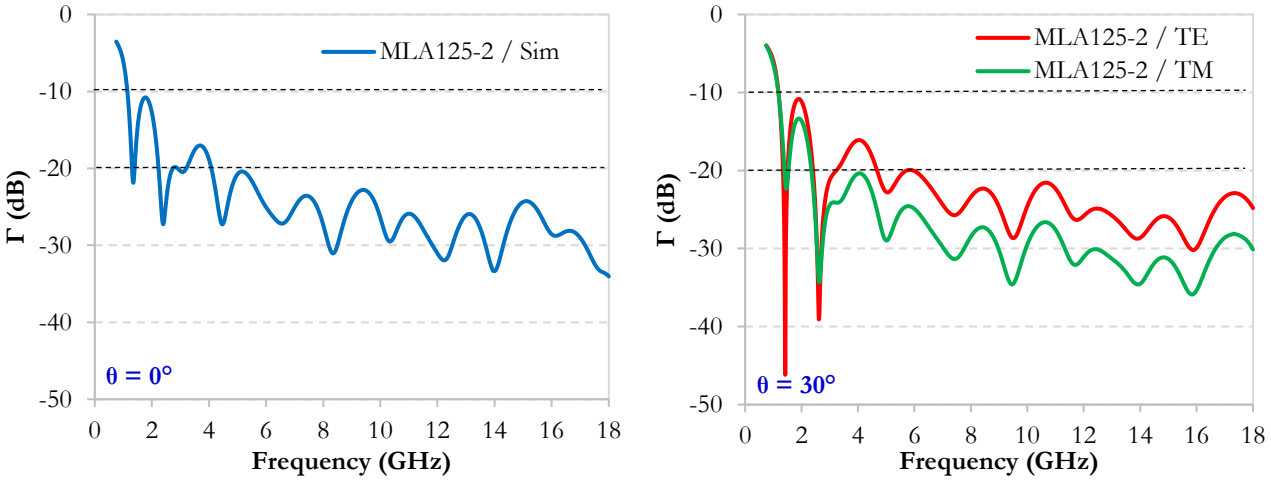

(a) (b)

Figure II.32. Simulated reflection coefficient of MLA125-2 for (a) normal incidence and (b) oblique incidence of θ=30° for TE and TM polarizations.

The photo of the realized prototype, using the composites loaded with low wt.% of CFs of 12 mm, is shown in Figure II.33 (a). A comparison between the simulated and the measured reflection coefficients of the proposed MLA125-2, for normal incidence and oblique incidence of 30° are presented in Figure II.33 (b), (c) and (d).

(a)

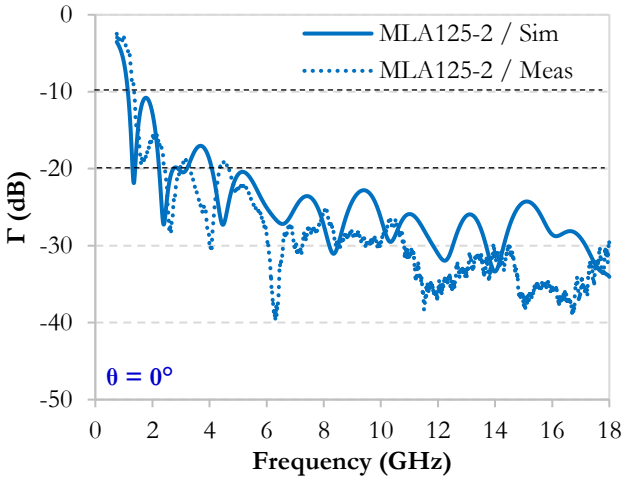

(b)

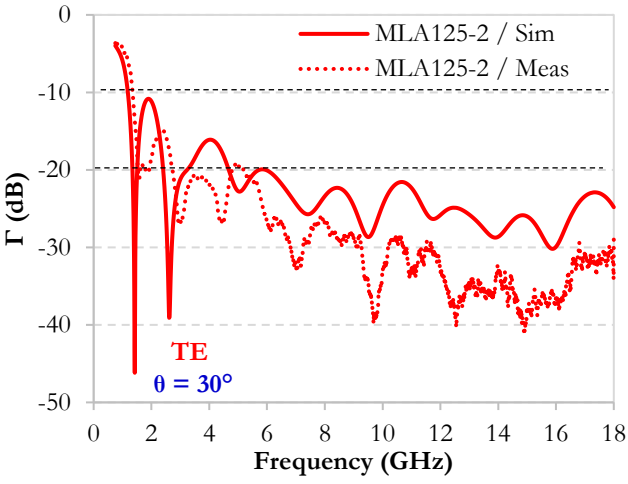

(c)

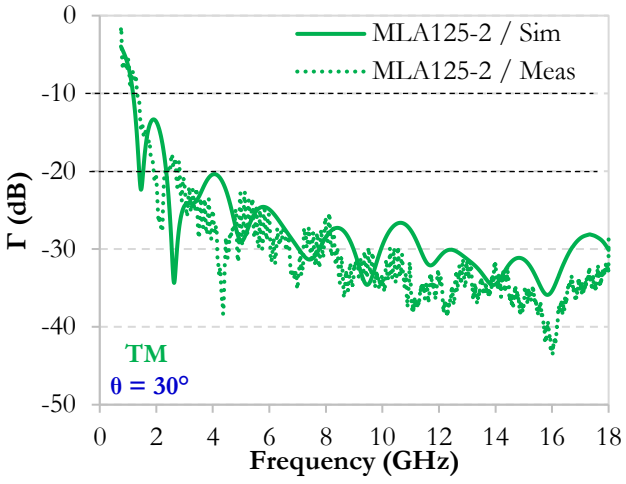

(d)

Figure II.33. MLA125-2 achieved prototype (a) and simulated and measured reflection coefficients for normal incidence (b), and oblique incidence θ=30° for TE (c) and TM (d) polarizations.

For normal incidence (Figure II.33 (b)), the reflection coefficient shows slightly lower values in measurement than simulation results. A reflection coefficient less than -15 dB from 1.15 GHz and less than -20 dB from 2.43 GHz are obtained. At oblique incidence of 30° (Figure II.33 (c) and (d)), better reflection coefficients, compared to that of simulation, are obtained at high frequencies, especially for TE mode.

6. CF loaded lightweight epoxy foams

In a parallel thesis, Ms. Hanadi Breiss has proposed a new method to reduce the density of the epoxy composite, from 0.12 g/cm^3 to 0.05 g/cm^3. Low-density composites, with the same CF length and rates as those used in previous part, are used here for the achievement of a multilayer absorber prototype.

The dielectric properties ε'_r and tanδ of these low density composites with respect to frequency are shown in Figure II.34 (a) and (b). A slight increase of the real permittivity associated with an important increase of the dielectric losses with respect to the weight percentage has been noted here. For example, at 4 GHz, the dielectric losses increase from 0.08 for 0.0125 wt.% to 0.61 for 0.075 wt.% associated with ε'_r ranging between 1.15 and 1.34. The maximum value of dielectric losses (tanδ_{max} = 0.66) is obtained at 2.2 GHz for the highest loaded sample (0.075 wt.%). However, which is important here is that lower permittivity values are obtained with these lightweight composites with respect to relative high density composites, presented in section 6. Here, the unloaded low-density epoxy foam was also elaborated and its dielectric properties are shown in Figure II.34. After 6 GHz, the real part of the permittivity of all composites are identical to the unloaded foam.

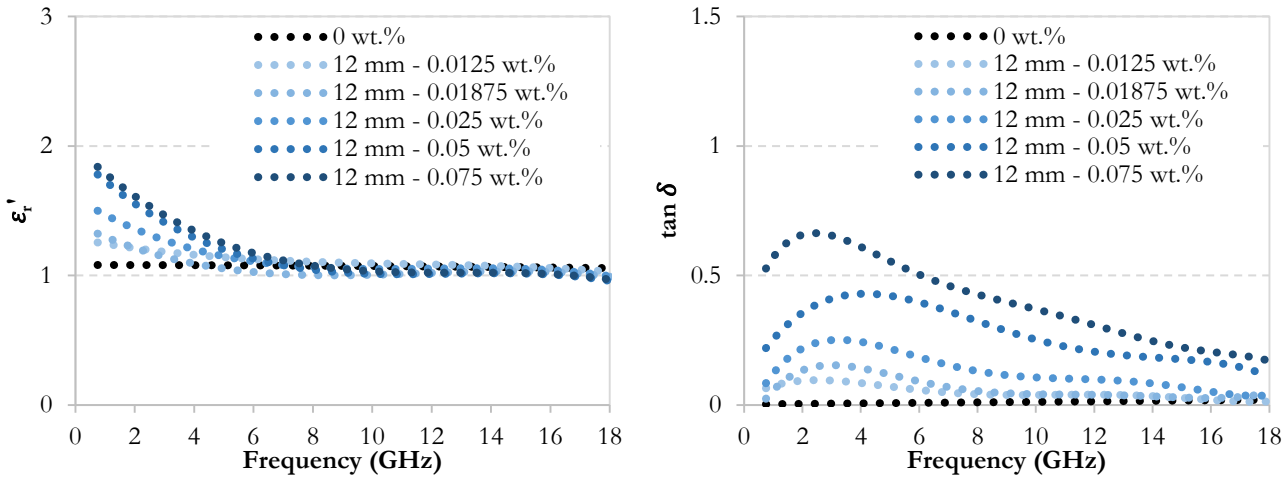

Figure II.34. (a) Dielectric permittivity ε'_r and (b) dielectric losses of the unloaded and low-loaded lightweight epoxy foam composites with 12 mm CFs.

A better smooth and gradual impedance has been used to realize the next prototype based on the elaborated low density epoxy foam composites (Figure II.35 (a)). To better show the gradual impedance that is realized here, the module of the intrinsic impedances of the elaborated composites were calculated and are presented in Figure II.35 (b). From one hand, very close impedances to each other were obtained,

and from the other hand, these impedances are closer to that of air than the previous elaborated composites. In addition to that, the characteristic impedances of these composites decrease with the increase of the weight percentage and remain the same for frequencies above 10 GHz.

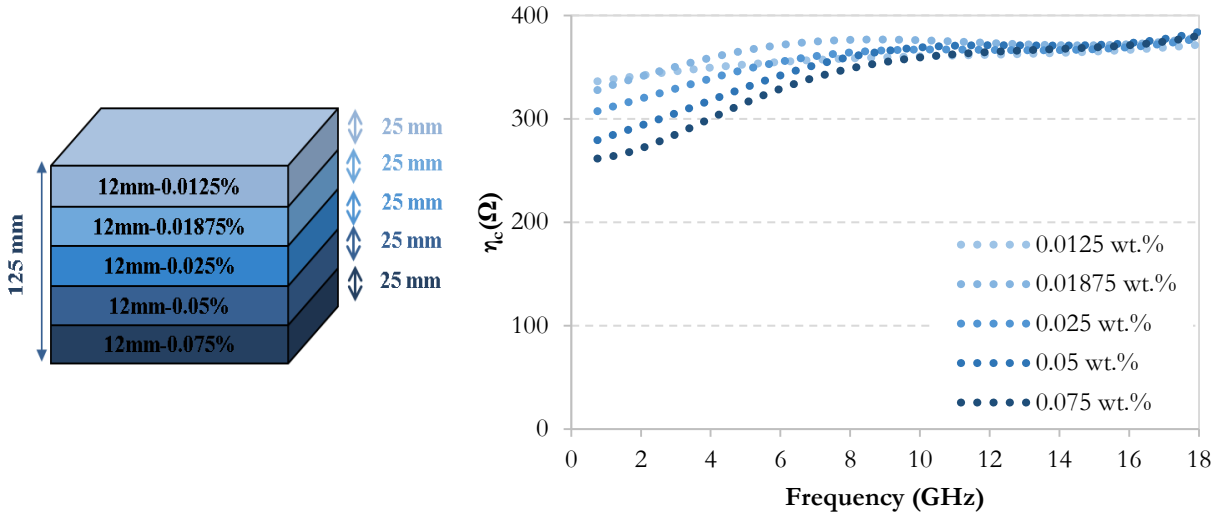

(a) *(b)*

Figure II.35. (a) Design of lightweight LW-MLA125-1 and (b) the module of the intrinsic impedances of the low-density loaded epoxy foam composites with 12 mm- low weight percentages.

The photo of the achieved lightweight prototype LW-MLA125-1 is shown in Figure II.36 (a). Simulated and measured reflection coefficients Γ of this prototype, for normal incidence, are compared in Figure II.36 (b); a good matching with only a slight difference is observed. The ultra-porous and lightweight prototype ensures a reflection coefficient less than -10 dB in the entire frequency band between 1.35 GHz and 18 GHz, and less than -20 dB between 2.6 and 18 GHz.

Simulated and measured reflection coefficients of this prototype, at oblique incidence of 30°, are compared in Figure II.36 (b) for TE and (c) for TM modes. For both modes, a good agreement between simulated and measured reflection coefficients has been also obtained and a reflection coefficient, less than -10 dB, predicted by simulation is obtained by measurement. A reflection coefficient less than -20 dB is obtained for TE from 2.8 GHz to 18 GHz and for TM from 3 GHz to 18 GHz. A lower measured reflection coefficient, compared to the simulated one, for TM mode is noted between 2 GHz and 9 GHz.

A comparison between the measured reflection coefficients of the MLA125-2 with relative high density, the LW-MLA125-1 with low density and the multilayer absorber of SIEPEL AH 125 is presented in Figure II.37. From the one hand, the lightweight LW-MLA125-1 shows a very close performance to that of the relative high density MLA125-2 composed of the same loads. Which is interesting here is that the new proposed prototype has a lower density (reduced to the half) than MLA125-2. From the other hand, and in the frequency band 2-18 GHz, results show that the performance of this lightweight prototype is close to the commercial absorber performance which is highly loaded with CB particles.

In conclusion, with very low CF loads (between 0.0125 and 0.075 wt.%) of 12 mm length, the lightweight LW-MLA125-1 presents a good absorption performance compared to the commercial one.

(a)

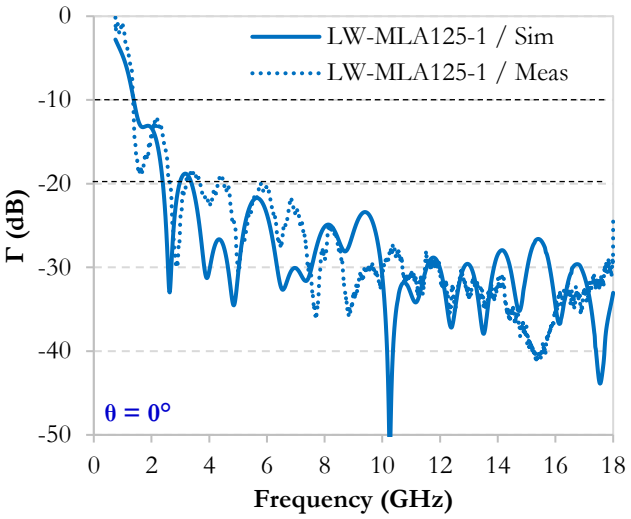

(b)

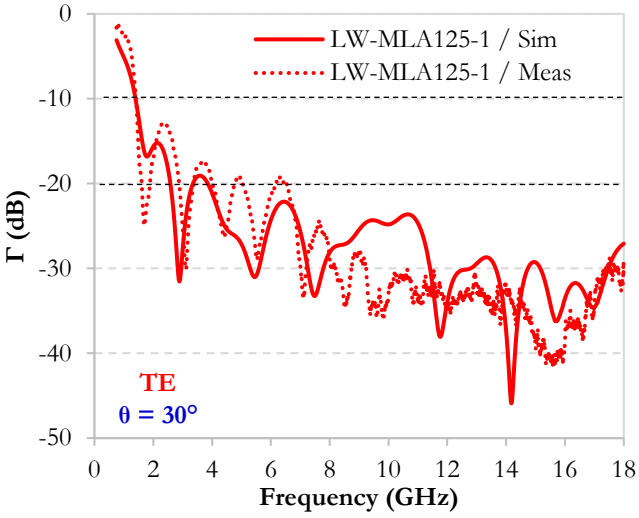

(c)

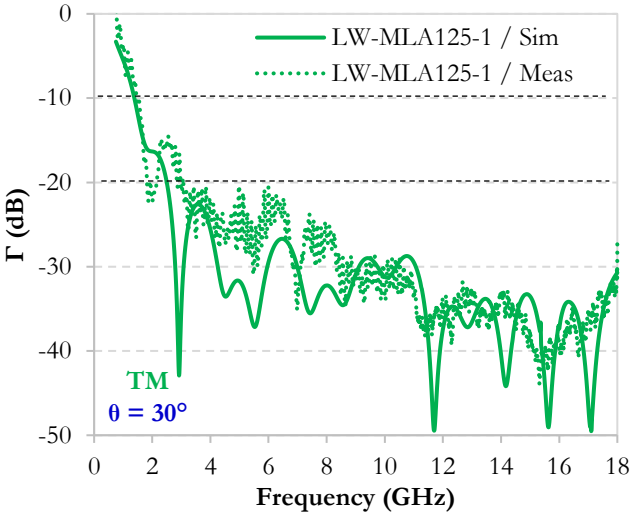

(d)

Figure II.36. Lightweight realized LW-MLA125-1 (a) and its simulated and measured reflection coefficients for normal incidence (b), and oblique incidence θ=30° for TE (c) and TM (d) modes.

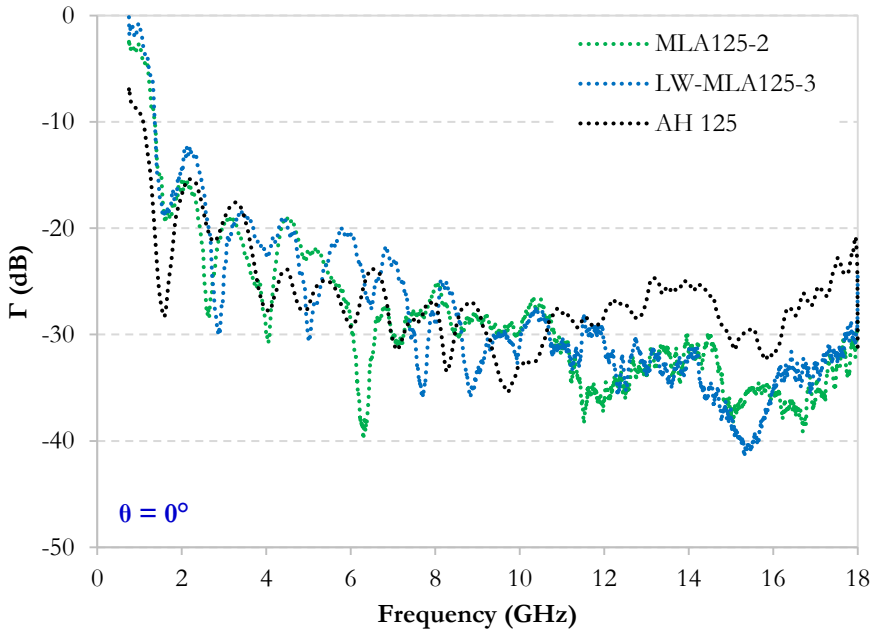

Figure II.37. Comparison between measured reflection coefficients of MLA125-2 and LW-MLA125-1 and with the commercial multilayer absorber AH 125.

7. Conclusion

In this chapter, the importance of using a smooth gradual impedance was emphasized and verified. A first prototype (MLA250), using the unloaded (0 wt.%) and the loaded epoxy foams with different CF lengths, 3 mm, 6 mm and 12 mm, with rates of 0.25 wt.%, 0.75 wt.% and 0/25 wt.%, respectively, is achieved. This prototype does not present a smooth gradient of impedance. Indeed, it shows many reflections between the different layers and low absorption performance, taking into account its thickness (250 mm). Therefore, a second set of composite materials were elaborated, especially to fill up the gap in the calculated characteristic impedances of the first set of blocks. This set includes the loaded epoxy foam composites with 12 mm CFs using different low weight percentages (from 0.0125 wt.% to 0.075 wt.%). The elaborated prototype, using these composites, shows a better absorption performance than the first prototype due to the smoother gradual impedance that was realized by the new set of composites, developed using low weight percentages of long CFs.

The third set of blocks have not only lower weight percentages of CFs, but also, low densities (ranging between 0.05 and 0.07 g/cm^3) than those of the first two set of blocks (0.12 g/cm^3). The new elaborated prototype LW-MLA125-1, using these lightweight composites, shows a very close performance to that of the relative high density MLA125-2 with the same CF rates. This same lightweight prototype presents also a reflection coefficient near to that of the commercial absorber AH 125 of the same dimensions and density. It ensures a reflection coefficient less than -20 dB from 2.6 GHz to 18 GHz. Furthermore, it is a rigid absorber where the CFs are trapped inside the epoxy foam matrix while the commercial multilayer absorbers are flexible and carbon particles may easily escape from the absorber resulting in its premature aging.

The next step will be the optimization of the reflection coefficient of the multilayer absorber, elaborated using epoxy foam composites, with the lowest possible total thickness of the absorber. The reflection coefficient is related to the thickness of each layer, as well as, the material composing each layer. Therefore, those two parameters will be the variables to be changed for further optimizations in the next chapter.

8. References

[1] C. A. Balanis, *Advanced engineering electromagnetics*. New York: Wiley, 1989.

[2] C. Méjean, "Élaboration de Nouveaux Matériaux absorbants : Application en Chambres anéchoïques," PhD, University of Rennes 1, Saint Brieuc, 2017.

[3] A. D. Lustrac, "Matériaux composites en électromagnétisme - Matériaux absorbants radar." Techniques de l'ingénieur, 2018.

[4] D. Micheli, C. Apollo, R. Pastore, and M. Marchetti, "X-Band microwave characterization of carbon-based nanocomposite material, absorption capability comparison and RAS design simulation," *Compos. Sci. Technol.*, vol. 70, no. 2, pp. 400–409, Feb. 2010, doi: 10.1016/j.compscitech.2009.11.015.

[5] H. Breiss, A. El Assal, R. Benzerga, C. Méjean, and A. Sharaiha, "Long Carbon Fibers for Microwave Absorption: Effect of Fiber Length on Absorption Frequency Band," *Micromachines*, vol. 11, no. 12, p. 1081, Dec. 2020, doi: 10.3390/mi11121081.

[6] L. Pometcu, "Matériaux et forme innovants pour l'atténuation en Hyper Fréquences," PhD, University of Rennes 1, Rennes, 2016.

[7] R. Benzerga, M. Badard, C. Méjean, A. El Assal, C. Le Paven, and A. Sharaiha, "Carbon Fibers Loaded Composites for Microwave Absorbing Application: Effect of Fiber Length and Dispersion Process on Dielectric Properties," *J. Electron. Mater.*, vol. 49, no. 5, pp. 2999–3008, May 2020, doi: 10.1007/s11664-020-07998-y.

Chapter III:

Optimizations of the Multilayer Absorbers

Table of contents

List of Figures 102

List of Tables 104

1. Introduction 105

2. MLA optimization using genetic algorithm of CST 105

2.1 Optimization results 106

2.2 Experimental results 109

2.3 Conclusion 111

3. Analytical solution and optimization technique using the GA of MATLAB 112

3.1 Reflection coefficient optimization by GA-MATLAB 112

3.2 Elaborated composites used for the optimization by GA-MATLAB 114

3.3 Optimization results 116

4. Conclusion 129

List of Figures

Figure III.1. Designs of (a) MLA125-1 and (b) MLA125-GA with optimized thicknesses by the GA-CST. 106
Figure III.2. Simulated reflection coefficients for MLA125-GA at (a) normal incidence and (b) oblique incidence of 30° for TE and TM polarizations. 107
Figure III.3. Comparison between the simulated reflection coefficients of MLA125 and the MLA125-GA. 107
Figure III.4. Reflectivity rate with respect to frequency between each two consecutive layers of MLA125-GA. 108
Figure III.5. Design of MLA77-GA with optimized thicknesses by the GA. 109
Figure III.6. Comparison between the simulated reflection coefficients of MLA77-GA and MLA125-GA. 109
Figure III.7. Realized prototypes (a) MLA125-GA and (b) MLA77-GA. 109
Figure III.8. Comparison between the simulated and the measured reflection coefficients for MLA125-GA at normal incidence (a) and at oblique incidence of 30° for TE (b) and TM (c) polarizations. 110
Figure III.9. Comparison between the measured and simulated reflection coefficients for MLA77-GA at normal incidence (a) and at oblique incidence of 30° for TE (b) and TM (c) polarizations. 111
Figure III.10. Flowchart showing the followed steps for the GA in MATLAB. 113
Figure III.11. Real part $\varepsilon r'$ (a) and imaginary part $\varepsilon r''$ (b) of the unloaded epoxy foam (0 wt.%), and the composites loaded with 100 μm CFs using different wt.%. 115
Figure III.12. Real part $\varepsilon r'$ (a) and imaginary part $\varepsilon r''$ (b) of the composites loaded with 3 mm CFs using different wt.%. 115
Figure III.13. Real part $\varepsilon r'$ and imaginary part $\varepsilon r''$ (b) of the composites loaded with 6 mm CFs using different wt.%. 115
Figure III.14. Real part $\varepsilon r'$ (a) and imaginary part $\varepsilon r''$ (b) of the composites loaded with 12 mm CFs using different wt.%. 116
Figure III.15. MLA98-GA-M layers' composition and thicknesses (a) and its simulated reflection coefficient for normal incidence (b) and comparison between MLA125-1, MLA125-GA and MLA98-GA-M (c). 117
Figure III.16. Photo of the realized MLA98-GA-M prototype (a), comparison between its measured and simulated reflection coefficients at normal incidence (b) and at oblique incidence of 30° for TE (c) and TM (d) polarizations. 118
Figure III.17. Comparison between the measured reflection coefficients of MLA98-GA-M and AH 125 at normal incidence. 119
Figure III.18. MLA70-GA-M layers' composition and thicknesses (a) and achieved prototype (b). 120
Figure III.19. Comparison between the simulated and measured reflection coefficients for MLA70-GA-M at normal incidence (a) and at oblique incidence of 30° for TE (b) and TM (c) polarizations. 120

Figure III.20. Design of MLA74-GA-M at [6-12] GHz (a) and MLA69-GA-M at [12-18] GHz (b)..... 122
Figure III.21. Comparison between reflection coefficients of MLA70-GA-M, MLA74-GA-M and MLA69-GA-M. 122
Figure III.22. MLA50-GA-M (a) layers' composition and thicknesses and (b) achieved prototype. 123
Figure III.23. Comparison between measured and simulated reflection coefficients for MLA50-GA-M at normal incidence (a) and at oblique incidence of 30° for TE (b) and TM (c) polarizations. 124
Figure III.24. Design of LW-MLA81-GA-M (a) and comparison between the reflection coefficients of LW-MLA125 and LW-MLA81-GA-M (b). 126
Figure III.25. Simulated reflection coefficient for LW-MLA81-GA-M at oblique incidence of 30° for TE and TM polarizations. 126
Figure III.26. Comparison between measured reflection coefficients of MLA50-GA-M, MLA70-GA-M and MLA77-GA. 127
Figure III.27. Comparison between the measured reflection coefficients of MLA50-GA-M, MLA70-GA-M, MLA98-GA-M, MLA77-GA, MLA125-2 and AH 125 at normal incidence. 128
Figure III.28. Calculated factor of merit of AH 125 compared to that of (a) MLA125-2 and MLA98-GA-M and (b) and MLA77-GA, MLA70-GA-M and MLA50-GA-M. 129

List of Tables

Table III.1. Thicknesses used for the optimization of the four layers absorber using GA CST. 106
Table III.2. Thicknesses used for the optimization of the four layers MLA77-GA. 108
Table III.3. The predefined database. 114
Table III.4. Parameters used for the optimization of the five layers absorber using MATLAB gatool. 116
Table III.5. Parameters used for the optimization of the five layers absorber using MATLAB gatool. 119
Table III.6. Parameters used for the optimization of the three layers absorber using MATLAB gatool. 123
Table III.7. The materials used for the optimization by the GA of MATLAB. 125
Table III.8. Parameters used for the optimization of the five layers absorber using MATLAB gatool. 125

1. Introduction

In the previous chapter, we have shown the approach to design a multilayered structure, using new absorbing materials, to exhibit the highest rate of absorption over the largest possible bandwidth. For this, the minimization of the reflection coefficient of an incident EM wave on a multilayer structure, over a wide frequency range, is required. The big challenge in designing such absorbers is to maintain a low total thickness and to guarantee their compactness. This could be achieved by evolutionary optimization techniques such as genetic algorithm (GA), which are used to find the best solution for such issues.

In this chapter, an optimization procedure, based on GA, is introduced to design a planar broadband absorber. Firstly, the GA implemented in CST will be used; it varies only the thickness of each layer to achieve the best solution, and consequently, the best and the nearest reflection coefficient to the goal. Secondly, we will use analytical equations to compute the total reflection coefficient of a multilayer absorber using a MATLAB code; this code, combined to the GA implemented in MATLAB, will be used for the optimization of the absorption bandwidth of the multilayer absorber. Here, the GA will use different combinations between materials/order/thicknesses for each layer, over many iterations, in order to approach the targeted reflection coefficient. So, the variable parameters are not only the thicknesses of each layer, but also the material composing each layer and its order. New designs of thinner multilayer absorbers, resulting from the proposed combinations, will be presented.

2. MLA optimization using genetic algorithm of CST

The logical function of the GA, implemented in the CST software, is summarized here. The GA generates points in the parameters range and then refines them through multiple generations using random parameter mutation. By selecting the fittest set of parameters at each generation, the algorithm converges to a global optimum. In other words, it consists of optimizing a solution, a result of the problem, over several iterations by selecting the best solutions and allowing them to train the next generation. Then, it creates a population of solutions and it applies genetic operators (mutation and crossing) to find the best one among them. Note that after defining the solution, the parameterization will be carried out over several iterations, giving at the end the optimized parameters of the best obtained result.

Because the GA is used for complex problems and models of many parameters, it could be also used in our case to optimize the thicknesses of the different layers composing the multilayer absorber. In our case, the solution of the problem is the reflection coefficient that should be as low as possible. Here, layers' thicknesses are the parameters to be modified at each iteration and the best result is represented by the nearest reflection coefficient to the goal (targeted reflection coefficient). Minimum and maximum values for each layer could be given also to the optimizer.

2.1 Optimization results

In this part, the GA was tested for the MLA125-1 composed of only 4 layers (Figure III.1 (a)) of loaded epoxy foams which was elaborated in the previous chapter. For this optimization, the same absorbing materials, which were used previously (Chapter II), are here introduced in GA. It consists of the unloaded (0 wt.%) and the loaded epoxy foam composites 3 mm-0.25 wt.%, 12 mm-0.25 wt.% and 6 mm-0.75 wt.%. The range of thicknesses of each layer, introduced in the GA, is presented in Table III.1; these values are chosen taking into account the reflections observed previously between the different layers of MLA125-1 (Figure II.27). Note that using the GA implemented in CST, the thickness of each layer will vary continuously at each iteration, but the overall thickness of the multilayer absorber is fixed; here the total thickness is fixed at 125 mm. The aimed reflection coefficient of -20 dB is set for the low frequency range of [0.75 - 6] GHz. In fact, we know that the low frequencies are the most problematic for absorption, for this reason, we have limited our goal of -20 dB for this low frequency range. The thicknesses of each layer are the parameters to be changed in order to enhance the absorption performance of the multilayer absorber. Note that during the running stage of the algorithm, the first computed reflection coefficient of the first iteration is taken as the reference to be compared to the result of the next computation. The algorithm will continuously replace the best achieved result of the reflection coefficient if and only if a better result is obtained by the new performed iteration.

After 496 iterations, the GA has stopped with the best thicknesses that it has found for each layer. The proposed thicknesses, by the launched GA, for the MLA125-GA prototype are shown in Figure III.1 (b). Note that the thicknesses chosen by GA are in the same logic as those imposed during the simulation (Table III.1). Indeed, the chosen thickness for the first layer is 43 mm (within a limit of 35 to 45 mm), and for the second layer, the chosen thickness is 18 mm within the limit between 15 and 40 mm.

Layer	Range of thickness (mm)
0 wt.%	35 - 45
3 mm - 0.25 wt.%	15 - 40
12 mm - 0.25 wt.%	25 - 40
6 mm - 0.75 wt.%	25 - 40

Table III.1. Thicknesses used for the optimization of the four layers absorber using GA CST.

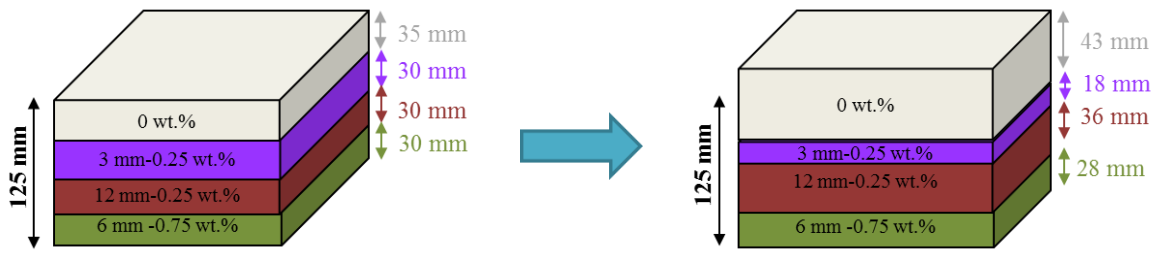

(a) *(b)*

Figure III.1. Designs of (a) MLA125-1 and (b) MLA125-GA with optimized thicknesses by the GA-CST.

The simulated reflection coefficients of the optimized MLA125-1 (MLA125-GA) are shown in Figure III.2 (a) and (b), for a normal incidence and oblique incidence of 30°, respectively. A reflection coefficient less than -13 dB has been obtained for both incidences in the studied frequency range between 0.75 GHz and 18 GHz. Here, the targeted reflection of -20 dB is not reached in the whole requested frequency range, but it has been obtained at the low frequencies between 1.19 GHz and 2.83 GHz, except the small bandwidth between 1.8 GHz and 2.1 GHz for the normal incidence, and between 1.3 GHz and 3.1 GHz for TM polarization at oblique incidence of 30°. Note that at oblique incidence of 30°, the reflection coefficient of the TM polarization is better than that of the TE polarization, as observed before with the MLA125-1 prototype (Figure II.32 (b)).

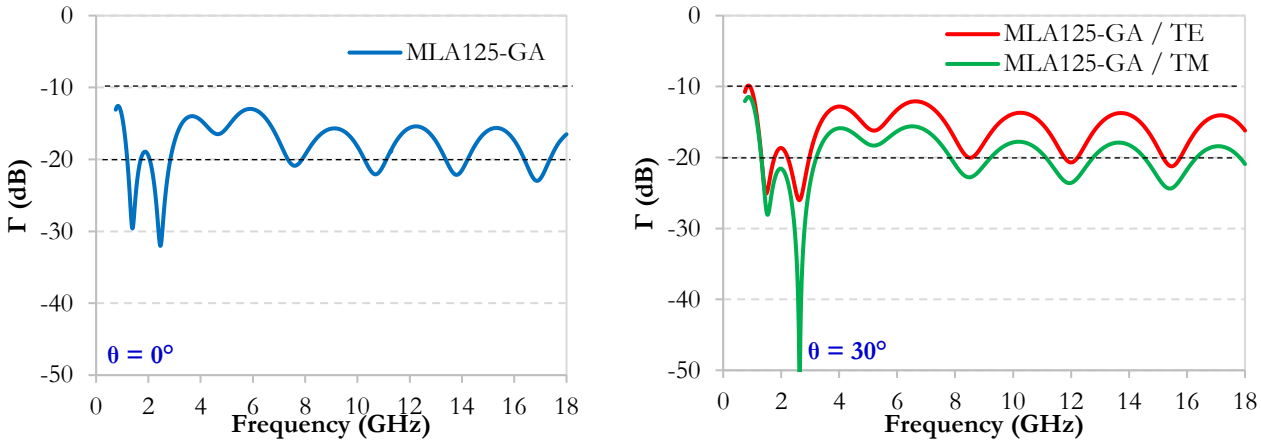

(a) *(b)*

Figure III.2. Simulated reflection coefficients for MLA125-GA at (a) normal incidence and (b) oblique incidence of 30° for TE and TM polarizations.

The obtained reflection coefficient, at normal incidence, of the optimized MLA125-GA is compared to that of the MLA125-1 in Figure III.3. The reflection coefficient of the optimized MLA125-GA is ameliorated between 0.75 GHz and 4.42 GHz, keeping the same performance for frequencies higher than 7 GHz, with a small deterioration of the performance between 4.42 GHz and 7 GHz; this is probably due to the change in thicknesses of the different layers. An improvement up to 10 dB in the low frequency band < 4 GHz could be noted here, while for frequencies > 6 GHz, the same performance of the reflection coefficient < -13 dB could be observed. It seems very difficult to improve the performance of the whole requested band, by only varying the layers' thicknesses.

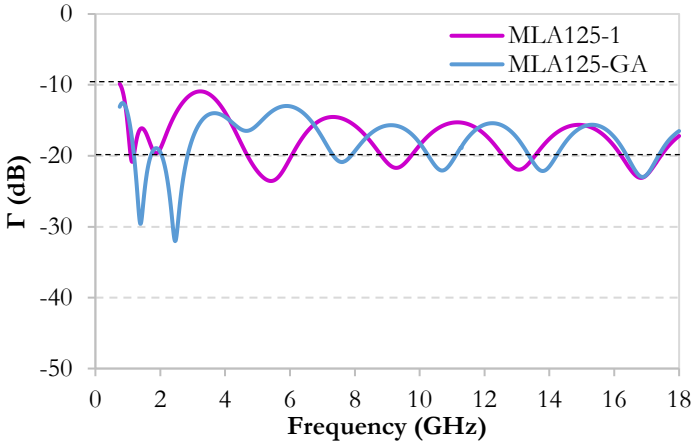

Figure III.3. Comparison between the simulated reflection coefficients of MLA125 and the MLA125-GA.

Reflectivities between each two consecutive layers for MLA125-GA were calculated (in %), and the results are presented in Figure III.4. Comparing this result with that obtained for MLA125-1 (Figure II.27), it is observed that the thickness of the first layer (0 wt.%) did not affect the reflectivity at this first interface. It also seems that the change of thicknesses by the GA affects slightly the reflectivity rate for frequencies higher than 6 GHz; therefore, a similar performance is obtained. However, for the low frequencies (<6 GHz), reflectivities are different between the layers. In fact, the maximum attained reflectivity between the first and the second layer is shifted to 3.1 GHz resulting in two minima at the low frequencies. This can explain the better performance of MLA125-GA over MLA125-1 at these low frequencies.

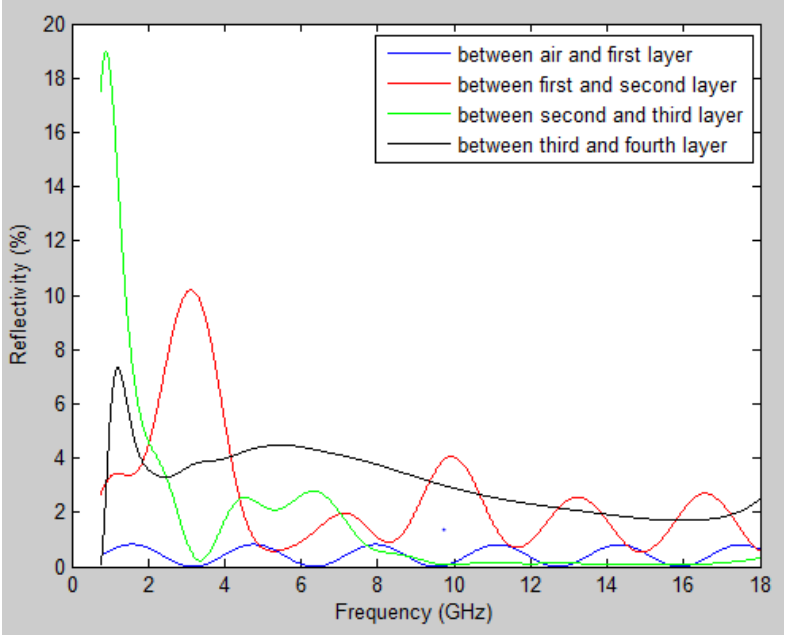

Figure III.4. Reflectivity rate with respect to frequency between each two consecutive layers of MLA125-GA.

Another optimization for a thinner multilayer absorber MLA77-GA (with total thickness of 77 mm), with the same compositions of the previous MLA125-1, was proposed to the GA. Here, the goal of the reflection coefficient less than -10 dB between 0.75 GHz and 6 GHz, is determined; the proposed minimum and maximum thicknesses are shown in Table III.2.

Layer	Range of thickness (mm)
0 wt.%	35 - 45
3 mm - 0.25 wt.%	15 - 30
12 mm - 0.25 wt.%	5 - 10
6 mm - 0.75 wt.%	5 - 10

Table III.2. Thicknesses used for the optimization of the four layers MLA77-GA.

The proposed thicknesses by the GA are shown in Figure III.5. In this proposed MLA77-GA, the first two layers were kept at the same thicknesses of 43 mm and 18 mm, respectively for the first and the second layer. However, the last two layers were reduced by 75% with thicknesses of 9 mm (for the 12 mm-0.25 wt.% layer) and 7 mm (for the 6 mm-0.75 wt.% layer), respectively.

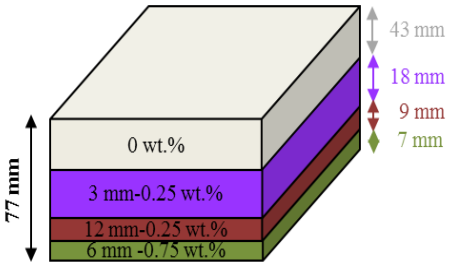

Figure III.5. Design of MLA77-GA with optimized thicknesses by the GA.

The obtained reflection coefficient, at normal incidence, of the optimized MLA77-GA is compared to that of the MLA125-GA in Figure III.6. The reflection coefficient of the optimized MLA77-GA is deteriorated between 1 GHz and 3.3 GHz while the same performances, between MLA77-GA and MLA125-GA, are observed beyond 4.5 GHz. This result shows that, for the chosen used composites, it is necessary to maintain a certain minimum total thickness of the multilayer in order to guarantee a good absorption at low frequencies.

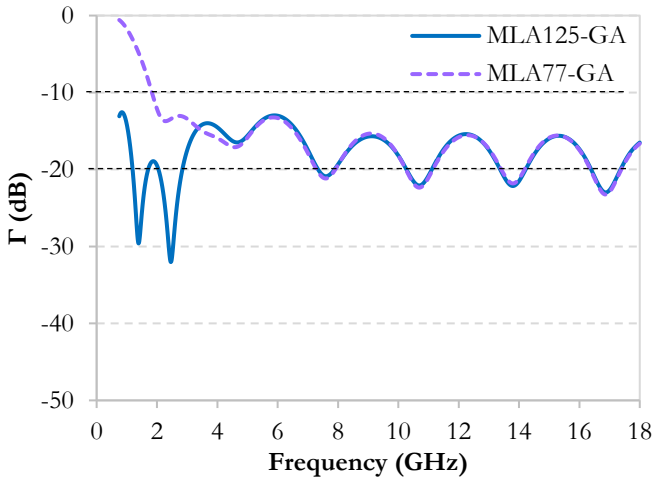

Figure III.6. Comparison between the simulated reflection coefficients of MLA77-GA and MLA125-GA.

2.2 Experimental results

The different layers of the loaded epoxy foam composites were cut to the proposed thicknesses by the GA in order to build the MLA125-GA and the MLA77-GA prototypes. The achieved prototypes are shown in Figure III.7 (a) and (b), for MLA125-GA and MLA77-GA, respectively. These prototypes have been measured in the anechoic chamber at normal incidence and oblique incidence of 30° for TE and TM polarizations to validate the simulation results.

(a) *(b)*

Figure III.7. Realized prototypes (a) MLA125-GA and (b) MLA77-GA.

The measured reflection coefficients compared to the simulated ones for MLA125-GA are presented in Figure III.8. At normal incidence, a very good matching is observed between measurement and simulation with a small deterioration in the low frequency range (Figure III.8 (a)). For TE and TM, at oblique incidence of 30°, a very good matching between simulation and measurement is also observed, with an overall better performance for the TE mode. At oblique incidence of 30° - TM mode, a small deterioration of the performance is also noted for some frequencies between 0.75 GHz and 3 GHz. It seems like a small shift has happened between measurement and simulation only in this frequency band.

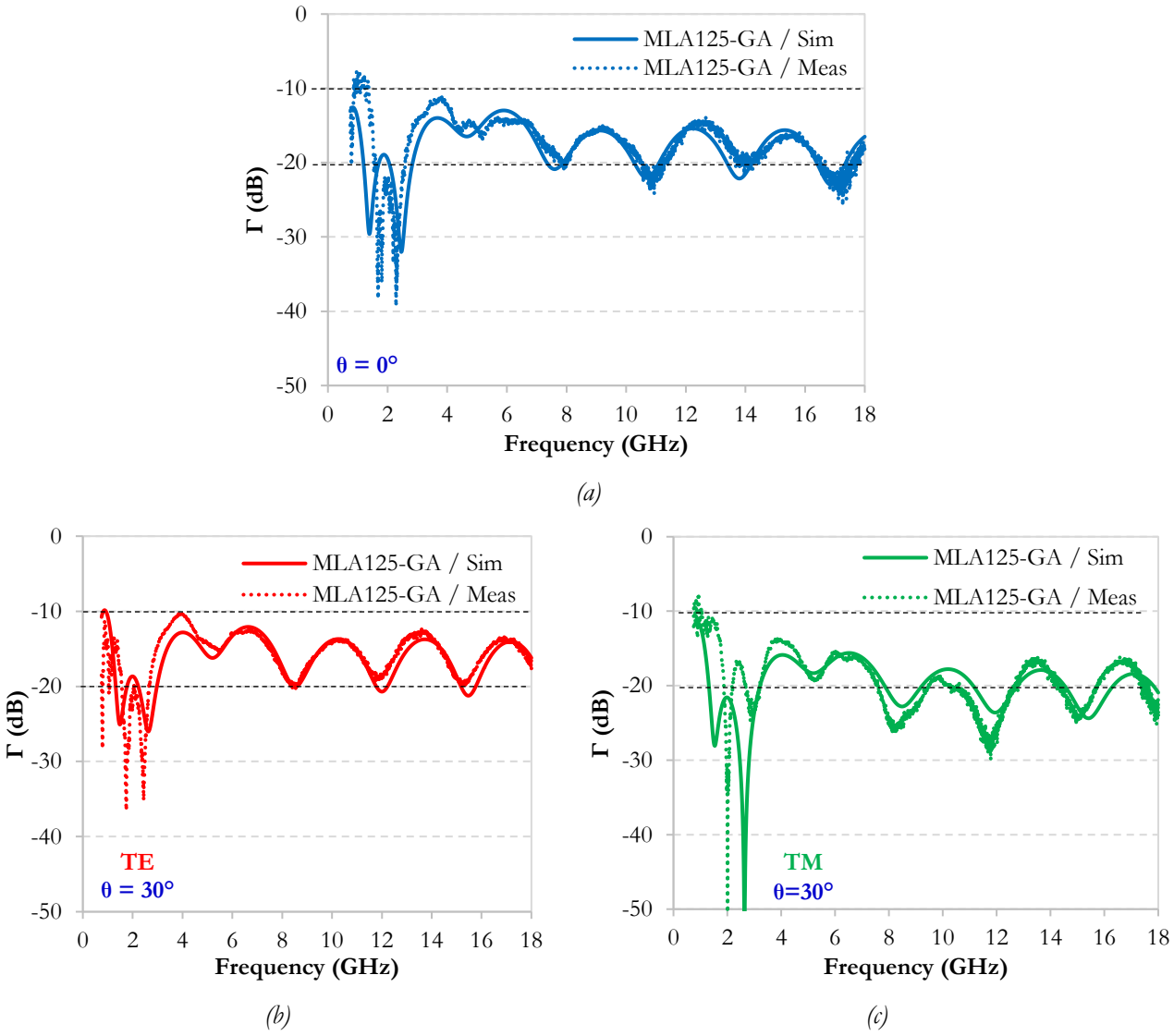

Figure III.8. Comparison between the simulated and the measured reflection coefficients for MLA125-GA at normal incidence (a) and at oblique incidence of 30° for TE (b) and TM (c) polarizations.

The measured reflection coefficients compared to the simulated ones for MLA77-GA are presented in Figure III.9, for normal incidence and oblique incidence of 30° for TE and TM polarizations. At normal incidence (Figure III.9 (a)), a very good matching has been observed between measurement and simulation with a small deterioration between 2.4 GHz and 5 GHz. This problem appears in most of our measurements in the used anechoic chamber. For TE polarization of the oblique incidence (Figure III.9 (b)), a very good matching between simulation and measurement was also observed, excluding the frequency band between 2.5 GHz and 5.7 GHz. At oblique incidence of 30° and TM mode (Figure III.9 (b)), the same small

deterioration of the performance has been noted for frequencies between 0.75 GHz and 4 GHz, but with a better measured performance for frequencies higher than 4.2 GHz. Probably, the observed differences between the measurements and the simulations may be partly due to the heterogeneity of the elaborated materials, especially highly loaded ones, as shown by the photos of the realized prototypes presented in Figure III.7 (a) and (b).

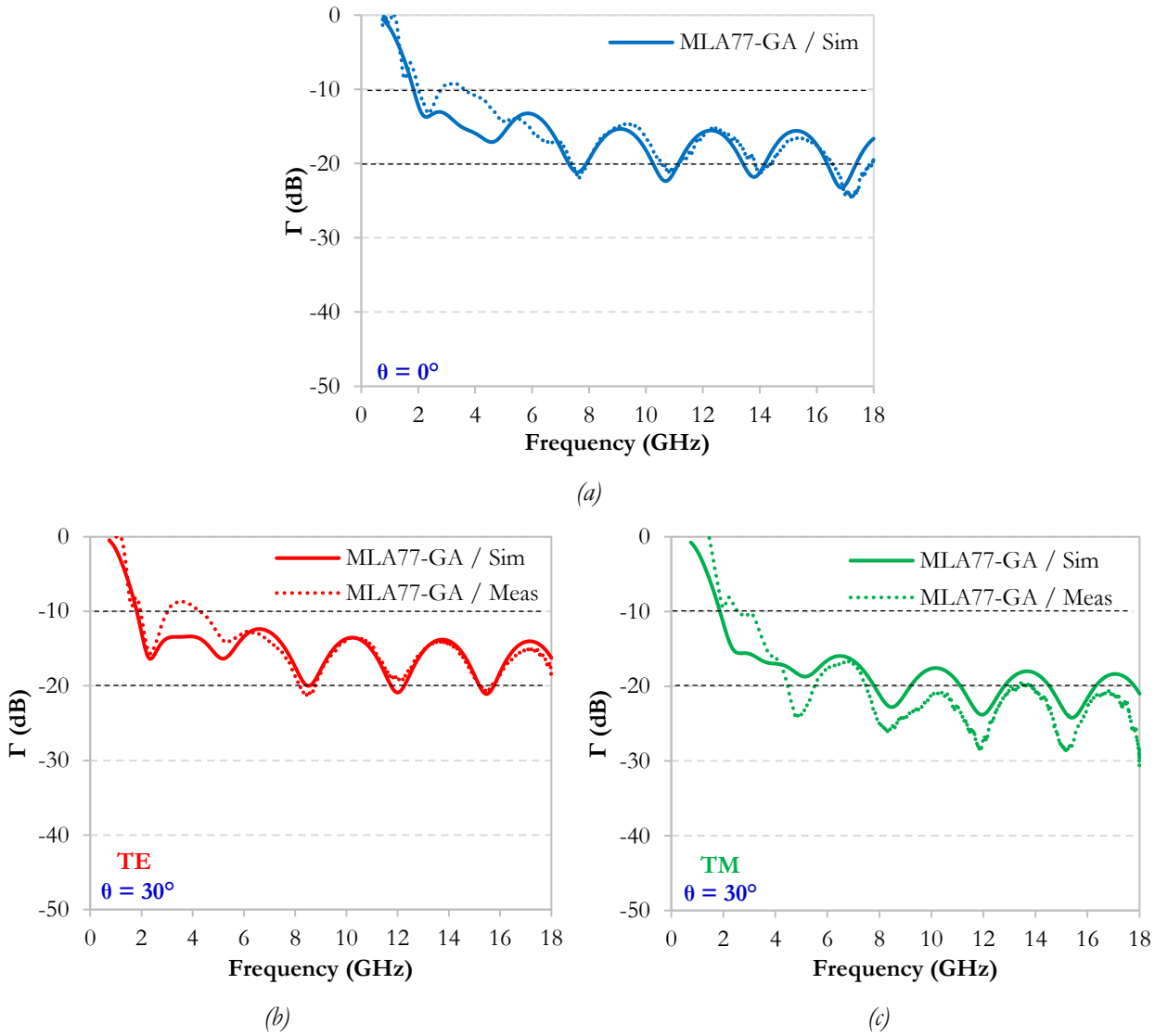

Figure III.9. Comparison between the measured and simulated reflection coefficients for MLA77-GA at normal incidence (a) and at oblique incidence of 30° for TE (b) and TM (c) polarizations.

2.3 Conclusion

In the conclusion of this section, even if GA implemented in CST allows the reduction of the reflections of the MLA125 at low frequencies, these reflections remain relatively high compared to the targeted values (-20 dB in the whole studied frequency range 0.75-18 GHz for a thickness of 125 mm). Indeed, this goal (a reflection coefficient less than -20 dB) was obtained at low frequencies between 1.19 and 2.83 GHz, but for the rest of frequencies, reflection coefficients ranging between -13 dB and -20 dB are obtained. When a thickness of 77 mm is used, a reflection of $\Gamma < -13$ dB was maintained from 2 GHz, but below this frequency, the reflection coefficient was deteriorated. From here, it can be concluded that the GA of CST

is not sufficient for further optimization of the absorption performance of the multilayer absorbers. In fact, the optimization of the problem here is limited to the thickness of each layer (the only parameter) that could be varied in order to obtain the best amelioration. In other word, it could not solve a multi-variable problem which involves multiple parameters such as the thickness and the material of each layer that composes the multilayer absorber. This is the weakness of the GA in CST. Moreover, this optimization is a time consuming since each optimization with GA of CST may take several days to be finished. For these reasons, the attention was oriented to develop an analytical method that could solve multiple problems to get the best solution; this will be discussed in the following section.

3. Analytical solution and optimization technique using the GA of MATLAB

As seen in the previous section, it is very difficult to solve a multi-variable problem, which involves a selection of various parameters at the same time, by only using GA of CST. In fact, a good absorption performance could be achieved via the selection of the suitable materials and their order, besides their thicknesses for achieving a multilayer absorber. For this task, an optimizing calculation plan is necessary to obtain the best multilayer absorber. The calculation of the total reflection coefficient involves many EM parameters that require complex mathematical expressions. The use of optimization techniques, like genetic algorithm (GA), combined to our calculation design, enables us to simplify the time and the process of several calculations to optimize the final result. In our case, this proposed calculation method will be used to design a thin broadband absorber. By this way, an optimal choice of the material composing each layer and layers' thicknesses, knowing the number of layers, could be obtained. It should be noted here that the most important part of the genetic algorithm is the calculation of the total reflection coefficient, which is the goal to be minimized. This will be discussed in the first part of this section, followed by the steps to run the genetic algorithm in the second section and finally with the obtained results by the optimization, which will be confirmed by measurements.

3.1 Reflection coefficient optimization by GA-MATLAB

GA uses the coding of the parameters instead of using the parameters themselves. The coding here is a mapping that transforms the set of parameters, usually consisting of real numbers (such as relative permittivities, relative permeabilities and thicknesses), to a finite-length of binary string. Consequently, the combination of all of the encoded parameters is a string of ones (1s) and zeros (0s). This will enable the GA to proceed in an independent manner of the parameters themselves. In addition to that, the binary coding has the shortest possible useful alphabet that yields to very simple GA operators (crossover and mutation).

One of the important parameters of the GA is the fitness function; it is the only connection between the physical problem and the GA optimization. In our case, it will be the connection between the calculated reflection coefficient of the multilayer absorber (as the physical problem) and the variable parameters (compositions and thicknesses of each layer), related to the problem, that will be used by the GA for the

optimization over several iterations. So, the fitness function holds the information about the value to be minimized, here, the reflection coefficient, and the target to be achieved.

The returned value by the fitness function, which should be positive, provides a measure of the goodness of a given trial solution. The fitness function is defined in equation (1); indeed, it is a comparison between two values 'Max' and 'f(x)'.

$$\text{Fitness} = \text{Max} - f(x) \tag{1}$$

'Max' is a positive number larger than the largest expected value of 'f(x)'; it is the target value that we want to reach by the optimization. In our case, f(x) is the calculated reflection coefficient (called $R_{computed}$) and 'Max' is the targeted reflection coefficient (called R_{Target}). So, the fitness function, here, is the comparison between the calculated and the targeted reflection coefficients as presented in equation (2). Here, the 'Max' ($R_{computed}$) and 'f(x)' (R_{Target}) are reversed to avoid the negative values in the returned values of the fitness function since they should be positive. These negative values come from both the calculated and targeted values of the reflection coefficients since both quantities are in dB (< 0).

$$Fitness = R_{computed} - R_{Target} \tag{2}$$

In our case, the obtained result by the fitness function is a vector of values that includes the reflection coefficients for each frequency at one iteration. However, GA optimization accepts only one positive number in the returned value by the fitness function, so it is impossible to run the GA in this case. Since the maximum value in the calculated vector is the maximum obtained value of the reflection coefficient by an iteration, this value will be the returned value by the fitness function to be minimized by the GA, as shown in equation (3).

$$F = Max\left\{R_{computed} - R_{Target}\right\} \tag{3}$$

The function that will compute the total reflection coefficient ($R_{computed}$) is based on the calculation of the total reflection coefficient presented in section 2.2.1 in chapter II. The next step is to relate this function, which will compute the total reflection coefficient of the multilayer absorber, to the GA that will vary the compositions, the thickness and the sequence of each layer over several iterations until it reaches the goal by the best combination with the best absorption performance. The flowchart that summarizes the steps for the GA optimization is shown in Figure III.10.

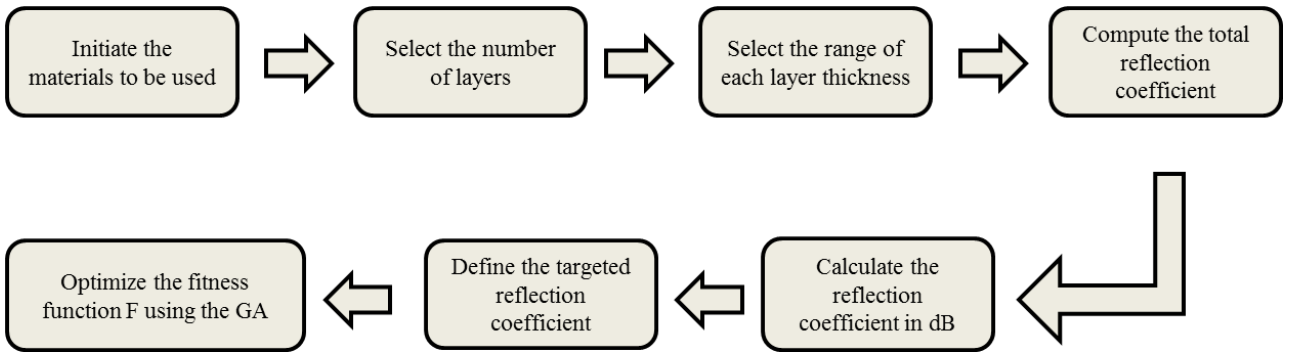

Figure III.10. Flowchart showing the followed steps for the GA in MATLAB.

It should be noted here that the fitness function F, called fitfun in our code MATLAB, includes the R_{target}, the goal, and $R_{computed}$, obtained by another function that computes the reflection coefficient at each iteration and returns the F value to be minimized by the GA. Here, the GA will stop in two cases: when the number of generations exceeds the maximum limit or when the GA achieves its goal. Note that the optimization by the GA may take only three minutes, to be finished; in fact, it depends on the difficulty of the band of frequencies where we want to optimize the absorption.

3.2 Elaborated composites used for the optimization by GA-MATLAB

First of all, a data base listing the available materials with frequency-dependent permittivities, presented in Table III.3, was developed. Note that all these materials are of density equals to 0.12 g/cm^3. The complex relative permittivity, represented by its real part ε_r' and imaginary part ε_r'', of these composites are shown in Figure III.11, from M1 to M4 for the unloaded and loaded epoxy foams with 100 μm CFs; Figure III.12, from M5 to M10 for the loaded epoxy foams with 3 mm CFs; Figure III.13 from M11 to M13 for the loaded epoxy foams with 6 mm CFs; and Figure III.14 from M14 to M24 for the loaded epoxy foams with 12 mm CFs. Here, M1 to M24 represent the sample codes; it's only an annotation for simplification. These loaded epoxy foam composites are elaborated using different CF rates (between 0.0125 wt.% and 1 wt.%). Note that we have 24 different materials with a large choice of ε_r' and ε_r'' in a large frequency band [0.75-18] GHz.

Sequence number	Composition	Sample Code
1	0 wt.%	M1
2	100 μm - 2.5 wt.%	M2
3	100 μm - 5 wt.%	M3
4	100 μm - 10 wt.%	M4
5	3 mm - 0.1 wt.%	M5
6	3 mm - 0.2 wt.%	M6
7	3 mm - 0.25 wt.%	M7
8	3 mm - 0.5 wt.%	M8
9	3 mm - 0.75 wt.%	M9
10	3 mm - 1 wt.%	M10
11	6 mm - 0.25 wt.%	M11
12	6 mm - 0.5 wt.%	M12
13	6 mm - 0.75 wt.%	M13
14	12 mm - 0.0125 wt.%	M14
15	12 mm - 0.01875 wt.%	M15
16	12 mm - 0.025 wt.%	M16
17	12 mm - 0.05 wt.%	M17
18	12 mm - 0.075 wt.%	M18
19	12 mm - 0.1 wt.%	M19
20	12 mm - 0.2 wt.%	M20
21	12 mm - 0.25 wt.%	M21
22	12 mm - 0.3 wt.%	M22
23	12 mm - 0.4 wt.%	M23
24	12 mm - 0.5 wt.%	M24

Table III.3. The predefined database.

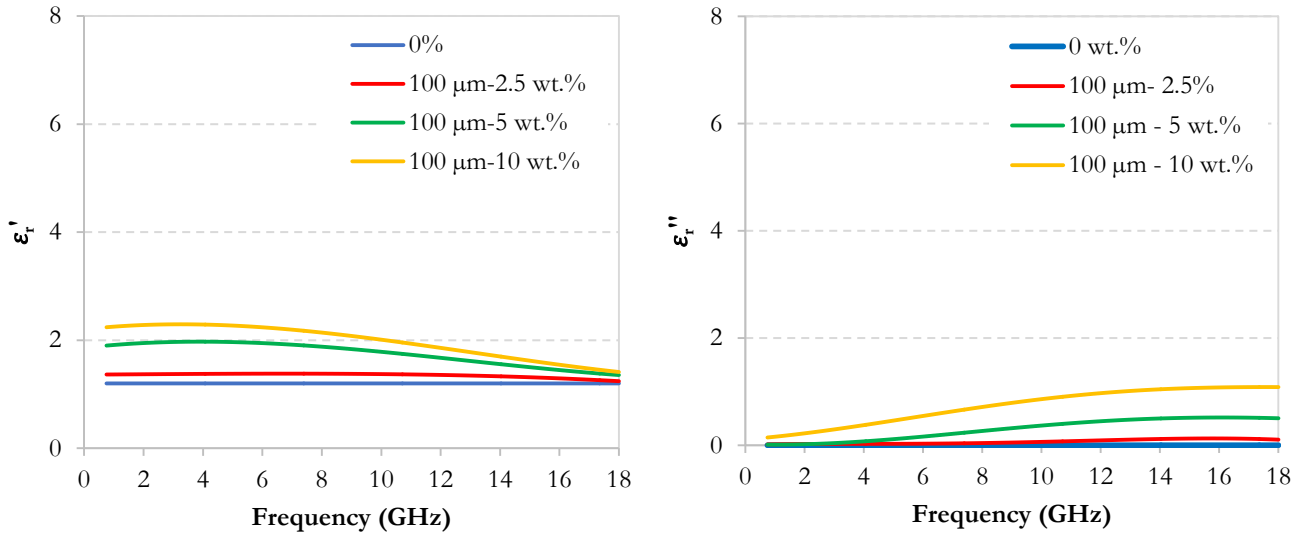

(a) (b)

Figure III.11. Real part ε_r' (a) and imaginary part ε_r'' (b) of the unloaded epoxy foam (0 wt.%), and the composites loaded with 100 µm CFs using different wt.%.

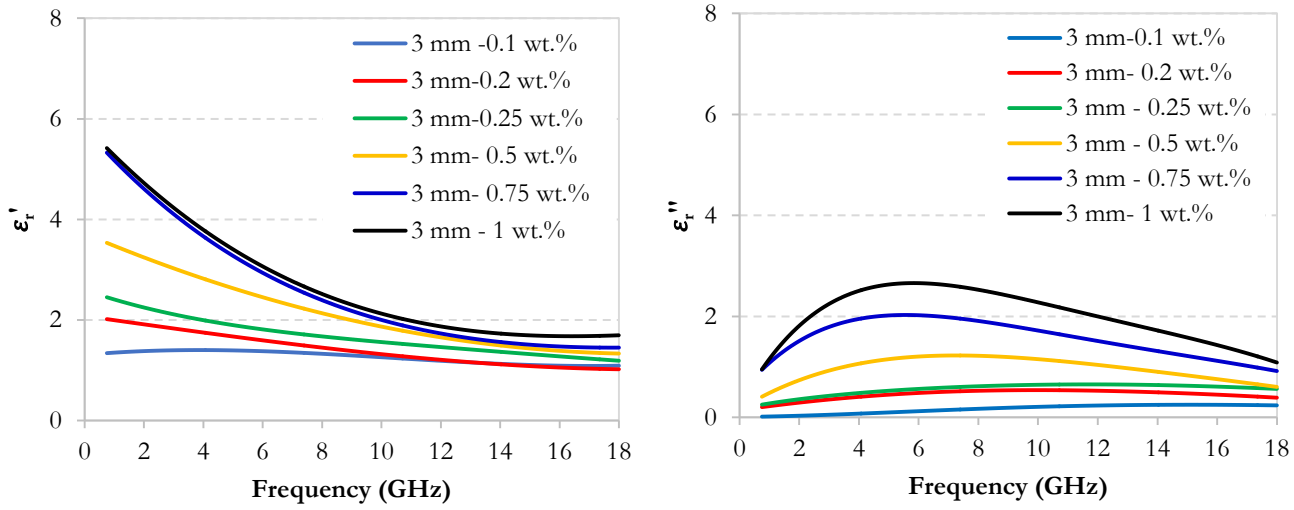

(a) (b)

Figure III.12. Real part ε_r' (a) and imaginary part ε_r'' (b) of the composites loaded with 3 mm CFs using different wt.%.

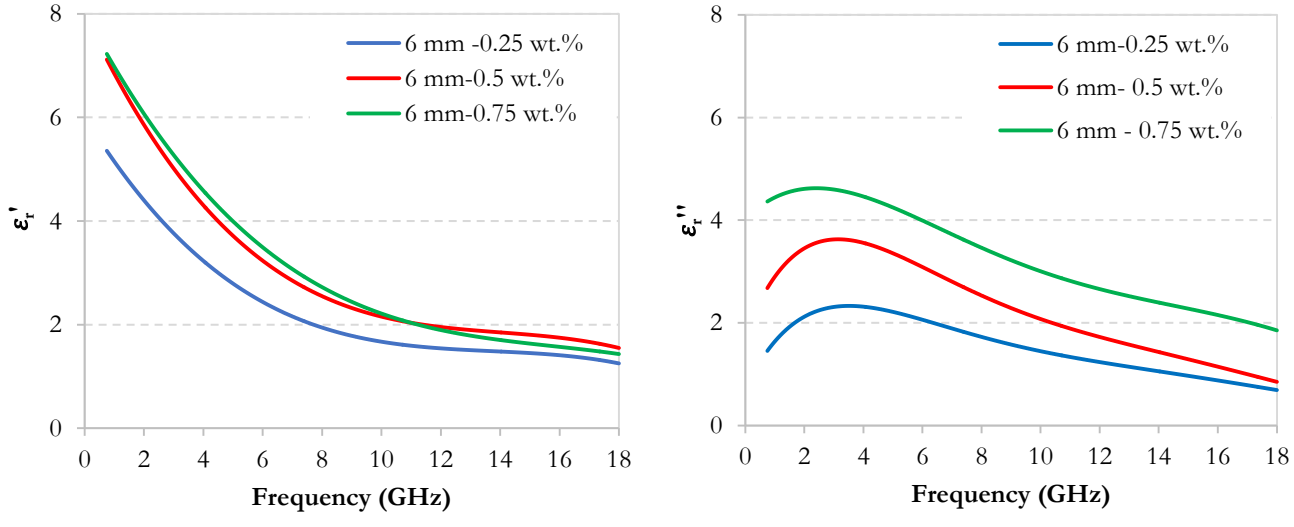

(a) (b)

Figure III.13. Real part ε_r' and imaginary part ε_r'' (b) of the composites loaded with 6 mm CFs using different wt.%.

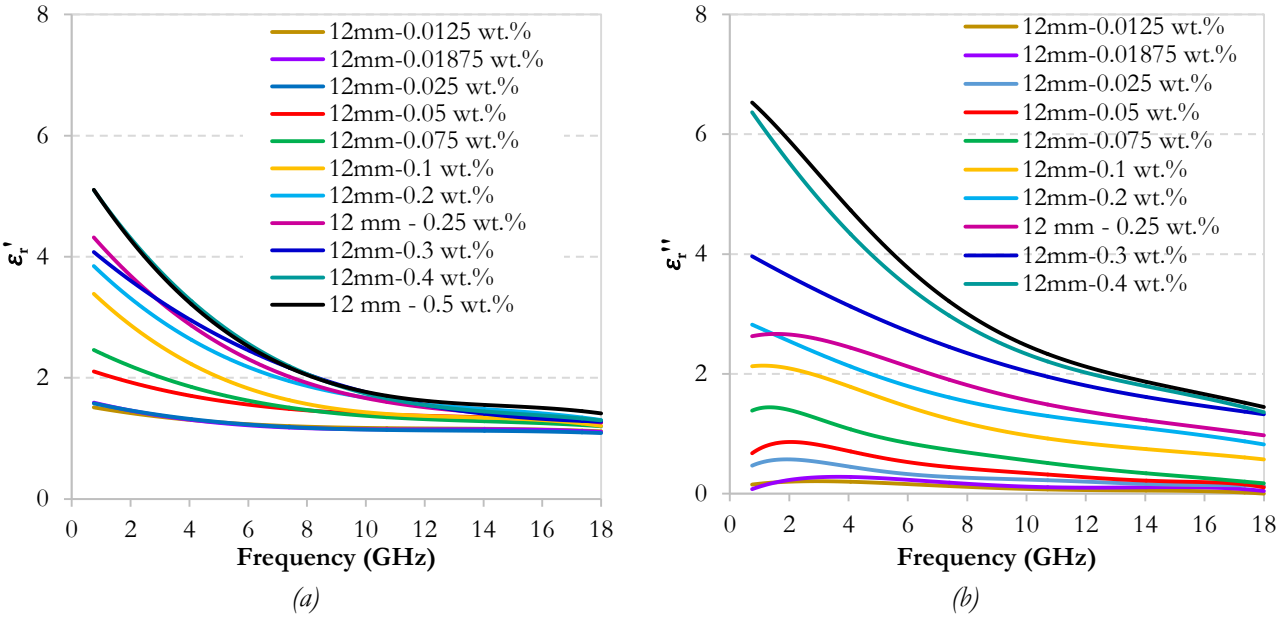

Figure III.14. Real part ε_r' (a) and imaginary part ε_r'' (b) of the composites loaded with 12 mm CFs using different wt.%.

From the presented complex permittivities, it is shown that the real and imaginary parts of the loaded epoxy foam composites increase with the increase of the CF rates. For example, at 4 GHz, the composites loaded with 0.0125 wt.% of 12 mm CFs presents ε_r'=1.3 associated with ε_r''= 0.4; these properties have increased with the CF rate to reach, ε_r'= 3.24 and ε_r''= 4.7 for the rate of 0.5 wt.%. One can note here that the peak of the imaginary part ε_r'' shifts toward a lower frequency when increasing the CF length. For example, the peak is around 18 GHz for the composites loaded with 100 µm (Figure III.11 (b)), around 5 GHz for the composites loaded with 3 mm (Figure III.12 (b)), around 3 GHz for the composites loaded with 6 mm (Figure III.13 (b)) and lower than 1 GHz for the composites loaded with 12 mm (Figure III.14 (b)).

3.3 Optimization results

3.3.1 Solution 1

First of all, the GA was used for the optimization of the multilayer absorber in the frequency range between 0.75 and 6 GHz. The used parameters for this optimization are listed in Table III.4; the number of layers was set to 5 and all the 24 materials were introduced to the GA code. A limit of thicknesses, between 10 and 25 mm, was given to each layer, thus, the total thickness of the absorber was limited between 50 mm (as a minimal thickness) and 125 mm (as a maximal thickness).

Entity	Selected parameters
Solver	ga
Fitness function	@fitfun
Number of layers	5
Number of predefined materials	24
Allowed thickness for each layer	10-25 mm

Table III.4. Parameters used for the optimization of the five layers absorber using MATLAB gatool.

The proposed optimized multilayer absorber presents a total thickness of 98 mm. It is composed first, of 10 mm of unloaded epoxy foam (M1) as a matching layer. Then, and for the next layers, the GA proposed three layers loaded with increasing rates of CFs of 12 mm lengths: M14 (0.0125 wt.%), M16 (0.025 wt.%) and M18 (0.075 wt.%) for the second, third and fourth layer respectively. Finally, a more loaded layer M23 (12 mm-0.4 wt.%) was chosen for the last absorbing layer. The proposed thicknesses, by the GA, of each layer are shown in Figure III.15 (a). The reflection coefficient of this proposed multilayer absorber, for normal incidence, is presented in Figure III.15 (b). Here, a reflection coefficient less than -20 dB is predicted for this absorber in the whole studied frequency range between 0.75 and 18 GHz.

A comparison between the reflection coefficients of MLA125-1, MLA125-GA and MLA98-GA-M is presented in Figure III.15 (c). A better reflection coefficient is obtained with the proposed multilayer absorber by the GA of MATLAB, than that obtained by the first MLA125-1 and by the GA of CST, and with a lower thickness. Indeed, this obtained solution predicts a very good absorption performance over a wide band of frequencies with a reduced thickness of 22 %.

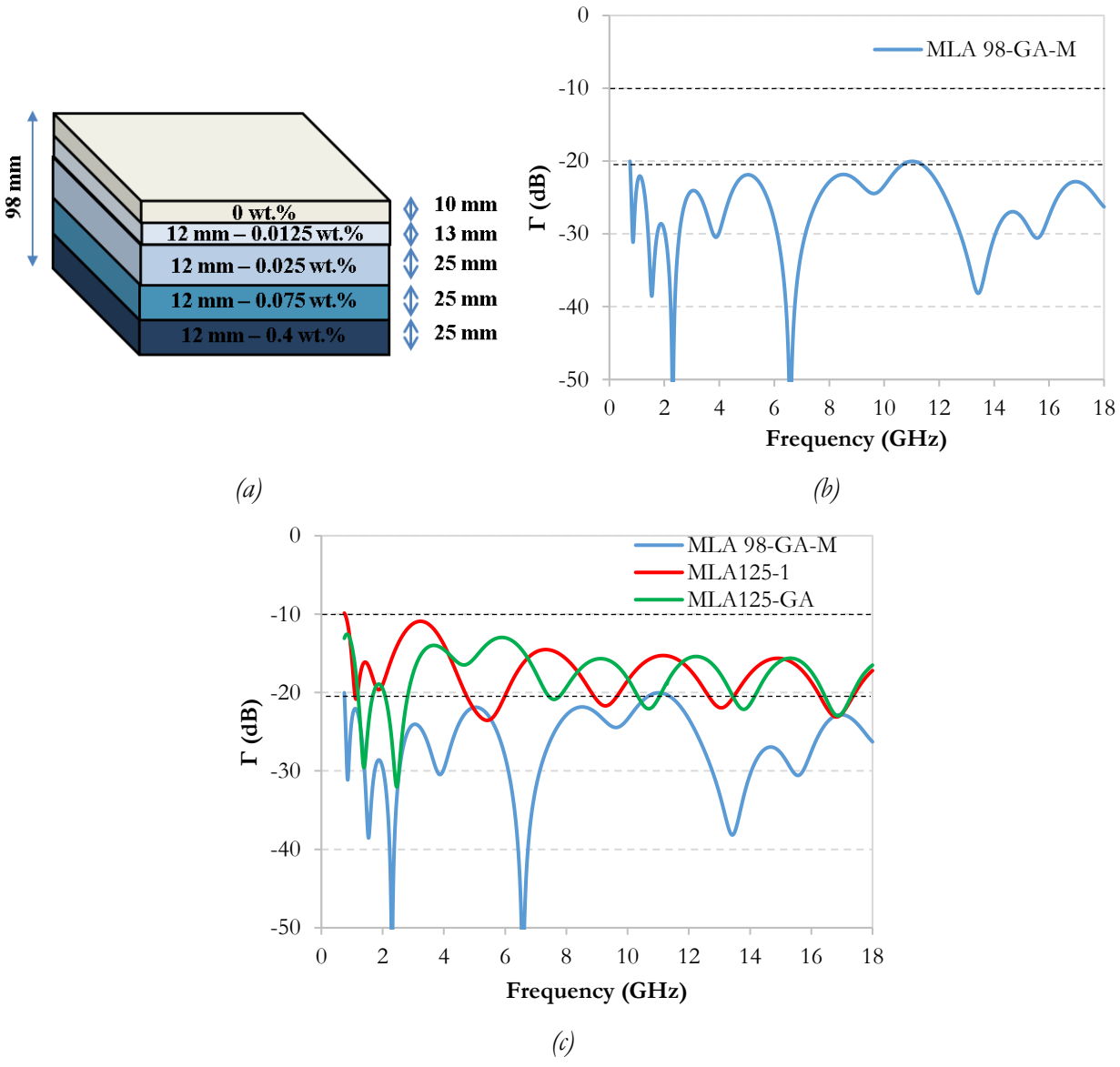

Figure III.15. MLA98-GA-M layers' composition and thicknesses (a) and its simulated reflection coefficient for normal incidence (b) and comparison between MLA125-1, MLA125-GA and MLA98-GA-M (c).

The photo of the achieved MLA98-GA-M prototype, proposed by this first optimization, is shown in Figure III.16 (a). The measured reflection coefficients of this prototype, compared to the simulated ones, are presented in Figure III.16 (b), (c) and (d) for normal incidence and oblique incidence (30°) for TE and TM polarizations, respectively. The reflection coefficients of <-20 dB over the entire studied frequency band (0.75 - 18 GHz), which was predicted by the simulation for the normal incidence, is confirmed by the measurement in the frequency range of 2 GHz to 18 GHz, but a degradation of this coefficient is observed at low frequencies (before 2 GHz); this is due to the limitation of the anechoic chamber used for the prototype measurement. In fact, all the measured results for this porotype (with different incidences) show the same reflection coefficient in this frequency range. It seems that below 2 GHz, we reach the limit of the anechoic chamber where we cannot measure reflection coefficients lower than -10 dB. Otherwise, comparing the measurement results for MLA98-GA-M to that of the commercial absorber (AH 125) in Figure III.17, a very comparable reflection coefficient to that of the commercial absorber is obtained in the whole studied frequency range and this is realized while having a reduction of 22 % in the total thickness. In the same figure, one can note that even for the commercial absorber, for which a reflection coefficient of -20 dB should be obtained at low frequencies, as announced by SIEPEL, a degradation of the performance is also observed.

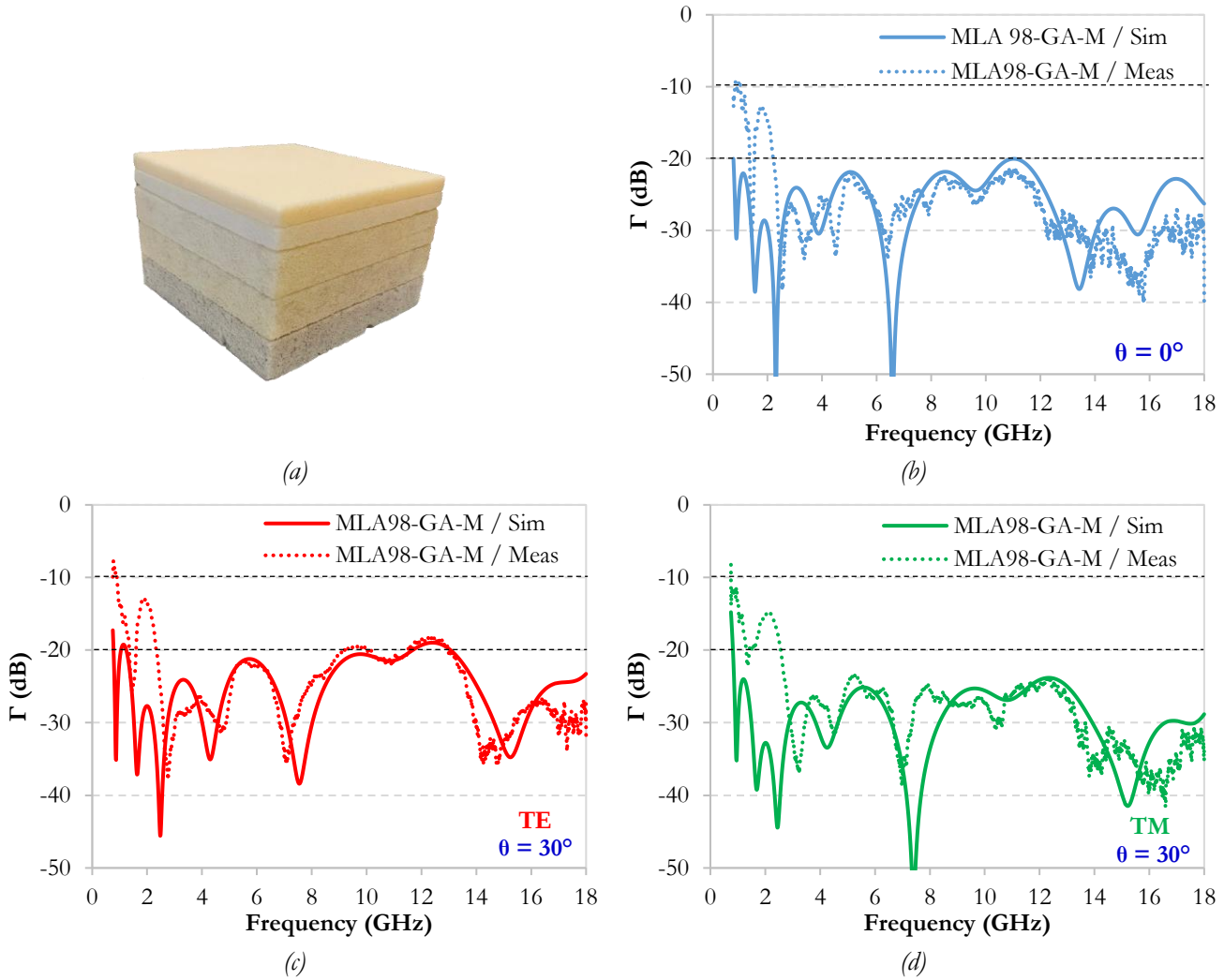

Figure III.16. Photo of the realized MLA98-GA-M prototype (a), comparison between its measured and simulated reflection coefficients at normal incidence (b) and at oblique incidence of 30° for TE (c) and TM (d) polarizations.

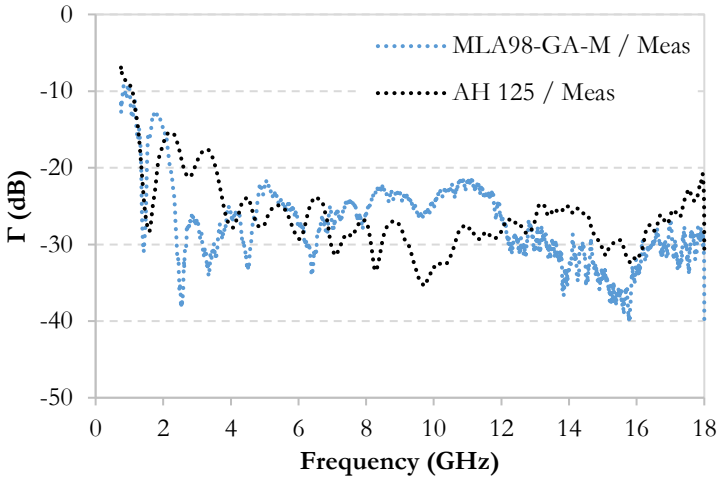

Figure III.17. Comparison between the measured reflection coefficients of MLA98-GA-M and AH 125 at normal incidence.

3.3.2 Solution 2

Despite the very good result obtained previously, we tend to further minimize the total thickness of the absorber; for this reason, other solutions will be presented in the next parts.

For the next prototype, the range of frequency for the optimization was also set to [0.75-6] GHz since it is the most critical and hard region for the absorption. The parameters used for the optimization of the five layers of the multilayer absorber using MATLAB's gatool are listed in Table III.5. As shown in this Table, the number of layers was set to five and the variable parameters are the predefined 24 materials in the database and the thickness of each layer, composing the multilayer absorber. A range of thickness between 10 and 20 mm was given to the first three layers, while the last two layers were given a range of thickness between 10 and 15 mm. By this, the total thickness of the absorber allowed by the GA was limited between 50 mm (as a minimal thickness) and 90 mm (as a maximal thickness). Thus, a thinner absorber could be obtained (< 90 mm); this simulation will be comparable to that of the MLA77-GA carried out with the GA-CST.

Entity	**Selected parameters**
Solver	ga
Fitness function	@fitfun
Number of layers	5
Number of predefined materials	24
Allowed thickness for three first layers	10-20 mm
Allowed thickness for last two layers	10-15 mm

Table III.5. Parameters used for the optimization of the five layers absorber using MATLAB gatool.

The proposed MLA is composed of four layers (Figure III.18 (a)) with a total thickness of 70 mm. The materials composing each layer and their thicknesses are presented below: M16 (12 mm-0.025 wt.%) was chosen twice with a total 30 mm thickness for the first and second layers. This layer will be able to ensure a good impedance transition between the air and the multilayer. M19, with moderate load of the same CF

length (12 mm-0.1 wt.%) was chosen for the second layer with a thickness of 20 mm; this layer will ensure a smooth gradual impedance and also, a small absorption. M23 (12 mm-0.4 wt.%) with a thickness of 10 mm, was chosen for the third layer of this multilayer absorber; here, a layer with higher load was implemented; this layer was probably chosen in order to ensure a good absorption. At the end, M19 (12 mm-0.1 wt.%) was re-used for the last layer with a thickness of 10 mm. Note that this optimization has taken only few minutes to be finished. The final achieved MLA70-GA-M prototype, proposed by the GA of MATLAB, is shown in Figure III.18 (b).

The achieved prototype has been measured in the anechoic chamber at normal incidence and oblique incidence of 30° for TE and TM polarizations. The measured reflection coefficients, compared to the simulated ones, are presented in Figure III.19.

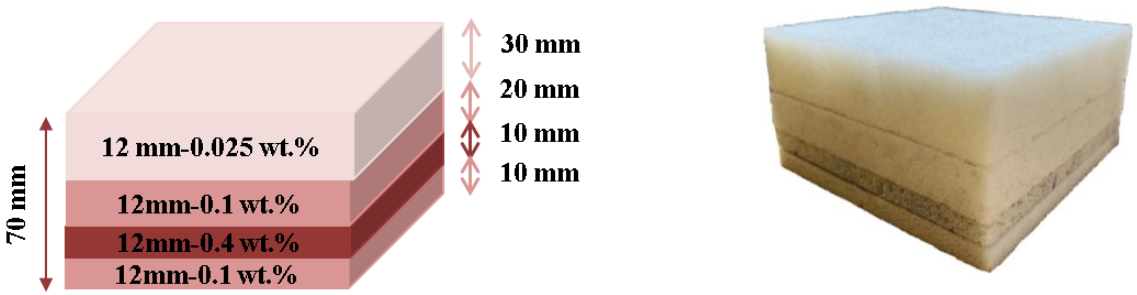

(a) (b)

Figure III.18. MLA70-GA-M layers' composition and thicknesses (a) and achieved prototype (b).

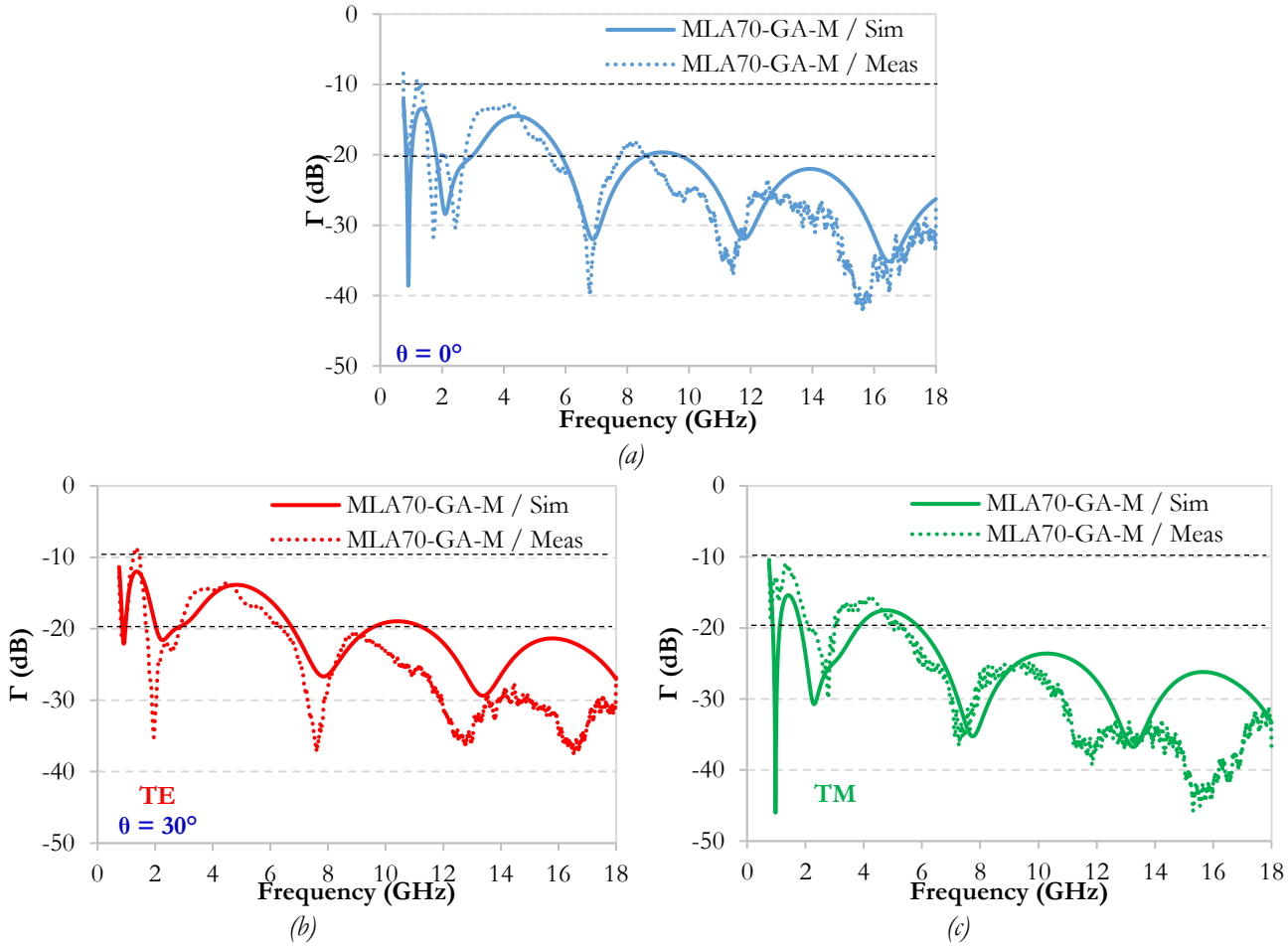

Figure III.19. Comparison between the simulated and measured reflection coefficients for MLA70-GA-M at normal incidence (a) and at oblique incidence of 30° for TE (b) and TM (c) polarizations.

A good matching has been observed between measurement and simulation at normal incidence (Figure III.19 (a)) and at oblique incidence of 30° for TE and TM modes (Figure III.19 (b) and (c)). Note that a better performance is expected for TM mode. The measured performance for TE mode shows better results at low frequencies (around 1.96 GHz and 7.63 GHz). For the two polarizations, a better measured performance is observed for all frequencies higher than 9.5 GHz. Finally, a reflection coefficient less than -10 dB is obtained in the frequency range 1 GHz - 18 GHz; for frequencies > 6 GHz, the reflection coefficient becomes lower than -20 dB.

For the two first optimizations, the GA has chosen particularly the composites loaded with 12 mm CF length; the choice of these composite was advantageous since it was seen before that these CFs provide a good absorption performance at the lowest frequencies, due to their low real permittivities (Figure III.14 (a)) and high losses (Figure III.14 (b)). In addition to that, we have also seen before that the frequency range where the composites show their maximum losses depends on the length of the fibers. Indeed, long fibers show high losses at low frequencies while short fibers show the maximum of their losses at high frequencies. In order to validate the reason behind the choice of the GA for the 12 mm CF lengths for the first prototypes (MLA98-GA-M and MLA70-GA-M), we decided to launch the same optimization, but at higher frequency ranges, once at [6-12 GHz] and the second time at [12-18 GHz]. The used parameters for the simulation (number of materials, thickness limits) are the same as the second optimization that is summarized in Table III.5.

From the obtained results (Figure III.20), it is shown that the GA has systematically chosen the 3 mm CF length to compose a multilayer absorber MLA74-GA-M that is efficient at the first frequency bandwidth of [6-12 GHz] while it has chosen the CFs of the lowest length (100 μm) to compose a multilayer absorber MLA69-GA-M that is efficient at the second frequency bandwidth of [12-18 GHz]. It should be noted here that for both prototypes a gradient of the charge was used. In fact, for MLA74-GA-M, GA has chosen the composite 100 μm-5 wt.% for the second layer instead of choosing one composite of the 3 mm CF lengths, and this is because it presents also high losses at high frequencies (Figure II.18). On the other hand, the GA has chosen the 100 μm-5 wt.% composite for MLA69-GA-M two times for the third (with a thickness of 14 mm) and fourth (with a thickness of 16 mm) layers; therefore, it is composed of four layers instead of five. Note that the choice of the unloaded composite (0 wt.%) for the first layer is because this layer presents the closest dielectric properties to that of air, thus it will ensure a smooth transition of the EM wave. From these results, the effect of the length of the CFs may be validated, the high length (12 mm) was chosen by the GA when the lowest frequencies were taken into account, and the low length was chosen for high frequencies.

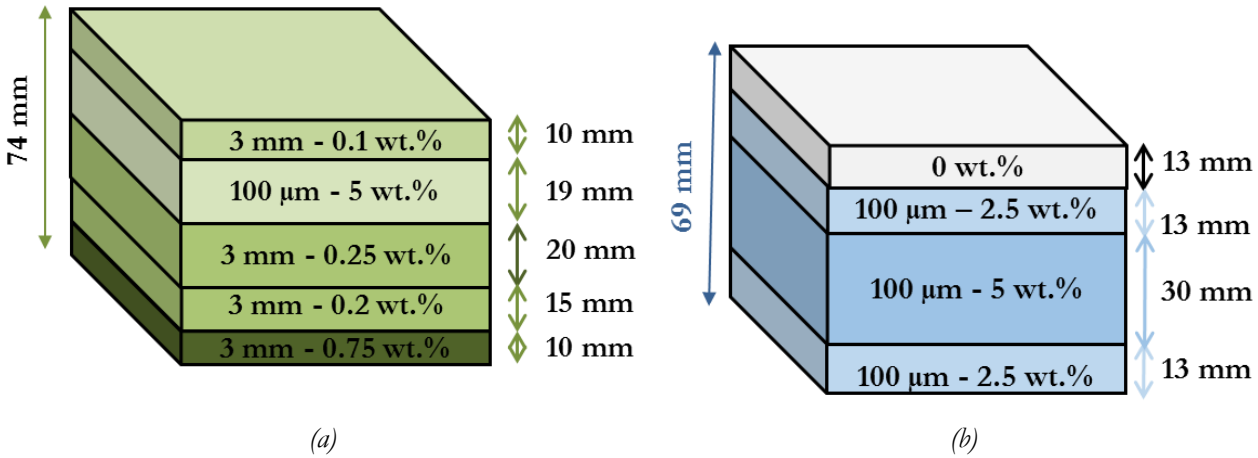

Figure III.20. Design of MLA74-GA-M at [6-12] GHz (a) and MLA69-GA-M at [12-18] GHz (b).

Comparison between the calculated reflection coefficients of MLA70-GA-M, MLA74-GA-M and MLA69-GA-M is shown in Figure III.21. Results show that the prototype made of epoxy foams loaded with 12 mm CFs (MLA70-GA-M) has the best absorption performance at the lowest frequencies (< 4 GHz), whereas, the prototype made with 3 mm CFs (MLA74-GA-M) has the best absorption performance at frequencies between 4 GHz and 10 GHz and the prototype loaded with 100 µm CFs (MLA69-GA-M) has the best absorption performance at high frequencies (> 12 GHz). Note that the GA has chosen the lowest thickness for this prototype; this is because no need for a high thickness to absorb at the high frequencies that are of small wavelengths. From these results, the effect of the length on the dielectric properties, especially on the losses and thus on the absorption band due to the peak shift is validated. In addition to that, it was noticed that to absorb at the low frequencies, a higher thickness is needed in comparison with absorber for high frequencies.

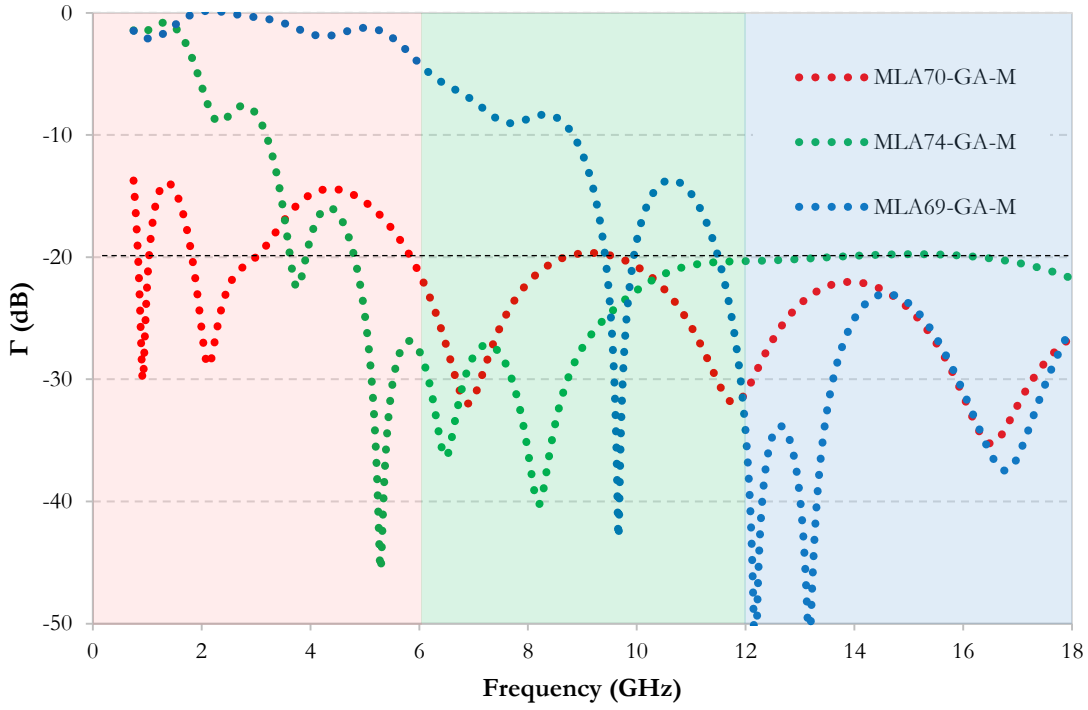

Figure III.21. Comparison between reflection coefficients of MLA70-GA-M, MLA74-GA-M and MLA69-GA-M.

3.3.3 Solution 3

For the third optimization, the number of layers was limited to three. The different parameters used for the optimization of the three layers of the multilayer absorber, using MATLAB gatool, are presented in Table III.6. A minimal total thickness of 30 mm and a maximal total thickness of 55 mm were introduced to the GA. The first layer was given a range of thickness between 10 and 25 mm, while the second and the third layers were given a range of thickness between 10 and 15 mm.

Entity	Selected parameters
Solver	ga
Fitness function	@fitfun
Number of layers	3
Number of predefined materials	24
Allowed thickness for the first layers	10-25 mm
Allowed thickness for last two layers	10-15 mm

Table III.6. Parameters used for the optimization of the three layers absorber using MATLAB gatool.

The new proposed MLA by the GA of MATLAB (named MLA50-GA-M) is composed of only two layers (Figure III.22 (a)) with a total thickness of 50 mm. In fact, as for the previous proposed multilayer absorber, the first layer was chosen also for this solution twice, for the first and the second layers. The materials composing each layer and their thicknesses are presented in Figure III.22 (a). The same first two layers of solution 2 were chosen for solution 3: a matching layer M16 (12 mm-0.025 wt.%) of 30 mm thickness followed by an absorbing layer, the M19 (12 mm-0.1 wt.%), with a thickness of 20 mm. This prototype, has been realized; it is shown in Figure III.22 (b).

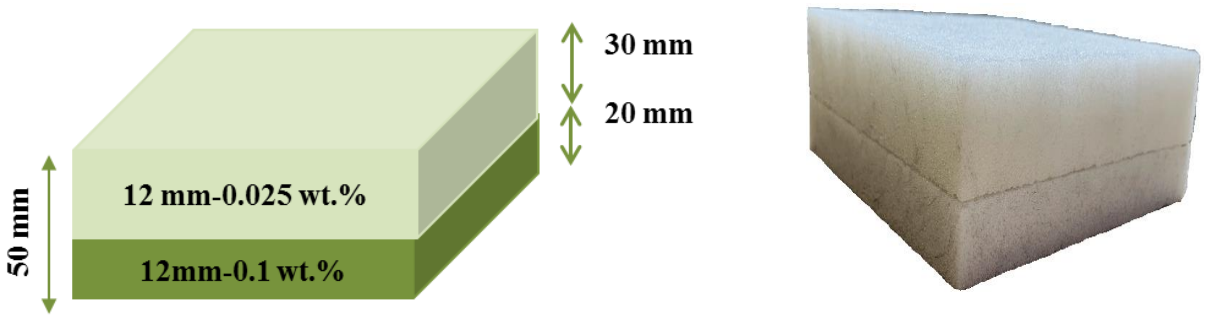

(a) *(b)*

Figure III.22. MLA50-GA-M (a) layers' composition and thicknesses and (b) achieved prototype.

The proposed prototype was measured in the anechoic chamber at normal incidence and oblique incidence of 30° for TE and TM polarizations. The measured reflection coefficients, of this prototype, are compared to the simulated ones and presented in Figure III.23. A relative good matching is observed between measurement and simulation for all studied incidences and polarizations (Figure III.23 (a), (b) and (c)), with a better measured performance for frequencies higher than 9.8 GHz, as observed for the previous

prototype of solution 2. A reflection coefficient less than -10 dB has been obtained from 1.18 GHz for normal incidence and from 1.14 GHz for oblique incidence and is ensured in the rest of the studied frequency range.

Our results show that with a thin and very lightly loaded multilayer absorber (< 0.1 wt.%) an absorption over a wide frequency band can be ensured. But this result confirms again that in addition to the optimal choice of materials and thicknesses of each layer, a minimal total thickness of the multilayer absorber is needed to ensure the absorption at low frequencies where the wavelengths of the EM waves become long.

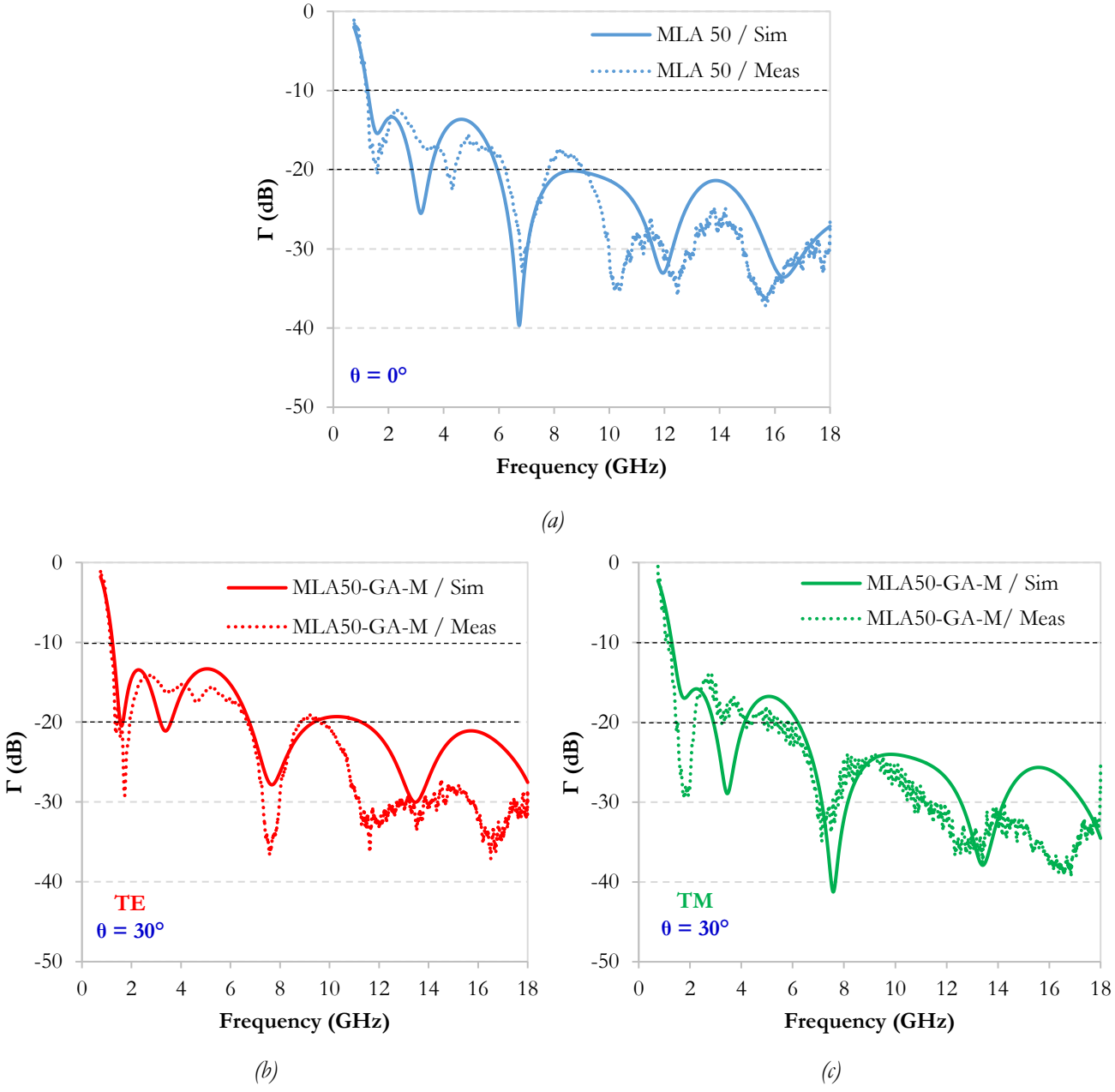

Figure III.23. Comparison between measured and simulated reflection coefficients for MLA50-GA-M at normal incidence (a) and at oblique incidence of 30° for TE (b) and TM (c) polarizations.

3.3.4 Solution 4

For the fourth optimized prototype, the chosen number of layers is five. For this optimization, only low density epoxy foam materials are used (Table III.7). The goal of this optimization is to ameliorate the

absorption performance of the lightweight multilayer absorber presented in chapter II with the minimal possible thickness; the dielectric properties of these composites are presented in Figure II.34. The different parameters, used for the optimization of the five layers using MATLAB gatool, are presented in Table III.8. Here, only five materials will be in the predefined database of the GA and the limit of each layer thickness is set between 10 mm and 20 mm (Table III.8). So, the total thickness of the absorber that is allowed by the GA is limited between 50 and 100 mm.

Sequence number	Composition	Sample Code
1	12 mm - 0.0125 wt.%	M1
2	12 mm - 0.01875 wt.%	M2
3	12 mm - 0.025 wt.%	M3
4	12 mm - 0.05 wt.%	M4
5	12 mm - 0.075 wt.%	M5

Table III.7. The materials used for the optimization by the GA of MATLAB.

Entity	Selected parameters
Solver	ga
Fitness function	@fitfun
Number of layers	5
Number of predefined materials	5
Allowed thickness for all layers	10-20 mm

Table III.8. Parameters used for the optimization of the five layers absorber using MATLAB gatool.

The proposed low density MLA by the GA, LW-MLA81-GA-M, is composed of three layers (Figure III.24 (a)) with a total thickness of 81 mm. In fact, the loaded epoxy foam composite with 12 mm-0.075 wt.%, was chosen three times for the second, third and fourth layers. Therefore, a multilayer with only 3 layers was obtained here. The materials composing each layer and their thicknesses are presented in Figure III.24 (a). The GA has chosen M4 (12 mm-0.05 wt.%) for the first layer with 20 mm thickness, followed by an absorbing layer, the M5 (12 mm-0.075 wt.%), with a thickness of 51 mm. Here, and contrary to our expectations, the last layer proposed by the GA, with a thickness of 10 mm, is the least loaded one among all proposed composites and therefore, with the lowest losses. Indeed, we were not able to find an explanation of the reason behind choosing this layer as the last layer.

Comparison between the simulated reflection coefficients of the lightweight LW-MLA125-1 (presented in chapter II) and the proposed LW-MLA81-GA-M, for normal incidence, are presented in Figure III.24 (b). A better performance has been obtained by LW-MLA81-GA-M at the lowest frequencies (< 2.5 GHz), keeping by that the good performance in the whole studied frequency range and with a lower total thickness (by 35%) compared to the MLA125.

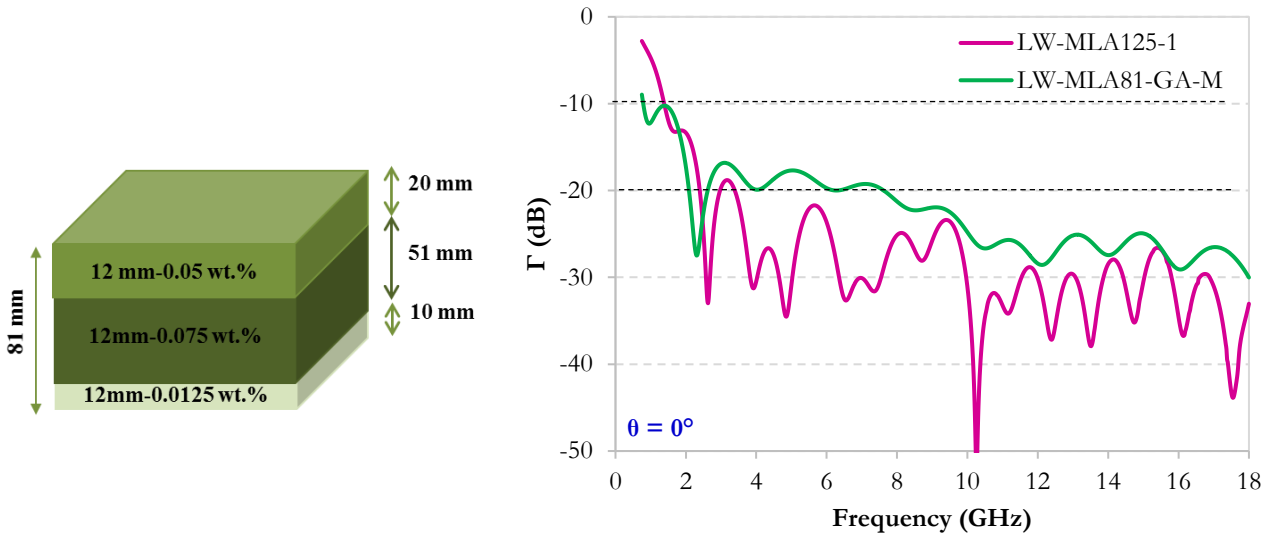

(a) *(b)*

Figure III.24. Design of LW-MLA81-GA-M (a) and comparison between the reflection coefficients of LW-MLA125 and LW-MLA81-GA-M (b).

The simulated reflection coefficients of the proposed LW-MLA81-GA-M, at oblique incidence of 30°, for TE and TM polarizations, are presented in Figure III.25. Reflection coefficients less than -10 dB are expected at the whole interval for TE mode and from 0.83 to 18 GHz for TM mode. A reflection coefficient less than -20 dB has been obtained from 2.21 GHz for TM and less than -15 dB from 2 GHz for TE. This prototype was unfortunately not realized for the validation of these obtained results.

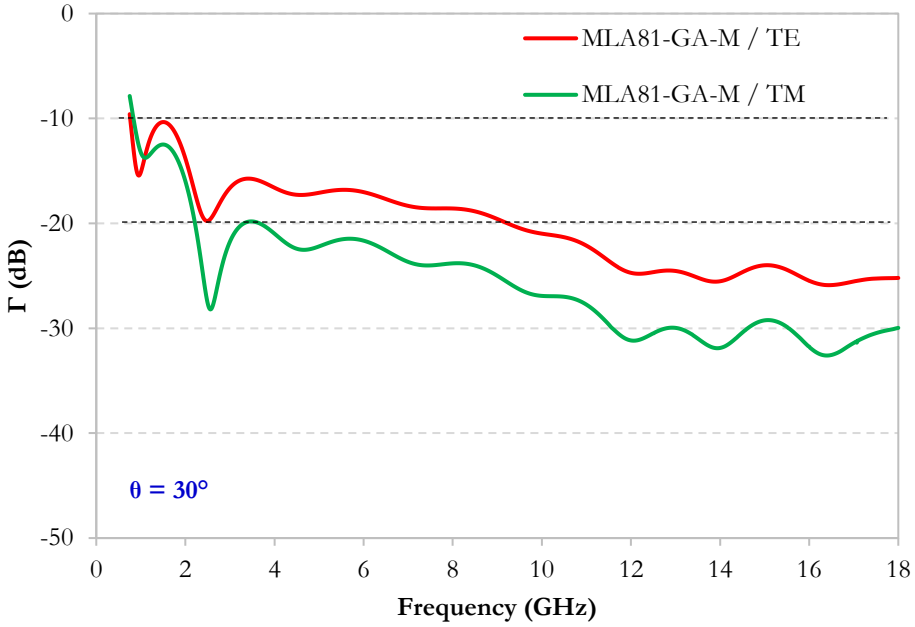

Figure III.25. Simulated reflection coefficient for LW-MLA81-GA-M at oblique incidence of 30° for TE and TM polarizations.

3.3.5 Comparison

Comparison between the measured reflection coefficients of MLA50-GA-M and MLA70-GA-M prototypes, optimized by the achieved MATLAB code, and the MLA77-GA (optimized thicknesses by GA CST) is presented in Figure III.26 for the normal incidence.

On the one hand, it is observed that both optimized prototypes by the MATLAB code (MLA70-GA-M and MLA50-GA-M) have a better absorption performance than that optimized by the GA CST (MLA77-GA), which has a higher thickness. On the other hand, the optimized MLA70-GA-M has a better performance than that of MLA50-GA-M. Indeed, MLA70-GA-M has a reflection coefficient less than -10 dB in the whole studied frequency range, and less than -20 dB from 2.2 GHz, whereas, MLA50-GA-M has a reflection coefficient higher than -10 dB for frequencies less than 1.18 GHz. It seems, from this latter, that the reduction in thickness has its limit since we observe a degradation of the absorption performance, when a total thickness of 50 mm is achieved. This is due, as explained before, to the very low overall thickness of this latest prototype (MLA50-GA-M) which does not allow the absorption of low frequencies. However, a comparable absorption performance is obtained with the two optimized prototypes, by the GA MATLAB, for frequencies higher than 5 GHz. This shows that the optimization with the developed code using GA of MATLAB is more efficient than that of GA implemented in CST software and means that the possibility of introducing the different materials / properties in the code is very important to realize a better optimization.

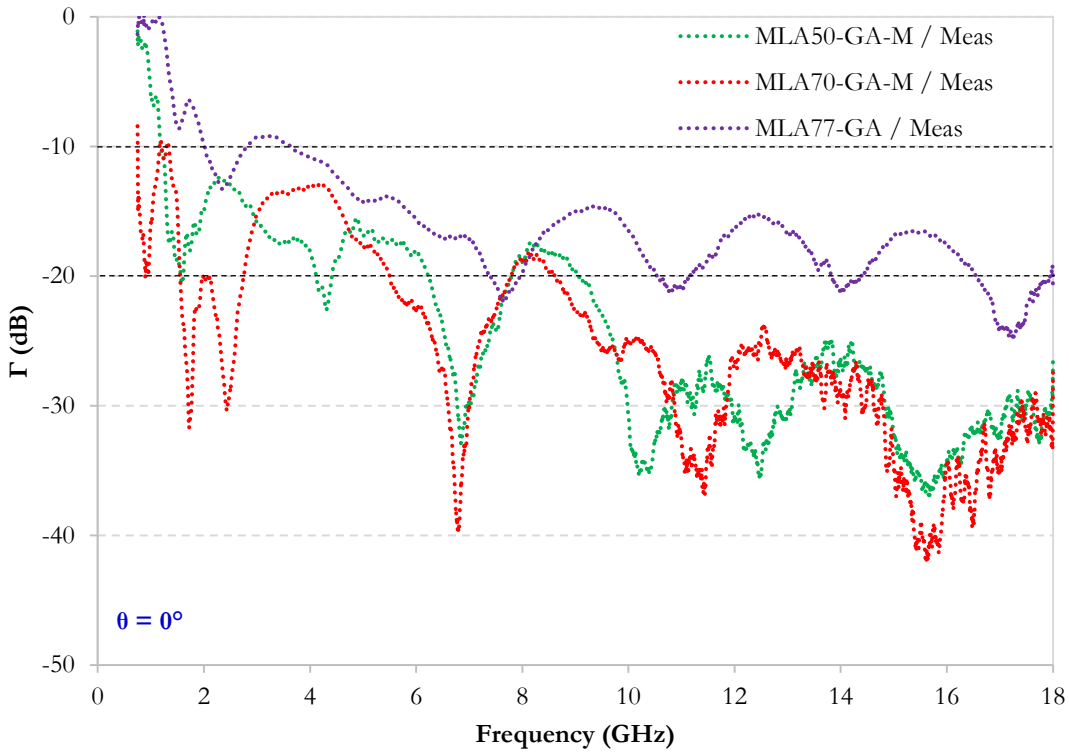

Figure III.26. Comparison between measured reflection coefficients of MLA50-GA-M, MLA70-GA-M and MLA77-GA.

In Figure III.27, the measured reflection coefficients of MLA50-GA-M, MLA70-GA-M, MLA98-GA-M (optimized by MATLAB) and MLA77-GA (optimized by CST) are compared, for normal incidence, to that of MLA125-2 (with the same thickness for all layers, and presented in the previous chapter in Figure II.33) and to that of the commercial absorber AH 125. It is observed that the MLA77-GA has the worst reflection coefficient and the MLA98-GA-M has the best one among all the achieved prototypes in the whole studied frequency range, especially at the lowest frequencies (less than 6 GHz). Moreover, MLA125-2, MLA98-GA-M, MLA50-GA-M and MLA70-GA-M have practically the same performances as the

MLA125-2 at the highest frequencies (higher than 10 GHz). One can note here that with a lower thickness of a multilayer absorber (reduction of 44 % for MLA70-GA-M and reduction of 22 % for MLA98-GA-M) and a very low CF loads, a better absorption has been obtained over a broadband frequency range.

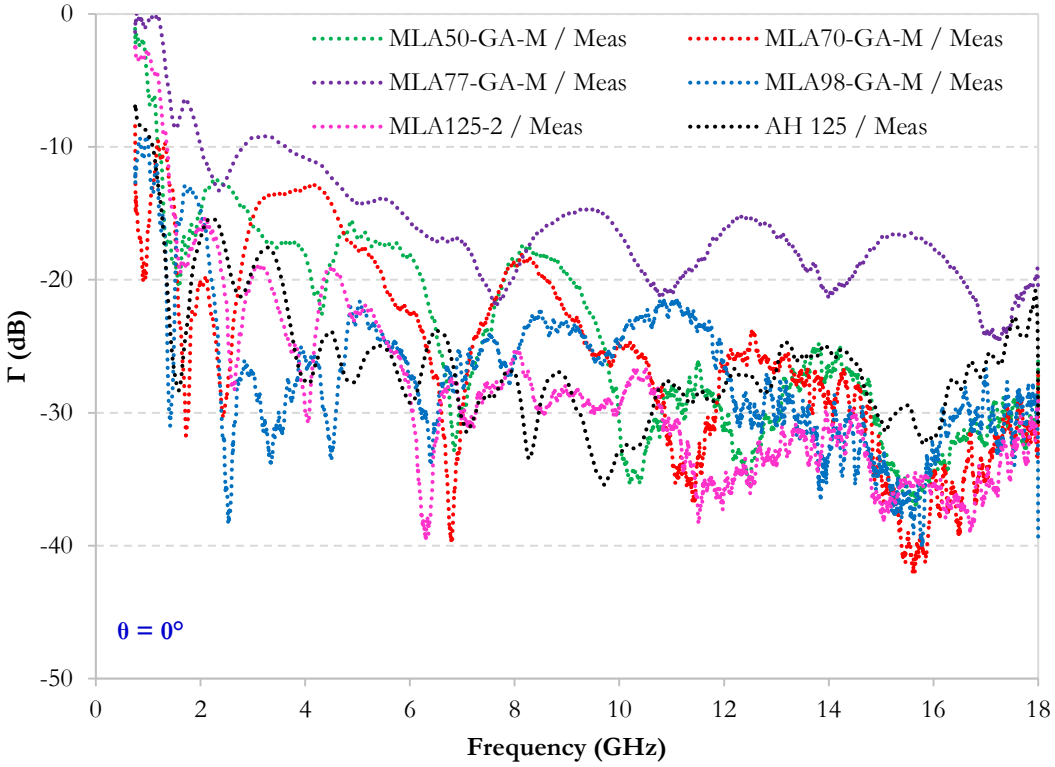

Figure III.27. Comparison between the measured reflection coefficients of MLA50-GA-M, MLA70-GA-M, MLA98-GA-M, MLA77-GA, MLA125-2 and AH 125 at normal incidence.

In order to compare the performances of the measured prototypes, taking into account their different thicknesses, we have established a Factor of Merit (FoM) that takes into account the two quantities that we are trying to reduce: the total thickness and the total reflection coefficient. The chosen FoM (equation (4)) is therefore inversely proportional to these two quantities.

$$FoM = \frac{1}{Total\ thickness * \Gamma_{linear}} \tag{4}$$

By comparing the calculated FoM of the five proposed prototypes MLA50-GA-M, MLA70-GA-M, MLA98-GA-M, MLA77-GA and MLA125-2 to that of the commercial absorber AH 125 (Figure III.28), we observe firstly that MLA77-GA has the worst FoM in all the studied frequency range (Figure III.28 (a)). Then, we can note that MLA125-2 has better FoM in high frequencies (> 10.7 GHz) than that of the commercial absorber AH 125 and practically the same FoM elsewhere (Figure III.28 (a)), while our prototype is composed of a very lightly loaded composite materials. Likewise, MLA98-GA-M has better FoM at low (< 7 GHz) and high (> 12 GHz) frequencies than that of AH 125 (Figure III.28 (a)) with a reduced thickness by 22 %.

Moreover, AH 125 also shows a lower FoM than both MLA70-GA-M and MLA50-GA-M prototypes (Figure III.28 (b)), optimized by our developed MATLAB program using GA, in all studied frequency range

and in particular from 10.5 GHz. Moreover, if we observe the entire studied frequency range, FoM of the two MLA50-GA-M and MLA70-GA-M prototypes can be considered as comparable.

In conclusion, firstly, our MLA98-GA-M prototype shows the best absorption performance among the proposed prototypes and even better than the commercial absorber in the studied frequency range between 0.75 GHz and 18 GHz. Secondly, MLA70-GA-M and MLA50-GA-M prototypes present the two best compromises of the absorption performance and the thickness, among all the measured absorbers.

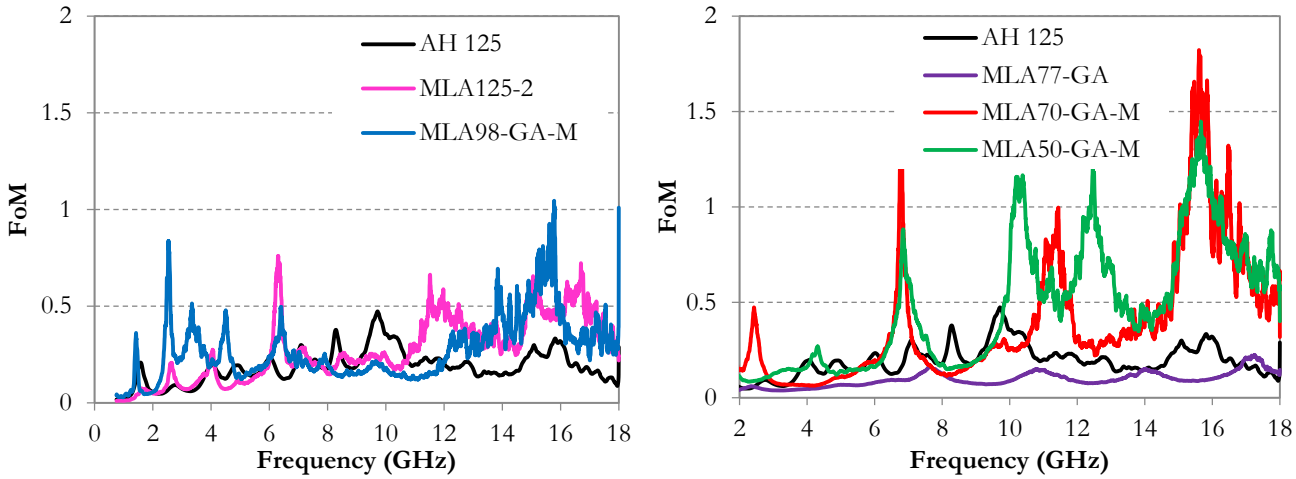

Figure III.28. Calculated factor of merit of AH 125 compared to that of (a) MLA125-2 and MLA98-GA-M and (b) and MLA77-GA, MLA70-GA-M and MLA50-GA-M.

4. Conclusion

In this chapter, a genetic algorithm was proposed to solve the problem of multilayer microwave absorber design. The purpose of this study is to find a set of layers with the smallest reflection coefficient, associated with a thin total thickness to compose a multilayer absorber that works, in a large frequency range. For this, a database of predefined materials was constructed with 24 different epoxy foam composites, loaded with different rates (from 0.0125 wt.% to 10 wt.%) and lengths of carbon fibers (100 µm to 12 mm).

Different proposed designs, by the developed code using GA in MATLAB, are presented and the results of the different designs are compared to those optimized by the GA implemented in CST software. The measured reflection coefficients of the achieved prototypes, MLA98-GA-M, MLA70-GA-M and MLA50-GA-M, show better performances than that of MLA77-GA (optimized by GA CST) and MLA125-2, which have higher thicknesses. Furthermore, the calculated FoM for all achieved prototypes, compared to that of AH 125, shows that MLA77GA has the lowest FoM and consequently the worst combination between absorption and thickness while MLA70-GA-M and MLA50-GA-M have the best compromise between absorption and thickness. In addition to that, our measurement results show that MLA98-GA-M has the best performance with a reduction of 22 % of the total thickness, compared to the commercial absorber.

Otherwise, an optimization was conducted using the five low density epoxy foam composites. The proposed LW-MLA81-GA-M design shows a good reflection coefficient < -20 dB in most of the studied

frequency band (2.21 - 18 GHz) with a total thickness reduced by 35 % compared to the lightweight LW-MLA125-1 which is composed with the same loaded materials; but in other order and layers' thicknesses.

This study shows that the use of the developed code combined with GA MATLAB improves the performance of multilayer absorbers while reducing their thickness. This improvement is possible because this code allows us to introduce, and therefore to optimize, the choice of the material, the thickness, as well as, the order of each layer constituting the multilayer absorber. In addition, for this code, the total thickness of the absorber is not imposed. Contrary to this, the GA of CST can only vary the thickness of the layers, but the choice of the materials, their order, as well as, the total thickness of the absorber must be determined.

The optimized design of the multilayer absorber in this study discusses only the case of normal incidence of the EM waves. The oblique incidence could be also used in the optimization process and may be discussed in future studies.

Chapter IV:

Hybrid Metamaterial Absorber

Table of Contents

List of Figures 134

List of Tables 136

1. Introduction 137

2. Metamaterial fundamentals 137

3. Flower shape metamaterial absorber 138

3.1 Simulation results of the first proposed MM absorber 138

3.2 Normalized input impedance and effective permittivity and permeability 147

4. The novel proposed symmetrical V-shape MM 150

4.1 Multi-resonance V-shape 10 x 10 MM 150

4.2 Multi-resonance V-shape 15 x 15 MM 153

5. Hybrid MM absorber 158

5.1 Simulation results 158

5.2 Measurement results 162

5.3 Comparison with other works 163

6. Conclusion 165

7. References 167

List of Figures

Figure IV.1. Proposed flower shape MM absorber (a), petal formation (b) and its absorption (c) for different radii values. 139
(a) 140
Figure IV.2. (a) Method used to draw each petal of the proposed flower shape MM absorber, (b) design and (c) side view of the proposed flower shape MM absorber. 140
Figure IV.3. Front view (a) and perspective view (b) of the proposed flower shape. 141
Figure IV.4. Reflection coefficients of the proposed flower shape MM absorber by varying L. .142
Figure IV.5. Reflection coefficients of the proposed flower shape MM absorber by varying a. ..143
Figure IV.6. Reflection coefficients of the proposed flower shape MM absorber by varying a and L. 144
Figure IV.7. Reflection coefficients of the proposed flower shape MM absorber by varying the radii with different steps. 145
Figure IV.8. Difference between the proposed structure and the previous one (a) and its perspective view (b). 146
Figure IV.9. Simulated reflection coefficient of the proposed flower shape MM 27 x 27 (a) and comparison between MM flower shape 27 x 27 with two orientations (b). 147
Figure IV.10. Calculated normalized input impedance of the proposed MM flower shape 27 x 27.148
Figure IV.11. Extracted effective permittivity (a) and permeability (b) of the proposed MM flower shape 27 x 27. 149
Figure IV.12. Comparison between simulated and analytical calculation of the reflection coefficients of the proposed MM using the extracted permittivity and permeability. 149
Figure IV.13. First three steps and the associated simulated reflection coefficients (a) to (c) and the second three steps and the associated simulated reflection coefficients (d) to (f) to obtain the final V-shape MM. 151
Figure IV.14. Front view (a), side view (b), perspective view (c) and periodic view (d) of the V-shape MM. 152
Figure IV.15. Simulated reflection coefficients at normal incidence (a) and at oblique incidence for TE and TM (b) polarizations. 152
Figure IV.16. From V-shape 10 x 10 to V-shape 15 x 15. 153
Figure IV.17. Front view (a), side view (b), perspective view (c) and periodic view (d) of the V-shape MM. 154
Figure IV.18. Comparison of the simulated reflection coefficients of the MM V-shape 10 x 10 and 15 x 15 at normal incidence. 154

Figure IV.19. Photo of the realized MM 15 x15 (a) and comparison between measured and simulated reflection coefficients, of the proposed MM, at normal incidence (b) and oblique incidence of 30° for TE (c) and TM (d) polarizations. 155
Figure IV.20. Calculated normalized input impedance of the proposed MM V-shape 15 x 15...156
Figure IV.21. Extracted effective permittivity (a) and permeability (b) of the proposed MM V-shape 15x15. 157
Figure IV.22. Comparison between simulated and analytical calculation of the reflection coefficients of the proposed MM using the extracted permittivity and permeability. 157
Figure IV.23. The proposed hybrid absorber. 158
Figure IV.24. Simulation results of the reflection coefficients of the MM alone and the hybrid absorber based on composites loaded with (a) CF loads ≤ 0.075 wt.% and (b) CF loads ≥ 0.075 wt.%. ..159
Figure IV.25. Simulation results of the reflection coefficients of the hybrid absorber based on composites loaded with 0.075 wt.% of different thicknesses. 160
Figure IV.26. Comparison between the simulated reflection coefficients of the proposed hybrid absorber and (a) the monolayer and (b) that of the proposed MM at normal incidence. 160
Figure IV.27. Simulated reflection coefficients of the proposed hybrid absorber compared to that of the proposed MM at oblique incidence of 30° (a) for the TE polarization and (b) for the TM polarization. 161
Figure IV.28. Simulation of the reflection coefficients of the hybrid absorber with different incidence angles ranging between 0° and 60° for (a) TE and (b) TM modes (The same scale is used for the two figures). 161
Figure IV.29. Simulation of the reflection coefficients of the hybrid absorber with different incidence angles (0°, 15°, 30°, 45° and 60°) for (a) TE and (b) TM modes.....162
Figure IV.30. The final proposed hybrid MM absorber (a) and comparison between simulation and measurement of the reflection coefficients of the hybrid absorber for normal (b) and oblique incidence for TE (c) and TM (d) polarizations. 162
Figure IV.31. Comparison between the relative bandwidth (in %) of the realized hybrid absorber and the different references in Table IV.8. 164
Figure IV.32. Comparison between the factor of merit (FoM) of the realized hybrid absorber and the different references in Table IV.8. 165

List of Tables

Table IV.1. Parameters of the proposed flower shape MM. 140
Table IV.2. Different radii used for the simulation. 144
Table IV.3. Parameters of the proposed flower shape MM. 146
Table IV.4. Complex normalized impedances at the resonant frequencies of the proposed MM. 148
Table IV.5. εeff and μeff at the resonant frequencies of the proposed MM. 149
Table IV.6. Parameters of the proposed V-shape MM 10 x 10. 151
Table IV.7. Comparison between MM V-shape 10 x 10 and MM V-shape 15 x 15. 153
Table IV.8. Complex normalized impedance at the resonant frequencies of the proposed MM. 156
Table IV.9. Comparison between the proposed structure and other presented MMs in literature. 163

1. Introduction

Traditional microwave absorbers based on magnetic or dielectric losses, such as Salisbury screen, Dällenbach layer and Jaumann absorber, suffer from narrow bandwidth. These structures consist of a resistive sheet located at a quarter wavelength above a perfect electric conductor (PEC) where a portion of the incident EM wave is reflected from the surface and another portion is reflected from the PEC at the back. At the frequency where the two reflected waves are at 180° out of phase, they cancel each other and the reflection coefficient tends to zero. A concept for achieving this absorber with a lower thickness was introduced by *Engheta* using the high impedance metasurface [1]. In this case, instead of using a quarter wavelength spacer between the PEC and the resistive sheet, a metamaterial was placed at a distance *d,* which is much smaller than the operating wavelength λ ($d << \lambda$), with a dielectric layer sandwiched between the metamaterial surface and the metallic plate. The aim of *Engheta* was to successfully fulfill the required phase difference for far field cancellation. However, the practical design of the metamaterial has been then realized by *landy and al.* [2]. Since then, many studies have been conducted concerning metamaterials for electromagnetic wave absorption in various frequency ranges.

In this chapter, MM fundamentals are first presented. After this, different multi-resonant MM absorbers will be proposed; the shape, size, effective parameters and absorption performance of these metamaterials will be shown. The absorption bandwidth of the best multi-resonant MM (presenting the highest number of resonant peaks, especially at low frequencies) will be then used to form a hybrid absorber. The measured absorption performance of the different porotypes will be systematically presented and compared to the simulated ones.

2. Metamaterial fundamentals

Metamaterials (MM), which acts as a frequency selective surface, consists of a periodic arrangement of metallic structures (resonators); they have a thickness that is much smaller than the guided wavelength. The resonators behave like artificial materials that scatter incident EM waves giving rise to macroscopic effective material parameters such as permittivity, permeability and refractive index; these parameters are influenced by the shape and the geometry of the resonators. Physically, when an incident plane wave arrives on MM, currents will be induced on the metal that forms the resonator creating a scattered field. This induced field is not uniform, it is strongest around the metal and decreases at a certain distance of it [3].

The reflection coefficient R of MM absorbers, at normal incidence of the EM wave, can be calculated using the transmission-line theory with equation (1) where z is the normalized input impedance of the MM absorber and z_o is the impedance of air ($z_o = 1$). Note that when $z = z_o = 1$, the reflection coefficient tends to zero and a total absorption will occur.

$$R = \frac{z - z_0}{z + z_0} \tag{1}$$

In order to find the normalized input impedance z, as well as, the permittivity and the permeability of a MM, we need to characterize the MM absorber as an effective homogeneous slab. For this, the simulated reflection (S_{11}) and transmission (S_{21}) coefficients data that are obtained by the simulation will be used. Using these data, the normalized input impedance of the MM absorber can be calculated using equation (2) [3]; here, S_{21} is equal to zero due to the presence of the backed metallic plate that cancels the transmission of the EM waves.

$$z = \pm\sqrt{\frac{(1+S_{11})^2 - S_{21}^2}{(1-S_{11})^2 - S_{21}^2}} = \pm\frac{1+S_{11}}{1-S_{11}} \tag{2}$$

Since the metamaterial under consideration is a passive medium, the ambiguity of the sign in equation (2) is determined, so that the real part of the normalized input impedance is non-negative $Re\,(z) \geq 0$ [4]. Therefore, for the sign of z, we distinguish two cases:

- The first case: if $Re\,(z) \geq 0 \rightarrow Z(\omega) = +\frac{1+S_{11}}{1-S_{11}}$
- The second case: if $Re\,(z) < 0 \rightarrow Z(\omega) = -\frac{1+S_{11}}{1-S_{11}}$

The effective permittivity and permeability (ε_{eff} and μ_{eff}) are two main parameters to study the metamaterial behavior. These parameters can be obtained using equations (3) and (4) where ***d*** is the thickness of the material in the direction of the incident EM wave and χ_e and χ_m are the surface electric and magnetic susceptibilities. These quantities are given by equations (5) and (6), respectively for χ_e and χ_m, where ***k*** is the wave number of the incident EM wave defined in equation (7), ***f*** is the frequency and ***c*** is the speed in free space (3 x 10^8 m/s) [5].

$$\tilde{\varepsilon}_{eff} = 1 + \frac{\chi_{es}}{d} \tag{3}$$

$$\tilde{\mu}_{eff} = 1 + \frac{\chi_{ms}}{d} \tag{4}$$

$$\chi_e = \frac{2}{k_0}\frac{j}{}\frac{S_{11}-1}{S_{11}+1} \tag{5}$$

$$\chi_m = \frac{2}{k_0}\frac{j}{}\frac{S_{11}+1}{S_{11}-1} \tag{6}$$

$$k_0 = \frac{\omega}{c} = \frac{2\pi f}{c} \tag{7}$$

3. Flower shape metamaterial absorber

3.1 Simulation results of the first proposed MM absorber

In [6], *Tuong and al.* have proposed a symmetrical four-petal flower shape resonator with a unit cell of 6 mm x 6 mm realized on FR-4 substrate with a total thickness of 0.2 mm (Figure IV.1 (a)). Note that each petal of the flower shape is the intersection of two circles of the same radii (Figure IV.1 (b)). They have shown that varying the radius of the circles composing the petals of the flower shape has an effect on the

resonant peak (Figure IV. 1 (c)). In the studied frequency range, the absorption rate is independent of the radius r of the circles that forms the petal, whereas, the resonant peak frequency shifts to lower frequencies with the increase of the radius of the circles and thus the increase of petals' dimension. For instance, by increasing the radius from 2 mm to 2.6 mm, the resonance shifts from 17 GHz to 12.75 GHz (Figure IV. 1 (c)).

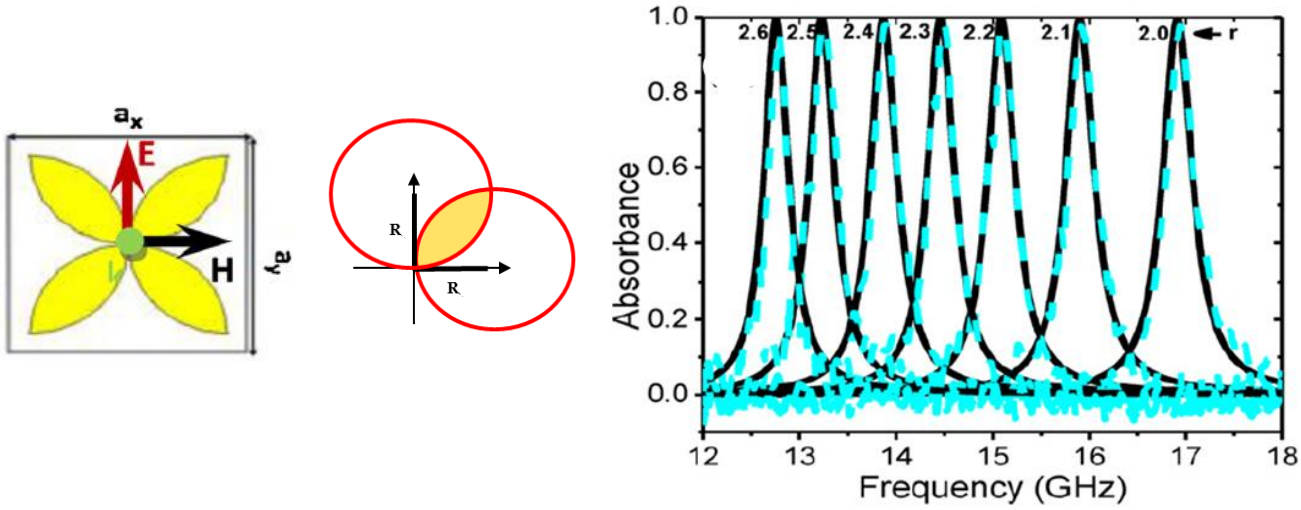

(a) *(b)* *(c)*

Figure IV.1. Proposed flower shape MM absorber (a), petal formation (b) and its absorption (c) for different radii values.

In this section, the first proposed MM is inspired from the flower shape of the literature presented above [6]. The idea here is to combine several dimensions of the flower shape resonator into the same unit cell in order to create multi-resonances, from one hand, and to use larger flower dimensions in order to shift the resonant frequencies to the low frequencies, from the other hand.

To investigate the absorption performance of the proposed structure, CST Studio software was used for the different simulations. Unit cell boundary condition is applied in the x and y directions and Floquet boundary condition is applied for the excitation in the z-direction. This numerical setup allows for the analysis of the MM absorber under different polarizations and incident angles of EM waves.

The design of all the proposed MMs consists of a periodic metal structure printed on the top of the substrate, while the underneath is fully covered with metal. The used metal in our studies is the copper with thickness t =17 µm. The same dielectric substrate FR-4, that has a relative dielectric constant $\varepsilon_r' = 4.3$ and tangent loss $\tan\delta = 0.025$, is used for all the proposed MM structures with the same thickness of h = 3.2 mm.

Figure IV.2 (a) illustrates the method of drawing the petals of each flower in CST for the first proposed flower shape MM. Here, each petal of the same flower is the intersection of two circles of the same dimension; this method will be used to form all the proposed flower based MMs of this section. The design of the flower shape MM is shown in Figure IV.2 (b) and (c). The different dimensions will be given later.

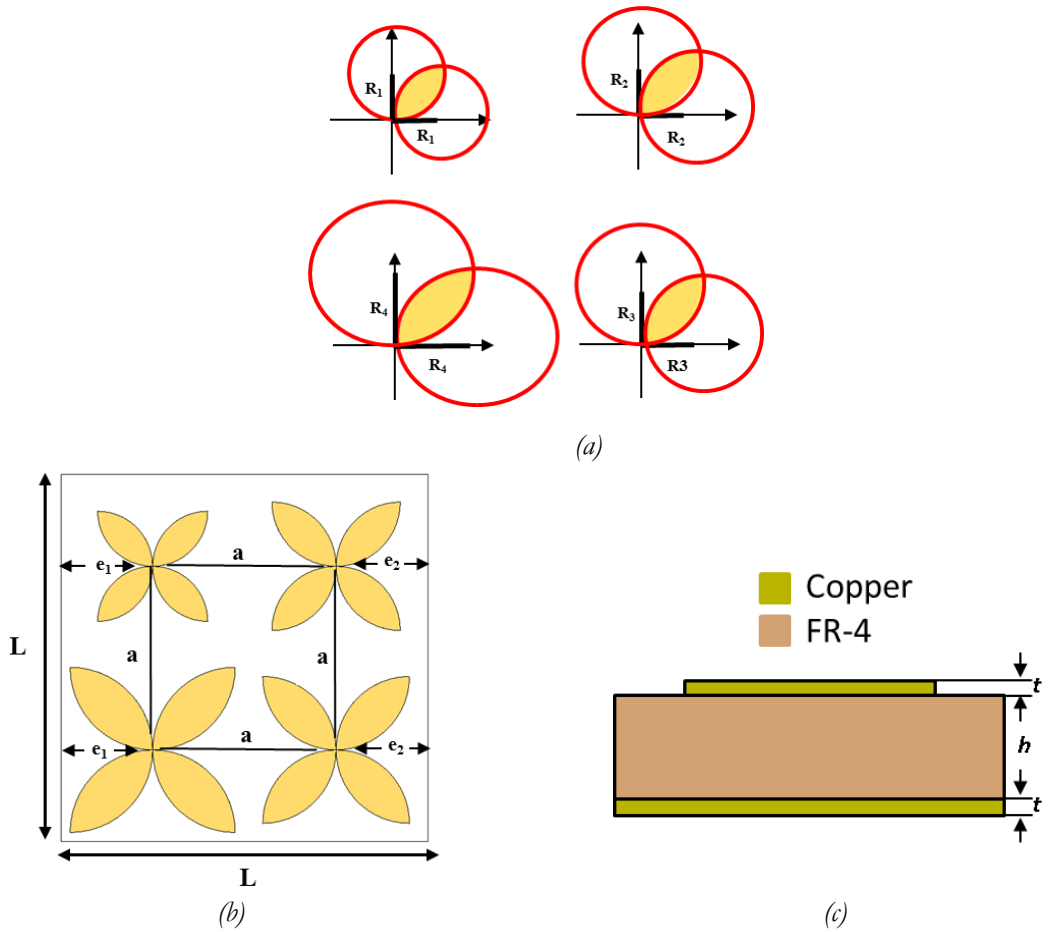

Figure IV.2. (a) Method used to draw each petal of the proposed flower shape MM absorber, (b) design and (c) side view of the proposed flower shape MM absorber.

A parametrical study of the flower shape was carried out during this thesis. Here, the influence of the dimensions of the flowers (represented by the radius R of the circles forming the petals), of the distance between the flowers (a) and of the size of the unit cell (L), are studied. The objective here is to determine the optimal value of each parameter that will allow us to achieve the MM absorber with the most resonances over a wide frequency band.

For the first study, the dimensions of the four flowers are fixed, as well as, the distance (a) between the flowers while the dimension of the unit cell L is variable. Here, near radii R_1= 3 mm, R_2= 3.5 mm, R_3= 4 mm and R_4= 4.5 mm are used to form the petals of the flowers. Table IV.1 summarizes the different dimensions of the structure of this first study and Figure IV.3 presents its design.

Parameters	Value (in mm)
a	10
e_1	Variable
e_2	Variable
h	3.2
L	Variable
R_1	3
R_2	3.5
R_3	4
R_4	4.5
t	0.017

Table IV.1. Parameters of the proposed flower shape MM.

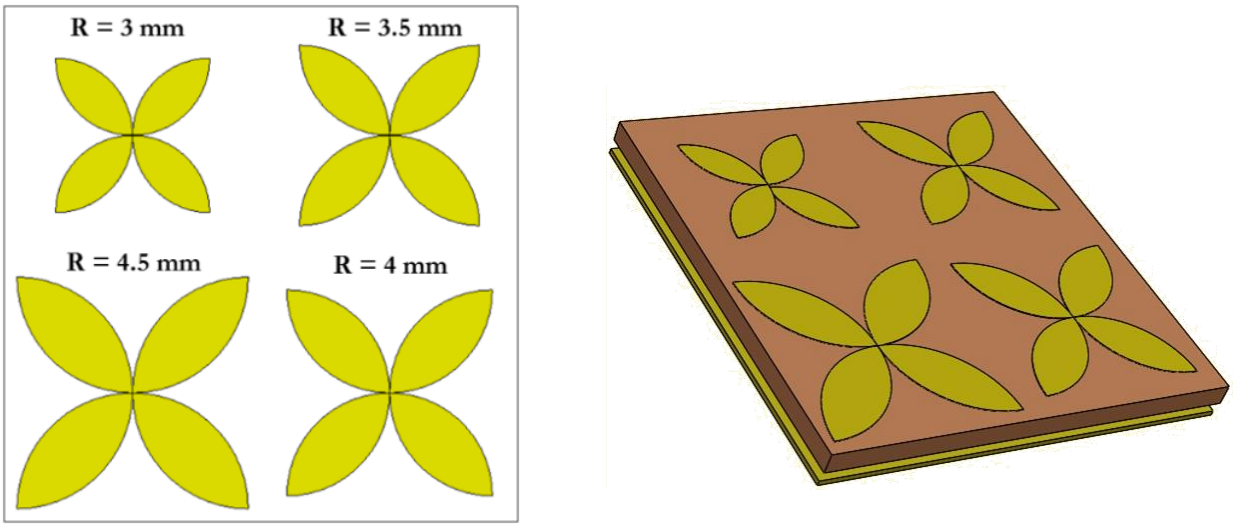

(a) (b)

Figure IV.3. Front view (a) and perspective view (b) of the proposed flower shape.

Simulated reflection coefficients of the proposed flower shape MM when varying the dimension of the unit cell L between 20 and 24 mm are shown in Figure IV.4. This latter shows that the use of different flower dimensions allows the obtaining of several resonances in the frequency range between 6 and 17 GHz, confirming by this the creation of a multi-resonant absorber. From the obtained results, it is also observed that the first resonance has appeared at the same frequency (around 6.4 GHz) whatever the L value is. Moreover, the frequencies of resonance at lower frequencies between 6 and 8 GHz are slightly affected by the increase of L; resonances occur approximately at the same frequencies or with a very small shift whatever is the value of L, but the intensity of these resonances decreases with the increase of L. For example, when L increases from 20 to 24 mm, the three obtained resonances slightly shifted toward lower frequencies; here the first resonance is shifted from 6.5 GHz with a reflection coefficient of -17.6 dB (when L = 20 mm) to 6.4 GHz with a reflection coefficient of -11.3 dB (when L = 24 mm).

For the obtained resonances at high frequencies (between 16 GHz and 18 GHz), the larger the L, the higher the intensity of the resonant peak. In the middle frequency range, two intense resonances have appeared at the frequencies of 9.86 GHz and 13.42 GHz when L = 24 mm is used. In fact, by increasing L, the resonances of high frequencies shift toward lower frequencies with higher intensities, and thus, lower reflection coefficient are obtained. For example, when L = 20 mm, a resonance is obtained at 14.2 GHz with a reflection coefficient of -4.3 dB; this resonance shifts to 13.4 GHz with a reflection coefficient of -31.3 dB when L = 24 mm.

In the conclusion of this study, L = 24 mm presents the highest number of resonances, therefore, it is chosen for the next study.

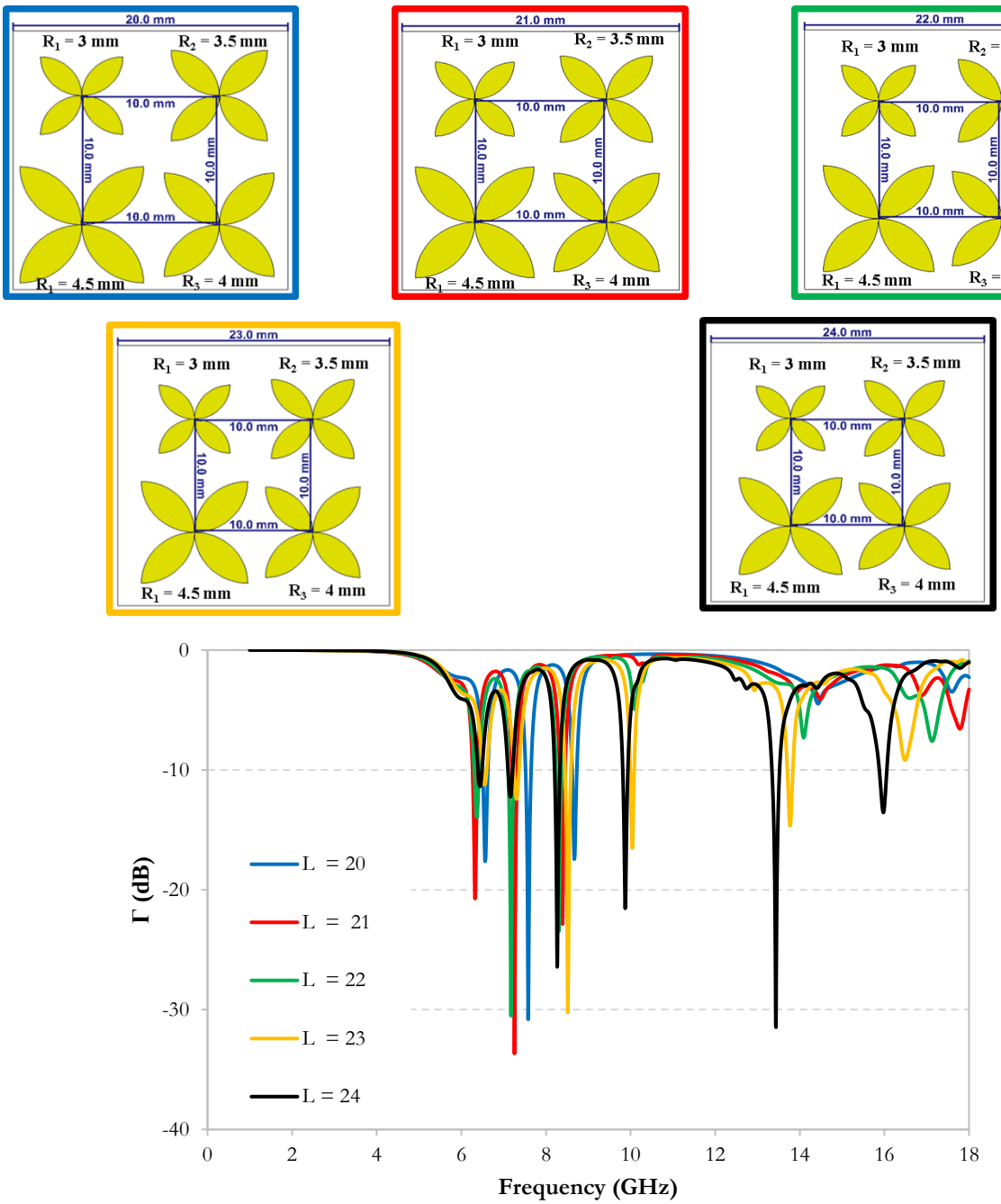

Figure IV.4. Reflection coefficients of the proposed flower shape MM absorber by varying L.

For the second study, and according to the obtained results above, the unit cell dimensions L x L are set to 24 mm x 24 mm and the distance between the four flowers (a) varies between 10 mm and 13 mm. Here, the same radii of R_1= 3 mm, R_2= 3.5 mm, R_3= 4 mm and R_4= 4.5 mm are also fixed, as for the first study. The schematic representation of this variation and the associated simulation of the reflection coefficients are presented in Figure IV.5.

From the obtained results, it can be observed that the intensity of resonances expected at the lower frequencies (between 6 and 7.5 GHz) are very close and still weak compared to those obtained at the high frequencies. Here, the best reflection coefficients, with two intense resonances (at 9.8 GHz and 13.4 GHz), is obtained when the distance between the flowers is 10 mm and it deteriorates when increasing the (a) value (Figure IV.5). For these reasons, a = 10 mm is chosen for the next study.

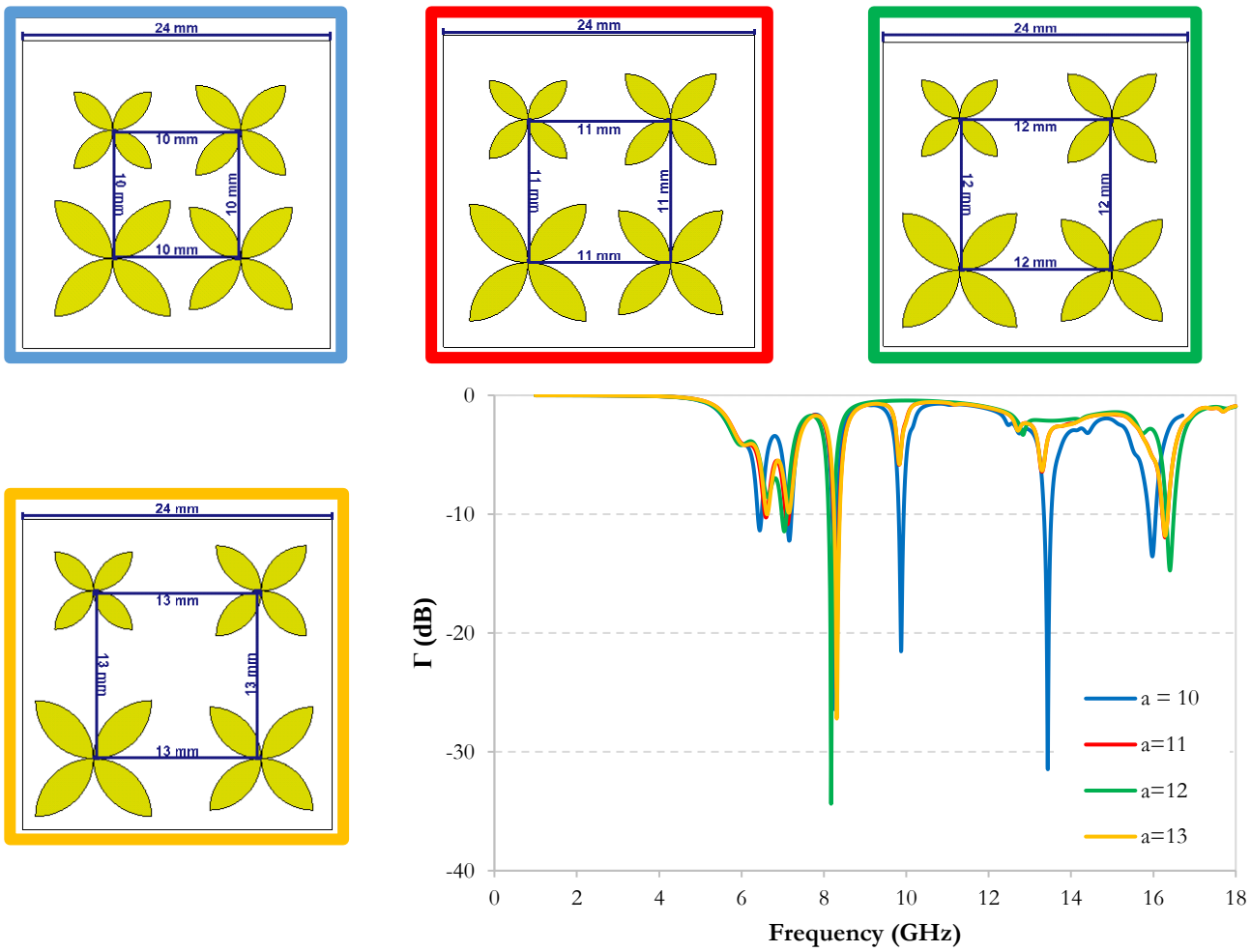

Figure IV.5. Reflection coefficients of the proposed flower shape MM absorber by varying a.

Following the previous results, another study was conducted by varying two parameters at the same time; the first one is L that varies between 20 mm and 23 mm respectively with the increase of the distance (a) between the flowers as the second variable parameter (Figure IV.6). For example, the unit cell of 20 x 20 is used when the distance between the flowers (a) is set to 10 mm, while the unit cell of 21 x 21 is used when the distance between the flowers (a) is increased to 11 mm. By this simultaneous modification of the (a) and L parameters, we can maintain the same distance between the flowers of two adjacent structures. Figure IV.6 groups the different structures and the associated simulated reflection coefficients.

From Figure IV.6, it could be observed that three intense resonances are obtained at the frequencies between 6 and 9 GHz, whatever are the values of (a) and L. In addition to that, resonances become more intense at high frequencies (> 8 GHz) when a = 13 mm. However, when a = 13 mm, associated with L = 23 mm, six resonances are obtained, where five of them are with a reflection coefficient less than -10 dB between 6 and 18 GHz. For these dimensions, three near resonances are obtained by simulation at the low frequencies 6.4 GHz, 7.3 GHz and 8.4 GHz with reflection coefficients of -15.4 dB, -17.62 dB and -20.5 dB, respectively, and three other resonances occurred at the high frequencies of 10.1 GHz, 14.03 GHz and 16.6 GHz with reflection coefficients of -31.2 dB, -21.4 dB and -9.6 dB, respectively. So, for this proposed flower shape MM, the optimal found values are a = 13 mm with L = 23 mm since it presents the highest number of resonances over a large bandwidth.

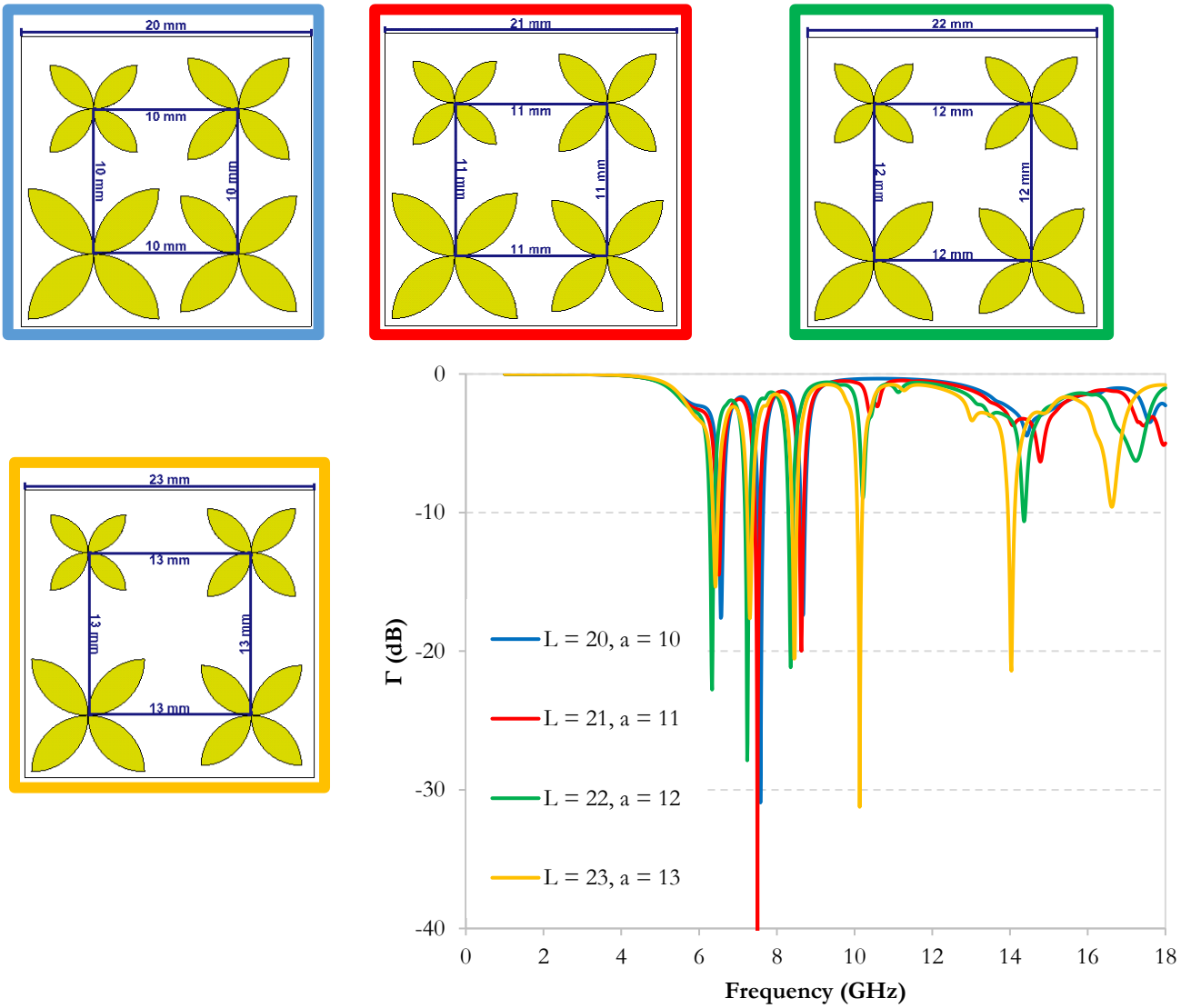

Figure IV.6. Reflection coefficients of the proposed flower shape MM absorber by varying a and L.

In the next study, the radii of the flowers are varied. Four different steps (R_step) of 0.5, 1, 1.5 and 2 mm are tested; varying by this the radius of the flowers between 1 and 7 mm. Table IV.2 summarizes these radii values for the different structures. Here, the (a) and L parameters are fixed to 13 mm and 27 mm, respectively; (a) is deduced from the previous study and L is chosen as 27 mm because higher radii are used. Indeed, we wanted to keep the same unit cell dimensions for the four structures, as well as, the distance between the flowers inside the same unit cell (Figure IV.7).

	R_1 (mm)	R_2 (mm)	R_3 (mm)	R_4 (mm)	R_step (mm)
Structure 1	3	3.5	4	4.5	0.5
Structure 2	3	4	5	6	1
Structure 3	1.5	3	4.5	6	1.5
Structure 4	1	3	5	7	2

Table IV.2. Different radii used for the simulation.

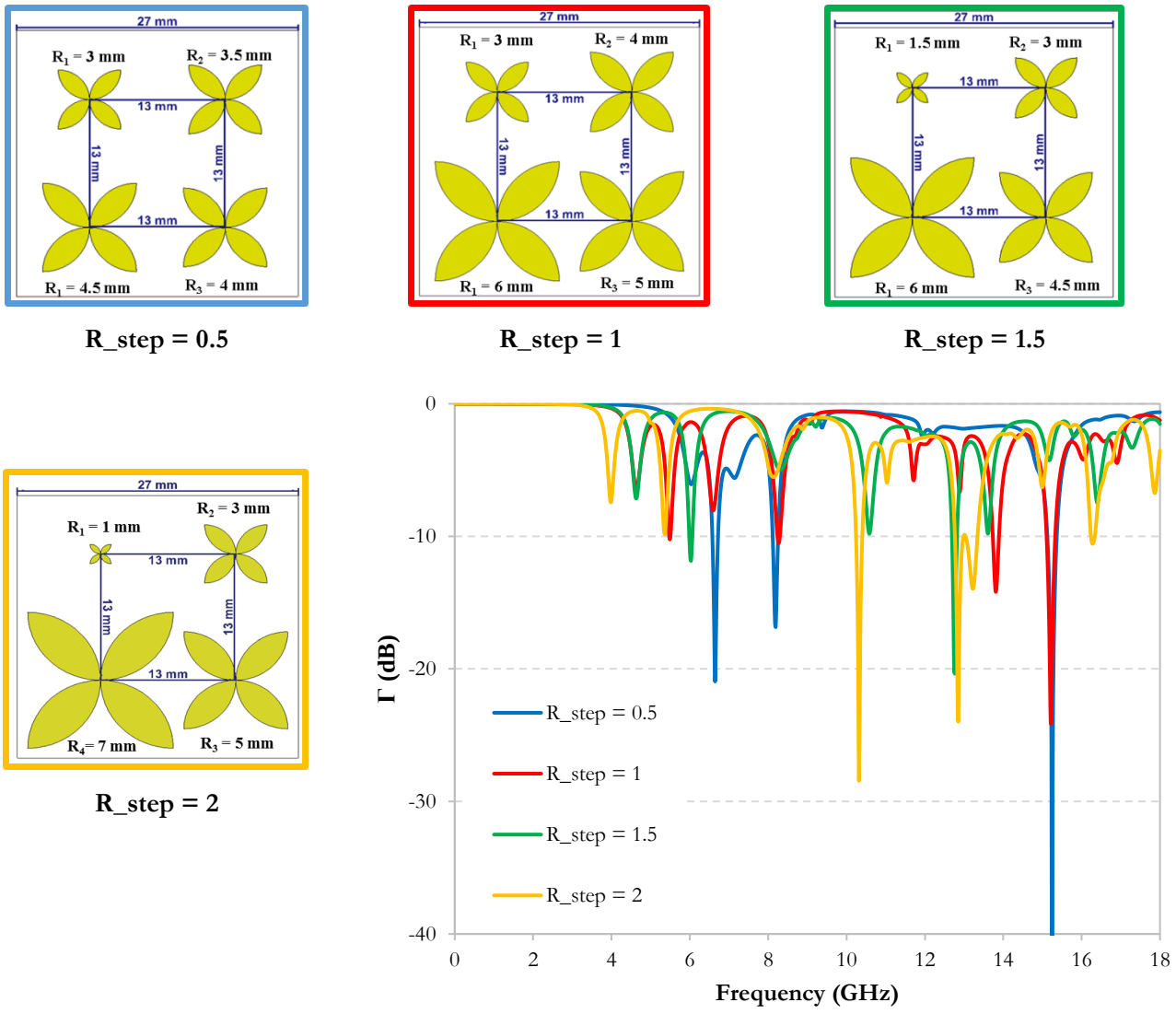

Figure IV.7. Reflection coefficients of the proposed flower shape MM absorber by varying the radii with different steps.

From the obtained results (Figure IV.7), it is observed that the resonance shift toward lower frequency when a higher step between the radii of the flowers is used. For example, when R_step = 0.5 mm, the lowest resonance is obtained at 6.64 GHz with a reflection coefficient of -21 dB; this resonance shifts toward 3.97 GHz when R_step is increased to 2, but with a higher reflection coefficient of -7.4 dB. In fact, the higher the step, the lower the frequency of resonances, but with a lower intensity. In addition to that, R_step = 2 presents multi-resonances with the greatest number of peaks over a large band. At the end, this structure, with R_step = 2, a = 13 mm and L = 27 mm, seems as the best compromise between resonance frequencies / reflection coefficients for a multi-resonant MM with several resonances between 3.99 GHz and 17.86 GHz.

In the last study of this section, the selected parameters for the best obtained result, of the previous study are reused (a = 13 mm, *L* =27 mm). One can note here that for this last structure, the location of the petals has been changed. In fact, in the previous structure, the flowers with successive radii were placed side by side in the unit cell (Figure IV. 8), while here, the flowers of successive radii are placed in the same

diagonal of the unit cell, as shown in Figure IV.8 (a) in order to investigate the effect of this position on the resonances. The different dimensions of this proposed MM are shown in Table IV.3.

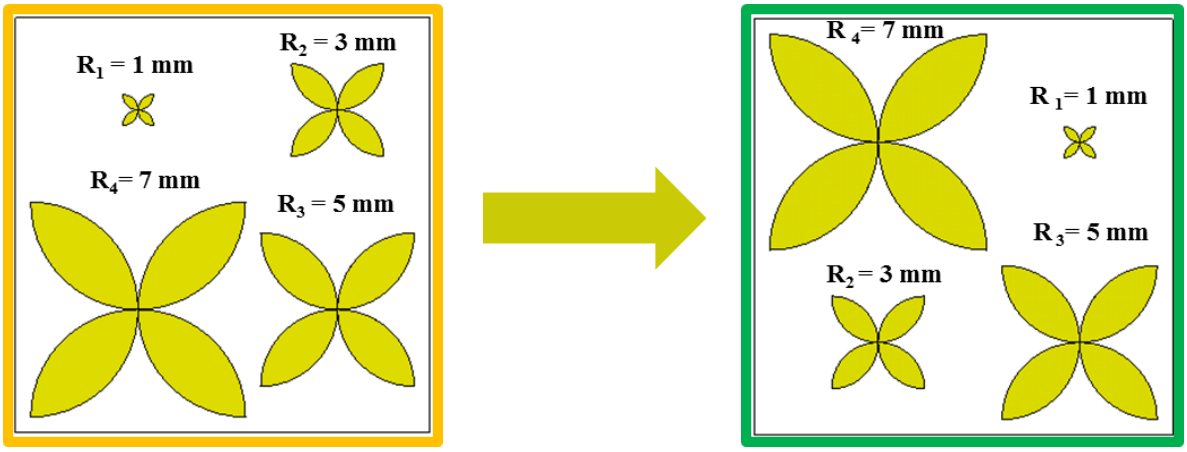

(a)

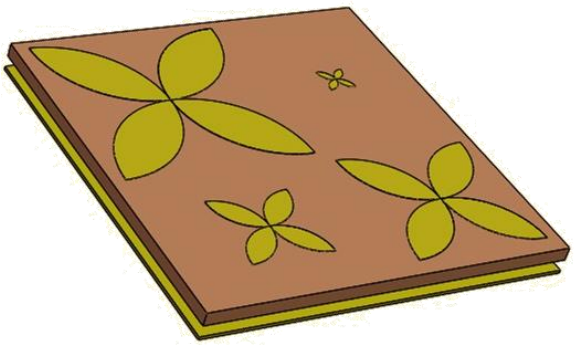

(b)

Figure IV.8. Difference between the proposed structure and the previous one (a) and its perspective view (b).

Parameters	Value (in mm)
a	13
e_1	8
e_2	6
h	3.2
L	27
R_1	7
R_2	1
R_3	5
R_4	3
t	0.036

Table IV.3. Parameters of the proposed flower shape MM.

The simulated reflection coefficient of this proposed flower shape based MM is shown in Figure IV.9 (a). Results show that multiple resonances are expected between 4 GHz and 16 GHz, with higher intensities for some frequencies such as at 8.3 GHz and with lower intensities for some other frequencies such as at 3.97 GHz, compared to the previous structure (Figure IV.9 (b)). Moreover, a new resonance has appeared at 14.4 GHz with a reflection coefficient of -36 dB and at other frequencies.

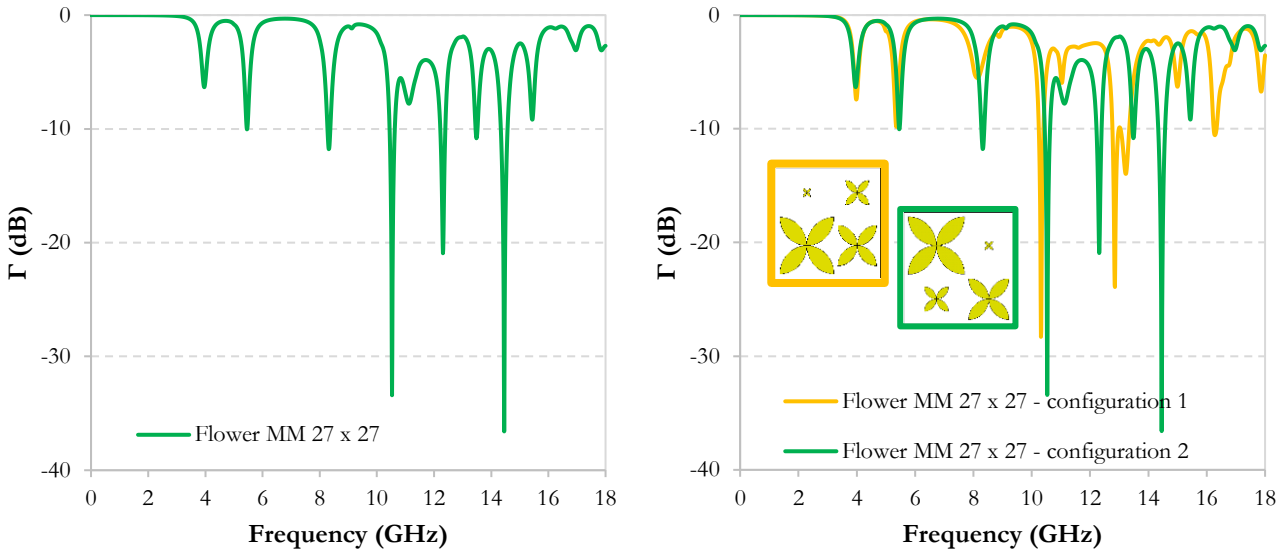

Figure IV.9. Simulated reflection coefficient of the proposed flower shape MM 27 x 27 (a) and comparison between MM flower shape 27 x 27 with two orientations (b).

Finally, the last structure presents the best compromise between the different flower-shape based MMs. Indeed, several resonances are obtained here with relative good intensities, but at the high frequencies (> 8 GHz). Moreover, resonant peaks are expected at low frequencies (between 3 and 8 GHz), but not below 3.90 GHz, and with low intensities. Here, simulated reflection coefficients are about -6 dB and -9.6 dB at resonant frequencies of 3.92 GHz and 5.43 GHz, respectively. In the conclusion, it should be noted that whatever are the dimensions (a, L and especially the radii Ri) of the proposed MM, this latter remains only adjusted to high frequencies between 10 and 18 GHz, the same studied range in the state of art.

3.2 Normalized input impedance and effective permittivity and permeability

Despite the relatively poor absorption performance of the proposed MM here, we proceeded to the extraction of the effective parameters; these will be used for the calculation of its reflection coefficient, and thus, the validation of our extraction method.

The S11 parameter, which is computed using CST software (Figure IV.10 (a)), was used to extract the effective parameters of the proposed MM flower shape of 27 mm x 27 mm unit cell. Based on equation (2), presented in section 2 of this chapter, the normalized input impedance (z) is extracted for the proposed MM backed with MP (Figure IV.10). The obtained values of the normalized input impedance (z) that corresponds to the resonating frequencies are presented in Table IV.4. It can be observed from the figure, and more clear in the table, that at the resonating frequencies where the reflection coefficient is less than -10 dB, the real part of the normalized input impedance Real (z) is close to one and the imaginary part Imag (z) is close to zero. In other words, the closer the Real (z) to 1 and Imag (z) to zero, the higher the absorption performance. This indicates a perfect matching at these frequencies, and hence, absorption higher than 90 % is obtained. For example, at 10.53 GHz, where a reflection coefficient of -33 dB is obtained, Real (z) = 1.02 and Imag (z) = 0.03.

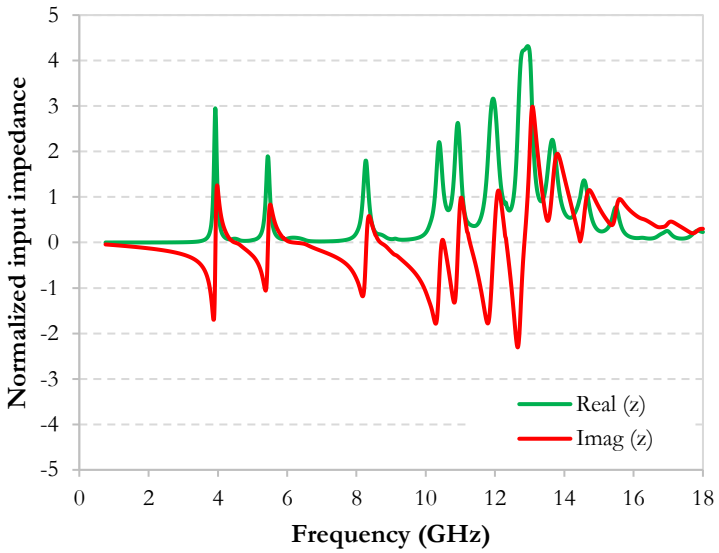

Figure IV.10. Calculated normalized input impedance of the proposed MM flower shape 27 x 27.

Frequency (GHz)	Impedance
3.96	2.08 – j 1.12
5.45	1.86 – j 0.17
8.33	1.26 – j 0.52
10.53	1.02 – j 0.03
12.31	0.87 – j 0.09
13.48	1.32 – j 0.53
14.45	0.98 – j 0.02
15.42	0.67 – j 0.44

Table IV.4. Complex normalized impedances at the resonant frequencies of the proposed MM.

The S_{11} parameter, was also used here in order to extract the effective parameters (ε_{eff} and μ_{eff}) of the proposed MM flower shape of 27 mm x 27 mm, using equations (3) to (7). The extracted effective permittivity (ε_{eff}) and permeability (μ_{eff}) are presented in Figure IV.11 (a) and (b), respectively. At the resonant frequencies, ε_{eff} and μ_{eff} are very close to each other approaching by that the impedance of the MM structure to that of air (Table IV.5). In other word, the normalized input impedance z, which is given by equation (8), should tend to 1 in order to obtain a good absorption, and hence, ε_{eff} and μ_{eff} should be very close to each other.

$$z = \sqrt{\frac{\mu_{eff}}{\varepsilon_{eff}}} \tag{8}$$

In fact, ε_{eff} and μ_{eff} are closer to each other when a reflection coefficient less than -20 dB is obtained. For example, at the resonant frequency that occurs at 10.53 GHz, the proposed flower shape MM 27 x 27 presents values of $\varepsilon_{eff} = 1.05 - j\,2.72$ and $\mu_{eff} = 0.9 - j\,2.94$ (Table IV.5); here, the $Real\ (\varepsilon_{eff})$ and $Real\ (\mu_{eff})$ are very close to each other and to 1 while $Imag\ (\varepsilon_{eff})$ and $Imag\ (\mu_{eff})$ are close to 0. Therefore, z tends to 1 at this frequency of resonance and a reflection coefficient of -33.4 dB is obtained. The same observations could be done for the intense peaks at 12.31 GHz and 14.45 GHz.

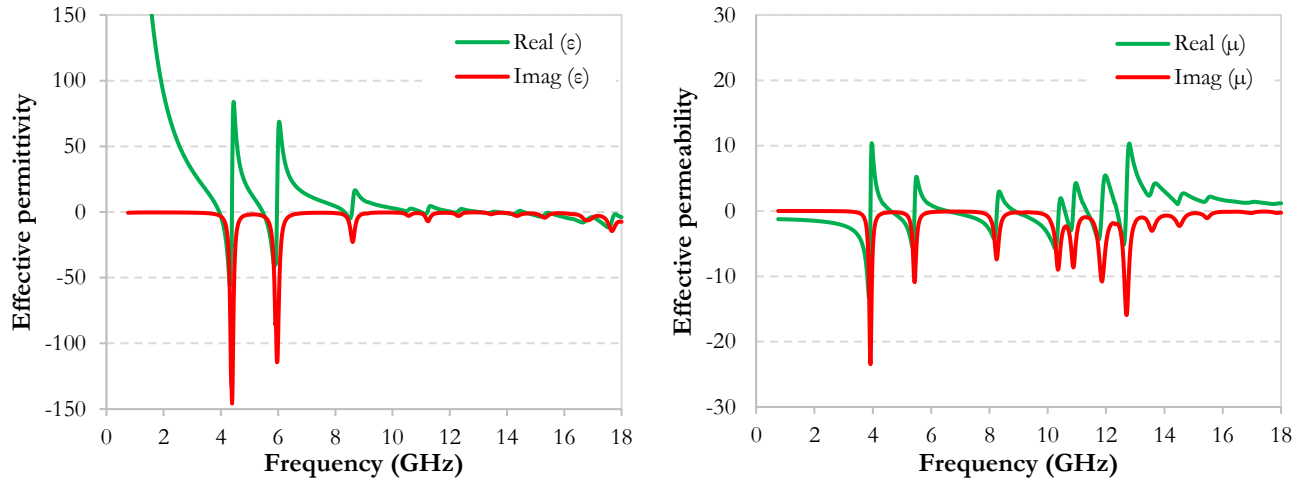

(a) *(b)*

Figure IV.11. Extracted effective permittivity (a) and permeability (b) of the proposed MM flower shape 27 x 27.

Frequency (GHz)	ε_{eff}	μ_{eff}
3.96	-0.98 – j 2.84	10.37 – j 13.4
5.45	0.35 – j 2.9	3.17 – j 9.8
8.33	-0.32 – j 2.6	2.99 – j 3.9
10.53	1.05 – j 2.72	0.94 – j 2.9
12.31	0.82 – j 2.8	1.12 – j 2.04
13.48	0.05 – j 1.59	2.3 – j 2.2
14.45	0.96 – j 2.11	1.02 – j 2.01
15.42	-0.49 – j 2.8	1.54 – j 1.03

Table IV.5. ε_{eff} and μ_{eff} at the resonant frequencies of the proposed MM.

Using the extracted effective permittivity and permeability of the proposed MM (Figure IV.11), the reflection coefficient is calculated using the transmission-line theory (equation (1)) where z is given by equation (8). The analytical calculation of the reflection coefficient is compared to the simulated one in Figure IV.12; a very good agreement is noted, which confirms the efficiency of the method of extraction that we have used to obtain the effective parameters of the proposed MM.

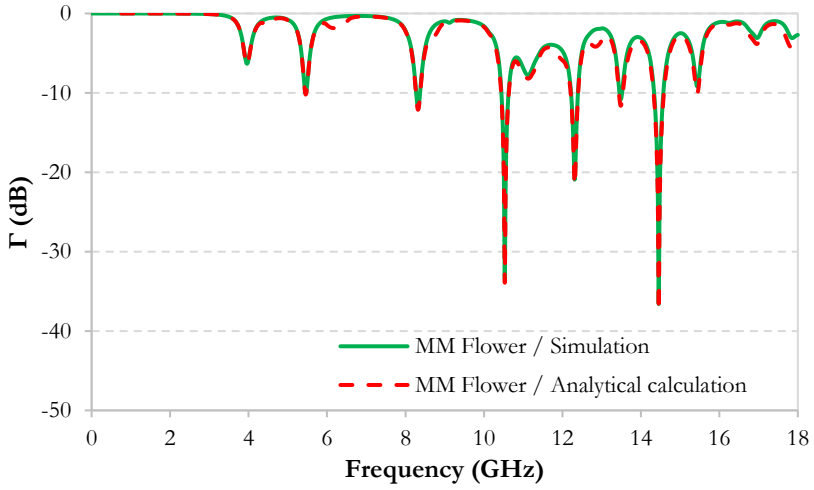

Figure IV.12. Comparison between simulated and analytical calculation of the reflection coefficients of the proposed MM using the extracted permittivity and permeability.

As explained before and despite of the multiple obtained resonances over a large band, the resonances at low frequencies (< 8 GHz) are weak; reflection coefficients higher than -10 dB are obtained. Our goal is to get more important absorption at the low frequencies. Therefore, other resonator shape will be tested. In addition, this MM is not symmetric; for these reasons, another symmetric and novel MM absorber design will be proposed in the next section.

4. The novel proposed symmetrical V-shape MM

In this section, a new symmetrical MM with a smaller unit cell dimensions than the MMs in the previous section, which presents multi-resonances, will be presented.

4.1 Multi-resonance V-shape 10 x 10 MM

The new proposed design of the MM consists of 10 mm x 10 mm unit cell using the same dielectric substrate FR-4 (dielectric constant $\varepsilon_r' = 4.3$, tangent loss $\tan\delta = 0.025$ and $h = 3.2$ mm) as that used for the first structure. The followed steps to obtain this new shape resonator are shown in Figure IV.13 (a) to (f) and the simulated reflection coefficient of each step is presented in Figure IV.13 (g).

A square shape alone (Figure IV.13 (a)) resonates at 2.29 GHz with -3.6 dB and at 15.7 GHz with -3.2 dB. On the other hand, X shape (Figure IV.13 (b)) alone resonates at 6.1 GHz with -1.7 dB and at 17.7 GHz with -7 dB. Combining the square and X shapes in the same unit cell (Figure IV.13 (c)), resonances at 2.9 GHz with -3.7 dB, at 6.2 GHz with -4.1 dB and at 16.2 GHz with -3.8 dB are obtained. Here, the observed resonances by each resonator alone are combined together; giving rise to the three obtained resonances at this step. When four additional symmetrical V shapes are added to the previous structure (Figure IV.13 (d)), the first two resonances appeared with two additional resonances that occur at 10 GHz with -24.9 dB and at 15.3 GHz with -6.4 dB. These two additional resonances surely come from the added resonators. When adding four other symmetrical V shapes, with smaller dimensions, to the previous structure (Figure IV.13 (e)), additional resonance occurs at a high frequency (15.9 GHz) with -17.2 dB. In order to increase the coupling effect, two gaps were created in the square shape in the previous obtained structure at the opposite corners (up right and down left), as shown in Figure IV.13 (f); these gaps induce a great amelioration in the resonances intensities compared to the previous structure. This final structure resonates at 3.57 GHz with -17.6 dB, at 6 GHz with -17.4 dB, at 8.4 GHz with -15.3 dB, at 10.1 GHz with -14 dB, at 14.8 GHz with -8 dB and at 16.3 GHz with -9.6 dB. This achieved structure is chosen as the final structure for the multi-resonance MM absorber.

The achieved dimensions of this proposed MM are summarized in Table IV.6. The chosen design of the proposed MM structure is shown in Figure IV.14.

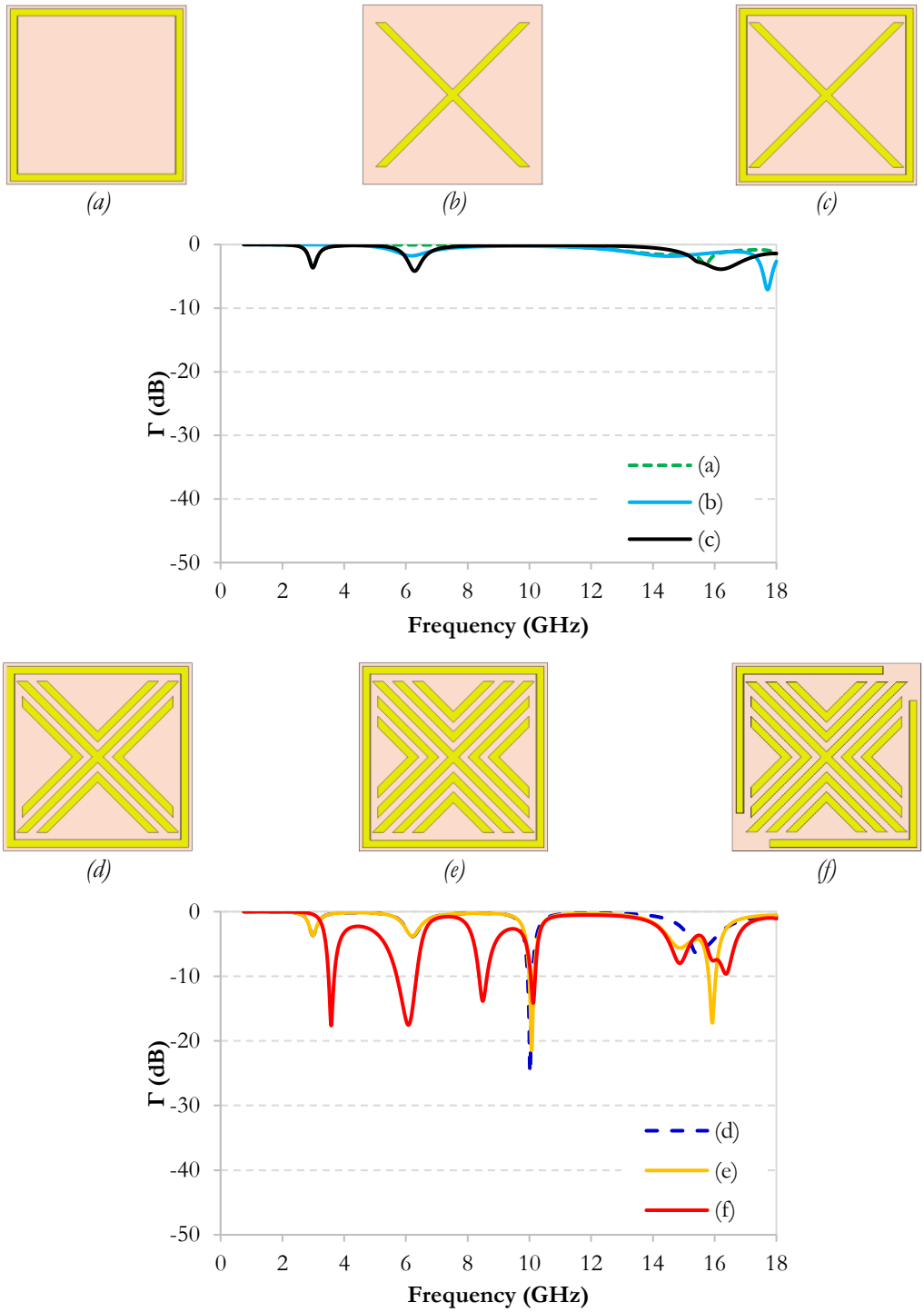

Figure IV.13. First three steps and the associated simulated reflection coefficients (a) to (c) and the second three steps and the associated simulated reflection coefficients (d) to (f) to obtain the final V-shape MM.

Parameters	Value (in mm)
e	0.5
h	3.2
L	10
ℓ	7.8
p	0.4
t	0.017
w_1	0.6
w_2	0.4

Table IV.6. Parameters of the proposed V-shape MM 10 x 10.

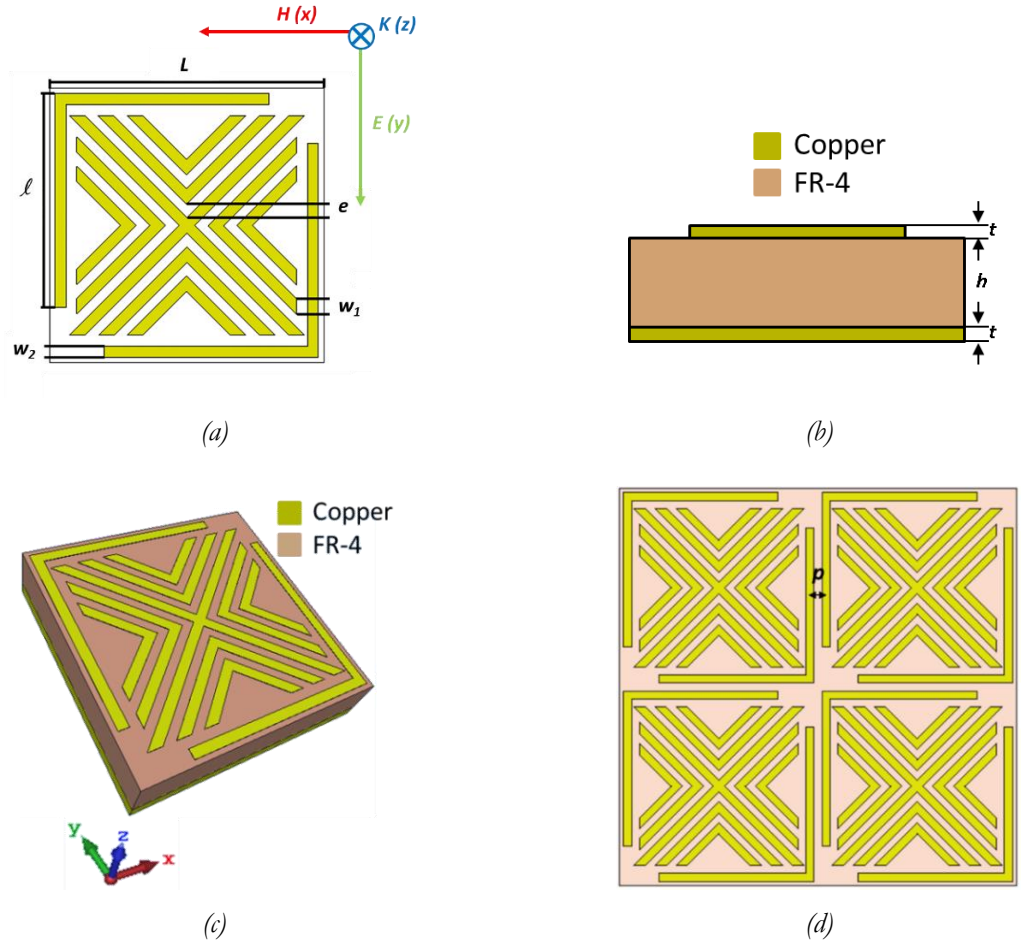

Figure IV.*14. Front view (a), side view (b), perspective view (c) and periodic view (d) of the V-shape MM.*

The simulated reflection coefficients of the proposed V-shape MM at normal incidence and oblique incidence of 30° are presented in Figure IV.15 (a) and (b), respectively. We note a multi-resonance behavior of the proposed MM where several resonances have been obtained between 3 and 18 GHz. At normal incidence (Figure IV.15 (a)), the proposed MM resonates at 3.57 GHz with -17.6 dB as the lowest frequency of resonance. Compared to the previous proposed flower shape MM, we obtained by this small unit cell a lower resonance frequency with a lower reflection coefficient. At oblique incidence of 30° (Figure IV.15 (b)), more new resonances are obtained for TM such as at 7.28 GHz and 13.1 GHz with reflection coefficients of -7.7 dB and -12.5 dB, respectively.

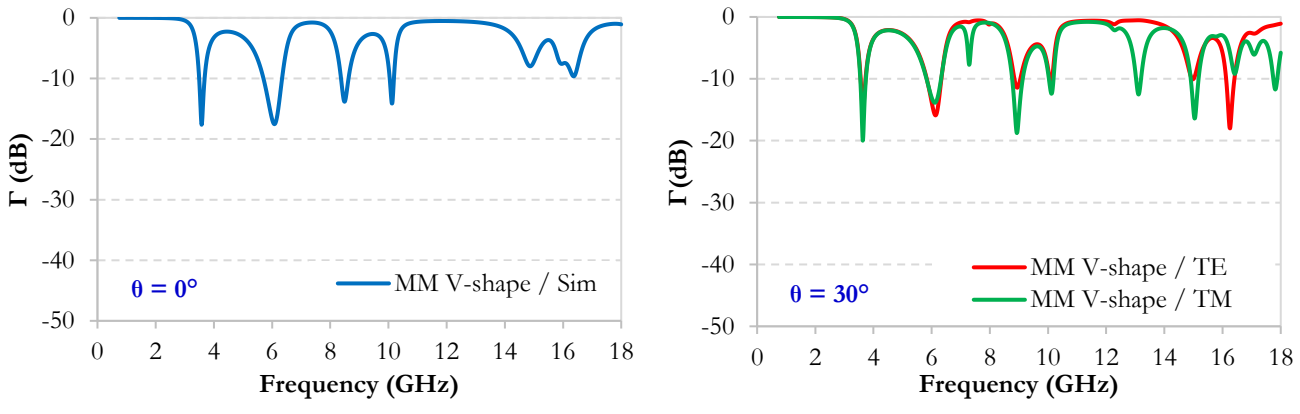

Figure IV.15. Simulated reflection coefficients at normal incidence (a) and at oblique incidence for TE and TM (b) polarizations.

In conclusion, this V-shape structure of 10 mm x 10 mm unit cell presents several resonances in the frequency range between 3 GHz and 18 GHz. But since we want to achieve a multi-resonant MM absorber between 2 and 18 GHz, with a reflection coefficient lower than -10 dB, we will proceed to the optimization of this V-shape MM in the next part.

4.2 Multi-resonance V-shape 15 x 15 MM

4.2.1 Unit cell design

The optimized proposed MM structure consists of 15 mm x 15 mm unit cell. Similar to the previous MM 10 x 10, which is composed of two L shapes (formed by the square cut on these two opposite sides) combined to X shape and several V shapes; this new shape presents at the end, larger L and X shapes with three additional V shapes, at each side of the X shape, in order to obtain several absorption peaks between 2 and 18 GHz. Figure IV.16 shows these differences between MM V-shape 10 x 10 and 15 x 15 where beside the added V shapes, longer lengths of the L, V and X shape dimensions are used. However, compared to the V-shape 10 x 10, V-shape 15 x 15 has also the same FR-4 substrate thickness (h = 3.2 mm), copper width and thickness (w = 0.4 mm and t = 0.017 mm) and the distance p (p = 0.4 mm). Table IV.7 shows the differences and the similarities between the two MM V-shapes. The proposed MM V-shape 15 x 15 is presented in Figure IV.17 from three side views.

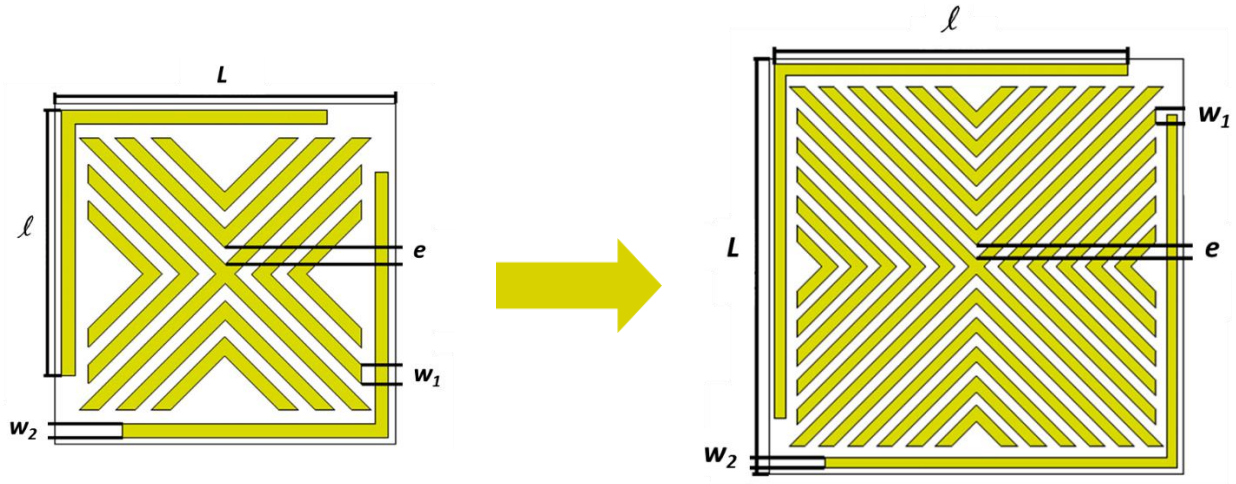

Figure IV.16. From V-shape 10 x 10 to V-shape 15 x 15.

Parameters	V-shape 10 x 10	V-shape 15 x 15
e	0.5	0.5
h	3.2	3.2
L	**10**	**15**
ℓ	**7.8**	**12.8**
p	0.4	0.4
t	0.017	0.017
w_1	0.6	0.6
w_2	0.4	0.4

Table IV.7. Comparison between MM V-shape 10 x 10 and MM V-shape 15 x 15.

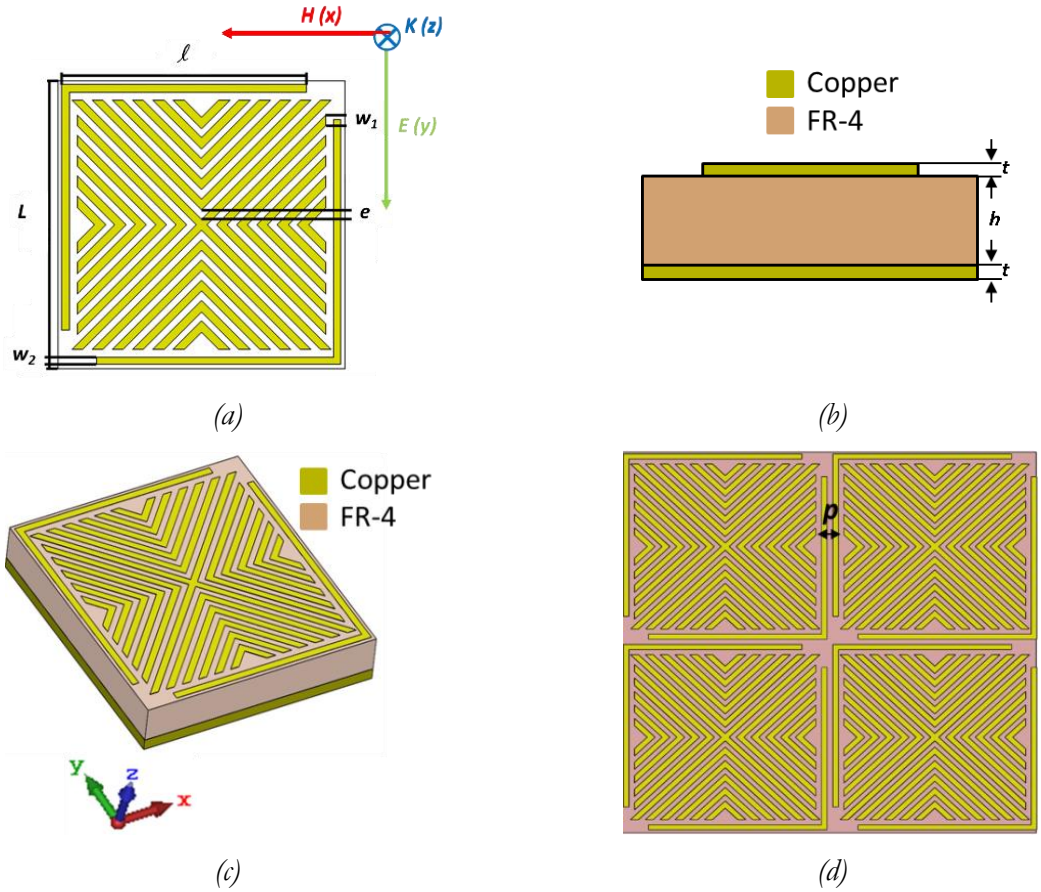

Figure IV.17. Front view (a), side view (b), perspective view (c) and periodic view (d) of the V-shape MM.

4.2.2 Simulation and measurement results

A comparison between the simulated reflection coefficients of MM V-shape 10 x 10 and 15 x 15 is presented in Figure IV.18. For MM V-shape 15 x 15, more resonances are obtained especially in the bands where MM 10 x 10 did not have any resonances. For example, a new resonance appears at 2.23 GHz, a lower frequency resonance than the first obtained one by the MM 10 x 10. Other new resonances have been appeared at 6.94 GHz, 12.4 GHz and 12.8 GHz. By this, the new proposed MM V-shape 15 x 15 presents more multi-resonances over a larger bandwidth.

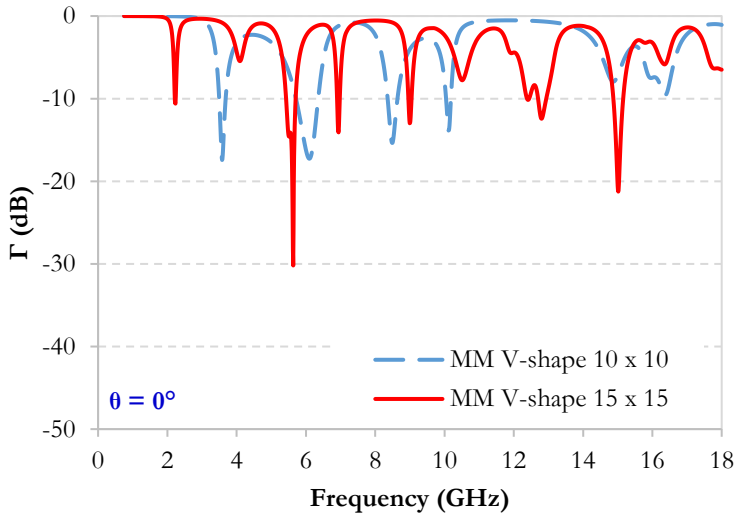

Figure IV.18. Comparison of the simulated reflection coefficients of the MM V-shape 10 x 10 and 15 x 15 at normal incidence.

The proposed MM absorber is fabricated with 10 × 10 unit cells of the total dimension of 150 mm × 150 mm × 3.2 mm where the dimension of each unit cell is 15 mm x 15 mm; the laser etching technique, using an LPKF station available at the IETR laboratory, is used for the elaboration of the proposed MM that is shown in Figure IV.19 (a).

Comparison between measured and simulated reflection coefficients, of the proposed MM of 15 mm x 15 mm, at normal incidence and at oblique incidence of 30° for TE & TM polarizations are shown in Figure IV.19 (b), (c) and (d). The same resonance is measured, but with a lower intensity, at 2.3 GHz; a reflection coefficient of -10.6 dB is expected by simulation while a reflection coefficient of -4.4 dB is measured. However, the other resonances are the same and they have a similar or even better reflection coefficient; for example, at 10.6 GHz, an expected reflection coefficient of -7.7 dB by simulation versus a reflection coefficient of -25.1 dB by measurement are obtained. The weak observed difference between simulation and measurement results is probably due to a geometric deviation between the perfect simulated structure of the MM and the produced one.

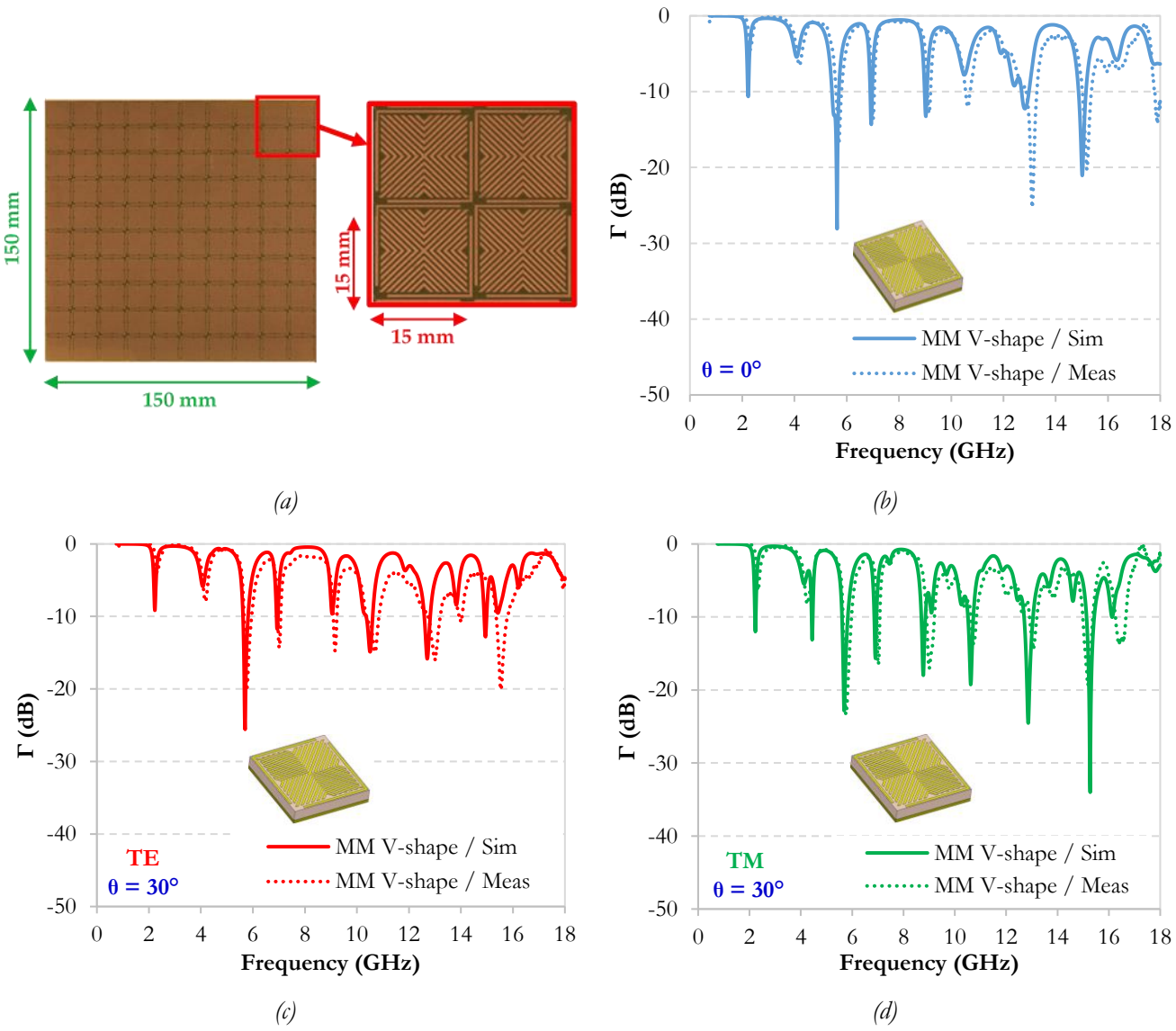

Figure IV.19. Photo of the realized MM 15 x15 (a) and comparison between measured and simulated reflection coefficients, of the proposed MM, at normal incidence (b) and oblique incidence of 30° for TE (c) and TM (d) polarizations.

On the other hand, the agreement between simulation and measurement could be observed for both TE & TM modes at oblique incidence of 30°. For TE, the same resonances are observed with a lower intensity only at 2.3 GHz, with an expected reflection coefficient of -9.2 dB by simulation and an obtained reflection coefficient of -4 dB by measurement, but the same or even better performance for the other resonances are observed. For TM, the same resonances are also observed with a lower intensity only at 2.3 GHz, with an expected reflection coefficient of -12 dB by simulation and an obtained reflection coefficient of -6.4 dB by measurement; the same or even better performance are also obtained for the other resonances. However, most of the resonances have reflection coefficients less than -10 dB as expected by simulation; so, this MM is considered as a good multi-resonant absorber over a broad band.

4.2.3 Normalized input impedance, effective permittivity and permeability

Using the simulated S_{11} parameter and based on equation (2), the normalized input impedance (z), for the proposed MM V-shape 15 x 15 backed with MP is calculated and it is shown in Figure IV.20. The obtained values of the normalized input impedance (z) that corresponds to the resonating frequencies are presented in Table IV.8. It can be noticed from both figure and table, and as previously, that at the resonating frequencies Real (z) is close to one and Imag (z) is close to zero. Here, and except at frequencies of 4.09 GHz, 10.51 GHz and 16.37 GHz, the other resonances indicate a perfect matching, and hence, a reflectivity less than -10 dB (90 % absorption) is obtained.

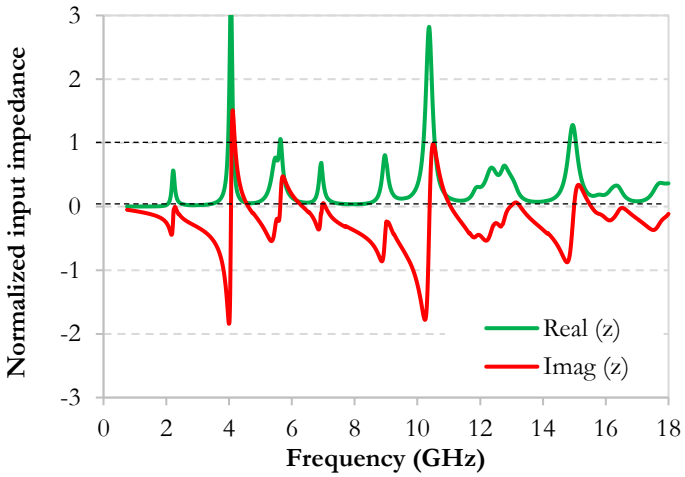

Figure IV.20. Calculated normalized input impedance of the proposed MM V-shape 15 x 15.

Frequency (GHz)	Normalized impedance
2.23	0.54 – j 0.05
4.09	2.34 – j 1.38
5.63	0.82 – j 0.43
6.94	0.68 – j 0.1
8.99	0.74 – j 0.3
10.51	1.32 – j 0.97
12.79	0.63 – j 0.16
15.01	1.14 – j 0.11
16.37	0.32 – j 0.09

Table IV.8. Complex normalized impedance at the resonant frequencies of the proposed MM.

The S_{11} parameter, was also used to extract the effective parameters (ε_{eff} and μ_{eff}) of the proposed MM V-shape 15 x 15. Based on equations (3) to (7), the extracted effective permittivity (ε_{eff}) and permeability (μ_{eff}) are presented in Figure IV.21 (a) and (b), respectively.

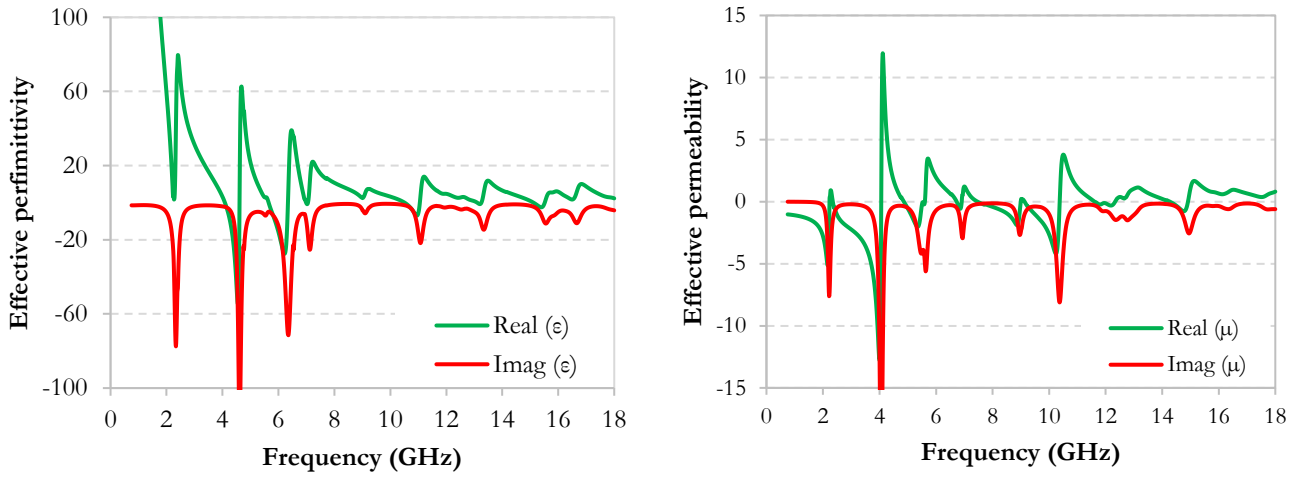

(a) *(b)*

Figure IV.21. Extracted effective permittivity (a) and permeability (b) of the proposed MM V-shape 15x15.

The analytical calculation of the reflection coefficient, using the extracted effective permittivity and permeability of the MM (Figure IV.21), is compared to the simulated one in Figure IV.22. A good agreement between these reflection coefficients is noted, which confirms again the efficiency of the extraction method used to obtain the effective parameters of the proposed MM.

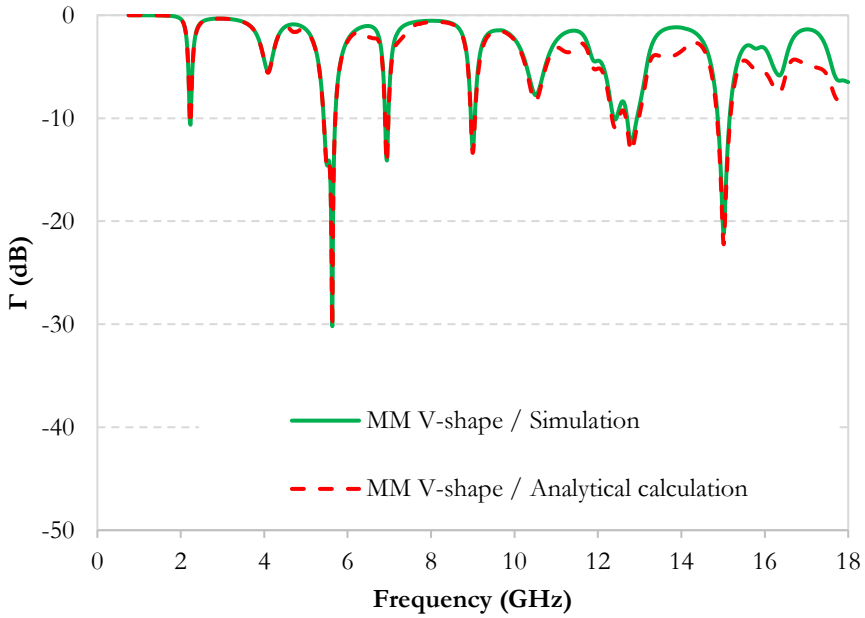

Figure IV.22. Comparison between simulated and analytical calculation of the reflection coefficients of the proposed MM using the extracted permittivity and permeability.

In conclusion, the MM V-shape 15 x 15 presents the best result, compared to the other proposed MMs, with more resonances, and the advantage of having a resonance at a low frequency (at 2.2 GHz) among all the proposed MM designs. For these reasons, this MM structure will be used in the following part in order to achieve a hybrid absorber in order to broaden its absorption bandwidth.

5. Hybrid MM absorber

MMs, which are based on a single layer, offer advantages in term of thickness, weight, and ease of fabrication. However, it is very difficult to broaden the absorption bandwidth even if using one of the methods detailed before in Chapter I, section 5.2. Indeed, most of these methods failed to cover several bands together where the design of a broadband microwave MM absorber has mostly focused on one or two frequency bands among the C-band (4-8 GHz) [7], [8], X-band (8–12 GHz) [9]–[11], Ku-band (12–18 GHz) [12] or K-band (18–27 GHz) [13], whereas very few MM designs for absorption in the S-band (2–4 GHz) [14] were reported so far. In fact because of the long wavelength of the electromagnetic waves in this band, developing a high efficient broadband microwave absorber is still a big challenge. Moreover, and today, most of the different proposed methods to broaden the MM bandwidth in the literature remain difficult to implement (such as 3D multilayers and MM with lumped elements). The aim of this work was to propose a simple method and a compact structure to broaden the MM absorber bandwidth, covering several bands, and to achieve a good absorption at the low frequencies.

In this section, a hybrid MM absorber is proposed. This hybrid absorber combines a layer of "natural" absorber, based on epoxy composites, with the artificial absorber, based on metamaterial. The proposed hybrid absorber is shown in Figure IV.23; it is composed of the V-shape MM 15 x 15 as an artificial absorber and of a layer of epoxy foam loaded with long carbon fibers, as a natural absorber.

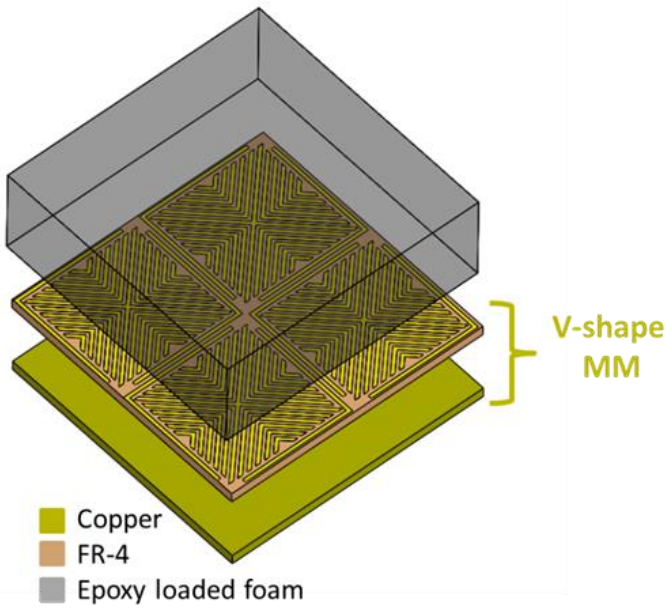

Figure IV.23. The proposed hybrid absorber.

5.1 Simulation results

Simulations of the reflection coefficient of the hybrid absorber using the loaded epoxy foam composites were carried out using CST software. These simulations were performed using the dielectric properties of different composites. Here, composites loaded with carbon fibers of 12 mm length were used. This length of fiber makes it possible, as shown before, to provide high losses at low frequency. Results are compared

to that of the MM absorber alone in Figure IV.24. These figures include, on the one hand, foam composites with very low loads (Figure IV.24 (a)) and on the other hand, more loaded foam composites (Figure IV.24 (b)); the metamaterial is represented by the black curve in both figures.

These figures show that when low weight percentages (< 0.075 wt.%) of the 12 mm CF length are used (0.025 wt.% or 0.05 wt.%), the reflection coefficient of the MM is improved (lower), but the losses are too low to broaden the bandwidth, and an uninterrupted large bandwidth (Γ < -10 dB) could not be obtained (Figure IV.24 (a)). On the other hand, when high CF loads (> 0.075 wt.%) are used (0.1 wt.% or 0.2 wt.%), higher reflections, compared to the one of the MM with 0.075 wt.% loaded foam, are obtained (Figure IV.24 (b)). Indeed, the complex permittivity of these composites are relatively high and the impedance matching is no longer ensured. This induces higher reflections (Figure IV.24 (b)) at the air/hybrid absorber interface (especially in the frequency range between 3 GHz and 8 GHz), affecting by that the absorption performance. These simulations confirm that for the hybrid absorber (as for planar absorbers) a low ε_r' that is near to that of air (ensuring an impedance matching at the air/material interface and so, the lowest reflection) and moderate dielectric losses (to ameliorate the absorption performance) are needed. For the next step, the composite loaded with 0.075 wt.% of 12 mm-CFs is adopted.

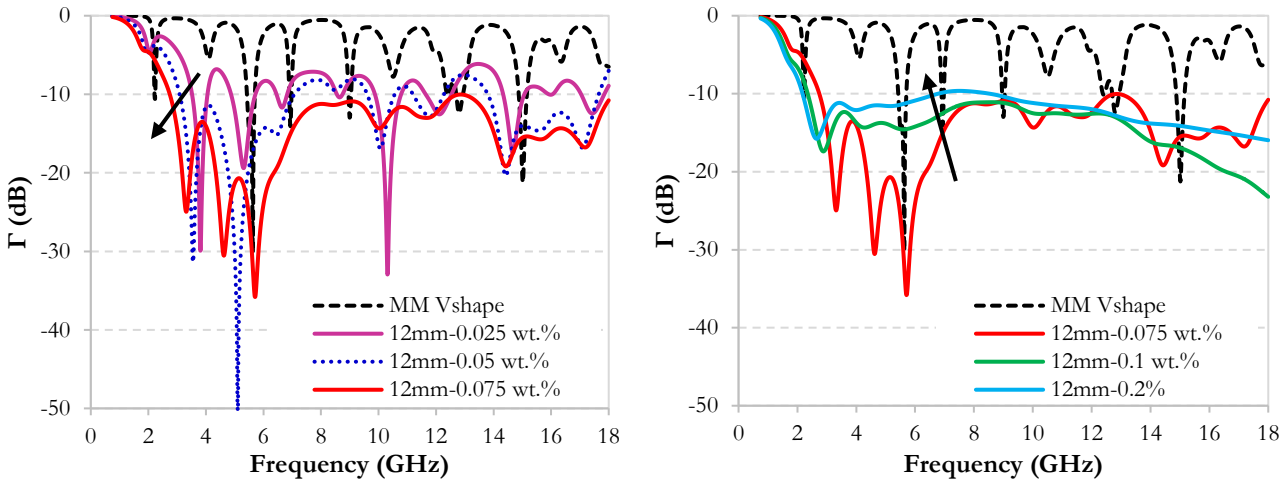

Figure IV.24. Simulation results of the reflection coefficients of the MM alone and the hybrid absorber based on composites loaded with (a) CF loads ≤ 0.075 wt.% and (b) CF loads ≥ 0.075 wt.%.

Simulations of the reflection coefficients of the hybrid absorber (with the composite loaded with 0.075 wt.% of CFs), using different thicknesses ***d***, were carried out (Figure IV.25). The worst reflection coefficient has been obtained by 10 mm thickness (***d*** = 10 mm) with a reflection coefficient less than -10 dB between 2.88 GHz and 15.3 GHz. The reflection coefficient becomes better (lower) and the absorption bandwidth becomes broader when increasing the thickness of the monolayer. With ***d*** = 13 mm, the reflection coefficient becomes less than -10 dB between 2.6 GHz and 18 GHz. However, when increasing the thickness to 14 mm and 15 mm the reflection coefficient has enhanced between 2.6 GHz and 6.7 GHz (for 14 mm thickness) and between 2.4 GHz and 5.97 GHz (for 15 mm thickness), but this was at the cost of the absorption performance between 6 GHz and 10 GHz that becomes lower (with higher reflection

coefficient). A compromise between the thickness and the absorption performance candidates the 13 mm as the better thickness to be used for the experimental measurements of the hybrid absorber.

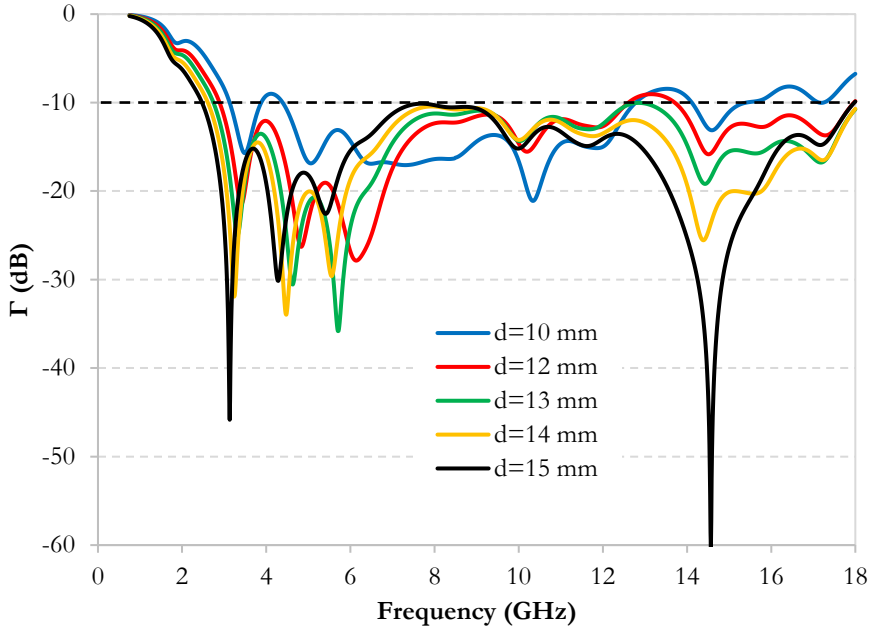

Figure IV.25. Simulation results of the reflection coefficients of the hybrid absorber based on composites loaded with 0.075 wt.% of different thicknesses.

The simulated reflection coefficient, at normal incidence, of the proposed hybrid absorber is compared to that of the monolayer (the loaded epoxy foam composite with 0.075 wt.% of 12 mm CFs) of 13 mm thickness backed with metallic plate, in Figure IV.26 (a). A better reflection coefficient is obtained by the hybrid absorber compared to the monolayer absorber alone; the absorption is here improved by the use of MM and the bandwidth is broadened by the proposed hybrid absorber.

On the other hand, a comparison between the simulated reflection coefficients of the proposed hybrid absorber and the MM 15 x 15 alone is shown in Figure IV.26 (b). A better and enhanced reflection coefficient is obtained by the hybrid absorber. In fact, a reflection coefficient less than -10 dB is obtained in an ultra-wide frequency band from 2.6 GHz to 18 GHz, covering 70% of the S-band and the entire C-band, X-band and Ku-band. By this, the absorption performance of the MM is broadened.

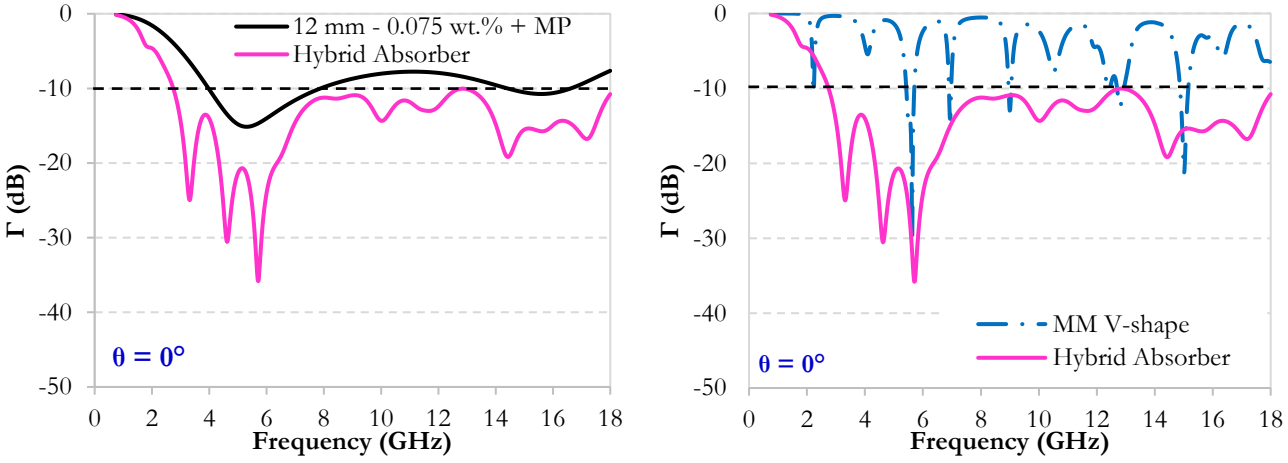

Figure IV.26. Comparison between the simulated reflection coefficients of the proposed hybrid absorber and (a) the monolayer and (b) that of the proposed MM at normal incidence.

The simulated reflection coefficients at oblique incidence of 30° for both TE and TM polarizations of the proposed hybrid absorber are shown in Figure IV.27. For both TE (Figure IV.27 (a)) and TM polarizations (Figure IV.27 (b)), reflection coefficients less than -10 dB are also obtained in an ultra-wide frequency range from 2.6 GHz to 18 GHz. A better performance of the TM polarization, compared to TE mode, is expected.

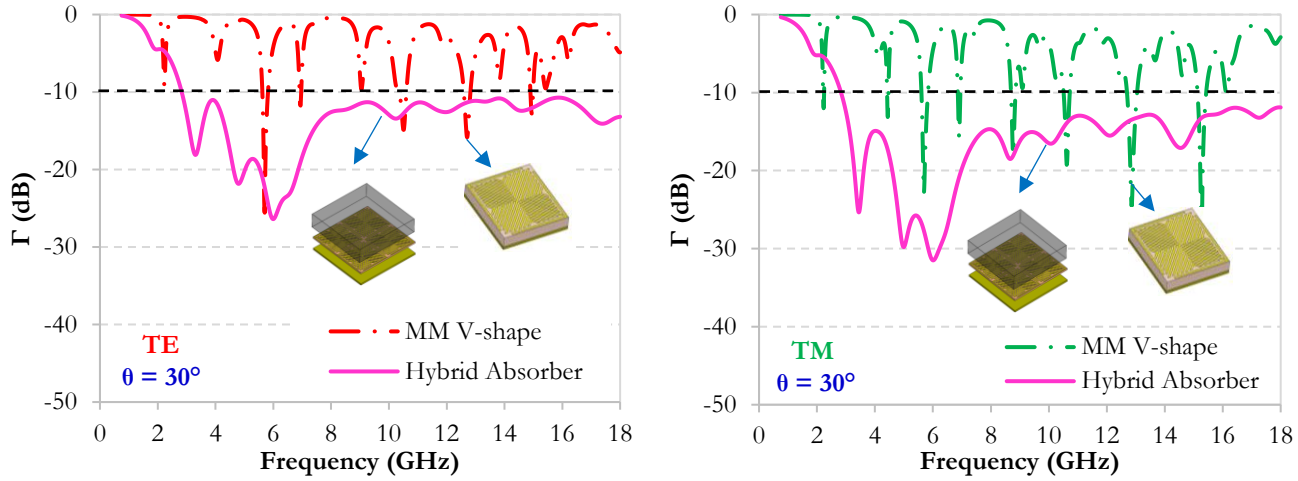

(a) *(b)*

Figure IV.27. Simulated reflection coefficients of the proposed hybrid absorber compared to that of the proposed MM at oblique incidence of 30° (a) for the TE polarization and (b) for the TM polarization.

Simulations of the reflection coefficients for other angle of incidence were conducted and are shown in Figure IV.28. A 3D plot of the simulation results for TE (Figure IV.28 (a)) and TM (Figure IV.28 (b)) polarizations, where θ varies between 0° and 60°, were performed. More clear view of the same simulated reflection coefficients for the angles of incidence 0°, 15°, 30°, 45° and 60°, for TE and TM polarizations, are shown separately in Figure IV.29 (a), for TE mode, and Figure IV.29 (b), for TM mode. These simulations predict a reflection coefficient less than -10 dB between 2.6 GHz and 18 GHz, for the different angles of incidence. However, for the TE mode and for the highest angles (θ ≥ 45°), the absorption performance is slightly affected at low (< 4.5 GHz) and high (> 16 GHz) frequencies (Figure IV.29 (a)).

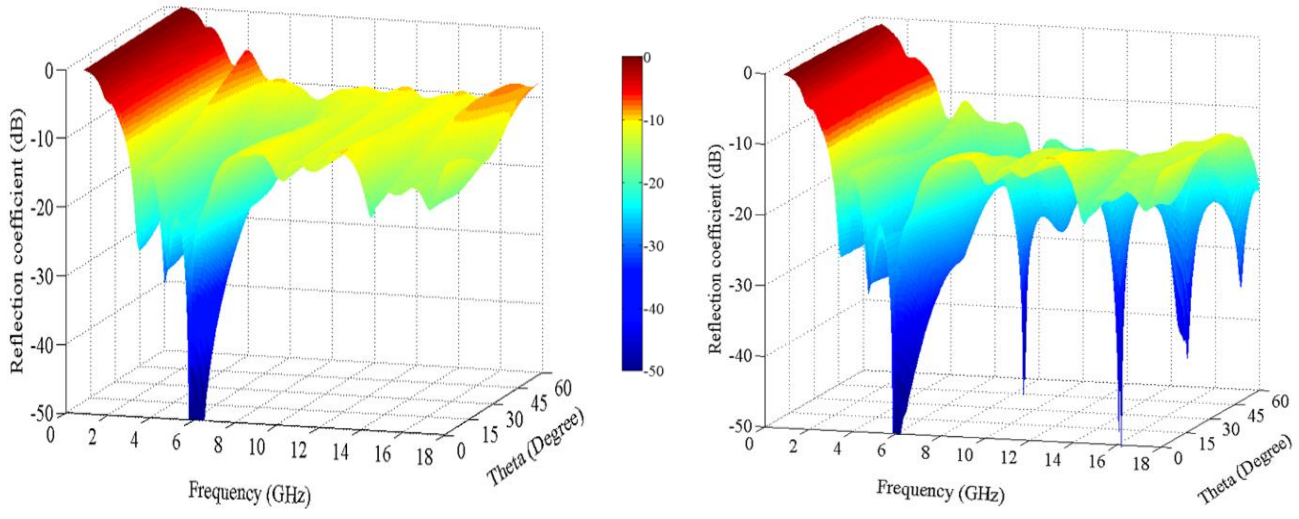

(a) *(b)*

Figure IV.28. Simulation of the reflection coefficients of the hybrid absorber with different incidence angles ranging between 0° and 60° for (a) TE and (b) TM modes (The same scale is used for the two figures).

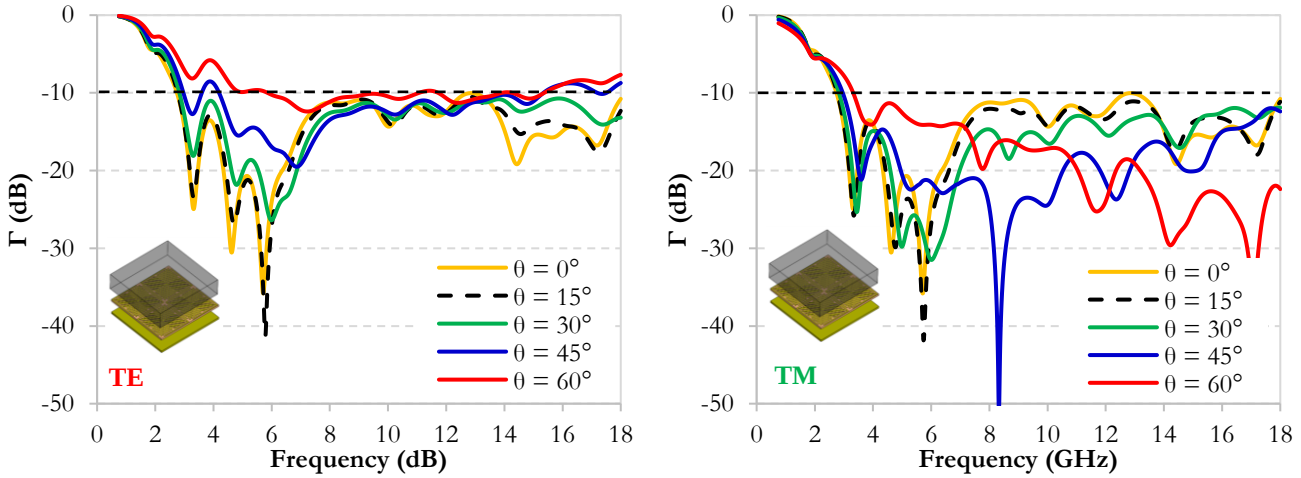

(a) *(b)*

Figure IV.29. Simulation of the reflection coefficients of the hybrid absorber with different incidence angles (0°, 15°, 30°, 45° and 60°) for (a) TE and (b) TM modes.

5.2 Measurement results

The achieved hybrid MM absorber prototype is shown in Figure IV.30 (a). The measurement results compared to that of simulations are shown in Figure IV.30 (b), (c) and (d).

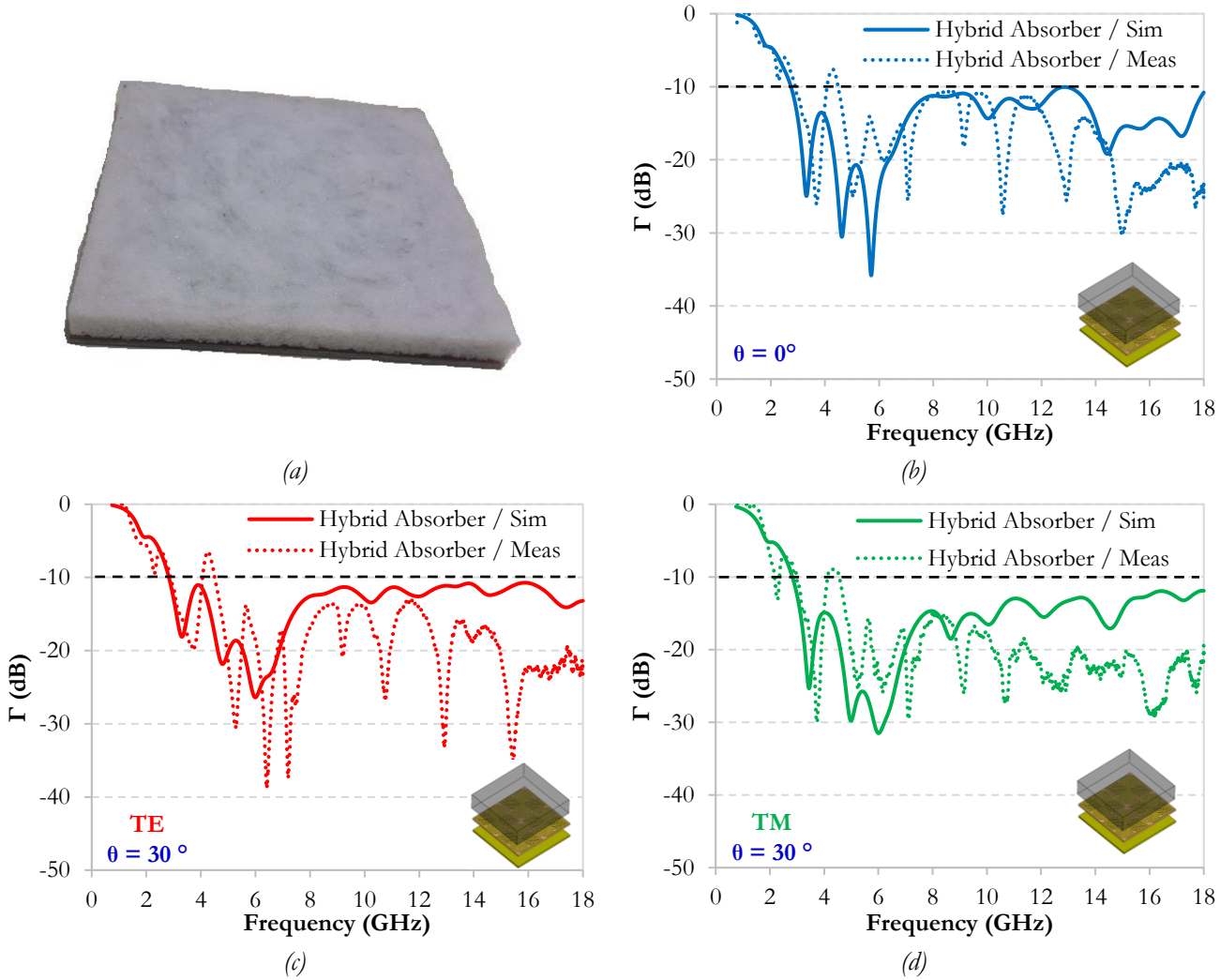

(a) *(b)* *(c)* *(d)*

Figure IV.30. The final proposed hybrid MM absorber (a) and comparison between simulation and measurement of the reflection coefficients of the hybrid absorber for normal (b) and oblique incidence for TE (c) and TM (d) polarizations.

The predicted absorption performance in ultra-wideband is confirmed here by the measurement. Note that, a slight difference between measurements and simulations is obtained. A decrease in the performance occurs at 4.2 GHz with a reflection coefficient -7.7 dB; this is due to the air gap between the monolayer and the MM absorber. Contrariwise, a better performance is obtained by measurement for the highest frequencies. For example, at 13 GHz and at normal incidence, a reflection coefficient of -25.6 dB has been obtained by measurement while the predicted reflection coefficient by simulation is -10 dB.

At oblique incidence of 30°, for TE polarization, a reflection coefficient of -28.3 dB has been obtained by measurement while a predicted reflection coefficient of -11.1 dB is obtained by simulation. Note that the measurement for the other angles of incidence (> 30°) were not carried out because of the space restrictions in the used anechoic chamber.

As a conclusion, the hypothesis of broadening the absorption bandwidth by associating a thin, light and low-loaded dielectric layer to the new mutli-resonance MM has been confirmed with an obtained reflection coefficient less than -10 dB between 2.6 GHz and 18 GHz forming an ultra-wideband compact hybrid absorber.

5.3 Comparison with other works

The absorption performance of the proposed hybrid absorber is compared to the other reported structures of microwave broadband MM absorbers. Table IV.9 presents the MM characteristics in terms of the frequency range with an absorption higher than 90 %, the total thickness (with respect to the highest wavelength λ_{max}) and the method of broadening the bandwidth. It can be observed that the proposed structure, with λ/7 (16.2 mm) thickness, has a measured absorption higher than 90 %, between 2.6 GHz and 18 GHz, forming an ultra-wideband thin hybrid absorber that covers 70 % of the S-band (2.6–4 GHz) and the entire C-band (4–8 GHz), X-band (8–12 GHz), and Ku-band (12–18 GHz); whereas, other achieved MMs cover only two or three bands with close thicknesses to that of the proposed hybrid absorber. To our knowledge, this table confirms that our result presents the best thickness/bandwidth/absorption frequency range compromise presented to date in the literatures.

Reference	Absorption > 90 %	Total thickness	Method of Broadening the BW
[15]	13.7–15.5 GHz	λ/46	Combining multiple resonating structures
[16]	10.5–12.5 GHz	λ/60	Combining multiple resonating structures
[17]	8.37–21 GHz	λ/10	Stacking multiple layers
[18]	3.7–17.5 GHz	λ/7	Stacking multiple layers
[19]	8–14 GHz	λ/8	Stacking multiple layers in 3 D
[10]	7.8–12.6 GHz	λ/12	Incorporating lumped elements
[20]	3.01–5.28 GHz	λ/20	Incorporating lumped elements
This work	2.6–18 GHz	λ/7	Associating a thin dielectric layer to the MM

Table IV.9. Comparison between the proposed structure and other presented MMs in literature.

From Table IV.9, it can be observed that the proposed structure, with 16.2 mm thickness, has a measured absorption higher than 90 %, between 2.6 GHz and 18 GHz, forming an ultra-wideband thin hybrid absorber that covers 70 % of the S-band (2.6–4 GHz) and the entire C-band (4–8 GHz), X-band (8–12 GHz), and Ku-band (12–18 GHz); whereas, other achieved MMs cover only two or three bands with close thicknesses to that of the proposed hybrid absorber. This table confirms, and to our knowledge, that our result presents the best thickness / bandwidth / absorption frequency range compromise presented to date in the literatures.

The comparison of the calculated relative bandwidth ($\Delta f/f_c$) of our realized hybrid absorber to that of the different structures of the literature, presented in Table IV.9, is shown in Figure IV.31. As shown in this figure, both references 15 and 16, where combining multiple resonating structures method is used, present the lowest relative bandwidth (< 20 %). The works using the method of stacking multiple layers (references 17, 18 and 19), to broaden the absorption bandwidth, show the highest bandwidths (between 55 % and 130 %). Here, our work presents the largest bandwidth (150 %) among all works.

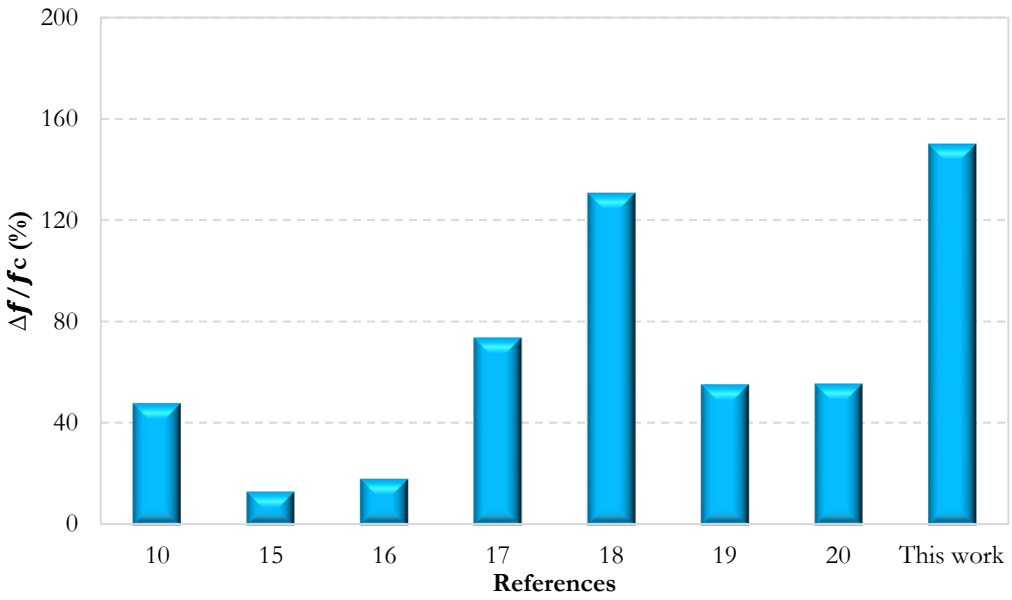

Figure IV.31. Comparison between the relative bandwidth (in %) of the realized hybrid absorber and the different references in Table IV.9.

However, as these different works present different frequency bands of absorption, as well as, different thicknesses, we cannot compare them directly; therefore, we propose to calculate here, for each work, a Factor of Merit (FoM) in order to better compare their performances. This FoM is calculated using equation (4) in which we seek to increase the absorption bandwidth and decrease both the lowest operating frequency and the total thickness of the proposed absorber.

$$FoM = \frac{Bandwidth}{Thickness * f_{min}} \tag{4}$$

The FoM is calculated for all the presented works except for references 15 and 16 because the MM structure used in these two references operate in a low bandwidth (< 20%) and at high frequencies. Our

FoM is placed here in the first position as seen in the representation of Figure IV.32. Therefore, our hybrid absorber, which is composed of two layers (epoxy foam based composite and V-shape metamaterial), presents the best compromise between bandwidth, minimal operating frequency and total thickness, achieved to date.

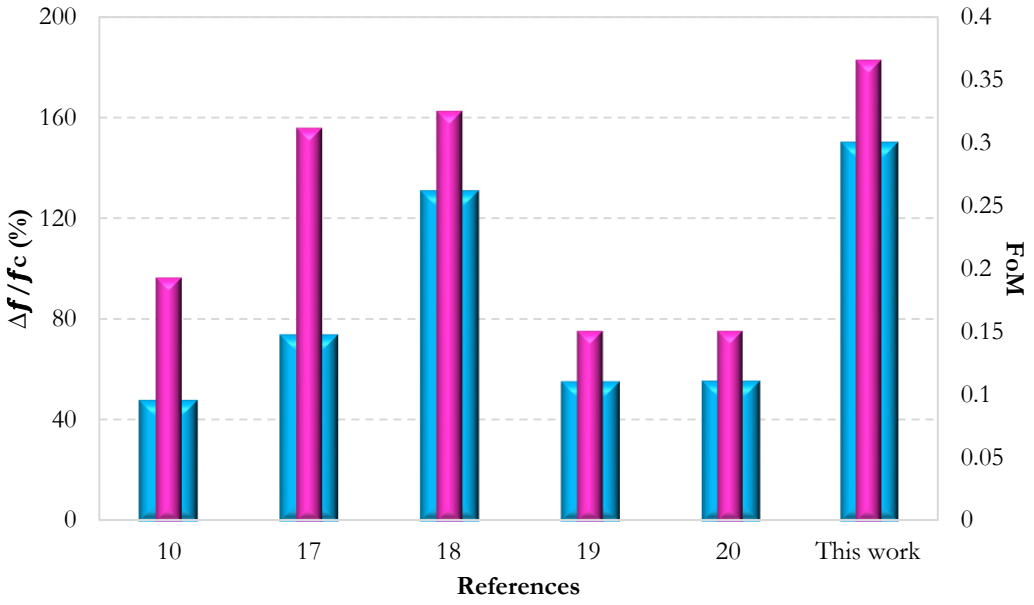

Figure IV.32. Comparison between the factor of merit (FoM) of the realized hybrid absorber and the different references in Table IV.9.

6. Conclusion

In this chapter, different new geometries of multi-resonant MM absorber are proposed. The flower shape MM, inspired from literature, was firstly proposed; here, several flowers with different dimensions were used in the same unit cell in order to obtain multiple resonances. The effect of the distance between the flowers, the dimension of the unit cell, as well as, the dimensions the flowers, on the resonance frequencies are studied. The best result is obtained when a unit cell of 27 mm x 27 mm with four flowers, with petals radii of R_1 = 1 mm, R_2 = 3 mm, R_3 = 5 mm and R_4 = 7 mm are used. These dimensions allow, as predicted, to several resonances over a large band between 4 and 18 GHz. Despite the multi-resonance behavior of the proposed MM flower shape over a broadband, the absorption performance is still weak at the low frequencies (< 7 GHz).

Another novel multi-resonance MM absorber, called V-shape MM, with unit cell dimensions of 10 mm x 10 mm was next proposed. This geometry presents several resonances between 3 and 18 GHz. However, the lowest resonance obtained with this MM occurs at 3.5 GHz. Moreover, this MM does not present resonances between 10 GHz and 14 GHz, and very weak resonances appear above 14 GHz. By increasing the unit cell of this proposed V-shape to 15 mm x 15 mm and consequently, the number of resonator elements, multiple resonances are obtained over larger bandwidth (between 2 and 18 GHz) than that obtained with MM V-shape 10 x 10. This final MM V-shape geometry combines between the good absorption performance with a multi-resonance over a large band and the small dimensions of the unit cell,

as well as, the symmetry of the resonator. For these reasons, it was chosen to be used to compose the hybrid absorber in the last part of this chapter.

A thin, light, and low-loaded dielectric layer, made of 0.075 wt.% CFs loaded epoxy foam, is associated to the front of the best MM absorber (V-shape 15 x 15), in order to broaden its absorption performance. The choice of this composite was a compromise between the low permittivity (to ensure the impedance matching at the air/absorber interface) and the moderate dielectric loss that has this composite material in order to improve the absorption performance. The dielectric layer has a thickness of 13 mm and the proposed MM has a thickness of 3.2 mm, so the hybrid absorber presents a total thickness of 16.2 mm. An absorption higher than 90% is obtained from 2.6 GHz to 18 GHz, for TE and TM polarizations at normal ($\theta = 0°$) and oblique ($\theta = 30°$) incidences. As a result, an ultra-wideband, light, and compact absorber that covers 70 % of the S-band (2.6–4 GHz) and the entire C-band (4–8 GHz), X-band (8–12 GHz), and Ku-band (12–18 GHz) is achieved. Moreover, a good agreement between measurement and simulation was obtained for both normal ($\theta = 0°$) and oblique ($\theta = 30°$) incidences for TE and TM modes for the measured prototypes based MM V-shape 15 x 15 and the hybrid absorber.

The normalized input impedance, effective permittivity and effective permeability of the MM were extracted for the proposed MMs. Analytical calculations of the reflection coefficient of the these MMs were performed and compared to that of simulation result; a very good agreement was obtained confirming by that the extraction method that was used. However, using these extracted parameters, it is possible to introduce the hybrid absorber to the genetic algorithm for further optimizations. Indeed, by introducing the MM absorber to the GA as a layer that has both the effective permeability and permittivity and the monolayer absorber as a dielectric layer that has only complex permittivity; GA will be able to vary the thickness and the composition of the dielectric monolayer for further optimizations in the absorption bandwidth and performance with a more compact thickness. This could be tested in a future work.

7. References

[1] N. Engheta, "Thin absorbing screens using metamaterial surfaces," in *IEEE Antennas and Propagation Society International Symposium (IEEE Cat. No.02CH37313)*, San Antonio, TX, USA, 2002, pp. 392–395, doi: 10.1109/APS.2002.1016106.

[2] N. I. Landy, S. Sajuyigbe, J. J. Mock, D. R. Smith, and W. J. Padilla, "Perfect Metamaterial Absorber," *Phys. Rev. Lett.*, vol. 100, no. 20, May 2008, doi: 10.1103/PhysRevLett.100.207402.

[3] X. Chen, T. M. Grzegorczyk, B.-I. Wu, J. Pacheco, and J. A. Kong, "Robust method to retrieve the constitutive effective parameters of metamaterials," *Phys. Rev. E*, vol. 70, no. 1, Jul. 2004, doi: 10.1103/PhysRevE.70.016608.

[4] D. Seetharamdoo, "Étude des métamatériaux à indice de réfraction négatif : paramètres effectifs et applications antennaires potentielles," PhD, University of Rennes 1, Rennes, 2006.

[5] L. Sun, J. Sun, B. Yang, X. Gao, H. Long, and Y. Shao, "A simplified design of broadband metamaterial absorber covering X- and Ku- band," *Mater. Res. Express*, vol. 6, no. 12, p. 125805, Jan. 2020, doi: 10.1088/2053-1591/ab62f6.

[6] P. V. Tuong, V. D. Lam, J. W. Park, E. H. Choi, S. A. Nikitov, and Y. P. Lee, "Perfect-absorber metamaterial based on flower-shaped structure," *Photonics Nanostructures - Fundam. Appl.*, vol. 11, no. 1, pp. 89–94, Feb. 2013, doi: 10.1016/j.photonics.2012.09.002.

[7] N. T. Q. Hoa, T. S. Tuan, L. T. Hieu, and B. L. Giang, "Facile design of an ultra-thin broadband metamaterial absorber for C-band applications," *Sci. Rep.*, vol. 9, no. 1, Dec. 2019, doi: 10.1038/s41598-018-36453-6.

[8] D. Shan *et al.*, "Comptibility of optical transparency and microwave absorption in C-band for the metamaterial with second-order cross fractal structure," *Phys. E Low-Dimens. Syst. Nanostructures*, vol. 116, p. 113756, Feb. 2020, doi: 10.1016/j.physe.2019.113756.

[9] P. Ranjan, A. Choubey, S. K. Mahto, R. Sinha, and C. Barde, "A novel ultrathin wideband metamaterial absorber for X-band applications," *J. Electromagn. Waves Appl.*, vol. 33, no. 17, pp. 2341–2353, Nov. 2019, doi: 10.1080/09205071.2019.1681299.

[10] T. Q. H. Nguyen, T. K. T. Nguyen, T. N. Cao, H. Nguyen, and L. G. Bach, "Numerical study of a broadband metamaterial absorber using a single split circle ring and lumped resistors for X-band applications," *AIP Adv.*, vol. 10, no. 3, p. 035326, Mar. 2020, doi: 10.1063/1.5143915.

[11] K. Ozden, O. M. Yucedag, and H. Kocer, "Metamaterial based broadband RF absorber at X-band," *AEU - Int. J. Electron. Commun.*, vol. 70, no. 8, pp. 1062–1070, Aug. 2016, doi: 10.1016/j.aeue.2016.05.002.

[12] J. B. O. de Araujo, G. L. Siqueira, E. Kemptner, M. Weber, C. Junqueira, and M. M. Mosso, "An Ultrathin and Ultrawideband Metamaterial Absorber and an Equivalent-Circuit Parameter Retrieval Method," *IEEE Trans. Antennas Propag.*, vol. 68, no. 5, pp. 3739–3746, May 2020, doi: 10.1109/TAP.2020.2963900.

[13] J. Sun, L. Liu, G. Dong, and J. Zhou, "An extremely broad band metamaterial absorber based on destructive interference," *Opt. Express*, vol. 19, no. 22, p. 21155, Oct. 2011, doi: 10.1364/OE.19.021155.

[14] Z. Zhang *et al.*, "Broadband metamaterial absorber for low-frequency microwave absorption in the S-band and C-band," *J. Magn. Magn. Mater.*, vol. 497, p. 166075, Mar. 2020, doi: 10.1016/j.jmmm.2019.166075.

[15] D. T. Viet *et al.*, "Perfect absorber metamaterials: Peak, multi-peak and broadband absorption," *Opt. Commun.*, vol. 322, pp. 209–213, Jul. 2014, doi: 10.1016/j.optcom.2014.02.037.

[16] T. Hien Nguyen *et al.*, "Metamaterial-based perfect absorber: polarization insensitivity and broadband," *Adv. Nat. Sci. Nanosci. Nanotechnol.*, vol. 5, no. 2, p. 025013, May 2014, doi: 10.1088/2043-6262/5/2/025013.

[17] H. Xiong, J.-S. Hong, C.-M. Luo, and L.-L. Zhong, "An ultrathin and broadband metamaterial absorber using multi-layer structures," *J. Appl. Phys.*, vol. 114, no. 6, p. 064109, Aug. 2013, doi: 10.1063/1.4818318.

[18] X. Begaud, A. C. Lepage, S. Varault, M. Soiron, and A. Barka, "Ultra-Wideband and Wide-Angle Microwave Metamaterial Absorber," *Materials*, vol. 11, no. 10, p. 2045, Oct. 2018, doi: 10.3390/ma11102045.

[19] F. Ding, Y. Cui, X. Ge, Y. Jin, and S. He, "Ultra-broadband microwave metamaterial absorber," *Appl. Phys. Lett.*, vol. 100, no. 10, p. 103506, Mar. 2012, doi: 10.1063/1.3692178.

[20] W. Yuan and Y. Cheng, "Low-frequency and broadband metamaterial absorber based on lumped elements: design, characterization and experiment," *Appl. Phys. A*, vol. 117, no. 4, pp. 1915–1921, Dec. 2014, doi: 10.1007/s00339-014-8637-3.

General conclusion

General Conclusion

Today, we are surrounded by several electromagnetic (EM) waves such as WIFI, 3G, 4G, Bluetooth, and many other electronic devices and systems, which induce an increasing electromagnetic pollution. For that, electromagnetic absorbing materials are more and more necessary in order to reduce this pollution; different forms and compositions of absorbing materials exist and they are used today in various fields, ranging from civil to military applications. The work of this thesis takes place in this context; it is dedicated to the use of the carbon fibers (CF) loaded epoxy foam composites for the elaboration of planar absorbers: multilayer and hybrid based metamaterial absorbers. For multilayer absorbers, the aim is to ensure a good absorption performance over a wide frequency range with the minimum thickness. However, for the metamaterial, the aim was to use a simple method to broaden the absorption bandwidth of a new elaborated metamaterial absorber, with also the minimal possible thickness.

In this manuscript, and first of all, the state of art of absorbing materials, their theory and principles were presented. Here, a classification of the microwave absorbers as function of their bandwidth from one hand, and their compositions from the other hand, was done. Then, the absorbers used in the anechoic chamber and their advantages and disadvantages were presented. Finally, the loaded epoxy foam composites that will be used in this work were introduced.

After this, a theoretical study was done in order to elaborate a MATLAB code that computes the total reflection coefficient of any multilayer absorber within few seconds. This elaborated code was verified on an example of the commercial absorber AH 125; a very good agreement was obtained between the simulation result, by the commercial software CST Microwave Studio Suite, and the analytical calculation result, thus validating the implemented calculation method.

The method of choosing the composition of each layer of the multilayer absorber, basing on the dielectric properties or on the characteristic impedance of each layer material, was also detailed. Indeed, a smooth and gradual impedance transition from front to back, associated with gradual losses in order to dissipate the EM waves, are required. For this, the calculation of the module of the characteristic impedance was presented for better observation of the gradual impedance.

In this work, different loaded epoxy foam composites were used. Some of them are elaborated by Ms. Hanadi Breiss. These composites were elaborated with a large panel of dielectric properties by using different CF lengths (between 100 μm and 12 mm) and different weight percentages (between 0.0125 wt.% and 10 wt.%). Here, it was seen that the maximum dielectric losses occurs at the high frequencies for the low CF lengths, and at low frequencies for long CFs (12 mm).

Two multilayer absorbers (MLA250 and MLA125-1), composed of the same composites (unloaded (0 wt.%) and loaded epoxy foams with different CF lengths, 3 mm, 6 mm and 12 mm, with rates of 0.25 wt.%, 0.75 wt.% and 0.25 wt.%, respectively) and with two different thicknesses (250 mm and 125 mm), were tested in order to prove the effect and the importance of using a smooth gradual impedance on the

absorption performance. The first prototype (MLA250) exhibited insufficient impedance transition, thus a low absorption performance was obtained. In fact, even when reducing the thickness of each layer to the half to compose MLA125-1, a similar performance has been obtained. From here, it was concluded that the high reflections between the layers are at the origin of this performance.

For the MLA125-2 prototype, the composites loaded with the 12 mm CFs using different low weight percentages (from 0.0125 wt.% to 0.075 wt.%), were used since they have interesting losses at low frequencies. This prototype, presenting the same thickness of 125 mm, shows a better absorption performance than the MLA125-1, due to the smoother gradual impedance that was observed when the composites are stacked from the lowest to the highest load in the direction of the EM wave.

A LW-MLA125-1 prototype was proposed using the elaborated composites by Ms. Hanadi Breiss with the same CF length (12 mm) and weight percentages (between 0.0125 wt.% and 0.075 wt.%) as MLA125-2, but with lower densities (ranging between 0.05 and 0.07 g/cm3) than those used before (0.12 g/cm3). LW-MLA125-1 presents a reflection coefficient less than -20 dB from 2.6 GHz to 18 GHz and it shows a very close performance to that of MLA125-2 which has the same CF rates but a relative higher density, and to that of the commercial absorber AH 125 of the same dimensions and density. However, LW-MLA125-1 is made of epoxy foam composites, which are rigid materials where CFs are trapped inside the foam matrix, unlike commercial multilayer absorbers which are flexible and carbon particles may easily escape from the material, since they are volatile loads, resulting in its premature aging.

An optimization of the absorption performance of the multilayer absorbers with the lowest thickness was conducted. Therefore, GA optimizer implemented in CST, which deals only with the thicknesses of each layer to enhance the absorption performance with a fixed total thickness, was tested for two thicknesses 125 mm (MLA125-GA) and 77 mm (MLA77-GA). The optimizer succeeded to improve the reflection coefficient at the low frequencies for MLA125-GA between 0.75 GHz and 4.42 GHz (-13 dB < Γ < -32 dB), keeping the same performance (Γ < -16 dB) for frequencies higher than 7 GHz, with a small deterioration of the performance between 4.42 GHz and 7 GHz. For MLA77-GA, the performance was deteriorated between 1 GHz and 3.3 GHz while the same performance (Γ < -13 dB), compared to MLA125-GA, is observed beyond 4.5 GHz. This result shows that it is necessary to keep a minimum thickness to guarantee a good absorption at low frequencies.

Another optimization of the multilayer absorber design was proposed by introducing the calculated reflection coefficient by the elaborated code (with MATLAB) to the GA optimizer in order to find the best compromise of layers compositions/thickness for a better absorption over a large frequency band. For this, a database of predefined materials was constructed with 24 different materials, the unloaded (0 wt.%) and several loaded epoxy foam composites, with different CF lengths (from 100 μm to 12 mm) and rates (from 0.0125 wt.% to 10 wt.%).

Different designs were proposed by the developed code. MLA70-GA-M, with a 70 mm thickness, presents Γ < -10 dB between 1 GHz and 18 GHz and Γ < -20 dB for frequencies > 6 GHz while MLA50-GA-M (50 mm) presents Γ < -10 dB for frequencies > 1.18 GHz. Simulated and measured reflection coefficients of the proposed prototypes, show a better performance than that of MLA77-GA (optimized by GA CST), which has a higher thickness (44%).

Otherwise, GA was also used to highlight, the effect of the length of the CFs on the absorption bandwidth. Indeed, for the absorption bandwidth, GA systematically chose the composites loaded with: the lowest CF lengths (mainly the CFs of 100 μm) and with the lowest total thickness (61 mm) for the frequency band [12-18] GHz, 3 mm CF length (with a total thickness of 79 mm) for the frequency band [6-12] GHz, and 12 mm CF length for the low frequencies [0.75-6] GHz, for the different layers.

Moreover, an optimization was conducted using the five lightweight epoxy foam composites; here the proposed LW-MLA81-GA-M design shows a good reflection coefficient < -20 dB in most of the studied frequency band (2.21 - 18 GHz) with a total thickness reduced by 35% compared to the lightweight LW-MLA125-1 which is composed with the same loaded materials, but in another combination between layers' compositions and thicknesses.

At the end, the developed code with GA MATLAB improves the performance of multilayer absorbers while reducing their thickness because of the variety of the combinations that could be generated and tested by the GA in few minutes, allowing a better absorption performance.

For metamaterial (MM) absorbers, different new geometries of multi-resonant MM absorber were proposed. For the first proposed MM, inspired from literature, the flower shape was chosen; here four flowers with different dimensions were combined together in the same unit cell. Several studies on the effect of the dimensions of the flowers, the length of the unit cell and distances between the flowers candidates a unit cell of 27 mm x 27 mm with four flowers, with petals radii of R1 = 1 mm, R2 = 3 mm, R3 = 5 mm and R4 = 7 mm. This proposed MM presents several resonances over a large band between 4 and 18 GHz. Despite the multi-resonance behavior of the proposed MM flower shape over a broadband, the absorption performance is still weak at the low frequencies (< 7 GHz).

Consequently, and in order to obtain more resonances in the studied frequency range [2-18] GHz, another novel multi-resonance MM absorber, called V-shape MM, with unit cell dimensions of 10 mm x 10 mm was proposed. This MM absorber presents several resonances between 3 and 18 GHz, but the lowest obtained resonance with this MM occurs at 3.5 GHz. In addition to that, there are no resonances between 10 GHz and 14 GHz, and very weak resonances appear above 14 GHz. When the unit cell of this proposed V-shape is increased to 15 mm x 15 mm and consequently, with an increase of the number of resonators, multiple resonances are obtained over a large bandwidth (between 2 and 18 GHz). This final symmetrical V-shape MM 15 x15 was chosen to be used to compose the hybrid absorber in the last part of the manuscript.

A thin, light, and low-loaded dielectric layer (epoxy foam loaded with 12 mm - 0.075 wt.%) of 13 mm was associated at the front of V-shape 15 x 15 of 3.2 mm in order to broaden its absorption performance, forming a hybrid absorber. The choice of this composite was a compromise between the low permittivity (to ensure the impedance matching at the air/absorber interface) and the moderate dielectric loss in order to improve the MM absorption performance. An absorption higher than 90% is obtained from 2.6 GHz to 18 GHz; thus, the hybrid absorber is considered as an ultra-wideband, light, and compact absorber that covers 70 % of the S-band (2.6–4 GHz) and the entire C-band (4–8 GHz), X-band (8–12 GHz), and Ku-band (12–18 GHz) with a small thickness (16.2 mm). A comparison of our hybrid material was made with planar based MM absorbers presented the literature, taking into account the thickness, the absorption bandwidth and the frequency range; this comparison shows that our prototype presents, to our knowledge, the best compromise presented to date in the literature.

Furthermore, the normalized input impedance, effective permittivity and effective permeability (ε_{eff} and μ_{eff}) of the MM were extracted for the different proposed MMs. ε_{eff} and μ_{eff} were used for the analytical calculations of the reflection coefficients of these MMs and the result was compared to the simulated one where a very good agreement was obtained confirming by that the extraction method.

In the perspective of this work, the optimized design of the multilayer absorber using the GA in MATLAB, which was used for normal incidence of EM waves, may be edited by including the adequate equations in order to also compute the reflection coefficients at oblique incidences. By this, the optimization will include all angles of incidence. Moreover, the extracted effective permittivity and permeability of the MM could be also used to introduce the hybrid absorber to the GA for further optimizations. Here, the MM could be represented as a layer that has both the effective permeability and permittivity and the monolayer absorber as a dielectric layer that has only complex permittivity. By this, GA will be able to vary the thickness and the composition of the dielectric monolayer to broaden the absorption bandwidth and performance with a more compact thickness.

List of communications

List of communications

Journal articles

1- H. Breiss, **A. El Assal,** R. Benzerga, A. Sharaiha, A. Jrad, A. Harmouch, "*Ultra-porous and lightweight epoxy foam loaded with carbon fibers for microwave absorber application", Materials Research Bulletin*, *137,* ***2021***, p.111188. https://doi.org/10.1016/j.materresbull.2020.111188

2- **A. El Assal,** H. Breiss, R. Benzerga, A. Sharaiha, A. Jrad, A. Harmouch, "*Toward an ultra-wideband and hybrid based metamaterial microwave absorber", Micromachines, 11*, *no. 10,* (**2020**): 930. https://doi.org/10.3390/mi11100930

3- H. Breiss, **A. El Assal**, R. Benzerga, C. Méjean, and A. Sharaiha, *"Long Carbon Fibers for Microwave Absorption: Effect of Fiber Length on Absorption Frequency Band," Micromachines, vol. 11, no. 12, p. 1081, Dec.* ***2020.*** https://doi.org/10.3390/mi11121081

4- R. Benzerga, M. Badard, C. Méjean, **A. El Assal,** C. Le Paven, A. Sharaiha, "*Carbon fibers loaded composites for microwave absorbing application: effect of fiber length and dispersion process on dielectric properties",* Journal of Electronic Materials, **2020**. DOI 10.1007/s11664-020-07998-y

5- Y. Lamri, R. Benzerga, A. Ayadi, L. Le Gendre and **A. El Assal,** "*Glass foam composites based on tire's waste for microwave absorption application",* Journal of Non-Crystalline Solids, Volume 537 (**2020**), pp-120017. https://doi.org/10.1016/j.jnoncrysol.2020.120017

6- Y. Lamri, R. Benzerga, A. Ayadi, L. Le Gendre and **A. El Assal,** *"Synthesis and characterization of foam glass composites for electromagnetic absorption application",* Materials Research Express, 6 (**2019**), pp- 035201. https://doi.org/10.1088/2053-1591/aaf42e

International Conferences

1- **A. El Assal,** H. Breiss, R. Benzerga, A. Sharaiha, A. Harmouch, A. Jrad, "*Hybrid Material For Broadband Microwave Absorbers",* MMA **2020**, International Conference on Microwave Materials and their Applications 30 august – 2 September 2020, Aveiro, Portugal. (reported to 4 july 2021)

2- H. Breiss, R. Benzerga, C. Méjean, **A. El Assal,** M. Badard, A. Sharaiha, "*Effect of fiber length on the dielectric properties and absorption frequency band of carbon loaded epoxy foam composites",* MMA **2020**, International Conference on Microwave Materials and their Applications 30 august – 2 September 2020, Aveiro, Portugal. (reported to 4 july 2021)

3- H. Breiss, **A. El Assal,** R. Benzerga, A. Sharaiha, A. Harmouch, A. Jrad, "*Ultra-porous epoxy foam loaded with carbon fibers for microwave absorber materials",* MMA **2020**, International conference on Microwave Materials and their Applications 30 august – 2 September 2020, Aveiro, Portugal. (reported to 4 july 2021)

4- Y. Lamri, R. Benzerga, A. Ayadi, L. Le Gendre, **A. El Assal,** *"Elaboration and characterization of foams glass composites for electromagnetic waves insulation application",* ISMSD2019 : 4th International Symposium on Materials and Sustainable Development, 11-14 November **2019** Boumerdes, Algeria

5- **A. El Assal,** H. Breiss, R. Benzerga, A. Sharaiha, A. Harmouch , A. Jrad, "*Electromagnetic multilayer absorber made of carbon fibers loaded epoxy foam",*APC 2019 "Antennas and Propagation Conference 2019", 11 – 12 November **2019**, Birmingham, UK

6- **A. El Assal,** R. Benzerga, A. Sharaiha, A. Harmouch , A. Jrad, "*Hybrid planar absorber: towards a compact absorber",* ISAP **2019** "International Symposium on Antennas and Propagation 2019", 27 – 30 October 2019, Xi'an, China

7- **A. El Assal,** R. Benzerga, A. Sharaiha, A.Harmouch, A. Jrad, "*Combination of Artificial and Natural Planar Absorbers: Towards a 70% Reduction in Thickness",* MS&T19 "Materials Science and Technology International Conference", Advances in Dielectric Materials and Electronic Devices Symposium, 30 September – 3 October **2019**, Portland, USA

8- **A. El Assal,** R. Benzerga, H. Breiss A. Sharaiha, A. Harmouch, A. Jrad, "*Genetic Algorithm for multilayer absorption performance optimization",* MS&T19 "Materials Science and Technology International Conference", Advances in Dielectric Materials and Electronic Devices Symposium, 30 September – 3 October **2019**, Portland, USA

9- **A. El Assal,** R. Benzerga, A. Sharaiha, A. Harmouch, A. Jrad, "*Foam Composites for Planar Absorber Application",* MS&T19 "Materials Science and Technology International Conference", Synthesis, Characterization, Modeling and Applications of Functional Porous Materials Symposium, 30 September – 3 October **2019,** Portland, USA

10- **A. El Assal,** R. Benzerga, A. Sharaiha, A. Harmouch, A. Jrad, "*Multilayer Absorber Based on Carbon Fibers Loaded Epoxy Foam",* URSI AP-RASC **2019**, URSI Asia-Pacific Radio Science Conference, 9 - 15 Mars 2019, New Delhi, India

11- **A. El Assal,** R. Benzerga, A. Sharaiha, A. Harmouch, A. Jrad, "*Planar Multilayer Absorber Based on Carbon Fibers Loaded Epoxy Foam: Design and Analysis",* MMA2018 (10th International Conference on Microwave Materials and their Applications 2018) Osaka, Japan, 1-4 October **2018**

12- Y. Lamri, R. Benzerga, A. Ayadi, L. Le Gendre, **A. El Assal,** F. Benhaoua, "*Waste tire-based glass foam composites for microwave absorption application",* MMA2018 (10th International Conference on Microwave Materials and their Applications 2018) Osaka, Japan, 1-4 October **2018**
Best Poster Award

13- Y. Lamri, R. Benzerga, A. Ayadi, L. Le Gendre, **A. El Assal,** F. Benhaoua, "*Glass foam composites based on used tires for microwave absorbing application",* ISMSD2017, 3rd International Symposium on Materials and Sustainable Development, 7-8 November **2017**, Boumerdes, Algeria,

14- Y. Lamri, R. Benzerga, L. Le Gendre, A. Ayadi, **A. El Assal,** "*Microwave absorbent material based on glass waste and carbon fibers",* ISMSD2017, 3rd International Symposium on Materials and Sustainable Development, 7-8 November **2017**, Boumerdes, Algeria

National Conferences

1- A. El Assal, R. Benzerga, H. Breiss, A. Sharaiha, A. Harmouch, A. Jrad, "*Absorbants planaires hybrides : vers l'optimisation de l'épaisseur",* JNM 2019 "21èmes Journées Nationales Microondes", 14-17 mai **2019** Caen, France.

2- L. Pometcu, C. Méjean, R. Benzerga, A. Sharaiha, **A. El Assal**, P. Pouliguen, "*Matériau et forme innovants pour les absorbants en chambre anéchoïque",* JCMM2018 "15èmes Journées de Caractérisation Microondes et Matériaux", 19-21 Mars **2018**, Paris, France.

Titre : **Matériaux absorbants en hyperfréquences à base de mousse époxy chargée en fibres longues de carbone**

Mots clés : Absorbants microondes, Multicouches, Métamatériaux, Composites, Absorbant hybride

Résumé : Ce travail de thèse porte sur la conception, la réalisation et la mesure d'absorbants microondes. Plusieurs types d'absorbant ont été étudiés dans la bande de fréquence allant de 0.75 GHz à 18 GHz. Il s'agit tout d'abord d'absorbants planaires à multicouches élaborés à partir de mousses époxy chargées avec différents pourcentages massiques (entre 0.0125 et 10 %) de fibres de carbone ayant des longueurs entre 100 µm et 12 mm. La performance d'absorption des multicouches a été optimisée, tout en réduisant leur compacité, grâce à un code MATLAB et à l'utilisation d'un l'algorithme génétique. La composition et l'épaisseur de chaque couche ont ainsi pu être optimisées, et ont conduit à la réalisation de plusieurs prototypes performants (absorption > 90%) de faibles épaisseurs (entre 50 mm et 98 mm), très faiblement chargés (<0.075 % de fibre) et présentant pour certains une très faible densité (0.06 g.cm-3). Par ailleurs, des absorbants à métamatériaux (MM) ont été étudiés. Une nouvelle géométrie multi-résonante (nommée Vshape), présentant une multitude de pics d'absorption sur la bande de fréquence étudiée, a pu être proposée ; un calcul analytique du coefficient de réflexion, utilisant les propriétés effectives extraites, a été mis en place. La simulation, la mesure ainsi que le calcul analytique de ce MM montrent des résultats très concordants validant ainsi nos modèles. Finalement, un absorbant hybride, associant une couche fine de mousse époxy chargée en fibres de carbone au métamatériau, a été proposé pour élargir sa bande passante. Ainsi, un absorbant plan ultralarge-bande (avec un coefficient de réflexion < -10 dB entre 2.6-18 GHz) a ainsi pu être obtenu. Cet absorbant montre le meilleur compromis épaisseur / bande d'absorption / fréquence d'absorption présenté à ce jour dans la littérature.

Title: **Microwave absorber materials based on epoxy foam loaded with long carbon fibers**

Keywords: Microwave absorbers, Multilayers, Metamaterials, Composites, Hybrid absorber

Abstract: This work focuses on the design, elaboration, and measurement of microwave absorbers. Several types of absorbers have been studied in the frequency range from 0.75 GHz to 18 GHz. First, planar multilayer absorbers have been made epoxy foams loaded with different weight percentages (between 0.0125 and 10%) of carbon fibers with lengths between 100 µm and 12 mm. The absorption performance of these multilayers has been optimized while reducing their compactness, thanks to a MATLAB code and the use of a genetic algorithm. The composition and thickness of each layer could thus be optimized and led to the production of several high-performance prototypes (absorption> 90%) of low thicknesses (between 50 mm and 98 mm), very lightly loads (<0.075% fiber), and with very low density (0.06 g.cm^{-3}). Second, metamaterial (MM) absorbers have been studied. A new multi-resonant geometry (called Vshape), presenting several absorption peaks on the studied frequency band, has been proposed; an analytical calculation of the reflection coefficient, using the extracted effective properties, was implemented. The simulation, measurement as well as analytical calculation of this MM show very consistent results thus validating our models. Finally, a hybrid absorber, combining a thin layer of epoxy foam loaded with carbon fibers to the metamaterial, was proposed to broaden its bandwidth. Thus, a planar ultra-wide-band absorber (with a reflection coefficient <-10 dB between 2.6-18 GHz) could thus be obtained. This absorber shows the best compromise between thickness/absorption band/absorption frequency presented to date in the literature.